The influence of Nicotinic Acid Adenine Dinucleotide Phosphate (NAADP) signalling and the significance of the organization of lysosomes in cardiac myocytes

SUBMISSION FOR THE DEGREE OF DOCTOR OF PHILOSOPHY

DANIEL ASTON
NEW COLLEGE, 639319

Acknowledgements

Contained within the following pages is a summary of the work that often felt all-consuming during the period between September 2012 and early 2017. The task of completing a DPhil sometimes seemed insurmountable, but thankfully I was not alone in my enormous task. That my name appears on the spine of this volume in solitude is an unrepresentative reflection of the number of people who really contributed to it, through the advice, encouragement and support that they generously offered.

I do not exaggerate when I say that my supervisor, Professor Derek Terrar, is one of the most optimistic and enthusiastic people I have had the pleasure of working with. I must thank him for inviting me to work in his laboratory and also for his wisdom and encouragement - especially during the times when my chips were down and I felt little optimism or enthusiasm myself!

There are a number of people in the Oxford departments of Pharmacology and DPAG to whom I must also offer my thanks:

The Beckies (Dr Rebecca Burton and Dr Rebecca Capel) have been good friends and always hugely helpful, encouraging and generous with their time. In particular, I must thank Becky Burton for her expertise and help with the electron microscopy experiments, without which this thesis would be much smaller and far less interesting!

Sam Lin Wee Khang, Dr Bobo Nazarov and Dr Emma Bolton, without whom working in Oxford would have been considerably less enjoyable and I am very pleased that our paths crossed while we were all in Derek's lab.

Dr Magarida Ruas da Silva who offered a vast amount of advice regarding my western blotting experiments and who also developed and donated the TPC2 knockout mice used in several of my experiments. Professor Manuela Zaccolo and Dr Nicoletta Surdo who were instrumental in facilitating the cell culture experiments. I would also like to thank Dr Gary Mirams for his Matlab coding skills, Dr Kerrie Ford for her help with many of the confocal microscopy experiments, and Professor Ming Lei for his help and the use of his lab to perform MAP recordings. Dr Eva A Rog-Zielinska and Professor Peter Kohl also allowed me to include their 3D electron tomography data in an appendix to this thesis - the results of which complement my own experiments - and I am very grateful for this.

Of course, I must thank my parents once again for their unremitting belief in me and everything I do. I must also thank my twin sons, Sam and Harry, who were born during my second week in Oxford. They have provided a continuous supply of joy and inspiration (even if they did their utmost to ensure that I did the first eighteen months of my DPhil in a state of permanent insomnia, and who - even as I type this - are singing to themselves in bed instead of settling to sleep).

Finally, and most importantly, I owe more thanks than I can express to my wife Lindsay who has been a source of unending love and patience, and who - in many ways - put her own life on hold to allow me to complete this DPhil.

Sincerely, thank you all.

Table of Contents

Acknowledgements		i
Table of contents		ii
Complete figure list		iv
Abbreviations		ix
Abstract		xi
1	**General Introduction**	**1**
1.1	General Introduction	2
1.2	The structure of the heart	3
1.3	Excitation-contraction coupling and calcium handling in the heart	17
1.4	Mechanisms of arrhythmogenesis	41
1.5	Lysosomes	46
1.6	Nicotinic Acid Adenine Dinucleotide Phosphate (NAADP)	52
1.7	Other calcium signalling molecules	70
1.8	Aims of this thesis	74
2	**Methods**	**75**
2.1	Generation of *Tpcn2*$^{-/-}$ mice	76
2.2	Murine electrocardiography	76
2.3	Monophasic action potentials and programmed electrical stimulation	77
2.4	Murine atrial contraction recordings	78
2.5	Rabbit ventricular cell isolation	79
2.6	Immunocytochemistry	80
2.7	Analysis of images obtained using immunocytochemistry	82
2.8	Live cell confocal microscopy	84
2.9	Electron microscopy	85
2.10	Western blotting	86
2.11	Neonatal rat ventricular cardiomyocyte isolation and culture	89
2.12	Analysis of cultured cells: size and viability measurements	91
2.13	Analysis of cultured cells: RNA isolation and measurement	92
2.14	Suppliers, solutions, drugs, reagents and consumables	96
2.15	Table of antibodies	97
2.16	Animals	98
2.17	Statistics	98
3	**Cardiac arrhythmias induced by acute adrenergic stimulation: involvement of TPC2**	**101**
3.1	Introduction	102
3.2	Results	107
3.3	Conclusion	125

4 Cardiac hypertrophy induced by chronic adrenergic stimulation: involvement of NAADP 134

4.1 Introduction 135
4.2 Results 139
4.3 Conclusion 160

5 The association of lysosomes with sarcomeric structures in ventricular muscle: Light microscopy 166

5.1 Introduction 167
5.2 Results 173
5.3 Conclusion 195

6 The association of lysosomes with sarcomeric structures in ventricular muscle: Electron microscopy 203

6.1 Introduction 204
6.2 Results 210
6.3 Conclusion 233

7 The structure and function of cardiac atrial tissue in the context of NAADP signalling 239

7.1 Introduction 240
7.2 Results 245
7.3 Conclusion 268

8 General Discussion 274

9 Appendices 280

9.1 Appendix A 281
9.2 Appendix B 289
9.3 Appendix C 299

10 Bibliography 306

Complete Figure List

Chapter 3: From page 112

Figure 3.1 Western blots of β1-adrenergic receptor protein with GAPDH loading controls in wildtype and *Tpcn2*$^{-/-}$ mice.

Figure 3.2 Expression of β1-adrenergic receptor protein in wildtype and *Tpcn2*$^{-/-}$ mice as detected by western blotting.

Figure 3.3 Representative electrocardiograph tracings from wildtype and *Tpcn2*$^{-/-}$ mice.

Figure 3.4 Resting electrocardiograph parameters from live anaesthetised wildtype and *Tpcn2*$^{-/-}$ mice.

Figure 3.5 Resting heart rates taken from electrocardiograph recordings of live anaesthetised wildtype and *Tpcn2*$^{-/-}$ mice.

Figure 3.6 There is no significant difference in duration of monophasic action potentials (MAPs) between wildtype and *Tpcn2*$^{-/-}$ mice.

Figure 3.7 Cumulative ventricular arrhythmia time (VT or VF) in isolated hearts from wildtype and *Tpcn2*$^{-/-}$ mice (variable cycle length).

Figure 3.8 Cumulative ventricular arrhythmia time (VT or VF) in isolated hearts from wildtype and *Tpcn2*$^{-/-}$ mice (variable pacing current).

Figure 3.9 The effect of isoprenaline on arrhythmia provocation in hearts from wildtype and *Tpcn2*$^{-/-}$ mice (variable pacing current).

Figure 3.10 The effect of isoprenaline on arrhythmia provocation in hearts from wildtype and *Tpcn2*$^{-/-}$ mice (variable cycle length).

Figure 3.11 Cumulative ventricular arrhythmia time (VT or VF) in isolated hearts from wildtype and *Tpcn2*$^{-/-}$ mice exposed to isoprenaline 50 nM (variable pacing current).

Figure 3.12 Cumulative ventricular arrhythmia time (VT or VF) in isolated hearts from wildtype and *Tpcn2*$^{-/-}$ mice exposed to isoprenaline 50 nM (variable cycle length).

Figure 3.13 Representative monophasic action potential (MAP) recordings from wildtype and *Tpcn2*$^{-/-}$ mice exposed to isoprenaline 50 nM.

Chapter 4: From page 145

Figure 4.1 Typical appearance of cardiomyocytes

Figure 4.2 Viability of cultured neonatal rat cardiomyocytes exposed to Ned-19 10 μM or bafilomycin-A1 100 nM over time.

Figure 4.3 The toxic effect of bafilomycin-A1

Figure 4.4 The effect of Ned-19 on the size of neonatal rat cardiomyocytes after 48 hours.

Figure 4.5 The effect of bafilomycin-A1 on the size of neonatal rat cardiomyocytes after 48 hours.

Figure 4.6 Hypertrophic effect of isoprenaline 10 μM compared with that of noradrenaline 10 μM.

Figure 4.7 Isoprenaline-induced hypertrophy of cells and the effect of Ned-19.

Figure 4.8 Differential interference contrast (DIC) images of cultured neonatal rat cardiomyocytes illustrating the effect of isoprenaline and Ned-19.

Figure 4.9 Atrial Natriuretic Peptide (ANP) mRNA expression in neonatal rat cardiomyocyte cultures exposed to isoprenaline 10 μM after 48 hours.

Figure 4.10 α-Actin mRNA expression in neonatal rat cardiomyocyte cultures exposed to isoprenaline 10 μM after 48 hours.

Figure 4.11 Hypertrophic effect of noradrenaline on cultured neonatal rat cardiomyocytes and the protective effect of Ned-19 10 μM.

Figure 4.12 Atrial Natriuretic Peptide (ANP) mRNA expression in neonatal rat cardiomyocyte cultures exposed to noradrenaline 10 μM after 48 hours.

Figure 4.13 α-Actin mRNA expression in neonatal rat cardiomyocyte cultures exposed to noradrenaline 10 μM after 48 hours.

Figure 4.14 Isoprenaline-induced hypertrophy of cells and the effect of bafilomycin-A1.

Figure 4.15 Mean total RNA yields from cultures of neonatal rat cardiomyocytes treated with different drugs.

Chapter 5: From page 181

Figure 5.1 Typical distribution of LAMP-2 in a rabbit ventricular cardiomyocyte using fluorescence immunocytochemistry.

Figure 5.2 Typical distribution of lysosomes labelled with lysotracker green in a rabbit ventricular cardiomyocyte.

Figure 5.3 Representative measurements of fluorescence intensity across rabbit ventricular cardiomyocytes.

Figure 5.4 Frequency of fluorescent intensity plots for type-2 ryanodine receptor (RyR2), phospholamban (PLB) and LAMP-2 in rabbit ventricular cardiomyocytes.

Figure 5.5 A representative example of a more sophisticated method for analysis of immunocytochemistry of cells co-labelled with antibodies against RyR2 and LAMP-2.

Figure 5.6 A representative example of a more sophisticated method for analysis of immunocytochemistry of cells co-labelled with antibodies against PLB and LAMP-2.

Figure 5.7 Correlation between dominant frequencies of RyR2/PLB and LAMP-2 images.

Figure 5.8 Co-labelling of LAMP-2 and type-2 ryanodine receptor (RyR2) using fluorescent immunocytochemistry in a rabbit ventricular cardiomyocyte.

Figure 5.9 Co-labelling of LAMP-2 and phospholamban (PLB) using fluorescent immunocytochemistry in a rabbit ventricular cardiomyocyte.

Figure 5.10 Estimating mean proximity between RyR2 and LAMP-2.

Figure 5.11 Proximity of RyR2 or PLB to LAMP-2.

Figure 5.12 Co-labelling of Ned-19 binding sites with Ned-19 and lysosomes using lysotracker red.

Figure 5.13 Co-labelling of T-tubules using the voltage-sensitive fluorescent dye di-8-anepps and lysosomes using lysotracker green.

Figure 5.14 Co-labelling of mitochondria using tetramethylrhodamine ethyl ester (TMRE) and lysosomes using lysotracker green in rabbit ventricular cardiomyocyte.

Chapter 6: From page 218

Figure 6.1 Annotated transmission electron micrograph of a single sarcomere in a rabbit ventricular cardiomyocyte.

Figure 6.2 Low magnification transmission electron microscopy of rabbit ventricular cardiomyocytes.

Figure 6.3 Typical examples of different organelles seen in rabbit ventricular cardiomyocytes with transmission electron microscopy.

Figure 6.4 The size of cardiac lysosomes found in rabbit ventricle.

Figure 6.5 The distance from the lysosome to the sarcoplasmic reticulum (SR) in rabbit ventricular cardiomyocytes.

Figure 6.6 Proximity of lysosomes to sarcoplasmic reticulum (SR) and T-tubules seen in rabbit ventricular cardiomyocytes on transmission electron microscopy.

Figure 6.7 Proximity of lysosomes to sarcoplasmic reticulum (SR) and T-tubules seen in rabbit ventricular cardiomyocytes on transmission electron microscopy.

Figure 6.8 Possible tethering of lysosome to sarcoplasmic reticulum (SR) membrane seen in rabbit ventricular cardiomyocytes on transmission electron microscopy.

Figure 6.9 The distance from lysosomes to the nearest T-tubule in rabbit ventricular cardiomyocytes.

Figure 6.10 The distance from lysosomes to the nearest Z-line in rabbit ventricular cardiomyocytes.

Figure 6.11 A wide-view image of a rabbit ventricular cardiomyocyte. Some lysosomes are in close proximity with Z-lines and T-tubules while others are more distant.

Figure 6.12 Lysosomal distribution in a rabbit ventricular cardiomyocyte seen on transmission electron microscopy.

Figure 6.13 Lysosomes in close proximity with mitochondria in rabbit ventricular cardiomyocytes seen on transmission electron microscopy.

Figure 6.14 The distance from the lysosome to the nearest mitochondria in rabbit ventricular cardiomyocytes.

Chapter 7: From page 252

Figure 7.1 Low magnification transmission electron microscopy of rabbit atrial cardiomyocytes.

Figure 7.2 The size of cardiac lysosomes found in rabbit atria.

Figure 7.3 Dimensions and distance to SR of atrial and ventricular lysosomes compared.

Figure 7.4 Dense clusters of lysosome-like structures in a cardiomyocyte from rabbit atrium.

Figure 7.5 Transmission electron micrograph showing a low magnification view of the submembrane region in a rabbit atrial cardiomyocyte.

Figure 7.6 The distance from the lysosome to the sarcoplasmic reticulum (SR) in rabbit atrial cardiomyocytes.

Figure 7.7 Lysosomes in rabbit atrial cardiomyocytes shown lying in close proximity with sarcoplasmic reticulum (SR).

Figure 7.8 The distance from the lysosome to the nearest mitochondrion in rabbit atrial cardiomyocytes.

Figure 7.9 Lysosomes lying in close proximity with mitochondria in rabbit atrial cardiomyocytes.

Figure 7.10 Comparison of baseline atrial contraction amplitudes between *Tpcn2*$^{-/-}$ and wildtype mice.

Figure 7.11 Contractile response of isolated left atria from wildtype and *Tpcn2*$^{-/-}$ mice to isoprenaline.

Figure 7.12 Rate response of isolated right atria from wildtype and *Tpcn2*$^{-/-}$ mice to isoprenaline.

Figure 7.13 Effect of drugs on left atrial contraction amplitude.

Figure 7.14 Contractile response of isolated murine left atria to isoprenaline or isoprenaline + Ned19 10 μM.

Figure 7.15 Contractile response of isolated murine left atria to isoprenaline or isoprenaline + bafilomycin-A1 1 μM.

Figure 7.16 Representative recordings of atrial contraction in response to isoprenaline.

Appendices: From page 280

Figure A1 Uncropped images of western blot membranes

Figure A2 Control images for immunocytochemistry experiments.

Figure A3 Live cell confocal control images.

Figure B1 Electron tomography reconstruction of a lysosome with SR, T-tubules and mitochondria.

Figure B2 Immunogold staining of LAMP-2 in mouse ventricular tissue.

Figure B3 Specific binding of Ned-19 in live ventricular cardiomyocytes.

Figure C1 Matlab code for analysis of immunocytochemistry images.

Abbreviations used in this thesis

β-AR	Beta-adrenergic receptor
ACh	Acetyl choline
ADP	Adenosine diphosphate
AF	Atrial fibrillation
ANOVA	Analysis of variance
ANP	Atrial natriuretic peptide
ARC	ADP-ribosyl cyclase
ASG	Atrial specific granule
ATP	Adenosine triphosphate
AVN	Atrioventricular node
AVNRT	Atrioventricular nodal re-entry tachycardia
BNP	Brain natriuretic peptide
cADPR	Cyclic adenosine diphosphoribose
CaMKII	Calmodulin-activated protein kinase 2
cAMP	Cyclic adenosine monophosphate
CD	Cluster of differentiation
CDI	Calcium-dependent inactivation
cDNA	Copy deoxyribonucleic acid
CICR	Calcium-induced calcium release
CREM	cAMP response element modulator
DAD	Delayed afterdepolarisation
DAG	Diacylglycerol
DIC	Differential interference contrast
DMEM	Dulbecco's modified eagle's medium
DMSO	Dimethyl sulphoxide
DNA	Deoxyribonucleic acid
EAD	Early afterdepolarisation
ECG	Electrocardiograph
EM	Electron microscopy
EPAC	Exchange protein directly activated by cAMP
ER	Endoplasmic reticulum
ERK	Extracellular signal-regulated kinase
ET	Electron tomography
FKBP	FK506-binding protein
GAPDH	Glyceraldehyde-3-phosphate dehydrogenase
GDP	Guanosine diphosphate
GPCR	G-protein coupled receptor
GPN	Glycylphenylalanine 2-naphthylamide
GTP	Guanosine triphosphate
HDAC	Histone deacetylase
ICC	Immunocytochemistry
IGF	Insulin-like growth factor
IP_3	Inositol 1,4,5-trisphosphate
JPH	Junctophilin
L-SR	Lysosome-sarcoplasmic reticular
L-TT	Lysosome-T-tubular
L-Z	Lysosome-Z-line

LAMP	Lysosome-associated membrane protein
LRO	Lysosome-related organelle
LTCC	L-type calcium channel
MAPK	Mitogen-activated protein kinase
MCS	Membrane contact site
MPR	Mannose-6-phosphate receptor
mPTP	Mitochondrial permeability transition pore
mRNA	Messenger ribonucleic acid
mTOR	Mammalian target of rapamycin
NAADP	Nicotinic acid adenine dinucleotide phosphate
NCX	Sodium-calcium exchange
NFAT	Nuclear factor activated by T-cells
PASMC	Pulmonary artery smooth muscle cell
PBS	Phosphate-buffered saline
PCR	Polymerase chain reaction
PI3K	Phosphoinositide-3-kinase
PIP_2	Phosphatidylinositol 4,5-bisphosphate
PKA	Protein kinase A
PKC	Protein kinase C
PKD	Protein kinase D
PLB	Phospholamban
PLC	Phospholipase C
PVDF	Polyvinylidene difluoride
qPCR	Quantitative polymerase chain reaction
RNA	Ribonucleic acid
RyR	Ryanodine receptor
S/ER	Sarco/endoplasmic reticulum
SAN	Sinoatrial node
SCW	Spontaneous calcium wave
SERCA	Sarco-endoplasmic reticulum calcium ATPase
SLN	Sarcolipin
SMC	Smooth muscle cell
SR	Sarcoplasmic reticulum
TAT	Transverse and axial tubule
TBS	Tris-buffered saline
TEM	Transmission electron microscopy
TGF	Transforming growth factor
TGN	Trans-Golgi network
TMRE	Tetramethyl rhodamine ethyl ester
TPC	Two-pore channel
$Tpcn2^{-/-}$	Two-pore channel-2 knockout
TRP-ML	Transient receptor potential mucolipin
UV	Ultraviolet
VDI	Voltage-dependent inactivation
VF	Ventricular fibrillation
VT	Ventricular tachycardia

The influence of Nicotinic Acid Adenine Dinucleotide Phosphate (NAADP) signalling and the significance of the organization of lysosomes in cardiac myocytes

Abstract

The central role of calcium ions in the generation of contractile force in the heart has been understood for many decades. In many mammals, a large proportion of the calcium responsible for activation of the contractile apparatus is released from the sarcoplasmic reticulum (SR), and this release is regulated via many mechanisms.

One regulatory factor that has earned much attention in recent years is Nicotinic Acid Adenine Dinucleotide Phosphate (NAADP) and its probable receptor, Two-Pore Channel-2 (TPC2), which is found on the surface of lysosomes. NAADP has been found to function in a wide range of tissues from both animals and plants. In the heart, it is thought that NAADP may be generated in response to stimulation of cardiomyocytes with β-adrenergic agonists and that it acts at the lysosome to cause release of calcium. This calcium may then regulate the release and reuptake of calcium by the SR.

Due to the importance of calcium in the heart, substances that modulate calcium release in cardiac cells may be expected to have a broad array of effects. Under some circumstances, the dysregulation of calcium signalling caused by these substances may also be expected to have pathological consequences, both acutely and over the long term.

The exposure of ex-vivo hearts perfused via Langendorff apparatus to the β-adrenergic agonist isoprenaline resulted in ventricular arrhythmias following electrical burst pacing in wildtypes, but not in hearts from TPC2 knockout (*Tpcn2*$^{-/-}$) animals. This data supports the hypothesis that NAADP is important in the acute cardiac response to β-agonists, and more specifically that it has an influence on the calcium handling events that lead to arrhythmogenesis in these cells.

Similarly, chronic treatment of cultured neonatal rat cardiomyocytes with the adrenergic agonists isoprenaline and noradrenaline is known to induce a hypertrophic response associated with re-activation of the foetal gene program. This response was found to be strongly attenuated by the NAADP antagonist Ned-19, which prevented both the increase in cell size and the increase in expression of foetal genes associated with hypertrophy. These results suggest that in addition to the role of NAADP in acute responses to β-adrenergic agonists, it may also be important in chronic responses.

Calcium released from the lysosome in response to NAADP action at TPC2 is thought to modulate calcium release from the SR. This process is likely to require a close spatial relationship between these organelles. Data from confocal microscopy experiments demonstrate an association between lysosomes and the SR, while membrane contact sites (MCS) between these structures are shown to exist using electron microscopy. These observations support the hypothesis that functional calcium signalling microdomains exist between lysosomes and the SR in the heart.

1

Introduction

1.1 General Introduction

The time taken for a substance to diffuse from where it is supplied to where it is needed is dependent on the square of the distance it has to travel. The time required for the diffusion of oxygen and other nutrients to occur over a distance such as the width of the muscular wall of the heart is far too great to allow supply to keep up with the high cardiac demand. Most multicellular organisms have solved this problem through the evolution of a specialised circulatory system in order to reduce the distance for diffusion as much as possible.

The blood circulates around the body and rapidly supplies the tissues with adequate nutrients and also removes waste products. The driving force of this circulation is the heart, which - in mammals - is a four chambered organ that functions as two pumps in series. The first (right side) sends deoxygenated blood returning from the periphery to the lungs and back to the second (left side), which pumps the newly-oxygenated blood back to the tissues.

Calcium ions play an essential role, both in the electrical excitation of the heart and in the generation of mechanical force. The subcellular pathways that function to regulate calcium concentration in the heart are complex, and have been the subject of decades of investigation. Additionally, knowledge of the mechanisms by which calcium regulation is altered or becomes abnormal in pathological circumstances is valuable in the search for therapeutic strategies.

1.2 The structure of the heart

1.2.1 Macroscopic anatomy

The heart is approximately cone-shaped and lies obliquely across the midline of the thorax with the base medial and cephalad, the apex lateral and caudad and the lungs lying laterally on either side. The base of the heart is an approximately oval-shaped ring composed of fat and fibrous tissue called the annulus fibrosus, which is electrically insulating. The four chambers of the heart and the great vessels are arranged around this, with the atria and vessels above and the ventricles below. The annulus fibrosus has four perforations; two allowing atrioventricular communication via valves, and two for the ventricular outflow tracts. There is also a connection through the annulus fibrosus that allows electrical communication between atria and ventricles - the atrioventricular node (AVN).

In transverse section through the ventricles, the left ventricle can be seen as a muscular ring which is approximately three times the mass and twice the thickness of the C-shaped right ventricle next to it. The left ventricular cavity is conical with muscle fibres wrapping around it in different directions: Endocardial and epicardial fibres run longitudinally from apex to base, while fibres between these layers run circumferentially. This allows the ventricle to shorten in both length and radius during contraction.

Blood enters the heart via the vena cavae, which are continuous with the right atrium. It then flows through the tricuspid valve into the right ventricle. As the name suggests, the

tricuspid valve usually has three cusps each of which are connected to prominences in the ventricular wall called papillary muscles by the fibrous cordae tendinae. The contraction of these muscles during systole prevents the valve inverting. Blood is pumped by the right ventricle through the pulmonary valve into the pulmonary artery and around the lungs before it returns to the left atrium. It then passes through the mitral valve (which usually has two cusps, also connected to papillary muscles) into the left ventricle. Finally, contraction of the left ventricle forces blood through the aortic valve into the systemic arterial system. After passing through the capillary network, blood flows into progressively larger veins until it returns to the vena cavae.

The heart is supplied with blood by the left and right coronary arteries, which originate from the coronary ostia in the proximal aorta, and run along the epicardial surface of the heart. Venous drainage is via the cardiac veins, which mostly drain via the coronary sinus into the right atrium. A small amount of venous blood drains directly into the ventricular cavity via the Thebesian veins. This drainage mechanism is more prominent on the right than on the left, since drainage of deoxygenated blood into the right ventricle does not increase shunt. The heart is innervated by both sympathetic and parasympathetic systems, and also has visceral sensory fibres.

The electrical conducting system of the heart begins at the sino-atrial node (SAN) in the right atrium, where the electrical activity that initiates each heart beat begins. From here, the electrical impulse spreads across the atria and passes through the base of the heart via the AVN. It then passes through specialised conducting tissue called the bundle of His and the bundle branches into the Purkinje fibres to excite the contractile myocytes.

1.2.2 Microscopic structure

Cardiomyocytes and cardiac tissue

Adult cardiomyocytes are approximately cylindrical (or rectangular in cross-section) with an approximate diameter and length of 10 - 25 μm and 50 – 120 μm respectively. They are usually mono- or binucleated and are connected end-to-end via intercalated discs, which are made up of three main types of junction; the adherens junction, the desmosome and the gap junction (Noorman et al., 2009). Adherens junctions and desmosomes are formed from transmembrane glycoproteins called cadherins which traverse the small (~20 nm) divide between adjacent myocytes. They allow the binding of cytoskeletal intermediate filaments which travel through the length of the cells, giving them tensile strength. In contrast, gap junctions are composed of six subunits of a protein called connexin. These subunits form the walls of a tunnel that pierces the plasma membrane of adjacent cells, allowing their cytoplasms to communicate. This connection is important for the transmission of electrical currents during the action potential. The presence of intercalated discs is unique to cardiac muscle, and these structures are not found in skeletal or smooth muscle.

As a result of these connections and gap junctions in particular, cardiac muscle behaves as an electrically continuous functional syncytium. Unlike skeletal muscle, in which more motor units can be recruited to increase the force of a contraction, cardiac muscle behaves as a single entity with each contraction of the heart being the combined result of the contraction of every myocyte.

Striations and contractile apparatus

Under light microscopy cardiac myocytes have alternating light 'I-bands' and dark 'A-bands' that run perpendicular to the long axis of the cell. Each I-band is bisected by a dark 'Z'-line. These patterns are known as striations, and represent the overlapping of the different proteins. A sarcomere is the smallest repetitive unit of the contractile apparatus, and is measured from one Z-line to the next. The sarcomere length is approximately 2 μm at rest, but reduces as the muscle contracts. See figure 4.1, panel A for an example.

More detail can be seen under electron microscopy. The A-band is seen to have a lighter zone in the centre known as the H-zone, which itself has a dark line running down the centre, called the M-line. The M-line is therefore half way between two Z-lines.

The proteins of the cytoskeleton and contractile apparatus are responsible for this unique striated appearance, and make up 45 - 55% of the cell volume in mammalian ventricle (Bers, 2001 p. 7). The Z-line is made of a cytoskeletal protein called α-actinin. The light I-band is formed by 'thin' actin filaments, which are anchored to α-actinin and run perpendicularly away from it. After a short distance, the actin filaments meet the 'thick' myosin filaments, which they run parallel with and with which they interlace. The dark A-band is formed by these heavier myosin filaments, which extend beyond the end of the actin filament. The H-zone is seen where the myosin filament is alone, without an accompanying actin filament. The M-line is at the centre of both the A-band and H-zone, and is made of a cytoskeletal protein called myomesin. The pattern then repeats in reverse from the M-line to the next Z-line to complete the sarcomere (Hwang et al., 2015). As the myocyte contracts, the actin and myosin filaments slide along each other and the

sarcomere becomes shorter due to narrowing of the I-band and H-zone. See figure 6.1 for an annotated electron micrograph of these structures.

The actin filaments are composed of F-actin, which in turn are long chains of globular (or G-) actin arranged in an α-helix. Tropomyosin and troponin are other sarcomeric proteins that play an important role in myocyte contraction (Solaro et al., 1998). The former wraps around F-actin, obscuring the myosin binding sites. In order for the muscle to contract, tropomyosin must move and expose these binding sites. It does this following the binding of calcium to troponin C, part of the troponin complex, which is a group of three comparatively small proteins bound to tropomyosin.

Other, non-contractile sarcomeric proteins also exist. Titin is a giant (3 MDa) protein that extends from the α-actinin Z-line to the myosin filament, and then runs along this protein to the M-line (Gautel et al., 1996). It is thought to have several functions including structural support for myosin.

Mitochondria

Unlike skeletal muscle, which can temporarily build up an oxygen debt, the heart is entirely dependent on aerobic metabolism as its energy source. As a result of this, cardiac myocytes are densely packed with mitochondria which may constitute a 22 - 37% of the cell by volume, depending on species (Barth et al., 1992).

Mitochondria are easily recognisable on electron microscopy, having a double membrane - the inner of which has many folds known as cristae. These organelles are abundant and found packed between the contractile apparatus.

T-tubules, sarcoplasmic reticulum and the dyad

Calcium ions play an essential and central role in cardiac muscle excitation-contraction coupling (see below). The binding of calcium to troponin-C lead to muscle contraction, and calcium ions can enter the cytoplasm via two routes; either through the plasma membrane, or via release from the sarcoplasmic reticulum (SR). These routes are also complementary, with entry of calcium through the plasma membrane leading to an amplification mechanism that causes the release of further calcium from the SR, known as calcium-induced calcium release (CICR) (Fabiato, 1983). Therefore, L-type calcium channels (LTCCs) on the plasma membrane are positioned in close proximity to calcium release channels on the SR (ryanodine receptors).

In order to avoid a delay in release of calcium in the centre of the cell compared to its release at the periphery, ventricular myocytes have deep invaginations of the plasma membrane into its interior. These transverse and axial tubules (usually known as 'T-tubules' or the 'TAT network') allow calcium entry deep in the interior of the cell as well as at the outer regions, leading to a synchronized and uniform rise in cytoplasmic calcium (Trafford et al., 2013). The absence of T-tubules leads to a rise in calcium concentration at the periphery of the cell which is temporally ahead of that in the centre (Dibb et al., 2013).

The presence of T-tubules varies depending on the tissue and the species from which it is taken (Richards et al., 2011; Tidball et al., 1991). They are abundant in mammalian ventricles, with a third to a half of the plasma membrane used in their formation. Smaller mammals (and therefore hearts with a higher resting rate) have a more dense TAT network in their ventricles than large mammals. In contrast, the presence of T-tubules in mammalian atria also depends on the size of the animal, but with small mammals such as mice and rabbits having only a crude atrial TAT network and larger mammals such as horses and humans having a more extensive one (Dibb et al., 2013). Reptilian, amphibian and avian hearts lack T-tubules altogether (Bers, 2001 p. 5).

T-tubules also exist in skeletal muscle, but are of a smaller calibre than those in the heart, with a diameter of 20-40nm compared with 20-450nm. LTCCs on the cardiac T-tubules are also known to outnumber those on the surface plasma membrane by up to nine times (Brandt, 1985; Scriven et al., 2000).

The SR is a large, membrane-bound and therefore isolated intracellular compartment, which contains a high concentration of calcium ions that can be released during systole to cause contraction. It is divided into three functional segments: The network SR (nSR) is densely covered with the sarco-endoplasmic reticular calcium ATPase pumps (SERCA), which function to remove calcium from the cytoplasm and return it to the SR lumen. The junctional SR (jSR) comes into very close proximity with the T-tubules and is covered with RyRs. The dyad is formed by the close apposition of the T-tubule plasma membrane with inflated areas of jSR known as terminal cisternae, and is usually found adjacent to the Z-line in cardiac muscle. This arrangement leads to a calcium signalling microdomain that allows CICR. The plasma membrane LTCCs and SR ryanodine receptors are not

randomly expressed over the T-tubule membrane and jSR, but are organised into groups known as couplons. A typical cardiac couplon may consist of approximately 100 ryanodine receptors and 10 - 25 LTCCs (Bers, 2001 p. 14; Franzini-Armstrong et al., 1999). The equivalent structure to the dyad in skeletal muscle (only rarely seen in cardiac muscle) is the triad, where a T-tubule is abutted by two terminal cisternae. The third part of the SR is the corbular SR (cSR, also sometimes known as the extended junctional SR, ejSR), which contains ryanodine receptors but exists independently and not in association with a T-tubule. It is particularly apparent in atrial and conducting tissue, and is also commonly seen in avian cardiac myocytes. It's specialised functions are not well understood.

Junctophilin-2 (JPH2) is a protein known to be present in the cardiac dyadic cleft that connects the plasma membrane to the SR, and whose absence is lethal. Mice lacking this protein die *in utero* at approximately the same time as the heart beat is established, and have an increased dyadic cleft width (Scriven et al., 2013). If the JPH2 is substituted with JPH1, which is usually expressed in skeletal muscle, the formation of the dyad is abnormal, although the triadic phenotype usually seen in skeletal muscle is not adopted (Komazaki et al., 2003). JPH2 therefore appears to be important in the formation and maintainance of the dyad.

1.2.3 Calcium signalling microdomains

The couplon provides a good example of a calcium signalling microdomain. The source of calcium (in this case the LTCC), and its target (the ryanodine receptor) are closely

apposed so that calcium in the space between them can rapidly rise to a locally high concentration, resulting in efficient signalling.

Calcium ions in aqueous solution can diffuse 40 μm per second (Einstein, 1905) - this is approximately half the length of a cardiomyocyte. However, in the subcellular environment this distance is scarcely achieved and calcium ions are not allowed to be free for that long. The freedom of calcium ions is tightly controlled, with the resting cytoplasmic calcium concentration kept extremely low (~100 nM), and its diffusion limited by the crowded environment and high number of calcium buffering substances. The diffusion of free calcium ions is limited to distances of a few nanometers and (with the exception of the whole cell calcium transient) they are generally permitted to exist unbuffered for only microseconds. The prevention of calcium diffusion is desirable since it allows localised calcium signalling to control different cellular processes simultaneously, and also because uncontrolled calcium diffusion can be cytotoxic and lead to apoptosis (Clapham, 2007).

Calcium signalling microdomains are found at membrane contact sites (MCS) between many intracellular structures, the S/ER often being one of them (Prinz, 2014). A critical feature of a microdomain or MCS is that the membranes of the two structures do not touch or fuse, but come within approximately 30 nm of each other (Eden, 2016; Penny et al., 2015). They are often tethered in this position by specialised tethering proteins, the absence of which leads to failure of MCS formation and interruption of the physiological processes associated with it (Helle et al., 2013).

MCS have been identified functionally and using electron microscopy between the S/ER and several organelles, including the plasma membrane as described above but also mitochondria, endosomes and lysosomes (Lam et al., 2013). Although the structure and function of the cardiac dyad has been understood for some time (Fabiato, 1985; Franzini-Armstrong et al., 1999), until recently there has been only a relatively small amount of evidence for other MCS in the heart. This is discussed further below.

1.2.4 Pathological changes in cardiac structure: Mechanisms of hypertrophy

Hypertrophy is the increase in size of cells. Cardiac hypertrophy may occur in physiological circumstances such as normal growth, pregnancy or athletic training, and this form of hypertrophy is associated with enhanced cardiac contractility and a normal structure of the heart (Bernardo et al., 2010). However, hypertrophy may also occur in pathological circumstances. These include inherited genetic syndromes such as hypertrophic obstructive cardiomyopathy (HOCM) or acquired abnormalities such as the pathological response to chronic arterial hypertension or aortic valve stenosis. In the latter, the left ventricle becomes hypertrophied either as a result of an abnormal protein, or in order to generate the larger pressure necessary to allow ejection of blood. Initially, this is considered reversible and adaptive, but in time the changes become permanent and cannot be reversed. This type of hypertrophy, sometimes called maladaptive hypertrophy, is characterised by fibrosis, cell death and cardiac failure (Bernardo et al., 2010).

On a cellular level, the signalling pathways involved in these two types of hypertrophy are known to be different. In physiological hypertrophy, increased cell size is promoted

by hormones such as insulin, insulin-like growth factor-1 (IGF-1) and thyroid hormone, and by intracellular pathways that involve proteins such as phosphoinositide-3-kinase (PI3K), Akt and the mammalian target of rapamycin (mTOR) (Shimizu et al., 2016). PI3K-Akt signalling was increased by exercise training in mice, but decreased by transverse aortic constriction (Kemi et al., 2008), and the over-expression of Akt was found to enhance the cardiac calcium transient via hyperphosphorylation of phospholamban, while knockout of PI3K had the opposite effect (Catalucci et al., 2009). Mechanosensors that involve sarcomeric proteins such as titin and muscle LIM protein (MLP) also promote cardiac remodelling in response to changes in mechanical load on the heart during training (Lyon et al., 2015).

In contrast, patients with maladaptive hypertrophy tend to have higher circulating levels of catecholamines and sympathetic nervous system output regardless of the aetiology (Osadchii, 2007; Scheuer, 1999), and there is also activation of the renin-angiotensin-aldosterone system. These neurohumoral factors lead to intracellular changes such as the increased activity of calcineurin, which dephosphorylates the nuclear factor of activated T-cells (NFAT), promoting its translocation to the nucleus where it increases the expression of genes leading to an increase in cell size (Houser et al., 2008). This pathway is not activated in physiological hypertrophy (Wilkins et al., 2004).

The involvement of adrenergic receptors in the development of cardiac hypertrophy is well accepted. However, the relative contribution of these receptors to the hypertrophic response under different conditions has been more controversial. Before the development of cell culture techniques, the study of cardiac hypertrophy was done in vivo and the emphasis had been on β-adrenergic receptors, since these make up the majority

(70-90%) of cardiac adrenergic receptors (Simpson et al., 1991). However, it was also suggested that since sympathetic nerves are intact and functional in in vivo models, it was possible that β-agonists were acting at the presynaptic membrane of the nerve terminal and promoting noradrenaline release, which subsequently acted primarily at α-receptors to induce hypertrophy (Simpson, 1985). It was also suggested that β-agonists may cause the release of growth factors such as TGFβ from non-myocytes such as fibroblasts which then subsequently also contributed to myocyte hypertrophy (Long et al., 1993).

Cultures of neonatal rat cardiac myocytes in the presence of noradrenaline demonstrated hypertrophy, and this response was not affected by the non-selective β-blocker propranolol or the selective α2-antagonist yohimbine, but was inhibited by the non-selective α-blocker phentolamine and the selective α1-antagonists prazosin and terazosin (Simpson, 1983).

Several years later, the survival benefit and protective effect of β-blockers against human cardiac remodelling was demonstrated in clinical trials (Eichhorn et al., 1994), and further experiments showed increased protein synthesis in cardiac myocytes exposed to adrenergic agonists that could be inhibited by β-blockers (Bogoyevitch et al., 1996). Subsequently, new experiments on cell cultures showed that hypertrophy could be induced via a β-adrenergic effect, but under subtly different conditions to those used by Simpson (Morisco et al., 2001). For example, insulin - originally included in the culture media - was removed due to its stimulatory action on PI3K, which is common to the β-adrenergic pathway. It was also noted that paracrine effects from non-myocyte cells in

the culture could affect myocyte response to catecholamines, although steps were taken in both sets of experiments to reduce non-myocyte contamination.

The action of catecholamines at α-adrenergic receptors also leads to activation of Gq, protein kinase C (PKC), and a number of other enzymes such as PKD and the mitogen-activated protein kinase (MAPK) cascade. This is a complex pathway that leads to involvement of proteins involved in up-regulation of genes causing hypertrophy such as p38MAPK, c-Jun N-terminal kinase (cJNKs) and extracellular signal-regulated kinase (ERK). This system has been found to be extensively activated in human hearts in end-stage cardiac failure, and also in animal models of this condition (Cotecchia et al., 2015; Shimizu et al., 2016). Activation of Gq leads to phospholipase C (PLC) activation and generation of inositol 1,4,5-trisphosphate (IP_3) and SR calcium release. Calcium-dependent activation of calmodulin and subsequently calcineurin can also lead to increased activity in nuclear transcription factors and CaMKII that promote hypertrophy (Cotecchia et al., 2015).

Hypertrophy induced by β-adrenergic receptors has some differences, but some of the intracellular pathways are common to α-receptor signalling. The stimulation of β-receptors leads to activation of Gs G-proteins and increased activity of adenyl cyclase, leading to cyclic AMP formation and protein kinase A (PKA) activation. PKA is able to phosphorylate and activate the cAMP-response element binding modulators (CREMs), which are a family of transcription factors responsible for the alteration in expression of many genes. There is also activation of the MAPK cascade, although exactly how this is coupled to β-activation is not well understood (Fu et al., 2012). β-adrenergic receptors are also linked to the calcineurin/NFAT pathway, activation of type-2 calmodulin-

activated protein kinase (CaMKII), and the exchange protein directly activated by cAMP (EPAC) (Fu et al., 2012). EPAC has been shown to be upregulated following experimental aortic constriction, and myocytes from these animals show an exaggerated growth response to EPAC activation by β-stimulation. Knockdown of EPAC strongly inhibited this response (Metrich et al., 2008).

The maladaptive hypertrophy that is seen in the context of adrenergic stimulation (α or β) and other pathological stimuli is associated with the re-expression of genes that are not usually seen in the healthy post-natal ventricle such as atrial and brain natriuretic peptide (ANP/BNP), α-actin, atrial myosin light chain-1 and β-myosin heavy chain (Frey et al., 2004). These proteins are known in this context as the foetal gene program, and their upregulation in adult hearts is associated with impaired contractility and calcium handling and alterations of myocardial metabolism (Cotecchia et al., 2015). Re-expression of the foetal gene program is seen in failing hearts, but is not seen in physiological hypertrophy (McMullen et al., 2007).

The hypertrophic response is regulated by many other factors, including autophagy. This is the cellular catabolic process by which old or dysfunctional proteins and organelles are degraded in lysosomes and recycled. The link between cardiac autophagy and hypertrophy is not straightforward. In some experiments, the inhibition of autophagy promotes hypertrophy. For example, a protein that is essential in the formation of autophagic vesicles is autophagy-related protein-5 (Atg5). Cardiac-specific knockout of the gene that encodes this protein resulted in cardiac hypertrophy, failure and dilatation after experimentally inducing pressure overload (Nakai et al., 2007). Similarly, the deletion of the gene for atrogin-1, a protein involved in an autophagic regulatory pathway

led to impairment of autophagy and an increase in pathological remodelling (Zaglia et al., 2014). However in contrast, genetic disruption of beclin-1, a protein that is required for early autophagosome formation also caused reduced autophagy, but resulted in reduced pathological remodelling while its overexpression had the opposite effect (Zhu et al., 2007). More investigation in this area will be required to fully elucidate the role of lysosomes and the autophagic system in the regulation of cardiac hypertrophy.

1.3 Excitation-contraction coupling and calcium handling in the heart

1.3.1 Cardiac electrophysiology

The resting potential

A resting ventricular cardiomyocyte has a stable negative charge with respect to the extracellular environment. This is known as the resting potential, or 'phase 4'. In order to contract, an electrical change occurs in the cell, which causes it to become briefly positively charged. This excitation, known as the 'action potential' causes intracellular changes that allow contraction to occur. The link between these two events is known as excitation-contraction coupling (Bers, 2002).

Potassium ions are distributed unevenly across the cardiac myocyte membrane, with an intracellular concentration, $[K^+]_{in}$, approximately thirty times the extracellular concentration $[K^+]_{out}$. In contrast, sodium ions are unevenly distributed with approximately the opposite intracellular and extracellular concentrations. This arrangement is largely a result of the activity of the Na^+-K^+-ATPase pump, which removes

sodium from the interior of the cell and replaces it with potassium in a 3:2 ratio (Shattock et al., 2015). If the membrane were freely permeable to both sodium and potassium ions, then these concentration differences would quickly disappear as both species of ion flowed down their respective concentration gradients, and equilibrated across the membrane. However, while resting cell membranes are freely permeable to potassium, they are relatively impermeable to sodium and other ions. Therefore, as potassium leaves the cell down its concentration gradient (inward rectifier current, I_{K1}), it is not replaced by sodium ions travelling in the opposite direction and a relative charge deficit occurs, leaving the inside of the cell negatively charged relative to the outside. Positively charged potassium ions are attracted to this negative intracellular charge.

There are therefore two forces working on potassium in opposite directions; the chemical force moving potassium down its concentration gradient out of the cell and the electrical force (or voltage) attracting it back in. At the point where these forces become balanced there is no net ionic movement across the membrane. The intracellular voltage at which this occurs is called the equilibrium potential for potassium (E_K) , and it can be calculated using the Nerst equation (Whalley et al., 1995):

$$E_K = \frac{RT}{zF} \cdot ln \frac{[K]_{out}}{[K]_{in}}$$

Where R is the universal gas constant, T is temperature in Kelvin, z is ion valency and F is the Faraday constant. If the extracellular potassium concentration is 4.5 mM and the intracellular concentration is 140 mM, then E_K=-91.8 mV at 37°C.

It can be seen from the Nernst equation that the membrane potential will be altered by changes in potassium ion concentration. Hypo- and hyperkalaemia will make the membrane potential more and less negative respectively. Additionally, potassium channels that carry I_{K1} are modulated by the extracellular potassium concentration, such that the conductance (g_{K1}) of these channels is proportional to the square root of the extracellular potassium concentration. This results in hypokalaemia causing both a reduction in I_{K1} due to reduced conductance, and hyperpolarisation of the membrane (El-Sherif et al., 2011).

In reality, although the cell membrane is freely permeable to potassium, there is also limited permeablity to sodium (and other ions), resulting in a small inward current and a membrane potential that is slightly less negative than that predicted by Nernst. The sodium ions that leak into the cell are pumped back out again in exchange for potassium via the Na/K exchanger. To calculate the overall resting membrane potential based on the concentrations of all the ions in the system, the Goldman-Hodgkin-Katz equation is used. In a ventricular cardiac myocyte, in the presence of normal physiological intracellular and extracellular concentrations of each electrolyte, the resting potential is approximately -80 to -90 mV.

The Action Potential

An action potential in a particular ventricular myocyte is stimulated by the depolarisation of adjacent myocytes, and the flow of current through the gap junctions between them. The arrival of a depolarising current causes the membrane potential to rise slightly. As it does so, voltage-gated sodium channels sense the change and begin to activate, allowing

further sodium current (I_{Na}) to flow which leads to a further rise in membrane potential. Sodium channels therefore activate progressively as the membrane potential becomes less negative. At potentials more negative than approximately -75mV, all sodium channels are in the resting state, but by the time the membrane potential reaches -20 mV, almost all are activated (Bers, 2001 p 73). As sodium channels activate, the probability of more activating increases, leading to a positive feedback process and rapid (200-400 $V.sec^{-1}$ in ventricular cells (Bers, 2001 p 92; King et al., 2013), but velocities of up to 900 $V.sec^{-1}$ have been recorded in Purkinje fibres (Weidmann, 1955)) membrane depolarisation, known as phase 0 of the action potential. There is consequently a large increase in the membrane permeability to sodium, and a large inward sodium current. As this occurs, there is also a reduction in the membrane permeability to potassium, as K_{ir} (which carry I_{K1}) channels begin to close as the membrane potential becomes less negative and moves away from E_K. The membrane potential therefore moves towards (although does not achieve) the equilibrium potential for sodium, E_{Na}. The peak membrane potential achieved during phase 0 is approximately +40 mV.

Phase 1 is a brief repolarisation carried by the transient outward current, I_{to}, which brings the membrane potential back to 0 to 20 mV. This current is carried by outward movement of potassium ions (I_{to-1}) and inward movement of chloride ions (I_{to-2}). The former is voltage-activated, whereas the latter is activated by calcium ions. The size of phase 1 is heterogeneous between cells from different parts of the heart - being more prominent in epicardial cells than endocardial cells, and also varies between species (Whalley et al., 1995).

The repolarisation of phase 1 is interrupted by the plateau, where the membrane potential stays relatively constant for 200-300 ms in humans. The plateau allows time for contraction to occur, and prevents re-activation of sodium channels producing the cardiac refractory period. The constant membrane potential is due to a balance between inward and outward currents and is known as phase 2. The main inward currents are the calcium current, I_{Ca}, and the sodium-calcium exchange current. The main outward current is carried by I_K.

I_{Ca} is the major inward current and is carried by two different channels, the transient 'T'-type, and the long-lasting 'L'-type. The former plays only a minor role in ventricular cells, and is more important in pacemaker cells and in the conducting system (Bean, 1989). Therefore, $I_{Ca\text{-}L}$ is the dominant calcium current. LTCCs are activated when the membrane potential becomes more positive than -40 mV, and therefore start to become active during phase 0. Peak calcium conductance (gCa-L) occurs 2 – 7 ms after LTCC activation, and while the sodium channels responsible for phase 0 inactivate after only 1-2 ms, the L-type calcium channels remain open for 100 - 200 ms, maintaining the depolarisation of the membrane during this time. The other function of the L-type channels is to allow calcium to activate adjacent ryanodine receptors on the SR. This results in calcium liberation from the SR (CICR), which is essential for excitation-contraction coupling (Bers, 2002; Whalley et al., 1995). The closure of LTCCs can be dependent on membrane potential (voltage-dependent inactivation, VDI) or the intracellular calcium concentration (calcium-dependent inactivation, CDI). CDI is the major mechanism of termination of $I_{Ca\text{-}L}$, and it occurs rapidly after release of calcium from the SR.

The Na-Ca exchange pump (NCX) moves three sodium ions in one direction across the membrane for every one calcium ion in the opposite direction, and is therefore electrogenic. At membrane potentials negative to the combined reversal potential for sodium and calcium (E_{Na-Ca}) the exchanger generates a net inward current (i.e. it transports three sodium ions into the cell and one calcium ion out). This is the state of affairs during the resting potential, and during the plateau. There is a brief period during the peak of phase 0, when the membrane potential may reach values above E_{Na-Ca} and so the exchanger will briefly generate an outward current at these times, by working in 'reverse mode' (Eisner et al., 1985).

The potassium current, $I_{K1,}$ which is responsible for the generation and maintenance of the resting membrane potential reduces considerably during depolarisation and the plateau due to its inward rectification. This means that while potassium channels freely conduct potassium ions into the cell at membrane potentials more negative than E_K, they become less permeable to potassium as the membrane potential becomes less negative, and their conductance (gK1) falls to zero at membrane potentials more positive than approximately -20mV. Therefore, I_{K1} falls as the membrane depolarises (Sakmann et al., 1984). This is essential to allow a stable plateau in phase 2: In order to maintain a plateau, the inward and outward currents must balance. If I_{K1} did not rectify, then its large outward current would be a strong repolarising influence that could not be equaled by the relatively small inward currents, and the plateau could not occur.

Instead of I_{K1}, a different potassium current known as the delayed outward rectifier, or I_K is responsible for potassium current after depolarisation. This current is activated during phase 2, and is made up of two components: I_{Kr} is a rapidly-activated current that flows

from the beginning of phase 2, and is later joined by a more slowly-activated current, I_{Ks}. These currents can be increased by protein kinase A (PKA) phosphorylation of the potassium channel proteins in response to β-adrenergic stimulation to shorten the action potential duration as heart rate increases (Marx et al., 2002). As is the case with I_{K1}, I_K is also modulated by extracellular potassium concentration, such that hypokalaemia results in reduced conductance (El-Sherif et al., 2011). Another 'ultra-rapid' potassium current, I_{ur}, occurs in atrial cells and causes a faster repolarisation - leading to the shorter action potential in this tissue (Grant, 2009).

Phase 3 is the repolarisation of the membrane to resting potential. As $I_{Ca\text{-}L}$ decays and I_K increases over the course of phase 2, the outward current begins to dominate. This leads to a drop in membrane potential back in the direction of E_K, and re-activation of the I_{K1} current as it falls more negative than approximately -20 mV (MacLeod, 2014 p. 205; Whalley et al., 1995). This re-establishes the resting potential, phase 4. There is also a small contribution from the Na-K exchange pump to phase 3, which removes sodium from the interior of the cell and replaces it with potassium in a 3:2 ratio, thereby producing a hyperpolarising influence (Shattock et al., 2015).

The action potential is different to that described above, and changes in membrane potential are mediated by different currents and channels in different parts of the heart - particularly the atria and sino-atrial pacemaker tissue.

It is important to realise that during the movement of sodium and potassium ions across the cell membrane during the action potential, their intracellular and extracellular concentrations do not change appreciably. This is because relatively large changes in

membrane potential can be the result of the movement of only a small fraction of the total number of ions in the cell (~0.02% for potassium). The exception is calcium, the intracellular concentration of which rises significantly (by an order of magnitude or more) during the action potential, although (depending on species) this is mostly due to release of calcium from the SR, rather than entry via the L-type channels.

1.3.2 Cardiac electrical conduction and the electrocardiograph

Conduction pathways

At the initiation of the cardiac cycle, an action potential is generated in a specialised group of cells in the right atrium known as the sino-atrial node (SAN). The depolarisation that originates here spreads rapidly via gap junctions between myocytes, and causes synchronised atrial depolarisation and contraction.

The ventricles are electrically insulated from the atria, except at a single location where conduction is able to take place. This is the atrio-ventricular node (AVN), which is activated by an incoming depolarisation from surrounding atrial tissue. The AVN has a latency that causes a short delay in the conduction of the wave of depolarisation from the atria to the ventricles, in order to give time for the atrial contribution to ventricular filling.

There follows a rapid co-ordinated spread of the action potential from the AVN via conducting tissue known as the bundle of His and the left and right bundle branches to the Purkinje fibres. These transmit the action potential to contractile ventricular myocytes. The bundle branches ensure that the depolarisation wave is transmitted to the

left and right ventricles simultaneously, leading to a co-ordinated contraction of both ventricles at the same time. The waves of depolarisation transmitted by each bundle branch travel around the heart in opposite directions until they meet. The refractory period of the myocytes prevents the wave travelling further and they return to their resting state.

The ECG

The electrical activity in the heart causes polarisation of charged particles throughout the body, and this polarisation can be detected using electrodes at the skin surface. The potential difference between two electrodes can be used to produce the electrocardiograph (ECG), which is a graph of this voltage against time.

Electrodes are placed on the body in standardised positions, and each electrode can be either positive or negative. A wave of cardiac depolarisation travelling towards a positive electrode (or a wave of repolarisation travelling in the opposite direction) will produce an upward (positive) deflection on the ECG. Conversely, a depolarisation wave travelling towards a negative electrode (or a repolarisation wave travelling away) will produce a negative ECG deflection. Thus, an ECG is a vector containing directional - and therefore anatomical - information about the cardiac electrical activity.

A typical ECG trace consists of an initial positive 'P'-wave, which represents atrial depolarisation. There is then a pause (the 'PR' interval) before the QRS complex. The 'Q'-wave is defined as the first negative deflection after the end of the P-wave, and - if present - represents septal depolarisation. The 'R'-wave is often the largest-amplitude wave on

the ECG, and is defined as the first upward deflection (even if Q-waves are absent) after the end of the P-wave. It represents early depolarisation of the bulk of ventricular muscle. There then usually follows an 'S'-wave, which is defined as the first negative deflection seen after an R-wave, and is said to represent late depolarisation. Another pause (the 'QT' interval) is then seen before the positive 'T'-wave which is due to ventricular repolarisation. The atrial repolarisation is not seen as an individual wave as it occurs more slowly in a diffuse fashion and occurs at the same time as ventricular depolarisation. It is therefore obscured by the QRS complex. The cycle then begins again with another P-wave. In steady state, the spacing between cardiac cycles does not vary, so that the time between two R-waves (the RR-interval), and therefore the heart rate, is constant.

The system described here is the normal pattern of electrical conduction through the heart and is known as 'sinus rhythm'. Aberrations from this pattern are known as arrhythmias, and can range from benign disturbances of regularity to severe malignant abnormalities that are incompatible with life.

1.3.3 Contraction

In order to produce a contraction, the intracellular concentration of calcium must rise. This process is highly regulated. The initial entry of calcium occurs via the LTCCs during the action potential. The location of these channels adjacent to the ryanodine receptors on the SR allows entering calcium to directly stimulate their opening, leading to calcium liberation from the SR (CICR, (Fabiato, 1983)). This calcium is then able to bind to and

activate the myofilaments and cause sarcomere shortening. The force of the contraction is a function of the intracellular calcium concentration.

Calcium entry via the cell membrane

L-type calcium channels consist of α1, α2, β, γ and δ subunits. However, the α1 subunit, which consists of four domains each of six transmembrane loops, seems to accommodate the functionally important part of the channel, forming the ion pore and containing sites for binding of drugs such as the dihydropyridines. This subunit also contains regulatory phosphorylation sites for regulatory enzymes such as PKA, CaMKII, and protein kinase C (PKC), and is sufficient to produce I_{Ca} in response to changes in membrane potential in cells lacking expression of the other subunits (Bodi et al., 2005; Kamp et al., 2000). LTCC β subunits also have phosphorylation sites for PKA, which may also cause increase channel activity (Kamp et al., 2000).

The magnitude of $I_{Ca\text{-}L}$ can be regulated in several ways: β-adrenergic stimulation results in activation of Gs proteins, generation of cyclic-AMP (cAMP) and activation of PKA, which is tethered close to the channel by A-kinase anchoring protein (AKAP). The phosphorylation of the L-type channel α1 subunit at Ser1928 results in a 2-4 fold increase in $I_{Ca\text{-}L}$ (McDonald et al., 1994). However, this is not due to an increase in individual channel conductance, but because of an increase in open probability at more negative membrane potentials. The channel will therefore open earlier and remain open for a longer period during the action potential (Yue et al., 1990).

Conversely, stimulation of receptors that are coupled with Gi-proteins, such as acetyl choline (ACh) and atrial natriuretic peptide (ANP) will reduce cAMP levels following an adrenergic-induced increase, and result in reduction of $I_{Ca\text{-}L}$ (Bers, 2001 p. 130).

The binding of dihydropyridine drugs can either increase or decrease channel activity and $I_{Ca\text{-}L}$. Nifedipine and nimodipine are clinically used antagonists of the L-type channel, while Bay K 8644 is an example of a stimulatory dihydropyridine (Bers, 2001 p. 123 - 127).

Termination of $I_{Ca\text{-}L}$ can be time-, voltage- or calcium-dependent. The time-dependent closure is very slow, and is unlikely to play a significant role in beat-to-beat regulation of the action potential (Shi et al., 2002). $I_{Ca\text{-}L}$ will also terminate as the membrane potential falls more negative than approximately -15mV, and at -45mV almost all L-type channels will be closed (Bers, 2001 p. 118). This demonstrates a voltage-dependent aspect to inactivation (Lee et al., 1985). Another mechanism of LTCC inactivation is thought to involve calcium and the calcium-binding protein calmodulin, which may be bound to the carboxy-tail of the channel protein. As a result of both the inward calcium current and the release of calcium from the SR, the local concentration of calcium will increase substantially. Some of this calcium binds to the calmodulin, and leads to channel closure. This is thought to be a major mechanism by which $I_{Ca\text{-}L}$ is terminated during an action potential.

Calcium release from the sarcoplasmic reticulum

Ryanodine receptors are very large proteins (approx 2.2 MDa) consisting of tetramers of a peptide consisting of almost 5000 amino acids and weighing just over 550 kDa each (Otsu et al., 1990). They are so-called due to their sensitivity to the alkaloid ryanodine, which is found in the stem and roots of *Ryania speciosa,* and irreversibly fixes the receptor into a subconducting "half-open" state at nanomolar concentrations (Fill et al., 2002). This leads to calcium depletion from the SR, and subsequent removal of calcium from the cell by the NCX leading to diastolic (flaccid) paralysis of the heart. The effect of ryanodine in skeletal muscle is to produce tetanic paralysis, since the calcium that leaks from the SR cannot easily leave the cell due to the low activity of calcium extrusion pumps in this tissue.

There are three subtypes of ryanodine receptor in mammalian tissue, RyR1 and RyR3 are both found in skeletal muscle, although the former is far more abundant. RyR2 is the predominant subtype found in cardiac cells. As described, the mechanism by which RyR2 opens requires stimulation by incoming calcium ions from nearby LTCCs. However, RyR1 in skeletal muscle can also be opened by the mechanical opening of the L-type channel, which is in directly physical contact, and does not necessarily require the flux of calcium (Fill et al., 2002).

The activity of ryanodine receptors may also be modulated by a wide range of other regulatory substances.

Calcium ions themselves, whether on the cytoplasmic or luminal side of the SR membrane regulate the release of calcium from the ryanodine receptor. The concentration of calcium in the dyadic cleft is related to $I_{Ca\text{-}L}$, so that a larger influx from outside the cell leads to a

higher concentration. In turn, this results in a larger release of calcium from the SR. However, very high levels of calcium inhibit ryanodine receptor opening. Its opening response is therefore bell-shaped with respect to calcium concentration (Fabiato, 1985). This may be one mechanism by which calcium release from the SR is terminated before relaxation begins.

In addition to the fact that higher concentrations of calcium lead to blunted ryanodine receptor opening, there is evidence that ryanodine receptors adapt to high local calcium concentrations over a short (ms) time period, leading to active channel closure under these conditions, and that this process is dependent on the intracellular concentration of magnesium (Valdivia et al., 1995).

Similarly, a high SR luminal calcium concentration leads to a higher open probability of the ryanodine receptor and longer opening times (Ching et al., 2000), whereas a low level of calcium within the SR has the opposite effect (Gyorke et al., 1998). This latter modulation may also help terminate release. Mutation of the glutamate (E) residue at position 4872 to a glutamine (Q) in RyR2 abolishes the detection of luminal calcium concentration, and protects against the effects of calcium overload such as spontaneous calcium waves (SCWs) and subsequent arrhythmias (Chen et al., 2014). Calcium within the SR is buffered by calsequestrin, an acidic calcium-binding protein that is anchored to the luminal surface of the SR membrane by two other proteins, junctin and triadin (Zhang et al., 1997). Mutations in calsequestrin can lead to the development of malignant ventricular arrhythmias (Terentyev et al., 2003b). Similarly, complete knockout of calsequestrin gene expression also results in SCWs, arrhythmias and cardiac hypertrophy. However, these effects can be mitigated if the RyR2 protein also contains

the E4872Q mutation (Zhang et al., 2014), suggesting that RyR2 calcium sensing is the more important.

In response to β-adrenergic receptor stimulation, the increased activity of PKA can lead to the phosphorylation of the RyR2. The exact phosphorylation sites and physiological significance of this is still a topic of ongoing research, and it is also likely that other serine/threonine kinases can also phosphorylate the ryanodine receptor. The physiological significance of PKA phosphorylation of the ryanodine receptor is also somewhat controversial. Addition of purified PKA to isolated RyR2 channels in planar lipid bilayer experiments increases open probability (Marx et al., 2000). It is likely that the most important phosphorylation site for PKA is Ser2808 (or Ser2809 in some species) (Dobrev et al., 2014). The increased activity in RyR2 caused by PKA was prevented by mutating the serine residue to an alanine (S2808A) so that it could not be phosphorylated (Wehrens et al., 2004). Conversely, a mutation that results in constitutive phosphorylation at this position (S2808D) resulted in permanent increased open probability compared with wildtypes in several studies (Wehrens et al., 2006; Wehrens et al., 2004). However, when hearts from animals with these mutations were studied in a more physiological context (either organ-level in vitro studies or in vivo experiments), the results were less clear-cut: Two independent groups reported opposite findings using the S2808A mutant. MacDonnell et al. (2008) was not able to detect an altered inotropic response to isoprenaline in the hearts of these animals, while subsequent experiments by Shan et al. (2010) reported a reduction in inotropic response and calcium transient amplitude. A second possible PKA phosphorylation site, Ser2030 (sometimes Ser2031) has also been identified (Xiao et al., 2006). It has been suggested that this site may

enhance RyR2 sensitivity to calcium concentration within the SR, although a functional effect of this has not been demonstrated in vivo (Huke et al., 2008; Wehrens et al., 2006).

The RyR2 can also be phosphorylated by CaMKII at Ser2814 (or Ser2815 in some species), and this seems to increase open probability in single channel experiments and spark frequency in isolated myocytes (Bers, 2012; van Oort et al., 2010; Wehrens et al., 2004). A S2814A mutation reduces the effects of CaMKII on RyR2, but does not abolish them completely, suggesting that there may be further - as yet unidentified - sites of phosphorylation by CaMKII on RyR2 (Respress et al., 2012). In contrast to the apparent effect of CaMKII, the binding of calmodulin to RyR2 is able to decrease open probability as a function of free calcium concentration (Balshaw et al., 2001).

The dephosphorylation of RyR2 is also regulated. Protein phosphatase type-1 (PP1) and PP2A are thought to be the principle two enzymes responsible (Dobrev et al., 2014). However, the effects and mechanisms of this are also controversial, with some studies reporting a reduction in RyR2 open probability in response to these enzymes and others reporting an increase (Carter et al., 2006; Terentyev et al., 2003a). In addition to dephosphorylation of RyR2, phosphodiesterases (particularly PDE4) are anchored near PKA and act to reduce levels of cAMP, which in turn will reduce the rate of ryanodine receptor phosphorylation. The absence of this enzyme may lead to hyperphosphorylation of RyR2 and cardiomyopathy (Lehnart et al., 2005).

FK506-binding proteins (FKBPs) are a family of proteins known to modulate a number of cellular processes and famously have an immunoregulatory function; FK506 is otherwise known as tacrolimus, a drug used to prevent rejection following organ

transplant due to its action in T-lymphocytes. FKBP12 and FKBP12.6 are known to exist in the heart, and may have a role in the regulation of calcium release from the SR via RyR2, although this is another controversial area. Tacrolimus and a related substance, rapamycin, prevent the binding of FKBP12.6 to RyR2, and have been reported to cause an increase in RyR2 opening, an increase in spark frequency, and a reduced SR calcium load (McCall et al., 1996; Xiao et al., 1997). This implies that the function of FKBP12.6 is to reduce the open probability of RyR2. However, other studies have found that FKBP12.6 had no effect on RyR2 gating (Timerman et al., 1996; Xiao et al., 2007). It has also been suggested that binding of FKBP12.6 to RyR2 can be regulated in response to β-adrenergic stimulation and PKA activity (Shan et al., 2010; Wehrens et al., 2006). However, this hypothesis has also been challenged (Bers, 2012). In addition, ryanodine receptors are known to be found in clusters with their cytoplasmic domains in physical contact. The opening of one channel may lead to an increase in open probability of adjacent channels, provided FKBP12.6 is bound. This co-operative process, which has become known as 'coupled gating' does not appear to occur in the absence of this regulatory protein (Gaburjakova et al., 2001; Marx et al., 2001).

Sorcin is another little-studied protein that regulates the ryanodine receptor. Found in the dyadic cleft, its role appears to be to reduce both spontaneous calcium release from the SR, and that released in response to $I_{Ca\text{-}L}$ (Farrell et al., 2004; Valdivia et al., 2004).

Mechanism of contraction

Due to entry of calcium into the cell via the LTCCs, and release of calcium from the SR, the cytoplasmic concentration of calcium rises by at least ten times, from 0.1 μM to more than

1 μM during systole (Bers, 2002). This change in calcium concentration is accepted to be the factor that activates muscular contraction, the mechanism of which is detailed in the sliding filament theory (Huxley et al., 1954a; Huxley et al., 1954b).

In the resting state, calcium levels are low and the troponin-C calcium binding sites are unoccupied. In this condition, the affinity of troponin-C for troponin-I is weak, and the latter is free to bind tightly to actin. As a result of this latter interaction, tropomyosin can only bind to actin in such a way that it blocks the actin binding sites for myosin.

As the free calcium concentration rises, calcium ions bind to troponin-C, causing a reversal in the attractions between these various subunits, such that troponin-C binds more tightly to troponin-I and the affinity of the latter for actin decreases. This leads to the movement of troponin-I and tropomyosin deeper into the groove in the actin helix, such that the myosin binding sites on the actin helix become exposed (Bers, 2001). Actin-myosin interaction can then occur.

The higher the number of troponin complexes that bind calcium, the more binding sites for myosin are revealed and the higher the force generated. The number of myosin binding sites available is also enhanced depending on the initial stretch of the sarcomere, and at longer sarcomere lengths there is an enhanced sensitivity of filaments to calcium (Kentish et al., 1986). In addition, the sensitivity of the filaments to calcium can be altered by modifications such as phosphorylation in response to drugs and autonomic influences, or a number of other factors such as pH and temperature (Bers, 2001). Consequently, the overall force of contraction depends upon the amplitude of the calcium transient, the

starting muscle fibre length, the presence of drugs or endogenous signalling molecules, and physiochemical factors.

Shortening of the sarcomere is a consequence of the actin-myosin interaction. The myosin heavy chain is a 'tadpole' shaped peptide with the 'tails' of several coiled around each other to form a helix. This leaves the 'heads', which incorporate ATPase enzyme activity, exposed to form cross-bridges with the binding sites on actin. In a process called cross-bridge cycling, which is dependent on ATP hydrolysis, the myosin heads repeatedly bind to actin, rotate and dissociate. The rotation causes the myosin filament to pull itself along the actin filament in a movement known as the 'power stroke', which leads to sarcomere shortening.

In the resting state, myosin has ATP bound. At the beginning of a cross-bridge cycle, ATP is hydrolysed to ADP and inorganic phosphate (Pi), causing priming or activation of the myosin head. In the presence of calcium to cause exposure of the binding sites, myosin then binds to actin and Pi is released. The myosin head then rotates, causing the power-stroke, releasing ADP. Actin and myosin then dissociate following the binding of a new molecule of ATP to the myosin head, and this completes the cycle. If the calcium concentration is still high, and the actin binding sites are still exposed, then further cycles will occur, leading to further shortening. If the calcium concentration has fallen to baseline levels, no further cycling will take place and the heart will relax.

1.3.4 Relaxation

Cardiac relaxation during diastole is essential for normal pump function. The period of relaxation allows adequate ventricular filling to occur before the next contraction. Reduction and termination of contraction is brought about by the clearance of calcium ions from the cytoplasm. This can occur in two main ways; extrusion of calcium from the cell to the extracellular environment via the NCX or sarcolemmal calcium ATPase, or return of calcium into the SR. There is also a small quantity of calcium transported into mitochondria via a uniporter (Bers, 2000).

Extrusion of calcium

There are two pumps located in the plasma membrane that are responsible for removing calcium from the cell. These are the NCX and the sarcolemmal calcium ATPase.

The proportion of calcium removed from the cell at the end of systole varies depending on species. In rabbit ventricle (which is thought to have similar calcium dynamics to human heart), 29% of calcium is removed from the cytosol to the extracellular space, with NCX being responsible for the vast majority (97%) of this. The sarcolemmal calcium ATPase therefore only makes a minor contribution to calcium removal (Bers, 2000). In contrast, rat and mouse ventricular cells only lose 8% of calcium from the cell, although the NCX is still the most important ion transporter in this process (Bassani et al., 1994).

The NCX is an exchange pump that transports three sodium ions in one direction across the membrane for a single calcium ion in the opposite direction. As explained above, the direction of this movement depends upon the myocyte membrane potential relative to

the $E_{Na\text{-}Ca}$. During the repolarisation and resting phases, the membrane potential is negative to $E_{Na\text{-}Ca}$ and so sodium is moved into the cell at the expense of calcium.

Return of calcium to the SR

The protein responsible for returning calcium ions to the SR is the sarco/endoplasmic reticulum calcium ATPase (SERCA), which is a P-type ion pump in the same family as the Na/K-ATPase in the plasma membrane and the sarcolemmal calcium ATPase. SERCA is found primarily in the nSR membrane, and there are three genes coding for it. These are highly conserved but found on different chromosomes, and alternative splicing of these genes leads to at least ten different protein isoforms of SERCA (Periasamy et al., 2007). SERCA1a is the principle isoform found in fast-twitch skeletal muscle, whereas SERCA2a is found in slow-twitch and cardiac muscle (Bers, 2001 p. 161; Periasamy et al., 2007).

SERCA transports two calcium ions into the SR against the concentration gradient for every molecule of ATP it consumes (Reddy et al., 1996), and it has been estimated that 10-15 calcium ions per pump per second can be transported (Levitsky et al., 1981).

There are two main regulators of SERCA function; Phospholamban (PLB) and sarcolipin (SLN). While both proteins are expressed in both atria and ventricles, PLB levels are much higher than SLN in the ventricles, while the reverse is true in the atria (Periasamy et al., 2008).

PLB is a 6 kDa protein consisting of 52 amino acids that forms a pentamer, and binds to SERCA, reducing the affinity of some isoforms - including SERCA2a - for calcium. It

therefore acts as a brake on the rate at which calcium is returned to the SR (MacLennan et al., 2003). Knockout of PLB leads to a hyperdynamic heart, with enhanced contractility and relaxation, that fails to respond to β-agonists (Luo et al., 1994) whereas over-expression results in cardiac depression (Kadambi et al., 1996). In human patients, mutations of phospholamban that prevent its binding at SERCA and result in lack of inhibition, or mutatations that prevent its phosphorylation and so result in permanent inhibition of SERCA both result in cardiomyopathy and premature death (Haghighi et al., 2003; Schmitt et al., 2003).

The phosphorylation of PLB by either PKA at Ser16 or CaMKII at Thr17 results in release of this brake, and calcium is pumped back into the SR faster. This has two effects: One is the lusitropic effect; the heart relaxes more rapidly after contraction, allowing filling to occur (Simmerman et al., 1986). The other is that there is an increase in the ratio of calcium pumped into the SR by SERCA to calcium pumped out of the cell by the NCX. This results in a higher availability of calcium for release from the SR during the next systole, and consequently a positive inotropic effect. Protein Kinase C (PKC) is also able to phosphorylate PLB at Ser10, although the physiological significance of this is controversial (Edes et al., 1990).

SLN is similar to phospholamban, insofar as it is a small peptide that inhibits SERCA and slows the movement of calcium into the SR. Experimental over-expression of SLN in ventricular cells from PLB knockout mice reversed the increase in calcium transient and contractility seen in PLB-null ventricular cells that did not over-express SLN. However, the effect of SLN over-expression could be overcome by treatment with isoprenaline,

suggesting that SLN can be phosphorylated to alter its inhibitory effect on SERCA in the same way as PLB (Gramolini et al., 2006).

1.3.5 Autonomic control of excitation-contraction coupling

Sympathetic and parasympathetic nervous systems have a regulatory influence over the heart. The sympathetic system, commonly known to be the mediator of the 'flight or fight' response has a stimulatory effect, increasing heart rate and contractility. In contrast, the parasympathetic system's 'rest and digest' influence has an inhibitory effect on the heart. In humans both systems are active at rest, but the parasympathetic influence dominates, leading to a heart rate that is slower than the intrinsic rate of the SAN.

Both branches of the autonomic nervous system exert their effects on the heart by releasing neurotransmitters.

The sympathetic nervous system

Sympathetic pre-ganglionic nerves originate from the lateral horns of T1-T5 levels of the spinal cord, and synapse with the post-ganglionic nerves in the sympathetic trunk. These post-ganglionic nerves travel through the cardiac plexus to innervate the heart, and their terminals release noradrenaline. This acts to increase the rate of depolarisation of the SAN, and therefore increase heart rate. Noradrenaline also acts at the AVN, bundle branches and Purkinje fibres to increase the rate at which action potentials are conducted and also at myocytes to increase rate of rise, peak amplitude and rate of fall of the calcium transient and therefore contraction force.

Noradrenaline (and also other catecholamine hormones such as adrenaline and dopamine, which reach the heart via the circulation rather than being released from the nerve terminal) act primarily on β1-receptors in the heart. These are G-protein coupled receptors (GPCRs).

GPCRs are found in the plasma membrane and consist of seven transmembrane domains. As their name implies, they are coupled to G-proteins, which consist of α and βγ subunits. The subunits depend on the binding of GDP to remain in the resting state. The stimulation of the receptor by an agonist leads to the substitution of GDP for GTP and the dissociation of the G-protein complex. The α and βγ subunits are then free to intracellular enzyme effectors, which mediate the cell's response to the agonist. Hydrolysis of GTP to GDP returns the G-protein to its resting state.

The β1-adrenergic receptor is coupled with $G\alpha_s$, which leads to activation of adenylyl cyclase and formation of cAMP. The latter signalling molecule is able to activate PKA, which phosphorylates several targets, including the ryanodine receptor, the LTCCs, potassium channels carrying I_{Ks}, and phospholamban, as discussed above. In addition, PKA may modulate other components of the excitation-contraction coupling system such as troponins and sodium and chloride channels. In addition to activating PKA, cAMP is known to cause another group of proteins, collectively known as exchange proteins directly activated by cAMP or Epac. The association of these proteins with cAMP was discovered relatively recently (de Rooij et al., 1998), and they have been found to mediate other actions of β-adrenergic stimulation such as activation of CaMKII and PKC. Epac has also been shown to mediate a positive inotropic effect (despite either no effect on or a

reduction in calcium transient) by increasing the sensitivity of the myofilaments to calcium. This effect is correlated with an increase in phosphorylation of myosin-binding protein C and troponin I, perhaps as a result of CaMKII and PKC activity (Cazorla et al., 2009).

The parasympathetic nervous system

Parasympathetic fibres that innervate the heart are branches of the vagus nerve, and synapse in ganglia within the heart. In contrast to the sympathetic fibres, the post-ganglionic parasympathetic nerves are short and use acetyl choline (ACh) as their neurotransmitter, and this acts mainly at type 2 muscarinic (M2) receptors to cause a reduction in heart rate and conduction velocity, although other subtypes have also been found in the heart (Olshansky et al., 2008). The majority of parasympathetic innervation to the heart acts at the SAN and AVN, with a much less significant influence on the ventricular muscle than the sympathetic system (Katz, 2011 p. 203).

Muscarinic receptors are also GPCRs, but which couple to $G\alpha_i$, leading to activation of phosphodiesterase and break-down of cAMP. There is therefore a reduction in the activity of PKA and Epac. Additionally, the $\beta\gamma$ subunits of this G-protein can act at specific inwardly-rectifying potassium (GIRK) channels to increase current and result in more rapid repolarisation of the cell membrane (Ito et al., 1995).

1.4 Mechanisms of arrhythmogenesis

As described above, a heart in normal 'sinus rhythm' generates an electrical signal at the SAN, and this signal spreads across the atria and then - after a brief pause - into the ventricles via the AVN, bundle branches and Purkinje fibres. The signal then spreads in two directions through the ventricular muscle to cause co-ordinated synchronised contraction (Katz, 2011 p. 403-6). Any deviation from this pattern qualifies as an arrhythmia, and there are a variety of classification systems. In general terms, arrhythmias occur when there is a problem with signal generation or signal propagation, or in other words, there must be a mechanism whereby the arrhythmia is initiated, and another by which it is maintained.

Arrhythmias vary in severity. At one end of the scale, there are mild physiological variations in the regularity of the heart beat (e.g. 'sinus arrhythmia', where the RR-interval varies with respiration), which have little or no effect on cardiac output. In contrast, some arrhythmias are severe disorders of ventricular conduction and contraction (e.g. asystole, where there is no electrical activity or contraction and ventricular fibrillation, where electrical activity is random and chaotic and there is no co-ordinated cardiac movement), which are incompatible with life (Katz, 2011 ch. 16).

Some of the more severe arrhythmias are initiated when an action potential spontaneously occurs in a part of the myocardium other than the SAN, and then this generates a signal that spreads in an abnormal pattern across the heart.

1.4.1 Arrhythmia initiation

The spontaneous firing of an action potential in an ectopic focus in the heart (i.e. a part of the heart distinct from the SAN) is known as automaticity (Cherry et al., 2012). There are many factors that may predispose to this, including acute or chronic ischaemia, infarction, abnormal morphology such as dilatation or hypertrophy, electrolyte imbalances, the action of various drugs or neurotransmitters, temperature and pH (Janse et al., 1989). If the ectopic focus fires action potentials at a higher rate than the SAN and these conduct, this focus may become the dominant pacemaker, leading to a tachyarrhythmia. Signals conducted as a result of automaticity are known as 'triggered activity'.

Automaticity and triggered activity are frequently the result of abnormal calcium handling in the heart. Any inward current that occurs during repolarising or resting phases of the action potential that is sufficient to re-activate sodium or calcium channels has the potential to trigger another premature membrane depolarisation. If this occurs during phase 2 or phase 3, it is known as an early after-depolarisation (EAD) whereas if it occurs during phase 4 it is known as a delayed after-depolarisation (DAD) (Levy, 1989).

As repolarisation begins to occur during phase 2, the membrane potential begins to fall towards zero, and then becomes more negative in phase 3. Between voltages of -20 mV to +10 mV, LTCCs can (re-)activate (MacLeod, 2014 p. 234). Therefore, any slight inward current at this point may overwhelm the normal repolarisation, and result in a small depolarisation which may re-activate the L-type channels. The EAD is then accentuated for two reasons: First, the inward current through the re-activated calcium channels will lead to further depolarisation. Second, the calcium that has re-entered the cell is pumped out again by the NCX, itself being electrogenic and producing a small inward current (Wagner et al., 2015). In addition, $I_{Ca\text{-}L}$ will also cause CICR and further release of calcium

from the SR, leading to an after-contraction. EADs are more likely in conditions where the action potential duration is prolonged, such as where there is a slow heart rate or where there is a reduction in outward, repolarising current (e.g. during hypokalaemia). They may also be more likely to occur when genetic ion channel abnormalities are present that cause long-QT syndromes (Chen et al., 2016).

In contrast, DADs are not dependent on re-activation of the L-type current, but are linked to overload of the SR with calcium. This may occur in hypertrophied or failing hearts, and also due to the influence of catecholamines and cardiac glycosides. High levels of calcium within the SR causes an increased open probability of ryanodine receptors, leading to calcium release into the cytoplasm (Levy, 1989). This calcium activates transient inward currents, collectively known as I_{ti}, consisting of that carried by NCX with smaller contributions from the calcium-activated chloride current, and a calcium-activated non-specific cation current (Bers et al., 2002). If I_{ti} causes the membrane potential to rise as far as the activation potential for voltage-gated sodium channels, a premature action potential will fire.

Propagation of EADs or DADs may result in individual premature beats, or severe re-entrant arrhythmias.

1.4.2 Arrhythmia maintenance

An initiating mechanism that occurs in a single cardiac myocyte or isolated focus is unlikely to cause a whole-heart arrhythmia unless there is also a maintenance

mechanism. An arrhythmia may be maintained in several ways which often either involve abnormalities of propagation or a re-entry mechanism, or both.

Propagation abnormalities may be caused by a delay or block in any part of the cardiac conducting system. Delayed conduction at the AVN will lead to first, second or third-degree heart block depending on the severity, whereas delay further down the system may result in bundle branch block or fascicular blocks.

Re-entry mechanisms can lead to a variety of arrhythmias including the supraventricular tachycardias (SVTs) as such atrioventricular nodal re-entry tachycardia (AVNRT), or ventricular arrhythmias such as ventricular fibrillation (VF) (Katz, 2011 ch. 16). Re-entry means that a wave of depolarisation travelling through the heart is able to enter an area of myocardium more than once during the same cardiac cycle. The wave is therefore able to continually propagate without being extinguished, and is sometimes known as a rotor (Vaquero et al., 2008). Due to the abnormal propagation, different areas of myocardium are left refractory at different times, leading to further re-entry circuits and the prevention of the re-establishment of sinus rhythm.

In order that an area of myocardium can undergo re-entry, there must be a unidirectional conduction block. An incoming excitation wave is unable to depolarise tissue behind the block until it has established an alternative path and can approach from the opposite direction, which allows conduction. This causes a delay, by which time the tissue in front of the block has repolarised and is no longer refractory. The wave can therefore re-enter this tissue (Kleber et al., 2004; MacLeod, 2014 p. 239).

Propensity to re-entry is increased by areas of ischaemia, heterogeneities in action potential duration and asymmetrical anatomical abnormalities, particularly in conducting tissue (Katz, 2011 p. 440-441).

If this mechanism occurs within the ventricle, the result can be disordered and chaotic waves of depolarisation and repolarisation spreading in random directions. This is known as ventricular fibrillation. If a re-entry circuit establishes itself in the AVN, then conduction can occur in the anterograde direction via the bundle of His, or in the retrograde direction back into the atria and leads to AVNRT. The cyclical depolarisation of the AVN caused by the re-entry circuit can therefore lead to a tachyarrhythmia, but with co-ordinated depolarisations and contractions of the ventricles (Kwaku et al., 2002).

1.5 Lysosomes

1.5.1 Discovery

Lysosomes were discovered in the early 1950s by Christian de Duve, who later won the Nobel Prize for his work (Bainton, 1981). De Duve was studying the location of glucose-6-phosphatase and other enzymes in rat hepatocytes, as part of his work on the mechanism of action of insulin on the liver, which was still controversial at that time. In one experiment, de Duve and his team were trying to separate glucose-6-phosphatase from another enzyme, acid phosphatase, by fractionation of liver cell homogenates. They found that the activity of acid phosphatase in homogenates that had been violently prepared using a Waring blender was an order of magnitude higher than that in

homogenates that were prepared more gently using fractional centrifugation. Furthermore, the activity in the latter preparation could be restored by various means, including leaving it in the refrigerator for five days. This behaviour was known as enzyme latency, and subsequently led to the realisation that the enzyme was enclosed by a membrane (Bainton, 1981; de Duve, 2005).

At that time, only four cell fractions were known; The heaviest was the nuclear fraction, followed by mitochondrial and microsomal fractions. The last was the supernatant. The microsomal fraction was thought to be predominantly made up of fragments of endoplasmic reticulum. However, the acid phosphatase activity was unusual because it was spread between the mitochondrial and microsomal fractions (de Duve, 2005). Soon, other enzymes were found that had the same distribution as acid phosphatase, and which all showed latency. They were also all acid hydrolases, but which targeted different substrates. This suggested a digestive function, and led to the collective naming of these enzymes and the fractions they were found in as 'digesting bodies' or lysosomes (De Duve et al., 1955).

Physical lysosomes were tentatively identified in liver cells a year later (Novikoff et al., 1956), and this was confirmed following their isolation and labelling using stains for acid phosphatase in 1965 (Baudhuin et al., 1965). They were first recognised in cardiac myocytes shortly after (Romeo, 1966) and they have subsequently been identified in all eukaryotic cell types (Appelqvist et al., 2013), being more abundant in those with high phagocytic activity such as macrophages. They are now known to contain over fifty types of acid hydrolase enzyme, including phosphatases, nucleases, glycosidases, proteases,

peptidases, ribonucleases, sulphatases, lipases and others (Bainton, 1981; Braulke et al., 2009).

1.5.2 Structure and function

Biogenesis and life cycle

Lysosomes are heterogeneous membrane-enclosed organelles, with a complex biogenesis. They contain a number of acid hydrolases capable of digesting a wide range of substrates, and their luminal pH is maintained at 4.5 – 5.5. They range in size from approximately 200 nm diameter to over 1 μm, and vary in shape. Traditionally, they are known for their recycling and degradative functions and have an intricate role in the immune system and autophagic processes (Alberts, 2015 ch. 13).

The acid hydrolase enzymes and other lysosomal proteins are manufactured in the rough endoplasmic reticulum (rER). From here, they are transported to the cis face of the Golgi apparatus and labelled with a mannose-6-phosphate tag (Braulke et al., 2009). These tags act as address labels, ensuring that the protein is transported to the lysosomal vesicle, or 'prelysosome', which is formed at the trans face of the Golgi. The vesicles contain mannose-6-phosphate receptors (MPRs), which bind to the tags and take up the correct proteins (Braulke et al., 2009; Saftig et al., 2009). Meanwhile, another vesicle is formed at the plasma membrane by endocytosis. This forms an early endosome and other proteins, including the hydrogen ATPase pump, are transported to it (Scott et al., 2014). As these proteins accumulate, the lumen becomes more acidic. As the pH approaches 4.5 – 5.5 the structure becomes known as a late endosome. The fusion of the lysosomal vesicle from

the trans-Golgi with the late endosome forms a primary lysosome (Kornfeld et al., 1989). The pH-related activation of proteases within the lysosome leads to dissociation of the MPRs (Diaz et al., 1998). The mannose-6-phosphate system also allows continuous trafficking of different proteins from the Golgi to endosomes and lysosomes at different stages of their development.

Phagocytosis is the process by which foreign bodies such as bacteria are taken up into membrane-bound vesicles by some cells – especially those of the immune system. These vesicles are known as phagosomes. Alternatively, autophagosomes are formed when native structures such as old or damaged mitochondria are enclosed within a membrane for breakdown and recycling (Alberts, 2015).

A secondary lysosome is formed when the primary lysosome fuses with a phagosome or autophagosome, leading to digestion of its contents by the acid hydrolases (Appelqvist et al., 2013). The resulting sugars, lipids, amino acids and other digestion products are transported out of the lysosome and into the cytoplasm for recycling or exocytosis. Some material is not digestible and this remains within the lysosome. Secondary lysosomes containing a significant amount of this indigestible material are known as dense bodies. In post-mitotic cells, dense bodies – also sometimes collectively known as lipofuscin – accumulate with age (Brunk et al., 2002; Terman et al., 1998; Terman et al., 2004).

Lysosomal membrane proteins

The lysosomal membrane is decorated with at least 25 different proteins, which are responsible for various functions such as the acidification of the lumen, transport of

degradation products to the cytoplasm, and the fusion of the lysosomal membrane with endosomes, phagosomes and other organelles (Eskelinen et al., 2003; Lubke et al., 2009). Approximately 50% of lysosomal membrane proteins are lysosome-associated membrane protein-1 (LAMP-1) and LAMP-2 (Eskelinen, 2006). These proteins consist of a small (11 amino acids) cytoplasmic carboxy-tail, a transmembrane domain, and a large glycosylated U-shaped intra-luminal domain. The amino terminus is anchored to the luminal aspect of the lysosomal membrane. These proteins are approximately 40 kDa, but the high level of glycosylation increases their apparent molecular weight to approximately 120 kDa (Fukuda, 1991; Mane et al., 1989). The presence of these proteins (in the absence of another membrane protein, the mannose-6-phosphate receptor (MPR)), is one of the major defining features of a lysosome (Appelqvist et al., 2013; Kornfeld et al., 1989). LAMPs are approximately specifically markers of the lysosomal membrane, although small proportions are also found on the membranes of late endosomes and on the cell plasma membrane (Fukuda, 1991).

While LAMP-1 has a single isoform, LAMP-2 has splice varients that lead to the expression of three isoforms, LAMP-2A, 2B and 2C (Eskelinen et al., 2005). The differences in expression and function of these isoforms have not yet been fully elucidated. Rare mutations in the human LAMP-2 gene (located on the X-chromosome) cause Danon disease, which is characterised pathologically by accumulation of late autophagic vacuoles in skeletal and cardiac muscle, and clinically by learning difficulties, skeletal muscle myopathy and hypertrophic cardiomyopathy. It usually leads to death in the teenage years in males, although its phenotype in females is less severe (Nishino, 2003).

The LAMP proteins' major function was initially thought to be to protect the lysosomal membrane from the noxious acidic luminal environment (Eskelinen, 2006; Granger et al., 1990). However, there is also now evidence that these proteins have a more important role in lysosomal function. Evidence from the study of conditions such as Danon disease and the effects of genetic knockout of LAMP1/2 suggests that these proteins are involved in degradative processes such as lysosome-phagosome fusion and the normal turnover of mitochondria (Eskelinen, 2006; Eskelinen et al., 2002; Eskelinen et al., 2003; Huynh et al., 2007; Saftig et al., 2008).

Lysosome-related organelles

Lysosome-related organelles (LROs) are a diverse group of intracellular vesicles that share some features with lysosomes (such as their acidic interior), but are distinct in function, morphology and composition (Huizing et al., 2008). Examples include melanosomes, platelet delta granules, lytic granules, lamellar bodies, azurophilic and basophilic granules, multivesicular bodies and others.

1.5.3 Lysosomes as a non-canonical acidic store of calcium

The major intracellular store of calcium is the sarco/endoplasmic reticulum, which (in the heart) has been reported to contain 1 - 1.5 mM calcium during diastole and 400 - 600 μM calcium during systole (Shannon et al., 2003). The factors that govern the release and reuptake of this calcium, along with its effects on the cardiac myocyte have been discussed above.

Measurements of lysosomal calcium concentration show very similar values to systolic S/ER concentration, and are related to luminal pH (Calcraft et al., 2009; Christensen et al., 2002; Lloyd-Evans et al., 2008). The low pH of the lysosome lumen is maintained by a vacuolar-type hydrogen ATPase. Alkalinisation of the lysosome with bafilomycin-A1 or ammonia leads to loss of calcium, and similarly, release of lysosomal calcium leads to alkalinisation. Therefore, it has been hypothesised that the entry of calcium into the lysosome is via an as-yet unidentified H^+-dependent calcium transporter (Morgan et al., 2011).

However, this idea has recently been challenged by experiments using a novel method of reporting lysosomal calcium concentration. Lysosome-targeted genetically-encoded calcium indicators (Shen et al., 2012) were used to show that inhibition of the V-type H^+-ATPase affected pH, but not calcium content (Garrity et al., 2016) – in contrast to other studies of this system (Calcraft et al., 2009; Christensen et al., 2002; Lloyd-Evans et al., 2008). Even more interestingly, antagonists of the IP_3 receptor blocked lysosomal calcium accumulation, suggesting that calcium released from the SR in response to IP_3 could enter lysosomes (Garrity et al., 2016).

Whatever the source of lysosomal calcium, the stimuli that result in its release, and the effects that it subsequently has on the myocyte, have been the subject of great recent interest.

1.6 Nicotinic Acid Adenine Dinucleotide Phosphate (NAADP)

1.6.1 Discovery

NAADP was discovered in 1980 as a derivative of the co-enzyme NADP, although its activity as a calcium-releasing intracellular messenger was not recognised at that time (Bernofsky, 1980).

In the late 1980s and early 1990s, shortly after the first published description of IP_3 as a calcium-releasing second messenger (see below), Lee and colleagues discovered that commercially available NAD and NADP were also capable of causing intracellular calcium release in sea urchin oocytes, albeit when used in large concentrations. They subsequently recognised that chemical derivatives of these compounds were responsible for their calcium-releasing activity, rather than the co-enzymes themselves.

Increased intracellular calcium concentration in response to NAD occurred several minutes after its application, suggesting an enzymatic reaction was needed to produce activity. After several years work, the resulting active metabolite of NAD was subsequently shown to be cyclic-ADP-ribose (see below), and this was published in 1989 (Lee et al., 1989). Its crystal structure was confirmed a few years later (Lee et al., 1994b).

In contrast, the calcium-releasing activity of NADP was almost instantaneous, and its activity could be increased by raising the pH, suggesting a change in ionisation state. The active metabolite of NADP was shown to have an extremely similar structure to its parent compound, and it took Lee and colleagues just a few months to confirm its structure as NAADP – that is, NADP with the nicotinamide moeity changed to nicotinic acid (i.e. the substitution of $-NH_2$ with an –OH group). Despite being discovered in 1990 (Lee, 2002 ,

p10.), the function of NAADP as a calcium-releasing second messenger, along with its structure, wasn't published until five years later (Lee et al., 1995) shortly before another group also published very similar findings (Chini et al., 1995).

NAADP has subsequently become recognised as an important intracellular second messenger in a wide range of species (including mammals) and tissues, and is the most potent calcium-mobilising molecule yet discovered, active at concentrations in the picomolar to nanomolar range, depending on the tissue in question (Chini et al., 1995; Galione et al., 2009).

1.6.2 Synthesis and metabolism

NADases (NAD glycohydrolases) are ubiquitous enzymes that metabolise NAD to ADP-ribose by hydrolysis, and were first studied in the middle of the last century (Lee, 2002). When it became possible to differentiate between ADP-ribose and cyclic-ADP-ribose in the laboratory, it was realised that NADases were a heterologous group; some metabolising NAD into ADP-ribose, but some using NAD to synthesise cADPR. One such example of the latter group was isolated from the sea slug *Aplysia californica,* and subsequently dubbed 'ADP-ribosyl cyclase' or ARC (Lee et al., 1991). The mammalian homologs of this enzyme, CD38 and CD157 were found not only to synthesise cADPR from NAD, but also to hydrolyse cADPR to ADP-ribose (Howard et al., 1993).

Unusually, as well as the metabolism of NAD to cADPR, CD38 was shown to be capable of synthesising NAADP from NADP. In acidic conditions, the base-exchange reaction leading

to the synthesis of NAADP is favoured, whereas in neutral or alkaline conditions the principle reaction is cyclization of NAD to cADPR (Aarhus et al., 1995).

The cardiac ARC may be distinct from CD38 and CD157. Both of the latter enzymes can be stimulated using zinc ions, but in the heart ARC they cause inhibition (Kannt et al., 2012; Xie et al., 2005).

In 1998, the synthesis of NAADP was linked to cytoplasmic levels of cAMP, adding to evidence that NAADP acts as an intracellular second messenger following extracellular stimulation (Wilson et al., 1998). In accordance with this observation, the synthesis of NAADP was subsequently shown in increase in response to β-adrenergic stimulation in isolated hearts (Gul et al., 2016; Lewis et al., 2012; Macgregor et al., 2007a).

Degradation of NAADP is either by alkaline phosphatase, which hydrolyses the 2'-phosphate to yield NAAD (Lee et al., 1997) or by nucleotide pyrophosphatase, which hydrolyses NAADP to produce phospho-AMP and nicotinic acid mononucleotide (Lee, 1997). Both of these enzymes are commonly found in a wide range of cell types and tissues, and all the breakdown products of NAADP are inactive in terms of causing calcium mobilisation. There is also some evidence that CD38 may also be able to degrade NAADP to 2'-phospho-ADP-ribose (Schmid et al., 2011). This would mean CD38 is capable of both the synthesis and breakdown of both NAADP and cADPR.

1.6.3 NAADP and calcium release

NAADP, cADPR and IP_3 release calcium via distinct mechanisms. The calcium response that occurs following the introduction of NAADP into sea urchin oocytes can be desensitized by high concentrations of NAADP. At this point, the addition of further NAADP will not produce a response. However, cADPR and IP_3 are still able to elicit calcium release in these circumstances, implying that these messengers act at a different site to NAADP (Aarhus et al., 1996; Genazzani et al., 1996). Similarly, the addition of heparin (an IP_3 receptor antagonist) or 8-amino-cADPR (an antagonist of cADPR) prevented the release of calcium in response to IP_3 and cADPR respectively, but not in response to NAADP (Lee et al., 1995).

Further evidence suggests that, while cADPR and IP_3 act at the sarcoendoplasmic reticulum (S/ER), NAADP does not. Experiments with sea urchin oocyte homogenates showed that while exposure of the system to inhibitors of SERCA such as thapsigargin and cyclopiazonic acid reduced the calcium release response to IP_3 and cADPR, the responses to NAADP were preserved (Churchill et al., 2001; Genazzani et al., 1996). Additionally, oocytes that underwent centrifugation and sucrose stratification so that their organelles became organised by density along the length of the cell demonstrated release of calcium at a site distant from the S/ER, in the region of mitochondria and acidic organelles following photorelease of caged NAADP (Churchill et al., 2002; Lee, 2001; Lee et al., 2000). Further evidence accumulated that suggested NAADP signalling is more complex than that mediated by cADPR or IP_3:

The introduction of NAADP into oocytes and also mammalian cells such as pancreatic acinar cells, not only rapidly led to a spike in calcium concentration but also to the long-term propagation of calcium waves and oscillations. Given that the continued

introduction of NAADP caused self-inactivation, this observation seemed paradoxical. Additionally, although the initial rise in calcium concentration caused by NAADP appeared to be independent of the S/ER, and remained unaltered in the presence of SERCA inhibitors and antagonists at IP_3 and ryanodine receptors, the long-term calcium oscillations that followed were abolished by these compounds (Cancela et al., 1999). This led to the suggestion of a 'two-pool' mechanism for calcium release by NAADP; that pool-1 was a non-canonical (non-S/ER) calcium store, released initially by NAADP. In turn, the calcium from pool-1 stimulated further calcium release (CICR) from pool-2, which was likely to be the S/ER (Churchill et al., 2001). This mechanism became known as the 'trigger hypothesis', and implied the existence of a calcium signalling microdomain between the two pools.

The identity of pool-1 was subsequently investigated. Sea urchin homogenates were subjected to fractionation using density gradient centrifugation and Percoll gradient purification, allowing isolation of different subcellular fractions (Churchill et al., 2002; Clapper et al., 1987). A unique fraction was identified that released calcium in response to NAADP, but not in response to cADPR or IP_3 and contained lysosome-related organelles ('reserve granules' in the sea urchin). These were identified by immunological labelling of acid phosphatase, glucosaminidase and β-galactosidase. Radioactive NAADP binding was also found to be higher in these fractions than cADPR. Additionally, glycyl-phenylalanine 2-naphthylamide (GPN) was used to cause selective osmotic lysis of lysosome-related organelles, and resulted in a significant reduction in the response to NAADP. Similarly, compounds that prevented the acidification of these organelles such as FCCP, nigericin, ammonia, and bafilomycin-A1 (see below) also prevented calcium uptake suggesting that calcium was co-transported into these structures with protons, or

that a proton gradient across the lysosomal membrane was required for calcium sequestration. Acidification was not prevented by thapsigargin (Churchill et al., 2002), but the release of calcium induced by NAADP caused alkalinisation of acidic compartments whereas cADPR and IP_3 had no effect on lysosomal pH (Morgan et al., 2007).

Following the identification of lysosomes as the likely candidates for calcium pool-1, the hunt for the exact molecular target of NAADP began. Identification of the NAADP receptor has proved controversial, and several possibilities have been investigated.

1.6.4 NAADP receptor candidates

Several possible molecular targets of NAADP have been put forward. The most frequently discussed are the transient receptor potential mucolipin-1 channel (Zhang et al., 2007), the ryanodine receptor types 1 and 2 (Hohenegger et al., 2002; Mojzisova et al., 2001), and the Two-Pore Channels (Brailoiu et al., 2009; Calcraft et al., 2009; Zong et al., 2009).

The transient receptor potential mucolipin type-1 channel (TRP-ML1) was reconstituted using purified rat liver lysosomes and shown to carry an ionic current in response to NAADP at low concentrations but desensitize at high concentrations. However, the experiments used caesium ions, and a calcium current was not sought. The response to NAADP could also be blocked using antibodies against TRP-ML1 in this model (Zhang et al., 2007). Furthermore, responses to NAADP could be abolished in fibroblasts by genetic deletion of TRP-ML1 and then rescued by transfection and re-expression of this protein (Zhang et al., 2011). In contrast to these findings, observations by other groups showed

no increase in the binding of radiolabelled NAADP in cells overexpressing TRP-ML1, and no exaggerated response to NAADP in these cells compared with controls (Pryor et al., 2006). Additionally, although lysosomal membrane currents were increased by NAADP in wildtypes and not in TRP-ML1 knockouts, calcium oscillations could still be elicited by NAADP in the knockout (Yamaguchi et al., 2011), and questions have also been raised regarding the specificity of the TRP-ML1 antibody that was able to block NAADP-induced current (Bayliss, 2014).

Ryanodine receptors (RyR) have also been suggested as putative NAADP targets. Some studies have reported activation of RyR2 by NAADP, although these were all at supra-physiological concentrations (Guse et al., 2016). Opening of partially purified RyR1 from skeletal muscle was detected in planar lipid bilayers in response to more physiological concentrations of NAADP (Hohenegger et al., 2002). However, there was no desensitization to higher concentrations and this was attributed to the loss of factors that are necessary for this process being lost when the receptors are reconstituted into lipid bilayers (Guse et al., 2016). Equally, this may simply demonstrate that RyR1 responses alter when removed from physiological conditions. Mojzisova et al. (2001) also reported direct activation of RyR using NAADP, although the concentrations required were high. Other groups have been unable to activate RyR in planar bilayers using NAADP (Copello et al., 2001; Pitt et al., 2010).

Depletion of calcium from the nuclear envelope was also detected in response to NAADP in pancreatic acinar cells (Gerasimenko et al., 2003). This effect of NAADP, in contrast to the results of other experiments discussed above, was sensitive to RyR blockers such as ryanodine and ruthenium red and to calcium depletion of the S/ER by inhibitors or

SERCA such as thapsigargin. The NAADP response in these experiments was insensitive to inhibitors of lysosomal function such as bafilomycin-A1 and nigericin (Gerasimenko et al., 2003). However, other groups were not able to reproduce this result using patch clamping of the nuclear membrane from HEK293 cells expressing RyR1 (Wagner et al., 2014). In other experiments using these cells, calcium release could not be elicited by intracellular release of NAADP (Ogunbayo et al., 2011).

In Jurkat T-lymphocytes, microinjection of NAADP caused a global calcium response that could be abolished by ruthenium red but not by the IP_3 antagonist heparin and genetic knockdown of RyR in these cells resulted in a lack of response to NAADP (Langhorst et al., 2004). However, differentiation between a possible short-lived localised calcium response to NAADP followed by a longer-lasting global response – respecting the two-pool and trigger hypotheses – was not attempted. Subsequent experiments addressed this problem; in fast calcium imaging studies a reduction in the initial short-lived localised calcium response was detected in T-cells lacking RyR expression (Dammermann et al., 2005; Wolf et al., 2015). The calcium response to NAADP was also unaffected by bafilomycin-A1 in these experiments, but was partly reduced by thapsigargin implying some dependence on the S/ER but not on lysosomes.

Although the evidence presented above suggests that NAADP may be acting at TRP-ML1 and RyR channels, their role as NAADP receptors remains controversial, and further work will be needed to clarify this area. Two-pore channels are more widely accepted as likely NAADP receptors.

1.6.5 Two-Pore Channels as NAADP receptors

The two-pore channels (TPCs) have two repeats of a pore-forming domain consisting of six transmembrane segments. This is in contrast with TRP-ML channels that have a single domain, and voltage-gated calcium channels that have four domain repeats (Calcraft et al., 2009; Morgan et al., 2014). There are three TPC isoforms, coded by *Tpcn1, Tpcn2* and *Tpcn3* genes. The latter is absent from human genomes and those of some rodents (Zhu et al., 2010), including mice. TPCs are found exclusively in the endolysosomal system and other acidic organelles in animals and also in plant vacuoles, and are not found on Golgi, S/ER or mitochondria (Galione, 2011). TPC1 tends to be distributed through early endosomes with a less acidic pH than TPC2, which is found on late endosomes and lysosomes (Morgan et al., 2011).

In 2009, three groups converged on the concept of TPCs as the molecular targets for NAADP (Brailoiu et al., 2009; Calcraft et al., 2009; Zong et al., 2009). TPC2 in particular showed promise as the most likely NAADP receptor. In addition to its lysosomal distribution, overexpression of TPC2 in HEK293 cells increased the specific binding of radiolabelled NAADP, and this allowed immunoprecipitation of the TPC2 protein. Application of NAADP to these cells caused a brief primary 'pacemaker-like' increase in calcium, followed by a larger secondary calcium rise. Both primary and secondary calcium signals could be inhibited by bafilomycin-A1, but antagonists at IP_3 receptors were only able to block the secondary response. This pattern is consistent with the trigger hypothesis. High concentrations of NAADP desensitized TPC responsiveness and knockdown of TPC2 expression also abolished responses. *Tpcn2*$^{-/-}$ mice were also created; pancreatic β cells from these animals failed to respond to NAADP where their wild-type counterparts did (Calcraft et al., 2009).

Cells overexpressing TPC1 also demonstrated the primary localised calcium release, but not the more widespread secondary phase. It was hypothesized that this was due to the early endosomal distribution of TPC1, which perhaps was more isolated from S/ER and therefore could not easily trigger further calcium release (Calcraft et al., 2009; Galione, 2011).

When TPCs were tested in lipid bilayer membranes (Pitt et al., 2010; Pitt et al., 2016), or in cells where the TPC had been redirected from the lysosome to the plasma membrane (Brailoiu et al., 2010), the current produced was dependent on NAADP and carried by calcium ions.

However, controversy arose when studies were published showing that TPCs could be activated by the lipid phosphatidylinositol 3,5-bisphosphate ($PI(3,5)P_2$) and not by NAADP, and selectively carried sodium ions instead of calcium (Cang et al., 2013; Wang et al., 2012). In the same study, this group also found that sodium, rather than any other ion was the predominant species in the lysosomal lumen, and that calcium responses to NAADP in pancreatic islet cells would still occur, even in cells from a double TPC knockout animal (*Tpcn1*$^{-/-}$ / *Tpcn2*$^{-/-}$).

In itself, the finding that TPCs could be activated by $PI(3,5)P_2$ was not surprising, having been demonstrated previously, and other channels – such as TRP-ML1 and RyR – are also known to be activated by this lipid (Dong et al., 2010; Touchberry et al., 2010). Ruas et al. (2015) performed several new experiments to re-test whether TPCs are likely NAADP receptor candidates. To start, the double knockout (DKO) animal used in experiments by

Wang et al. (2012) was regenerated and shown not to be TPC-null, since the method used to silence the *Tpcn* genes only caused truncation of the protein and not complete deletion. The truncated proteins were shown to be still functional and responsive to NAADP – explaining why pancreatic islet cells from these animals still demonstrated calcium responses. Although Wang et al. showed data confirming loss of the *Tpcn* genes using Southern blotting, there was no confirmation of loss of mRNA or protein. Ruas et al. developed new DKO mice using a different method, and showed that not only did cells from these mice not respond to NAADP, but transfection with viral vectors carrying replacement TPC genes restored responsiveness (as did transfection of the truncated versions of TPCs used in the original 'DKO' experiments, confirming their functionality). The transfection of vectors carrying genes coding for TRP-ML1 were not able to restore responses to NAADP.

Additionally, transfection of a mutant TPC2 protein (E643A) that conducts a non-specific cationic current but is not permeable to calcium was unable to rescue responses to NAADP. This suggests that TPC proteins that allow non-specific (but non-calcium containing) cation flux are not adequate for a response to NAADP – a calcium current is necessary. Other experiments studying the specificity of ionic permeability of TPCs in native intact lysosomes also demonstrated a 270-fold preference for calcium over potassium and a slight preference for sodium over calcium (P_{Ca} / P_{Na} = 0.6 – 0.8). This confirmed that although several ionic species can pass through TPCs, they are not selective or specific for sodium. Furthermore, in sea urchin oocyte homogenates suspended in a sodium-free medium, calcium release can still be observed in response to NAADP.

The reason why Wang et al. were unable to elicit responses to NAADP in cells from wildtype animals remains unknown. To date, TPCs remain the most credible contenders as molecular NAADP receptors.

1.6.6 The pharmacology of substances that affect NAADP signalling

Substances that can be used to pharmacologically manipulate the NAADP signalling pathway fall into three broad groups; those that interfere with NAADP synthesis (or breakdown), those that prevent normal lysosomal function and those that disrupt NAADP binding at its receptor.

Inhibition of NAADP synthesis can be achieved using small molecule inhibitors of the CD38 / CD157 and other ARC enzymes, and also by deletion of the genes that code for these proteins. The latter approach has been shown to abolish NAADP production in pancreatic acinar cells following stimulation with CCK, and subsequently interfere with calcium signalling (Cosker et al., 2010).

Two structurally dissimilar compounds, SAN4825 and SAN2589 were identified as ARC inhibitors by high-throughput screening using porcine cardiac SR membranes, and have both been shown to possess anti-arrhythmic properties (Kannt et al., 2012). Due to the use of cardiac SR membranes, these drugs appear to inhibit a cardiac-specific ARC that is distinct from CD38 or CD157. The suggestion that a novel ARC is present in the heart is supported by the finding that CD38 knockout animals showed an attenuated rise in cADPR production, but not in NAADP production following isoprenaline stimulation (Gul et al., 2016).

There are several compounds that interfere with normal lysosomal function. Bafilomycin-A1 is a macrolide antibiotic isolated from the *Streptomyces* bacterium that inhibits the vacuolar-type H^+-ATPase. This pumps hydrogen ions into the lysosome and consequently maintains a low luminal pH. Transport of calcium ions into the lysosome depends upon this proton gradient, and inhibition of the pump by bafilomycin-A1 therefore prevents both acidification and calcium loading (Churchill et al., 2002). Lysosomes devoid of calcium are unable to respond to NAADP. Similarly, nigericin is also produced by *Streptomyces* and inhibits the K^+/H^+ exchange pump, hampering lysosomal pH regulation (Tapper et al., 1990). Ammonia can also be used to raise lysosomal pH (Churchill et al., 2002). Another compound, glycylphenylalanine 2-naphthylamide (GPN) causes selective osmotic lysis of lysosomes via inhibition of exopeptidase cathepsin C (Berg et al., 1994; Jadot et al., 1984). Since all these compounds act indirectly on the NAADP pathway by disruption of the lysosome, a reasonable criticism of their use could be lack of specificity.

There are two compounds known to act as NAADP antagonists, *trans*-Ned-19 and BZ-194. The cell-membrane permeant Ned-19 was discovered following a process using ligand-based virtual screening using a large electronic library of small molecules (Naylor et al., 2009). Following its identification and the confirmation of its inhibitory effect on NAADP-induced calcium release in sea urchin oocyte homogenates and in mouse pancreatic β-cells, the *cis*- and *trans*- stereoisomers were tested separately. In these experiments Naylor et al. (2009) showed that *trans*-Ned-19 was far more potent (IC_{50} 6 nM vs 800 nM). Ned-19 is a non-competitive and irreversible antagonist of NAADP, and it is also specific as calcium responses to cADPR and IP_3 were unaffected, as were L-type calcium

channels and mitochondrial metabolic function. Ned-19 is also fluorescent with a peak excitation wavelength of 368 nm and a peak emission wavelength of 425 nm. A variant of Ned-19, Ned-K has also been synthesised and used in one study to date (Davidson et al., 2015).

BZ-194 was synthesised following the observation that nicotinic acid was able to reduce NAADP-mediated responses when the two were co-administered. This was in contrast to nicotinamide, which had no effect. BZ-194 was therefore produced as an alkylated derivative of nicotinic acid. However, in contrast with the low nanomolar IC_{50} of *trans*-Ned-19, the IC_{50} of BZ-194 is in the micromolar range. Despite this, it did not appear to inhibit the activity of other calcium signalling molecules such as IP_3 and cADPR (Dammermann et al., 2009).

1.6.7 Extra-cardiac effects of NAADP

The NAADP/TPC signalling pathway has been studied in a wide range of plants and animals, and in a broad range of tissues. Although many aspects of this system are still being elucidated, a great deal is already known about its function.

The sea urchin oocyte was the first system in which NAADP signalling was studied, and further experiments showed that the system was important in fertilization in this species (Churchill et al., 2003; Vasudevan et al., 2010). It was subsequently also demonstrated that NAADP functions in a very similar way in human fertilization (Sanchez-Tusie et al., 2014). In mice, NAADP has been shown to act at TPC1 receptors to promote the acrosome

reaction at fertilization. *Tpcn1*$^{-/-}$ mice colonies can be difficult to generate and maintain, and this may be the reason (Galione, 2015).

NAADP has been implicated in the contraction of smooth muscle from a variety of sources and in response to several different agonists. Gastric fundus and bladder contraction in response to muscarinic agonists were shown to involve NAADP signalling, as were contractions in pulmonary, renal and coronary artery, the latter in response to endothelin-1, trachea in response to carbachol, and uterus in response to oxytocin (Aley et al., 2010; Aley et al., 2013; Boittin et al., 2002; Pereira et al., 2014; Tugba Durlu-Kandilci et al., 2010; Zhang et al., 2006).

Pancreatic function has also been extensively studied in the context of NAADP signalling (Zhao et al., 2012). Endocrine function and insulin secretion from β-cells is linked to an increase in intracellular calcium caused by NAADP signalling that can be blocked by Ned-19 (Johnson et al., 2002; Naylor et al., 2009). NAADP also plays an important role in pancreatic exocrine function, and acinar cells were the first mammalian cells in which this pathway was investigated (Cancela et al., 1999). Cholecystokinin (CCK)-induced production of NAADP was reduced in cells from animals lacking CD38 (Cosker et al., 2010), and calcium responses to NAADP are inhibited by desensitizing concentrations of NAADP (Cancela et al., 1999).

Other areas where a role for NAADP signalling has been found include haematological cells such as T-lymphocytes, natural killer cells (Berg et al., 2000; Rah et al., 2010) and platelets (Mushtaq et al., 2011), hepatocytes (Mandi et al., 2006), a variety of renal cells (Cheng et al., 2001), various tissues from the central nervous system (Bak et al., 1999;

Barcelo-Torns et al., 2011; McBrayer et al., 2013), and adipocytes (Song et al., 2012). NAADP is also involved in autophagy (Lu et al., 2013; Pereira et al., 2011), and has even been shown to be important in ebola virus infectivity (Sakurai et al., 2015).

1.6.8 The influence of NAADP on cardiac physiology

A cardiac role for NAADP has become more clear in recent years. In paced cardiomyocytes, the photorelease of NAADP from a 'caged' compound by a brief (500 ms) ultraviolet (UV) flash causes a gradual increase in both the amplitude of the calcium transient and the resting (diastolic) calcium concentration over the next minute. This occurs in both ventricular (Macgregor et al., 2007a) and atrial (Collins et al., 2011) myocytes, and could also be demonstrated using the cell membrane permeant ester of NAADP, NAADP-AM (Capel et al., 2015; Collins et al., 2011). There was no detectable effect on the L-type calcium current, but following NAADP photorelease caffeine-induced calcium liberation was increased, suggesting that NAADP causes calcium loading of the SR (Macgregor et al., 2007a). Increased spark frequency was also observed, lending weight to this idea. These effects could be blocked by concurrent use of bafilomycin-A1 or Ned-19, or by genetic deletion of *Tpcn2* (Capel et al., 2015). Additionally, inhibitors of CaMKII such as KN93 and AIP were also able to abolish the increase in calcium transient observed following NAADP photorelease, suggesting a role for this enzyme in the pathway (Capel et al., 2015).

Nebel et al. (2013) also demonstrated the release of calcium in response to NAADP in intact cardiac myocytes, and its inhibition by bafilomycin-A1. These calcium signals could also be blocked with BZ-194, ruthenium red (an antagonist of RyR) and ryanodine itself.

Similarly, the combined use of ryanodine and thapsigargin to render the SR non-functional resulted in loss of calcium signals in response to NAADP (Macgregor et al., 2007a). Bak et al. (2001) made similar observations, but used isolated cardiac microsomes; in these experiments, NAADP resulted in a calcium signal that could be prevented with bafilomycin-A1. However, antagonists of RyR were not able to prevent the signal in these experiments. Taken together, these results suggest that the SR is important in NAADP signalling in intact cells, but less so when studying isolated organelles. This may mean that structural integrity of the myocyte and aposition between lysosomes and the SR are important in physiological NAADP signalling.

NAADP synthesis seems to be linked to β-adrenergic stimulation of cardiac myocytes (Gul et al., 2016; Lewis et al., 2012; Macgregor et al., 2007a). Moreover, the increase in calcium transient and force of contraction in response to β-agonists can be significantly reduced using bafilomycin-A1 or Ned-19 (Capel et al., 2015), suggesting NAADP involvement in the β-adrenergic transduction pathway. In agreement with this idea are the results of experiments using *Tpcn2*$^{-/-}$ animals, which demonstrate reduced responses to isoprenaline in terms of calcium transient and force of contraction in comparison with their wildtype counterparts (Capel et al., 2015).

1.6.9 The influence of NAADP on cardiac pathology

There have also been several investigations regarding the potential pathological effects of NAADP in the heart. The influence of NAADP on cardiac arrhythmias, hypertrophy and ischaemia-reperfusion injury have all been examined to varying degrees:

Ventricular arrhythmias caused by SR calcium overload in isolated guinea pig papillary muscle could be prevented using the inhibitors of cardiac ARC, SAN2589 and SAN4825 (Kannt et al., 2012). The latter could also prevent arrhythmias in isolated myocytes (Warszta et al., 2014) and in vivo (Kannt et al., 2012). Similarly, the NAADP antagonist BZ-194 was also shown to abolish arrhythmias in response to stimulation by isoprenaline in both isolated myocytes and in live mice (Nebel et al., 2013), and bafilomycin-A1 increased the time taken for isolated ventricular myocytes to develop arrhythmic contractions when exposed to isoprenaline (Bolton, 2014).

Cardiac hypertrophy may also be reduced by blockade of the NAADP signalling pathway. *Tpcn2*$^{-/-}$ mice chronically exposed to isoprenaline via osmotic mini-pumps suffered less hypertrophic effects than wildtypes. Additionally, ex-vivo hypertrophied hearts from the wildtype animals displayed a higher propensity to arrhythmias than those from the knockout (Capel et al., 2015). In another study, Gul et al. (2016) demonstrated reduced isoprenaline-induced hypertrophy in hearts from CD38 knockout animals. However, Gul et al. also reiterated the finding that while cADPR seems to be produced by CD38, NAADP appears to be synthesised by a non-CD38, non-CD157 ARC. Therefore, these experiments may suggest a role for cADPR in cardiac hypertrophy as well as NAADP.

Finally, a role for NAADP was shown in hearts subjected to ischaemia-reperfusion injury. Extracellular NAADP has been shown to act at cell membrane purinergic receptors such as P2Y11 to induce intracellular NAADP production (Djerada et al., 2013a), and confer protection during ischaemia-reperfusion (Djerada et al., 2013b). In another study, the addition of the NAADP antagonist Ned-K reduced the effects of this injury in isolated cardiac myocytes, and genetic deletion of *Tpcn1* significantly reduced myocardial infarct

size in vivo. It was suggested that these effects were due to prevention of opening of the mitochondrial permeability transition pore (MPTP) by NAADP (Davidson et al., 2015).

1.7 Other calcium signalling molecules

In addition to NAADP, there are two other major calcium-mobilising messengers. These are inositol trisphosphate and cyclic ADP-ribose. Both of these substances have been shown to play an important role in the mobilisation of calcium in a wide variety of tissues, including in the heart.

1.7.1 Inositol 1,4,5-trisphosphate (IP_3)

In contrast to the GPCRs linked to $G\alpha_s$, which lead to activation of adenylyl cyclase, generation of cAMP and activation of PKA, those coupled to $G\alpha_q$ lead to activation of a different pathway. Release of $G\alpha_q$ following stimulation of the receptor leads to activation of PKC, which then cleaves phosphotidylinositol 4,5-bisphosphate (PIP_2) and generates diacylglycerol (DAG) and inositol 1,4,5-trisphosphate (IP_3) (Kockskamper et al., 2008b). The latter then acts at specific receptors on the SR membrane and nuclear envelope, which are distinct from ryanodine receptors but also release calcium (Zima et al., 2007). Examples of receptors coupled to $G\alpha_q$ include the α1-adrenergic receptor, the type-1 angiotensin-2 receptor, the type-1 histamine receptor and the endothelin receptor. In contrast to the result of the actions of PKA, IP_3 does not lead to increased activity in SERCA or enhanced loading of the SR with calcium (Kockskamper et al., 2008a).

There are three subtypes of IP_3R, with IP_3R2 being the predominant isoform expressed in the heart (Wojcikiewicz, 1995). They are expressed at a level approximately 1-10% of that of ryanodine receptors, and produce a much smaller and slower calcium release (Bers, 2001 p. 242; Kockskamper et al., 2008b; Moschella et al., 1993). Atrial abundance of IP_3R2 has been reported as six times higher than that in the ventricle (Lipp et al., 2000).

The role of IP_3 in the heart is yet to be fully elucidated. IP_3 and substances acting at $G\alpha_qPCRs$ are able to cause intracellular release of calcium leading to enhancement of the calcium transient in ventricles (Proven et al., 2006) and atria (Collins et al., 2012). However, how this relatively small increase in calcium release might be physiologically significant in the face of much larger changes in calcium concentration mediated by the far more abundant ryanodine receptor is not clear (Kockskamper et al., 2008b). Interestingly, the increase in calcium transient amplitude caused by the α1-adrenergic receptor agonist phenylephrine could be blocked by α1 receptor antagonists such as prazosin and antagonists of the IP_3R such as 2-aminoethoxydiphenylborane (2-APB), but also by adenylyl cyclase inhibitors and PKA inhibitors. This led to the hypothesis that calcium-activated adenylyl cyclases (AC1 and AC8) were responsible for enhanced PKA activity following calcium release caused by IP_3 (Collins et al., 2012).

There is also evidence that IP_3 release in the ventricle is associated with the development of arrhythmias, in response to both neurohumoral transmitters and ischaemia-reperfusion (Mackenzie et al., 2002; Proven et al., 2006; Woodcock et al., 2000).

In addition, the location of IP_3Rs on the nuclear membrane has led to the suggestion that IP_3 may be involved in the regulation of gene expression, and IP_3 mediated activation of

CaMKII has been linked to the phosphorylation of factors involved in transcription regulation such as histone deacetylase 5 (HDAC5), leading to its removal from the nucleus (Wu et al., 2006). Chronic stimulation of α1 adrenergic receptors and endothelin receptors are known to result in hypertrophic changes (Singal et al., 2004; Sugden et al., 2005).

1.7.2 Cyclic adenosine diphosphate ribose (cADPR)

As discussed above cADPR is closely related to NAADP, in that it is derived from nicotinamide-containing co-enzymes and also functions as a calcium-mobilising second messenger in a wide variety of tissues (Lee et al., 2000). The first demonstration of this was in sea urchin oocytes, where it was shown to cause calcium release that was independent of that caused by IP_3 (Clapper et al., 1987). Later, studies implicated cADPR in the potentiation of CICR via the ryanodine receptor (Lee, 1993). An interaction between cADPR and the ryanodine receptor was later confirmed, although there are still some questions regarding whether cADPR modulates it directly, or via an intermediate protein such as calmodulin or an FKBP (Lee et al., 1994a; Tang et al., 2002).

In the heart, cADPR enhances the amplitude of the calcium transient and increases the spark frequency and these effects can be prevented using competitive antagonists of cADPR such as 8-amino-cADPR and 8-bromo-cADPR (Cui et al., 1999; Iino et al., 1997). The increase in calcium transient amplitude caused by cADPR is not associated with an increase in $I_{Ca\text{-}L}$, implying that increased release of calcium from the SR is responsible (Macgregor et al., 2007b). This is consistent with the above evidence that cADPR acts at

the ryanodine receptor. An increase in SR loading was calcium was seen, but only after a prolonged (10 minute) period of observation (Macgregor et al., 2007b).

Antagonists of cADPR have also been shown to reduce the frequency of calcium waves, spontaneous action potentials, DADs, and I_{ti} caused by the presence of ouabain and isoprenaline (Rakovic et al., 1999). This finding, along with the observation that cADPR production is increased in the presence of β-adrenergic agonists (Lewis et al., 2012) suggest that the pathway may also be a future target for antiarrhythmic therapy.

1.8 Aims of this thesis

This thesis further explores the function of NAADP in the heart, and also investigates the subcellular structural specialisations of cardiac myocytes that support it. In chapters three and four, data is presented showing the effects of interruption of the NAADP signalling pathway on cardiac rhythm and growth respectively. Chapter five examines the organisation of the ventricular myocyte with respect to the lysosome using light microscopy, while chapter six presents related data from electron microscopy studies. Finally, chapter seven presents data relating to both structure and function of NAADP in atrial myocytes.

2

Methods

2.1 Generation of *Tpcn2*$^{-/-}$ mice

Two-Pore Channel-2 (TPC2)-null animals were generated using a gene trap mutation in the *Tpcn2* gene of a YHD437 strain of mouse, as described previously (Calcraft et al., 2009; Ruas et al., 2015). This work was carried out by Margarida da Silva of the laboratory of Professor Antony Galione, Department of Pharmacology, University of Oxford, and animals were kindly donated to me for work presented in this thesis.

2.2 Murine electrocardiography

Electrocardiograph (ECG) recordings were obtained from wildtype and *Tpcn2*$^{-/-}$ mice. Animals were anaesthetised using an intraperitoneal injection of tribromoethanol (approximately 250 mg.kg^{-1}). Once unconscious, transcutaneous electrodes were placed into the limbs and ECGs were recorded from lead II. LabChart software (ADInstruments Ltd, Oxford, UK) was used to make recordings and also for analysis. Parameters measured were heart rate, P-R interval, QRS duration, and QT interval. The QT interval was corrected using Bazett's formula:

$$QT_c = \frac{QT}{\sqrt{RR}}$$

2.3 Monophasic action potentials and programmed electrical stimulation

Mice anaesthetised for ECG recordings were subsequently sacrificed by cervical dislocation. Hearts were rapidly excised and cannulated via the aorta for retrograde perfusion on a constant-flow Langendorff apparatus. Perfusion was maintained at 3.5 $ml.min^{-1}$ with a warmed and gassed (37 °C, 95% O_2 / 5% CO_2 to give pH 7.4) modified Tyrode solution containing (in mM) NaCl 125, $NaHCO_3$ 25, KCl 5.4, NaH_2PO_4 1.2, $MgCl_2$ 1, glucose 5.5, $CaCl_2$ 1.8.

Monophasic action potentials (MAPs) were recorded from the epicardial surface of the left ventricle, while a second electrode delivered pacing stimuli adjacent to the ventricular septum. In order to assess the susceptibility to arrhythmia, hearts were subjected to programmed electrical stimulation (PES) first in the absence and then in the presence of 50 nM isoprenaline.

Pacing first occurred with a progressively increasing current (from 1 to 10 mA in 1 mA steps and from 10 to 35 mA in 5 mA steps). At each current amplitude, three bursts of 50 stimuli were delivered. The cycle length between stimuli was held at 20 ms and the bursts were separated by a 2 second pacing-free interval. Data were expressed as a cumulative percentage of pacing-free time during which ventricular arrhythmias were observed. A second set of experiments was then performed in which the basic cycle length was progressively reduced (from 90 to 10 ms in 10 ms steps) and the pacing current was held at 10 mA. These data were analysed using the same method.

Recordings and analysis of MAP data were performed using Spike-2 software (Cambridge Electronic Design Ltd, Cambridge, UK). Comparisons were made between wildtype and *Tpcn2*$^{-/-}$ and between hearts exposed to isoprenaline and those not exposed to isoprenaline.

2.4 Murine atrial contraction recordings

CD1 Mice were sacrificed by concussion followed by cervical dislocation. Hearts were rapidly excised and the ventricular tissue discarded. The atria were separated and fine suture was used to tether one side of each atrium to a fixed point in an organ bath, while the opposite side was connected via more suture to a tension transducer. The organ baths were filled with 20 ml modified Tyrode solution to submerge the atria and gassed with 95% O_2 / 5% CO_2.

Stretch across the atria was adjusted to give a baseline diastolic tension of 0.3 grams. The right atrium was allowed to beat spontaneously, while the left atrium was paced at 5 Hz. Tissues were allowed to settle for 20 minutes and then the bath solution was changed. Ned-19 10 μM, Bafilomycin-A1 1 μM or DMSO 0.01% were added to the bath at this point and allowed to equilibrate with the tissue for 60 minutes before the isoprenaline dose-response curve was commenced.

These experiments were also performed using YHD437 mice lacking the gene coding for TPC2 (*Tpcn2*$^{-/-}$) and their wildtype counterparts. Ned-19 and Bafilomycin-A1 were not used.

Cumulative dose-response curves to isoprenaline were obtained between 0.3 nM to 100 nM in both sets of experiments.

2.5 Rabbit ventricular cell isolation

Cardiomyocytes were isolated using a method modified from Powell (Powell *et al.*, 1980).

Male New Zealand White rabbits (6-8 weeks, approximately 1kg) were sacrificed by intravenous overdose of sodium pentabarbitone, causing asystole. The heart was then rapidly excised and washed in a zero-calcium solution containing heparin 5 U/ml. Any blood trapped in the ventricular lumens was removed. The aorta was then cannulated and the heart mounted on constant-pressure Langendorff apparatus. The heart was initially perfused for 2 minutes with a warmed (37°C) solution containing (in mM) NaCl 136, KCl 5.4, $NaHCO_3$ 12, sodium pyruvate 1, NaH_2PO_4 1, $MgCl_2$ 1, EGTA 0.04, glucose 5 that had been gassed with a mixture of 95% O_2 and 5% CO_2 to maintain pH 7.4. This solution was then replaced with an identical solution containing 0.5 $mg.ml^{-1}$ type II collagenase (Worthington Biochemical Corp, Lakewood, NJ, USA) with 100 μM $CaCl_2$ instead of EGTA, and allowed to recirculate for 30-35 minutes.

At the end of this period of digestion, the heart was removed from the Langendorff apparatus and the atria removed and discarded. The ventricles were

diced using a scalpel blade and placed into 10 ml of the collagenase-containing solution where they were mechanically agitated for five minutes.

The suspension was then filtered through a 200 μm mesh and subjected to a gentle spin (20 turns in 30 seconds) using a hand-operated centrifuge. The supernatant was discarded and the pellet resuspended in warmed Dulbecco's Modified Eagle Medium (DMEM). This procedure was then repeated in order to ensure that the residual collagenase concentration was negligible.

Cells were stored in DMEM at room temperature until use. In experiments where cells were fixed for studies of cellular structure / architecture (e.g. immunocytochemistry or electron microscopy), fixation occurred within 60 minutes of isolation.

2.6 Immunocytochemistry

Isolated rabbit ventricular cardiomyocytes suspended in DMEM were allowed to settle for 20 minutes on flamed glass coverslips. Typically, 200 μl of cell suspension was placed on each coverslip. The cells were then flooded with an excess of 4% paraformaldehyde solution, and allowed to fix for 15 minutes. After three five-minute washes with phosphate-buffered saline (PBS), the cells were then flooded with 0.2% Triton-X 100 (Sigma-Aldrich, Dorset, UK) detergent to increase permeability, and left for another 15 minutes. Blocking for 60 minutes

with 5% donkey serum was performed after a second set of washes. All these steps were performed at room temperature.

The coverslips were then placed in a humidified gas-tight container. Primary antibodies were added to 5% donkey serum to dilute, and 100 µl was placed on each coverslip. For experiments where cells were to be co-labelled with two primary antibodies, both were added to the same serum. This allowed cells to be incubated with both primary antibodies concurrently, and using the same overall volume of serum as used for cells being labelled with only one primary antibody. Control cells were incubated with 5% donkey serum alone with no primary antibody.

Primary antibody incubations were for 60 minutes at room temperature followed by overnight (approximately 14-16 hours) at 4°C.

The following day, cells were washed again before highly cross-adsorbed secondary antibodies that had been raised in donkey and conjugated with fluorescent groups were again diluted in freshly-prepared 5% donkey serum. Each coverslip was covered in 200 µl of diluted secondary antibody. Again, co-labelling was performed with both secondary antibodies incubated concurrently.

Secondary antibody incubations were for 60 minutes at room temperature followed by overnight (approximately 14-16 hours) at 4°C. All cells, and solutions containing fluorescent secondary antibodies were protected from light at all times.

Details of antibody suppliers, concentrations, species and wavelengths can be seen in the table at the end of this chapter.

On the third day, the coverslips and cells were washed again. Excess liquid was then removed from each coverslip and they were mounted on glass slides using 5 µl Vectashield Hardset mounting medium with DAPI (Vectorlabs, Peterborough, UK). When the mounting medium had begun to harden, the edges of the coverslip were sealed with nail polish.

Slides were stored in the dark at 4°C, and images were obtained within 48 hours of their preparation.

Images were taken using an Olympus Fluoview FV1200 confocal microscope.

2.7 Analysis of images obtained using immunocytochemistry

Images of cells co-labelled with antibodies against RyR2 or PLB and LAMP-2 were analysed in order to ascertain if there was a periodicity in the LAMP-2 signal, and if so how that compared to the signal from RyR2 or PLB in the same cell. The images were also analysed to measure the average distance between the SR structures and the lysosomal LAMP-2.

In the initial basic analysis, ImageJ software (http://imagej.nih.gov/ij/) was used to draw a line of interest across the cell and a plot of fluorescence intensity along the line was obtained. The frequency of this plot was then calculated by counting the number of major peaks and dividing by the distance of the line. This method was used for all three labels, RyR2, PLB and LAMP-2. Where LAMP-2 labels were analysed, the line was not drawn in a random place, but deliberately across a number of LAMP-2 signals.

In order to eliminate the bias that is apparent in this method, a different analysis technique was also employed. In the second method, the image of the cell was rotated into an orientation such that the striations of RyR2 or PLB were vertical. Thresholding was then performed to remove any background noise, and the fluorescence intensity in each individual pixel in the image was then obtained. The sum of all intensities in each vertical column of pixels was then calculated.

The column sums were then plotted in order of distance across the image to give a waveform similar to that obtained using the intensity plot in the simpler method described above. This was done for both labels in each cell (RyR2 or PLB and LAMP-2), and the two waves were overlaid. The offset between the peaks could be used as a marker for distance between the SR marker and the lysosomal marker. As well as being overlaid, the column sums were also plotted against each other to obtain a correlation between the signals.

The waveforms obtained from the column sums were also subjected to Fourier analysis to give their component frequencies in order to establish whether there

was a common dominant frequency (and therefore periodicity) between the labels.

Matlab (MathWorks, Cambridge, UK) code to perform the above analysis and mathematics was kindly written by Gary Mirams, Wellcome Trust and Royal Society Sir Henry Dale Fellow, Department of Computer Science, University of Oxford.

2.8 Live cell confocal microscopy

Isolated rabbit ventricular myocytes were incubated with either 100 μM of the fluorescent NAADP antagonist, Ned-19 for 40 minutes at room temperature, 500 nM lysotracker Red or 500 nM Lysotracker Green to label acidic compartments such as the lysosome, 10 μM tetramethylrhodamine ethyl ester (TMRE) to label mitochondria, 10 μM di-8-anepps to label the cell membrane and T-tubules, or a combination of these. Cells were then allowed to adhere to a glass coverslip and superfused with Tyrode's solution containing (in mM) 135 NaCl, 4.5 KCl, 11 glucose, 20 HEPES, 1 $MgCl_2$, $1CaCl_2$, pH 7.4.

Imaging was performed with an Leica SP5 inverted confocal microscope with a 1.25 NA, 40x oil-immersion objective lens.

Peak excitation and emission wavelengths are shown in the following table:

Compound	Excitation wavelength (nm)	Emission wavelength (nm)
Ned-19	355	415 ± 30
Lysotracker red	514	590 - 747
Lysotracker green	504	511
TMRE	549	575
Di-8-anepps	475	630

2.9 Electron microscopy

Images were prepared from samples of either ventricular tissue or isolated myocytes (n=3 animals) or atrial tissue (n=1 animal).

Rabbit ventricular cardiomyocytes isolated using the method described above, or approximately 1 mm^3 pieces of tissue from atria or ventricles were rapidly dissected. Tissue samples were placed directly in Karnovsky (Karnovsky, 1965) fixative (paraformaldehyde 4%, glutaraldehyde 5%, cacodylate buffer 80mM, pH 7.4), while cells were gently pelleted in a centrifuge before fixation. Samples were kept in fixative for 24 hours at 4°C.

Following rinsing in cacodylate buffer, 1% osmium tetroxide was used for post-fixing for a further 2 hours at 4°C. Samples were then dehydrated at room temperature, by placing in progressively higher concentrations (50%, 75%, 95%) of ethanol, before being placed in 100% propylene oxide. Embedding was performed using Spurr (Spurr, 1969) resin at progressively increasing concentrations in propylene oxide until the sample was in 100% resin. This was then heated to 65°C for 48 hours to harden.

Sections were cut to approximately 80 nm thick (Reichart Ultracut) and placed on grids for drying. Post-staining to achieve contrast was carried out using 2% aqueous uranyl acetate for 20 minutes and Reynold's (Reynolds, 1963) lead citrate for 5 minutes.

Images were obtained using transmission electron microscopy (TEM, Joel 1200EXII). Analysis and measurements were made using Gatan and ImageJ software.

Lysosomes were identified by their previously well-documented appearance; a matrix slightly more electron dense than the surrounding cytoplasm enclosed by a single lipid bilayer membrane (Fameli et al., 2014).

2.10 Western blotting

Mice, 10-15 weeks old were sacrificed by concussion followed by cervical dislocation. The heart was rapidly excised and the ventricles isolated before being submerged in liquid nitrogen. Tissue was then ground into powder using a mortar and pestle and placed into ice-cold lysis buffer containing NaCl 150 mM, Tris base 50 mM, Triton-X 100 1%, Na-deoxycholate 0.5%, Sodium dodecyl sulphate 0.1%, cOmplete protease inhibitors and PHOSstop phosphatase inhibitors (both from Roche, UK). Homogenisation was then completed using the

Precellys®24 homogeniser and brief sonication. Six wildtype and six *Tpcn2*$^{-/-}$ hearts were prepared in this way.

Protein quantification was then performed on each sample using the Bicinchoninic Acid (BCA) method with bovine albumin as a standard. Homogenates were then aliquoted and stored at -80°C until use.

On the day of use, protein homogenates were diluted using Lithium Dodecyl Sulphate (LDS) loading buffer (Thermofisher, Paisley, UK) and dithiothreitol (DTT, final concentration 50mM). A 12% acrylamide gel was used and 50 µg of protein was loaded per lane. Pageruler™ protein ladder (Thermofisher) was used to indicate molecular weight. Electrophoresis was performed at 150 Volts for 60 minutes using a mini-Protean tetra-cell system with PowerPac™ power supply (Bio-Rad, Hertfordshire, UK) in a buffer containing tris base 25 mM, glycine 190 mM, and SDS 0.1% (w/v).

Wet transfer onto Immobilion-Fl polyvinylidene difluoride (PVDF) membrane (Millipore, Hertfordshire, UK) was then performed at 300 milliamps for 60 minutes in a transfer buffer containing tris base 25 mM, glycine 190 mM and methanol 20% (v/v).

Blocking of the membrane to prevent non-specific binding of antibody was performed using 50% Odyssey TBS blocking buffer (Licor, Cambridge, UK) for 60 minutes at room temperature.

The membrane was then divided horizontally between the 36 and 55 kDa molecular weight markers. The half of the membrane with the heavier molecular weights was incubated with the primary antibody against β1-adrenergic receptor (β1-AR), while the lower half of the membrane was incubated with a primary antibody against glyceraldehyde-3-phosphate dehydrogenase (GAPDH). Incubations were overnight (14-16 hours) at 4°C. The membranes were then washed four times for ten minutes each in PBS with 0.1% Tween-20 detergent before being incubated with the secondary antibody for 60 minutes at room temperature. The membranes were then subjected to another set of washes before imaging.

Samples from each animal were blotted twice.

Membranes containing samples from three wildtype and three *Tpcn2*$^{-/-}$ mice were also incubated with antibodies using the same method as in standard experiments, but in the presence of a β1-AR antibody blocking peptide.

Imaging was carried out using a typhoon flatbed scanner with a 633 nm laser.

Analysis was performed using ImageJ software. The fluorescence density of each band corresponding to β1-AR (approximately 55 kDa) was measured and divided by the density of the GAPDH band (approximately 36 kDa). This method therefore controls for differences in the amount of protein loaded between lanes (assuming that GAPDH expression is constant). The relative densities were then compared between wildtype and from *Tpcn2*$^{-/-}$ animals: The mean measurement

of the two blots from each individual was expressed as a ratio to the mean wildtype β1-AR:GAPDH relative density.

2.11 Neonatal rat ventricular cardiomyocyte isolation and culture

Primary cardiac ventricular myocytes were isolated from 1-2 day old Sprague-Dawley rats (Charles River Laboratories, UK). For each culture, a litter of pups (approximately 12 individuals) was sacrificed by cervical dislocation and decapitation. Hearts were rapidly excised under aseptic conditions and placed in an ice-cold, filtered (0.22 μm) preparation buffer containing (in mM) NaCl 106, HEPES 20, NaH_2PO_4 0.8, glucose 5, KCl 5.3, $MgSO_4$ 0.4 with pH adjusted to 7.4. Non-ventricular tissue was dissected away and discarded.

The ventricles were then cut into 1 mm^3 pieces before being transferred into 9 ml fresh buffer at 37 °C with 0.45 $mg.ml^{-1}$ type A collagenase (Roche, UK) and 1.25 $mg.ml^{-1}$ pancreatin (Sigma-Aldrich, UK). The pieces were agitated in a water bath for five minutes before being triturated using a 10 ml pipette. The buffer was then removed and discarded, as at this stage it is likely to be rich in connective tissue and fibroblasts.

Fresh digestion buffer (9 ml) was then added along with 1 ml newborn calf serum and the pieces agitated for 20 minutes. This buffer was then removed from the remaining large pieces of tissue and centrifuged at 1250 rpm for five minutes. The supernatant was then discarded and the pellet – containing the

cells – resuspended in 2 ml newborn calf serum and stored at 37 °C. Further fresh digestion buffer was then added to the undigested pieces of ventricle, and the procedure repeated until all pieces of ventricle were fully digested.

At this point, the cell suspensions from each digestion were amalgamated and centrifuged again at 1250 rpm for five minutes. The supernatant was discarded and the pellet resuspended in first-day medium containing DMEM 67%, M-199 17%, horse serum 10%, newborn calf serum 5%, Glutamine 1% and Penicillin/Streptomycin 0.1%. The volume used was 2 ml per heart.

This suspension was then divided onto several plastic petri dishes (one dish for every five hearts) and incubated at 37 °C for two hours. This step allows non-myocytes (e.g. fibroblasts and endothelial cells) to adhere to the plastic, leaving the myocytes in suspension. After two hours the suspension was removed from the petri dishes, which were discarded.

The suspension was then centrifuged again at 1250 rpm for 5 minutes and the pellet resuspended in fresh first-day medium. A small (20 µl) sample was taken and diluted by 10 times and placed on a counting chamber, allowing quantification of the density of cells in the suspension. Only well-rounded bigger cells with a well-defined dark membrane and clear cytoplasm were counted.

The density of cells in the suspension was then adjusted to approximately $3x10^5$ cells per ml, plated on laminin-coated coverslips, and incubated at 37°C in an atmosphere containing 95% air and 5% CO_2.

Twenty-four hours later, the first-day medium was removed and cells were washed in warmed preparation buffer. This was then replaced with second-day (serum-free) medium containing DMEM high glucose 75%, M-199 17%, glutamine 1%, penicillin/streptomycin 0.1% and insulin-transferrin-selenium-X supplement. The cells were then allowed to rest for at least two hours before the addition of drugs (DMSO 0.01%, isoprenaline 10μM, Ned-19 1 – 10 μM, bafilomycin-A1 100 nM – 1 μM, noradrenaline 10 μM, or combinations of these). Cultures were then maintained at 37°C in an atmosphere of 95% air and 5% carbon dioxide for 48 hours.

2.12 Analysis of cultured cells: size and viability measurements

After 48 hours, each culture was visualised under an Olympus IX71 inverted microscope using a 60x oil objective lens. 12-15 images of random areas of each culture were taken using Metamorph software (Molecular Devices, Berkshire, UK). The cross-sectional areas of the myocytes in these images were then measured using ImageJ software by drawing a region of interest around each cell and counting the number of pixels within them. Each pixel corresponds to 0.1075 μm^2 using this system. The investigator performing photography and measurements was blinded to the culture conditions.

A differential interference contrast (DIC) microscope was also used to obtain images of the cells for illustrative purposes.

Cell viability was measured after 24 and 48 hours of exposure to the different culture conditions using a modifed tetrazolium compound. CellTiter 96 Aqueous One Solution (Promega, Southampton, UK) reagent was added to cells cultured in a 96-well plate and incubated for two hours in the standard culture conditions described above, as per the manufacturer's instructions. Spectrophotometry was then used to record the absorbance of light at 490 nm by each well, and this was used as a marker of cell viability, with higher absorbance reflecting a higher proportion of viable cells.

Absorbance measurements taken at 24 and 48 hours were normalised to the mean control culture (DMSO 0.01% alone) at that time.

2.13 Analysis of cultured cells: RNA isolation and measurement

Protein synthesis is the process by which cells manufacture new protein. DNA is made up of genes that contain code for making proteins and each gene codes for a single peptide. However, not all of the DNA within a gene is translatable. The areas of DNA that contain peptide code are known as exons, but they are interspersed with areas that do not need to be included in the peptide that are known as introns. When a cell needs to increase the amount of a protein, gene expression is upregulated. The first step in this procedure is transcription, which is the process of making a messenger RNA (mRNA) copy of the gene. Only the gene exons are transcribed, so the mRNA strand does not include any non-coding

portions. The mRNA is then translated into a peptide by the sequential binding of amino acids as dictated by the code.

In order to quantify the expression of genes associated with cardiac hypertrophy, the Taqman® real-time quantitative polymerase chain reaction (qPCR) system was used. This is a method of amplifying specific pieces of DNA to allow the calculation of their relative abundance in experimental samples.

In the first step of this system, mRNA is isolated from the cell or tissue sample, and a viral enzyme called reverse transcriptase makes a DNA copy of the mRNA. This copied DNA (cDNA) differs from the DNA native to the sample in two important respects; it is single stranded and it only contains the coding exons. All the mRNA in the sample will be copied, so the population of cDNA represents all the genes that are expressed by the sample.

The cDNA is then incubated at 50°C with short strands of DNA called primers that are specific complimentary sequences for parts of the gene of interest. At this temperature, they bind to one end of the relevant strands of cDNA. Importantly, these primers span the end of one exon and the beginning of the next so that they cannot bind to the native DNA due to obstruction by introns. This means that only cDNA is amplified.

In the Taqman system, the primers have a fluorescent reporter molecule and a quencher molecule bound to them. The reporter and the quencher are in close proximity, such that the photon emitted by the reporter as fluorescence is

absorbed by the quencher. Therefore, in the resting state the overall fluorescence signal is very low.

In the presence of a mix containing an excess of DNA bases, the temperature is then increased to 72°C and another enzyme called polymerase synthesises an exact complimentary copy of the cDNA strand starting at the primer. Because the primers only bind to the genes of interest, only the cDNA strands coding these genes are amplified. As polymerase binds to the primer to begin elongation and synthesis of the new DNA strand, it cleaves the bond between the fluorescent reporter and the quencher, causing fluorescence to increase.

Once the synthesis is complete, the resulting double-stranded DNA is 'melted' (i.e. separated into two single strands again) by increasing the temperature to 95°C. The temperature is then reduced back to 50°C, allowing more primer to bind to the single strands and the 50°C, 72°C, 95°C cycle starts again.

Each strand of cDNA is copied once in each cycle, and therefore the overall amount of cDNA for the gene of interest doubles in every cycle. In turn, this means that the fluorescence signal also doubles in every cycle.

If the gene of interest was expressed at low levels, then there will be small amounts of mRNA and small amounts of cDNA at the start of the process. The number of cycles of PCR required to get to a particular ('threshold') level of fluorescence will therefore be greater than if the gene was highly expressed and there was a large amount of mRNA in the original sample.

By observing the fluorescence of the reaction in real time, the point at which the fluorescence crosses the threshold (Ct) can be recorded. The Ct is the number of cycles that were needed to reach threshold, and if sample A (which was treated with a drug) reached threshold four cycles before sample B (which was not), then the abundance of the mRNA for the gene of interest must be 16 times higher in sample A than in sample B (2^4=16). In other words, the drug caused a 16-fold increase in the expression of the gene.

It is difficult to ensure that the size of the original samples are exactly the same. Therefore, it may seem that the expression of the gene of interest is higher in one sample than the other, simply because that sample was bigger, rather than because the expression was increased. In order to account for this, a reference gene whose expression is known not to alter in response to the drug treatment is often used: Two different primers with different coloured fluorescence can be used in the same sample to amplify the reference gene and the gene of interest respectively. The Ct value for both can then be measured, and the difference between them is known as ΔCt. If ΔCt is then measured for both sample A and sample B, then the relative expression of the gene of interest between the two samples is $\Delta Ct_a - \Delta Ct_b$.

In the experiments presented here, total RNA was extracted from cultured cells using an RNeasy® Mini Kit (Qiagen, Manchester, UK) and quantified using a NanoDrop Lite spectrophotometer (Thermo Scientific, UK). Generation of cDNA

was conducted using a QuantiTect® Reverse Transcription Kit (Qiagen) according to manufacturers instructions.

To quantify expression of Atrial Natriuretic Peptide (ANP) and α-actin in each culture, the Taqman® Gene Expression Assays Rn00664637_g1 and Rn01641150_m1 respectively were used (Thermofisher, UK). The reference gene used to normalise the expression of both ANP and α-actin was GAPDH (Rn01775763_g1). Real-time PCR reactions were prepared using Platinum Quantitative PCR SuperMix (Invitrogen) and performed in a 7300 real-time PCR system (Applied Biosystems).

2.14 Suppliers, solutions, drugs, reagents and consumables

All salts for solutions, isoprenaline, noradrenaline, DMSO, and TritonX-100 were obtained from Sigma-Aldrich, UK. Solutions were made using double-deionised water with a resistivity of 18 MΩ.cm from a Millipore MilliQ Biocel CT water processor.

Consumables for western blotting were as follows: NuSep precast protein electrophoresis gels, 12% acrylamide, Generon, UK, CatNo: NG21-012. Immobilion-Fl PVDF membrane, Millipore, UK, CatNo: IPFL10100. TBS blocking buffer, Licor, Cambridge, UK.

Animal sera, DMEM, M-199, Pen/strep, lysotracker, TMRE and Taqman ® assays were purchased from Thermofisher, UK.

Ned-19 and bafilomycin-A1 were obtained from Tocris Biotechne, Abingdon, UK. RNeasy® RNA quantification minikit and QuantiTect® reverse transcriptase kits were purchased from Qiagen, Manchester, UK.

2.15 Table of Antibodies

Primary Antibodies			
Target & technique	Supplier & catalogue number	Species & clonality	Dilution
LAMP-2 ICC	Thermofisher PA1-655 (Lot: PA189864)	Rabbit polyclonal	1:100
Type-2 Ryanodine receptor ICC	Abcam ab2827	Mouse monoclonal	1:100
Phospholamban ICC	Abcam ab2865	Mouse monoclonal	1:100
β1-adrenergic receptor WB	Alomone labs AAR-023	Rabbit polyclonal	1:500
Glyceraldehyde-3-phosphate dehydrogenase (GAPDH) WB	Abcam ab181602	Rabbit monoclonal	1:5000
Secondary Antibodies			
Target & technique	Supplier & catalogue number	Conjugate & wavelength	Dilution
Anti-rabbit ICC	Thermofisher A-21206	AlexaFluor-488 nm	1:1000
Anti-mouse ICC	Newmarket Scientific AS12-1935	Dylight-555 nm	1:1000
Anti-rabbit WB	Newmarket Scientific AS12-2034	Dylight-633 nm	1:1000

2.16 Animals

Unless otherwise stated, animals were sourced from Harlan Laboratories, UK. All procedures involving animals described here were performed in accordance with Schedule-1 of the Animals (Scientific Procedures) Act 1986 (HMSO).

2.17 Statistics

Statistical comparisons of groups of data sampled from normally distributed populations were made using parametric tests. Student's paired or unpaired t-tests were used when two groups were being compared and Analysis of Variance (ANOVA) was used when more than two groups or repeated measures at more than two points were compared. One-way and two-way ANOVA were used when one (e.g. isoprenaline dose) or two (e.g. isoprenaline dose and genotype) variables were being manipulated respectively.

If a significant effect was detected using ANOVA, post-hoc testing using Tukey's method (when the mean of every group is compared to the mean of every other group) or Bonferroni's method (when the means of particular groups were selected for comparison) were used.

In cases where it was thought that data was sampled from non-Gaussian populations, a non-parametric test was employed. Either a Mann-Whitney test (for two groups) or a Kruskal-Wallis test (for more than two groups or repeated

measures at more than two points) were used. If a significant effect was detected using a Kruskal-Wallis test, a post-hoc Dunn correction was used.

Post-hoc tests were used to correct for the problem of multiple comparisons. A p-value is the probability of seeing a difference between the two groups being compared that is at least as big as the difference that was actually observed in the experiment, if in fact the two groups are the same. The arbitary cut-off where this probability is said to be low enough to declare that the difference between the groups is 'significant' is known as alpha – usually set to 0.05 or 5%. There is therefore a 95% chance of correctly rejecting the null hypothesis (that there is no difference between the groups) when p=0.05 following a single comparison of two groups.

However, if two comparisons are made, and both p-values are calculated at 0.05 then the chance of correctly rejecting both null hypotheses is 0.95 x 0.95 = 0.9025. In other words there is a 1 – 0.9025 = 0.0975 = 9.75% chance of incorrectly rejecting at least one of the null hypotheses. As more comparisons are made, this chance increases (= $1 - 0.95^n$, where n is the number of comparisons). At the point where 13 comparisons are made, there is an approximately 50% chance of incorrectly rejecting the null hypothesis in at least one of the comparisons, and where 60 comparisons are made the chance of incorrectly rejecting the null hypothesis at least once is almost inevitable (95%). The post-hoc corrections are mathematical methods of accounting for this problem, and deliver amended p-values that are adjusted for the number of comparisons.

P-values of less than 0.05 were considered significant. Exact p-values are given except when they are less than 0.0001 or greater than 0.05. Values where $0.01 \leq p < 0.05$ are indicated by *, $0.001 \leq p < 0.01$ are indicated by **, $0.0001 \leq p < 0.001$ are indicated by *** and $p < 0.0001$ are indicated by ****.

Data are expressed as mean ± standard error of the mean (SEM) for normally distributed data, and median with inter-quartile range (IQR) for non-parametric or skewed data. Outliers were identified using ROUT analysis with Q=1%. Pearson's product-moment correlation coefficient (r) was calculated to give the degree of correlation between two variables.

All statistical calculations and analysis were performed using Prism 6 software (Graphpad Software Inc., California, USA).

3

Cardiac arrhythmias induced by acute adrenergic stimulation: Involvement of TPC2

3.1 Introduction

Preservation of normal cardiac output is ensured by the co-ordinated and regular depolarisation and contraction of the myocardium. Every atrial contraction is followed by a contraction of the ventricle and every ventricular contraction is preceded by an atrial one. This is known as sinus rhythm, and each heart beat in this scheme is initiated by the sinus node pacemaker in the right atrium. Deviations from this pattern are known as arrhythmias, and they are often triggered by mechanisms that involve abnormal calcium handling.

Well-recognised arrhythmogenic triggers include delayed after-depolarisations (DADs), which are inextricably linked with overloading of the sarcoplasmic reticulum (SR) with calcium (Bers, 2001; Wagner et al., 2015). A very high SR luminal calcium concentration causes an increased open probability of ryanodine receptors which may result in spontaneous calcium release from the SR into the cytoplasm (Wagner et al., 2015). This has two major consequences: The first is activation of the transient inward current (I_{ti}) which is mostly carried by the sodium-calcium exchange (NCX), although there are also smaller contributions from calcium-activated chloride channels and from a calcium-activated non-specific cation channel, depending on which species is being studied (Bers, 2001 p. 297.). The NCX allows three Na^+ ions to enter the cell for every Ca^{2+} ion extruded, resulting in a net inward movement of charge (Shattock et al., 2015). The I_{ti} therefore results in an after-depolarisation of the cell membrane, and possibly leads to an action potential if the threshold membrane potential is reached. The second consequence of spontaneous calcium release

from the SR is activation of the contractile apparatus, leading to an 'after-contraction'.

If the DAD is propagated to adjacent cells, a whole-heart ectopic premature beat may occur (Myles et al., 2012). If this is combined with pathological processes, such as genetic abnormalities of ion channels, ischaemia, or areas of myocardium that are scarred (e.g. post infarction), it is possible that the propagating DAD may interact with a 'normal' sinus depolarisation, re-activating areas of recently-repolarised myocardium and predisposing to reentrant patterns of impulse propagation and more serious, possibly lethal arrhythmias (Pogwizd et al., 2001; Wagner et al., 2015).

The activation of β-adrenergic receptors is likely to compound these factors further due to intracellular enzyme cascades that are triggered following receptor stimulation. These can have several consequences, including phosphorylation of phospholamban (PLB) by activated protein kinase A (PKA) at Serine-16 and by calmodulin-dependent protein kinase II (CaMKII) at Threonine-17 (Bers, 2002; Stammers et al., 2015). Consequently, there is increased loading of the SR with calcium because of the removal of the inhibition of the Sarco-Endoplasmic Reticulum Calcium ATPase (SERCA). This allows an increased amount of calcium to be pumped into the SR at the end of systole. The activation of PKA also leads to an increase in open probability of the ryanodine receptor for any given SR luminal calcium concentration (Bers, 2002; Bers, 2006). At low levels of β-adrenergic stimulation, these mechanisms lead to positive inotropic and lusitropic effects that characterise the sympathetic flight-

or-fight response, and are physiologically beneficial. However, at high levels of β-adrenergic stimulation, they may lead to DADs and be arrhythmogenic (Bers, 2001; Levy, 1989; Wagner et al., 2015).

Some of the downstream effects of β-adrenergic stimulation are likely to be the result of the action of NAADP. There is good evidence that cardiac production of NAADP is increased when the heart is exposed to isoprenaline (Gul et al., 2016; Lewis et al., 2012; Macgregor et al., 2007). Application of NAADP into the cytoplasm of isolated cardiomyocytes in the absence of β-adrenergic stimulation (either using a cell-permeant ester or photorelease from a caged compound) has been shown to increase calcium spark amplitude and frequency and also to increase the amount of calcium released from the SR in response to caffeine (Macgregor et al., 2007). These are both indicators of increased SR calcium loading. NAADP also causes an increase in the calcium transient amplitude in these cells, an effect that appears to be dependent on the presence of functional CaMKII (Capel et al., 2015). Also in isolated myocytes, antagonists of NAADP such as Ned-19, interference with lysosomal function with bafilomycin-A1 or knockout of the Two-Pore Channel-2 (TPC2) protein have been shown to attenuate the increase in calcium transient and contraction amplitude seen following exposure to isoprenaline (Capel et al., 2015).

There is a large body of compelling evidence that TPCs conduct calcium ions and act as the receptor for NAADP (Pitt et al., 2016). Three groups simultaneously converged on this idea in 2009 (Brailoiu et al.; Calcraft et al.; Zong et al.), and although there have been challenges (Cang et al., 2013; Wang et al., 2012), TPCs

remain strong candidates for likely NAADP receptors, and are conductors of calcium ions (Pitt et al., 2016; Ruas et al., 2015). The evidence is discussed in more detail in chapter 1.

As an overall scheme, it has been suggested that NAADP causes release of calcium from lysosomes by acting at TPC2; this calcium then stimulates ryanodine receptors on adjacent SR and results in calcium-induced calcium release. The lysosomal calcium may also activate CaMKII which is also known to phosphorylate PLB to relieve its inhibition of SERCA, and also to phosphorylate the ryanodine receptor to increase open probability, thereby leading to an enhancement of the overall calcium transient. This 'trigger' or 'modulator' hypothesis is postulated to be the mechanism by which NAADP contributes to the β-adrenergic response in the heart (Capel et al., 2015).

An interesting addition to this scheme has also been suggested: ADP-ribosyl cyclases (ARCs) such as CD38 are the enzymes thought to be responsible for the synthesis of NAADP and the related calcium signalling molecule, cyclic ADP-ribose (cADPR). Following experiments using ARC inhibitors and temporal analysis of NAADP and cADPR production, it has been suggested that cADPR may act as an intermediary between NAADP and the SR, its synthesis being promoted by NAADP (Gul et al., 2016). It is possible that both molecules could then act at different targets on the SR.

Given the evidence suggesting that NAADP and TPC2 are integral parts of the downstream pathway following activation of the β-adrenergic receptor, and

given that β-adrenergic stimulation is known to be arrhythmogenic under certain conditions, it was hypothesised that NAADP and TPC2 may also play a role in arrhythmogenesis.

Some evidence to this effect already exists: Nebel et al. (2013) looked at the arrhythmogenicity of isoprenaline on isolated murine ventricular cardiomyocytes and on hearts in vivo in the presence or absence of another antagonist of NAADP, BZ194. In both of these contexts, the addition of BZ194 reduced the number of isoprenaline-induced arrhythmias. Similar results have been found in guinea pig cardiomyocytes using bafilomycin-A1 (Bolton, 2014), and in other experiments, Capel et al. (2015) found that hearts from *Tpcn2*$^{-/-}$ mice that had been chronically exposed to isoprenaline were less likely to develop arrhythmias during burst pacing than their wildtype counterparts.

It was therefore hypothesised that as well as being less susceptible to the chronic effects of β-adrenergic stimulation, hearts from *Tpcn2*$^{-/-}$ mice may also be acutely less susceptible to isoprenaline-induced arrhythmias. Experiments in this chapter were designed to evaluate this possibility.

3.2 Results

3.2.1 No difference was detected in expression of β1-adrenergic receptor protein between wildtype and *Tpcn2*$^{-/-}$ mice.

Due to the possibility that differences in response to β-adrenergic agonists between wildtype and *Tpcn2*$^{-/-}$ hearts are due to differences in expression of the β_1-adrenergic receptor protein between these genotypes, quantitative western blotting was performed to detect levels of this protein.

Blots of protein from wildtype and knockout mouse ventricles were each performed in duplicate and probed for β_1-adrenergic receptor protein and a control protein, in this case glyceraldehyde-3-phosphate dehydrogenase (GAPDH). Representative blots from each mouse are shown in figure 3.1.

The density of each β_1-adrenergic receptor band relative to the corresponding GAPDH control band was measured and the result normalised to the mean wildtype result. No significant difference was detected between the two genotypes ($P>0.05$, Unpaired Student's t-test, $n=6$). There was a slight (less than 1.4-fold) non-significant increase in expression seen in the knockout (see figure 3.2).

3.2.2 Electrocardiograph parameters between wildtype and *Tpcn2*$^{-/-}$ mice do not differ, but a small difference in resting heart rate was detected.

As part of the investigation into the hypothesis that wildtype mice and those lacking the Tpcn2 gene had different susceptibility to ventricular arrhythmias, the resting ECG from live anaesthetised animals was analysed. Any differences in electrocardiographic phenotype may give important clues regarding the influence of the Tpcn2 gene on cardiac physiology.

Figure 3.3 shows representative electrocardiograph traces from one wild type (panel A) and one *Tpcn2*$^{-/-}$ (panel B) mouse. Markers along the x-axis can be seen that show different events as detected by LabChart software.

When the ECGs were analysed, no significant differences could be detected in PR-interval, QRS duration, or QT interval regardless of whether Bazett's correction was applied ($P>0.05$, one-way ANOVA with Tukey's multiple comparisons test, n=9). The mean data is shown in figure 3.4.

Wildtype heart rates were 56±11 beats per minute faster than those from *Tpcn2*$^{-/-}$ animals ($P=0.0003$, one-way ANOVA with Tukey's multiple comparisons test, n=9). Mean heart rates were 482±19 beats per minute in wildtype compared with 426±18 beats per minute in the *Tpcn2*$^{-/-}$ animals, a difference of 13% (mean data is shown in figure 3.5).

3.2.3 No difference was detected in monophasic action potential (MAP) duration between wildtype and *Tpcn2*$^{-/-}$ mice.

While ECGs were recorded in live anaesthetised mice, MAP recordings were made from isolated hearts perfused via Langendorff apparatus. Recording electrodes were placed on the epicardial surface of the left ventricle while pacing occurred via a nearby electrode positioned adjacent to the ventricular septum.

MAPs were analysed to measure their duration at 10%, 50% and 90% of repolarisation (APD-10, APD-50 and APD-90 respectively) both before and after exposure to isoprenaline 50 nM. Pacing frequency was held constant. Mean data is shown in figure 3.6. No significant differences were found between wildtype and knockout hearts ($P>0.05$, two-way ANOVA with Bonferroni's multiple comparisons test, n=6).

3.2.4 No difference in susceptibility to ventricular arrhythmias was detected between hearts from wildtype and *Tpcn2*$^{-/-}$ mice in the absence of β-adrenergic mediated stress.

Susceptibility to arrhythmias was tested in hearts from wildtype and *Tpcn2*$^{-/-}$ animals using two different pacing protocols. In the first protocol, pacing current amplitude was held constant while the basic cycle length of the pacing stimulus

was progressively reduced. In the second protocol, the cycle length was held constant while the current amplitude was progressively increased.

A set of three trains of fifty stimuli was delivered at each cycle length or current amplitude and a two second pause in pacing was left between trains. The cumulative proportion of this pacing-free time in which ventricular arrhythmias was observed is shown in figures 3.7 (varying cycle length) and 3.8 (varying current amplitude).

In these experiments, a small increase in arrhythmias was seen at low basic cycle lengths, but this was not significant ($P>0.05$, two-way ANOVA, $n=10$). There was also no significant difference in arrhythmias between wildtype and *Tpcn2*$^{-/-}$ hearts when provoked by increasing pacing current.

3.2.5 Hearts from *Tpcn2*$^{-/-}$ mice were protected against ventricular arrhythmias compared with wildtypes when exposed to β-adrenergic stimulation.

The same protocols were repeated in the presence of high-dose (50 nM) isoprenaline.

Using the increasing pacing current protocol, the additional stress of β-adrenergic stimulation provoked an increase in ventricular arrhythmias in the wildtype ($P=0.0005$, 2-way ANOVA, $n=7$), but not in hearts from *Tpcn2*$^{-/-}$ mice,

which were protected from the effect of isoprenaline (P>0.05, 2-way ANOVA). This data is shown in figure 3.9.

No increase in arrhythmias was observed in either wildtype or knockout using the reducing cycle length protocol following addition of isoprenaline (P>0.05, 2-way ANOVA, n=9). Mean data is shown in figure 3.10.

In the presence of isoprenaline, hearts from *Tpcn2*$^{-/-}$ mice were therefore significantly protected from arrhythmias provoked by the increasing pacing current protocol compared with wildtypes (P=0.0002, two-way ANOVA). There was also significant protection from arrhythmias between wildtype and knockout hearts using the reducing cycle length protocol (P=0.0146, two-way ANOVA). These comparisons are shown in figures 3.11 and 3.12.

Representative pacing bursts and MAP recordings from the increasing pacing current protocol can be seen in figure 3.13.

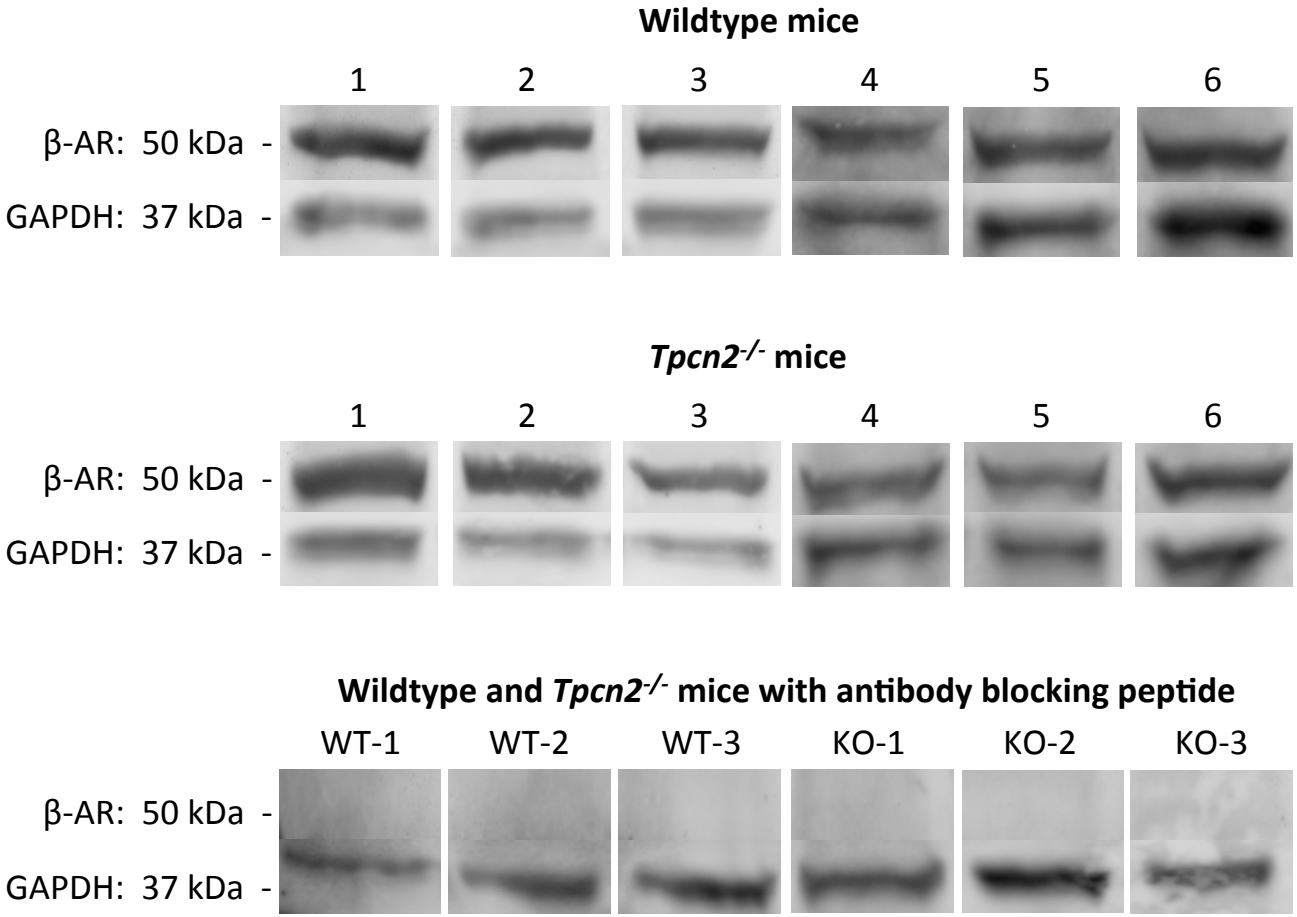


Figure 3.1: Western blots of β1-adrenergic receptor protein with GAPDH loading controls in wildtype and *Tpcn2*$^{-/-}$ mice. Top and middle panels show example blots from wildtype and *Tpcn2*$^{-/-}$ mice respectively. Samples from each animal were blotted twice (only one of each is shown above – please see appendix A for whole membranes). The bottom panel shows blots from three wildtype and three *Tpcn2*$^{-/-}$ mice when the β1-adrenergic receptor antibody was pre-incubated with blocking peptide.

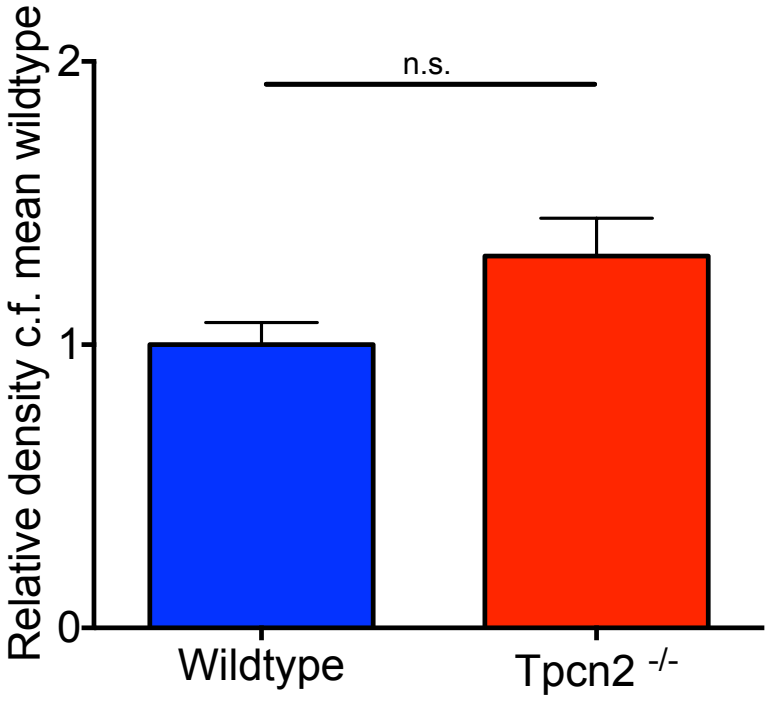


Figure 3.2: Expression of β1-adrenergic receptor protein in wildtype and *Tpcn2*$^{-/-}$ mice as detected in western blotting. There was no significant difference between expression of β1-adrenergic receptor between the two genotypes (P>0.05, unpaired Student's t-test, n=6 for both groups).

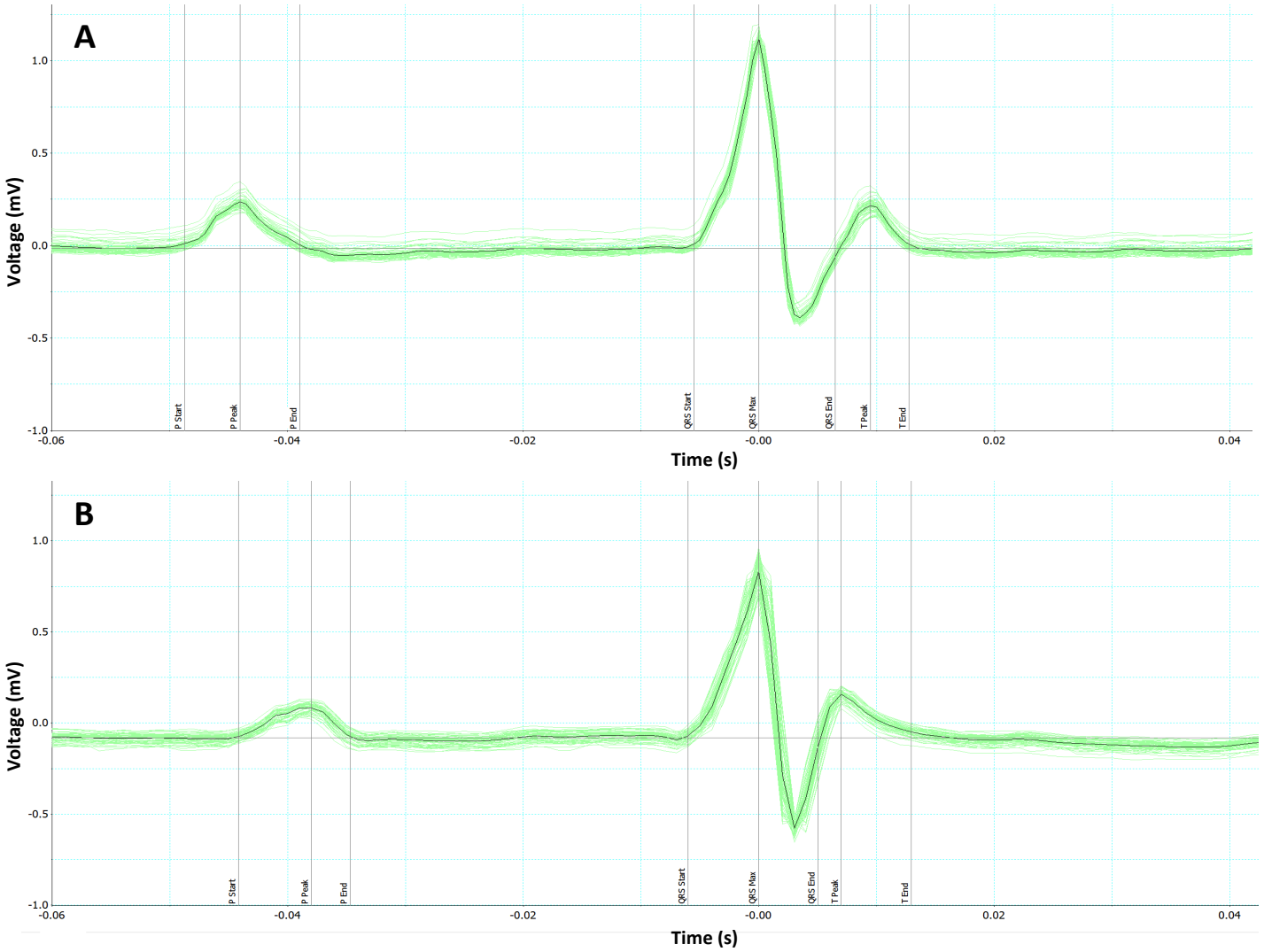


Figure 3.3: Representative electrocardiograph tracings from A, wildtype and B, *Tpcn2*$^{-/-}$ mice. Each trace shows an average (black line) of fifty individual cardiac cycles (green lines). Markers along the time axis indicate times at which different events were detected using LabChart ECG analysis software. Recordings were made from live anaesthetised mice.

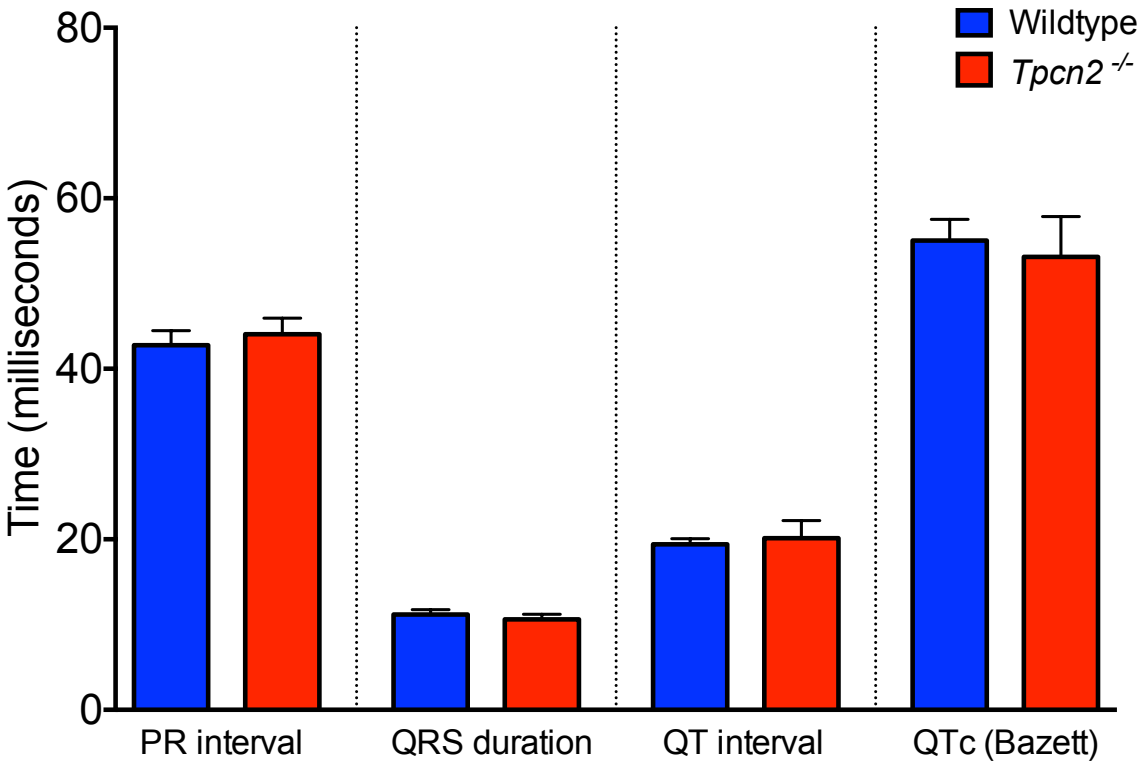


Figure 3.4: Resting electrocardiograph parameters from live anaesthetised wildtype and *Tpcn2*$^{-/-}$ mice. QT intervals were corrected for heart rate using Bazett's formula. No significant differences were found between the groups for any parameter ($P > 0.05$, one-way ANOVA, n=9 for both genotypes).

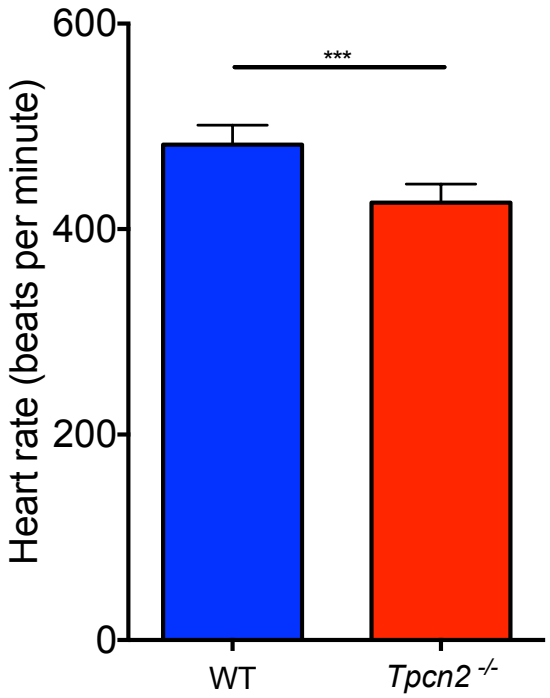


Figure 3.5: Resting heart rates taken from electrocardiograph recordings of live anaesthestised wildtype and *Tpcn2*$^{-/-}$ mice. Wildtype heart rates were 56±12 beats per minute faster than those in *Tpcn2*$^{-/-}$ mice (P = 0.0003, one-way ANOVA with Tukey's post-hoc testing, n=9).

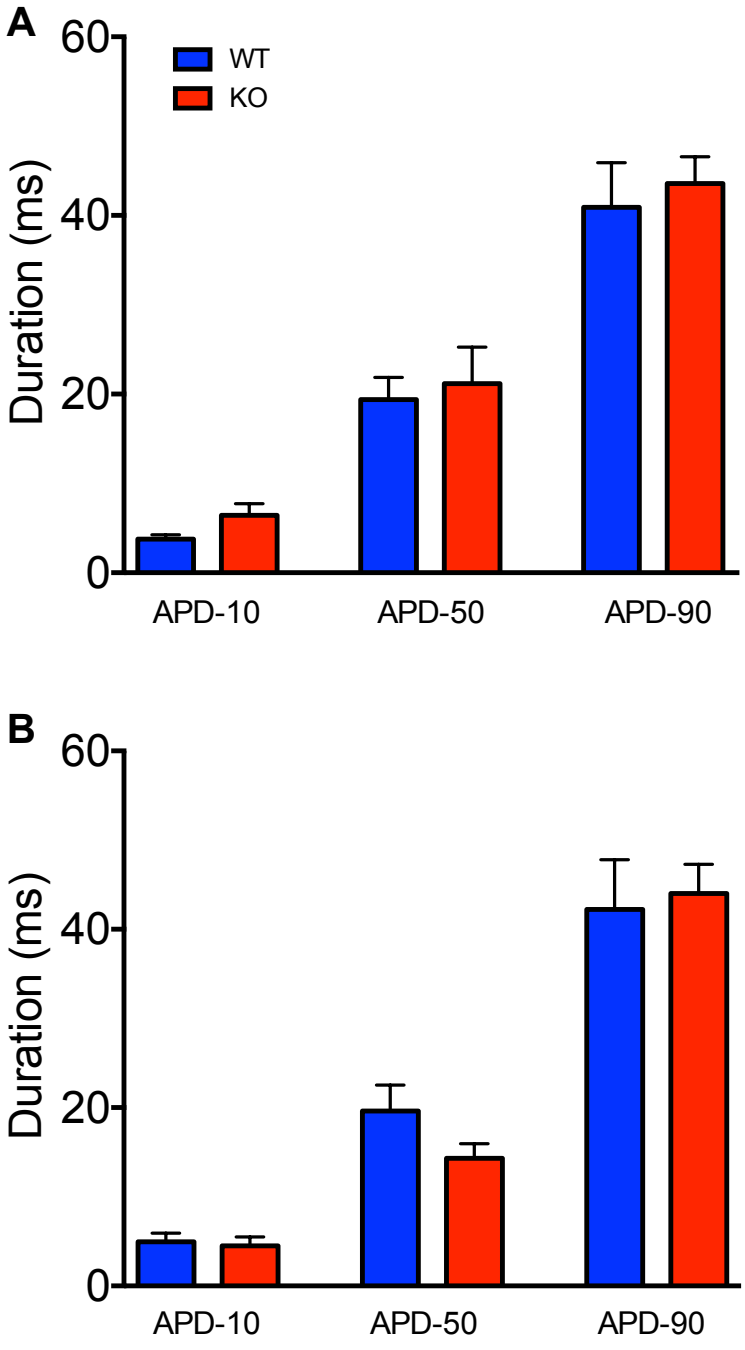


Figure 3.6: There is no significant difference in duration of monophasic action potentials (MAPs) between wildtypes and *Tpcn2*$^{-/-}$ mice. MAPs were recorded from the epicardial surface of the left ventricle of hearts mounted on and perfused using Langendorff apparatus. Action potentials were recorded from each heart first in the absence of isoprenaline (panel A) and then in the presence of 50nM isoprenaline (panel B). ($P>0.05$, two-way ANOVA with Bonferroni's multiple comparisons test, n=6 for each group).

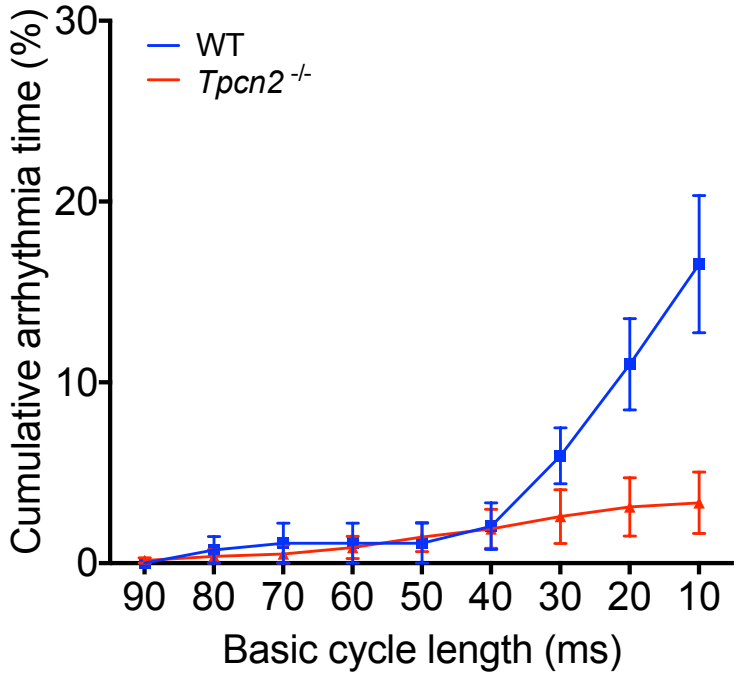


Figure 3.7: Cumulative ventricular arrhythmia time (VT or VF) in isolated hearts from wildtype and *Tpcn2*$^{-/-}$ mice. Hearts perfused via Langendorff apparatus were subjected to a burst pacing protocol. A set of three trains of fifty stimuli were delivered to the heart with a pause of two seconds between each train. The cycle length between stimuli was varied after each set of trains from 90 ms down to 10 ms. The proportion of pacing-free time in which re-entrant ventricular arrhythmias were observed was recorded cumulatively and is summarised above. Arrhythmias were observed at low cycle lengths, but there was no significant difference between wildtypes and *Tpcn2*$^{-/-}$ hearts ($P>0.05$, two-way ANOVA, n=10 in both groups).

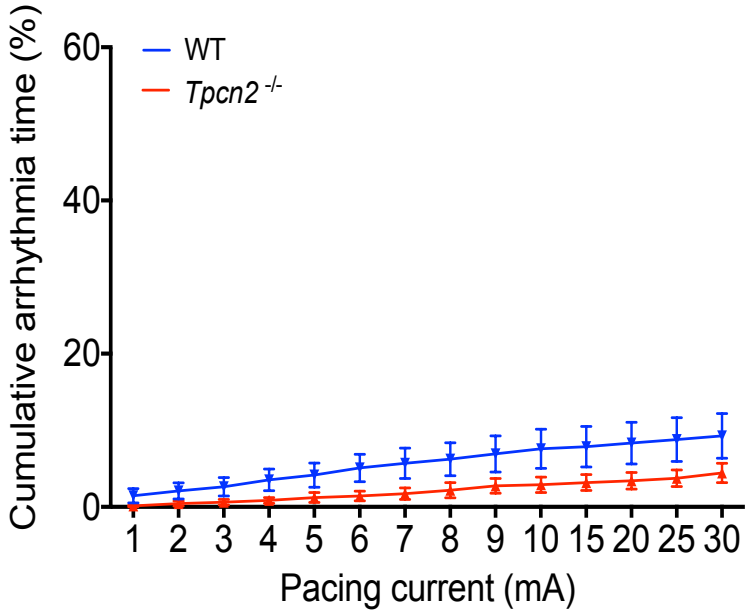


Figure 3.8: Cumulative ventricular arrhythmia time (VT or VF) in isolated hearts from wildtype and *Tpcn2*$^{-/-}$ mice. Hearts perfused via Langendorff apparatus were subjected to a burst pacing protocol. A set of three trains of fifty stimuli were delivered to the heart with a pause of two seconds between each train. The stimulus current was increased after every set of trains from 1 to 30 mA. The proportion of pacing-free time in which re-entrant ventricular arrhythmias were observed was recorded cumulatively and is summarised above. No significant difference between wildtype and *Tpcn2*$^{-/-}$ was observed ($P>0.05$, two-way ANOVA, n=10 in both groups).

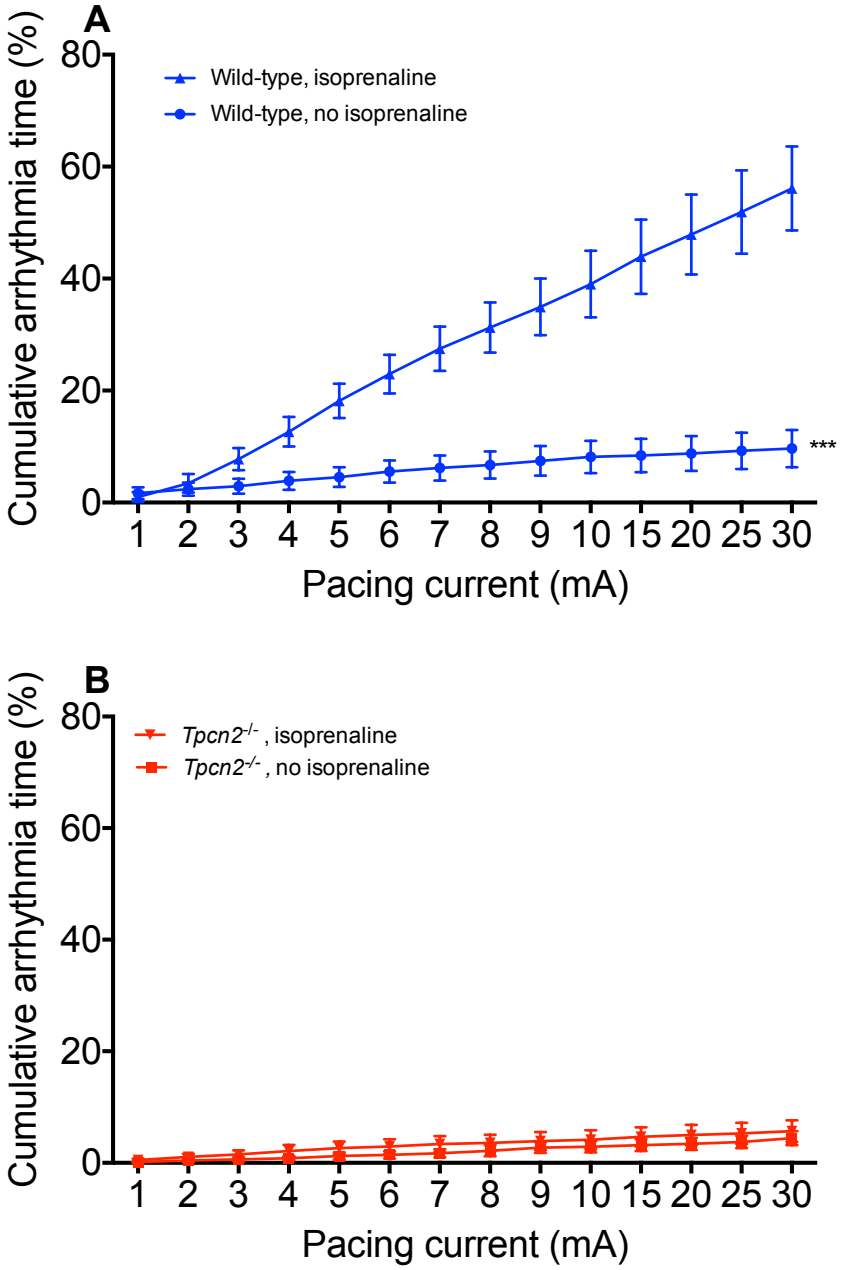


Figure 3.9: The effect of isoprenaline on arrhythmia provocation in hearts from wildtype and *Tpcn2*$^{-/-}$ mice using the increasing current burst pacing protocol. Wildtype hearts experienced significantly more arrhythmias in the presence of isoprenaline than they did in its absence (panel A, P=0.0005, two-way ANOVA, n=7). However, no increase in arrhythmias was seen when knockout hearts were exposed to isoprenaline (panel B, P>0.05, two-way ANOVA).

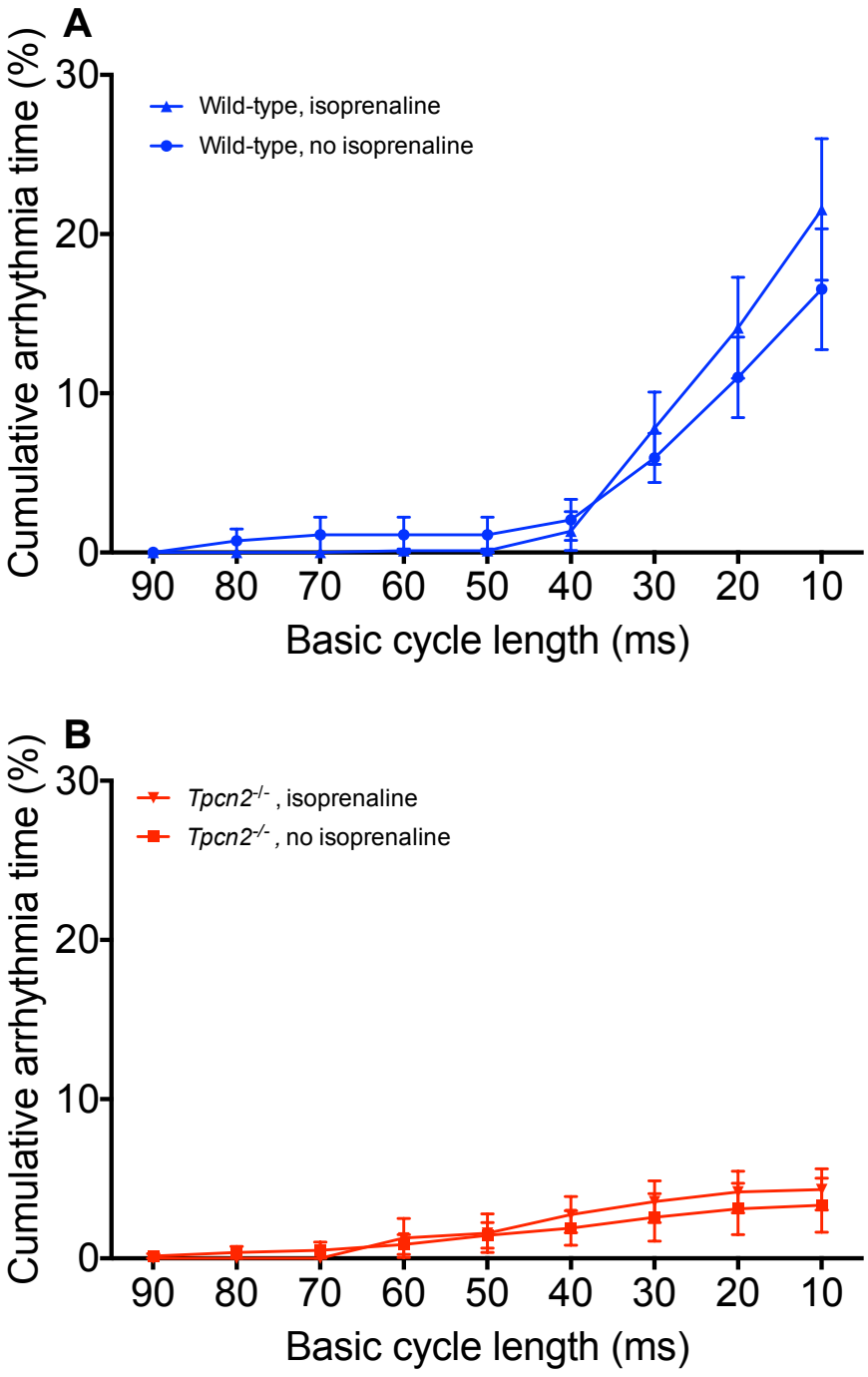


Figure 3.10: The effect of isoprenaline on arrhythmia provocation in hearts from wildtype and *Tpcn2*$^{-/-}$ mice using the reducing basic cycle length burst pacing protocol. Neither wildtype (panel A) nor knockout (panel B) hearts experienced an increase in arrhythmia occurrence following exposure to isoprenaline using this protocol ($P>0.05$, two-way ANOVA for both comparisons).

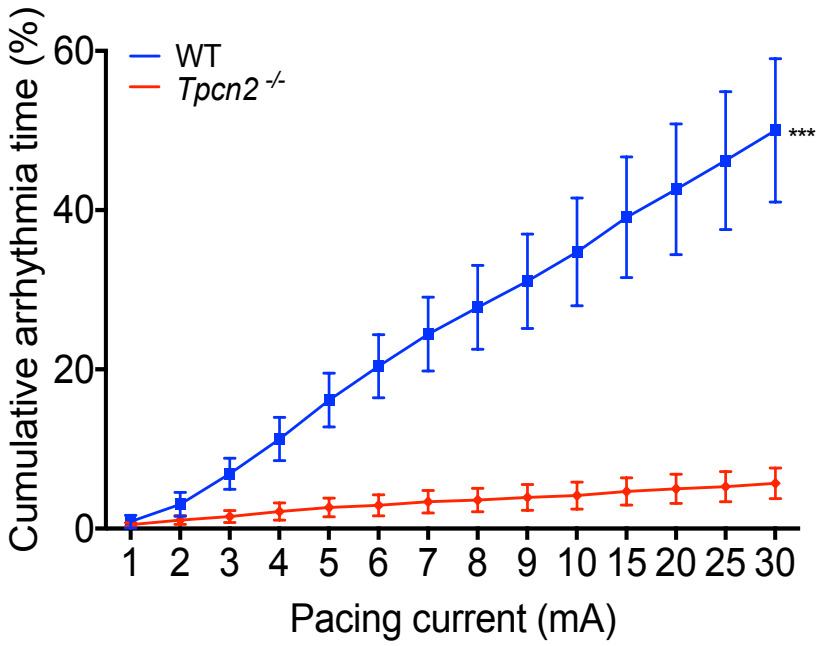


Figure 3.11: Cumulative ventricular arrhythmia time (VT or VF) in isolated hearts from wildtype and *Tpcn2*$^{-/-}$ mice exposed to isoprenaline 50 nM. Hearts perfused via Langendorff apparatus were subjected to a burst pacing protocol in the presence of isoprenaline. A set of three trains of fifty stimuli were delivered to the heart with a pause of two seconds between each train. The stimulus current was increased after every set of trains from 1 to 30 mA. The proportion of pacing-free time in which re-entrant ventricular arrhythmias were observed was recorded cumulatively and is summarised above. *Tpcn2*$^{-/-}$ mice were significantly protected against arrhythmias compared with wildtypes (P=0.0002, two-way ANOVA, n=9 in the wildtype group and n=10 in the *Tpcn2*$^{-/-}$ group).

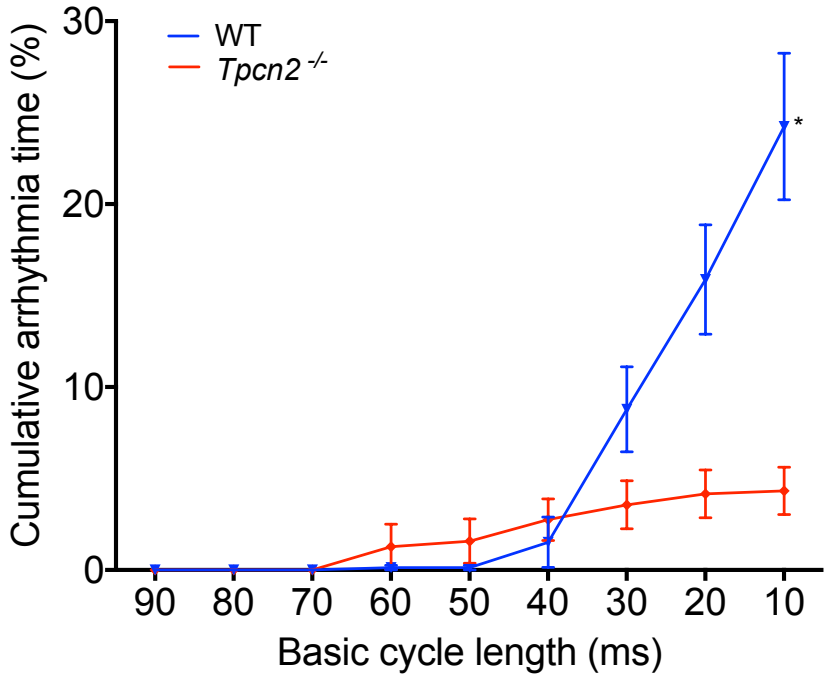


Figure 3.12: Cumulative ventricular arrhythmia time (VT or VF) in isolated hearts from wildtype and *Tpcn2*$^{-/-}$ mice exposed to isoprenaline 50 nM. Hearts perfused via Langendorff apparatus were subjected to a burst pacing protocol in the presence of isoprenaline. A set of three trains of fifty stimuli were delivered to the heart with a pause of two seconds between each train. The cycle length between stimuli was varied after each set of trains from 90 ms down to 10 ms. The proportion of pacing-free time in which re-entrant ventricular arrhythmias were observed was recorded cumulatively and is summarised above. Arrhythmias were observed at low cycle lengths, but *Tpcn2*$^{-/-}$ hearts were significantly protected compared with wildtypes (P=0.0146, two-way ANOVA, n=8 in wildtype group and n=9 in *Tpcn2*$^{-/-}$).

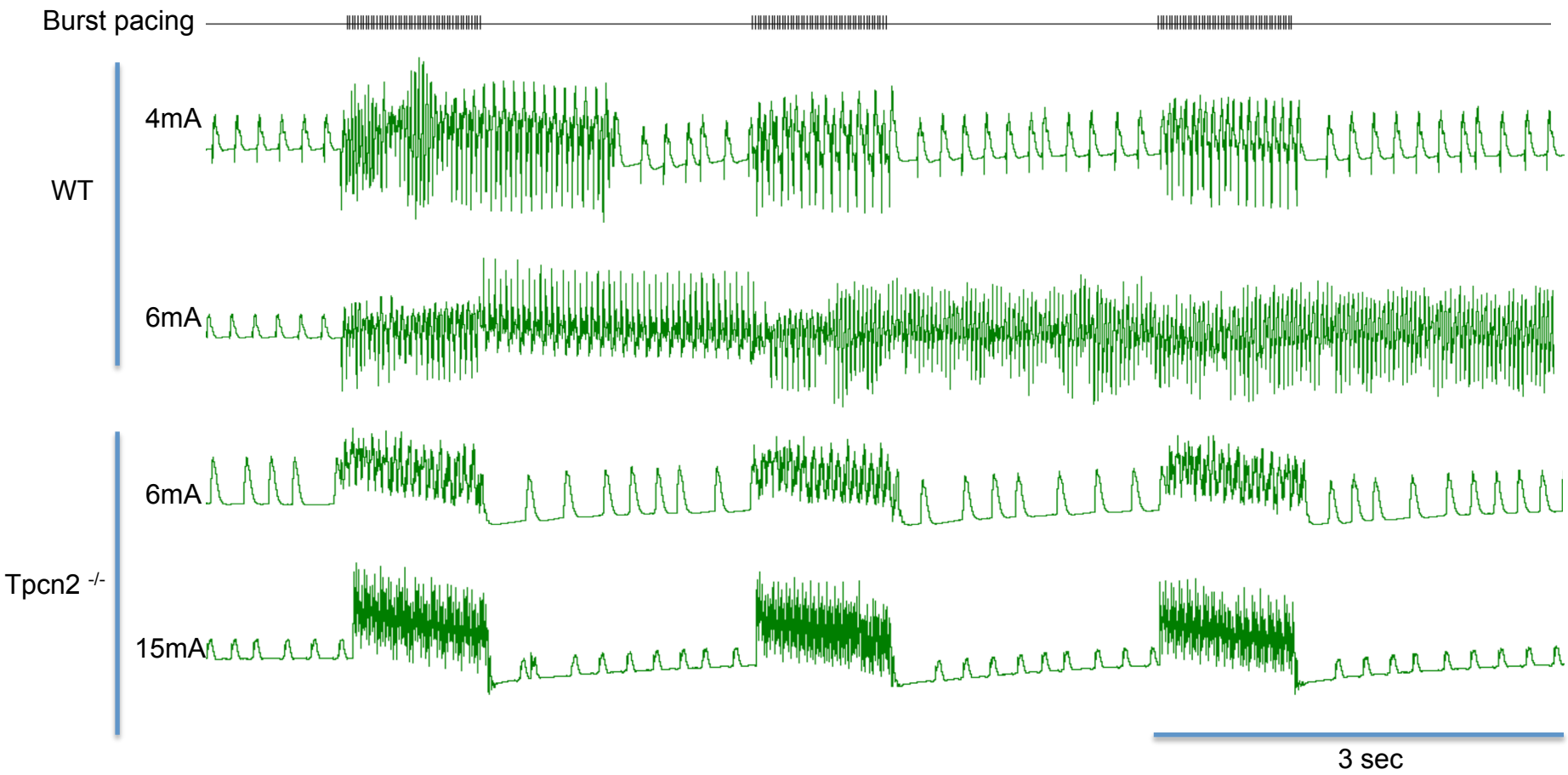


Figure 3.13: Representative monophasic action potential (MAP) recordings from wildtype and *Tpcn2*$^{-/-}$ mice exposed to isoprenaline 50 nM. Hearts were subjected to a burst pacing protocol in the presence of isoprenaline. A set of three trains of fifty stimuli were delivered to the heart (top trace, black) with a constant cycle length of 20 ms. The trains were separated by two second pauses and the proportion of this time occupied by re-entrant arrhythmias (VT or VF) was recorded. Another set of three trains was then delivered with a higher stimulation current. Above traces (green) show reaction of wildtype and *Tpcn2*$^{-/-}$ mice to this protocol at different stimulation currents.

3.3 Conclusion

The data presented in this chapter show that hearts from *Tpcn2*$^{-/-}$ mice are protected against the arrhythmias induced by isoprenaline following burst stimulation, compared with their wildtype counterparts. The difference in arrhythmia susceptibility only became apparent following the application of isoprenaline, due to the increase in arrhythmias seen in the wildtype under these conditions. There was no difference between the genotypes in the absence of β-adrenergic stimulation. The levels of expression of β1-adrenergic receptor protein were not significantly different between these genotypes, and so this is unlikely to be the explanation for the difference in arrhythmia susceptibility, although other differences in the β-adrenergic transduction pathway cannot be ruled out. In-vivo electrocardiograph analysis revealed no differences in resting gross cardiac conduction phenotype, although the wildtype resting heart rate was 13% higher than the knockout. This difference has not previously been detected. No significant difference was detected in action potential durations (APD) in ex-vivo hearts between the two genotypes.

These findings are broadly consistent with the findings of other studies that looked at the role of the NAADP signalling pathway in arrhythmogenesis, but these are the first observations to be made from the point of view of acute β-adrenergic stimulation in a TPC2 knockout model instead of using pharmacological NAADP antagonism.

There were no differences in the frequency of arrhythmias in the absence of isoprenaline, which is consistent with previous observations of the effect of TPC2 knockout on ventricular calcium handling. No difference was detected between the calcium transient amplitudes in resting ventricular myocytes isolated from *Tpcn2*$^{-/-}$ mice and controls, and differences only became apparent following the exposure of these cells to isoprenaline, and similarly, the contraction force of resting myocytes from these animals was not different (Capel et al., 2015). The difference in susceptibility to arrhythmia between these genotypes is therefore consistent with the hypothesis that NAADP/TPC2 signalling is an important part of the acutely-activated β-adrenergic pathway.

Nebel et al. (2013) looked at the arrhythmogenicity of isoprenaline on isolated murine ventricular cardiomyocytes and also on hearts in vivo using the NAADP antagonist, BZ194. Isolated cells were electrically stimulated to produce an action potential, and the number of after-depolarisations that occurred were counted. Calcium transients were also measured using the fluorescent calcium probe Indo-1. High-dose isoprenaline (200 nM) resulted in a three to four-fold increase in after-depolarisations and spontaneous diastolic calcium transients compared with cells that had no isoprenaline exposure. The addition of bafilomycin-A1 (1 μM) returned the number of after-depolarisations and spontaneous calcium transients to basal levels. Similarly, the addition of BZ194 abolished the arrhythmogenic effect of isoprenaline in a dose-dependent manner. BZ194 also had no effect on action potential duration, which is consistent with the lack of effect of TPC2 knockout on this parameter in observations presented here.

In addition, Nebel et al. also studied SR luminal calcium concentration using the low-affinity calcium probe mag-Fura-2 during high-dose β-adrenergic stimulation. In isoprenaline-exposed cells, a cyclical fall and recovery of SR calcium concentration was observed in an inverse pattern compared with the spontaneous calcium transients, suggesting the release of calcium from the SR was responsible for these events. Stronger evidence that this is the case was presented in a further study where cytosolic and SR luminal calcium concentrations were measured simultaneously in the same cell using fluo-4 and mag-fura-2 respectively (Warszta et al., 2014). The rise in cytosolic calcium was synchronised with the fall in luminal SR calcium during both a stable rhythm and during arrhythmias. Interestingly, in this study the arrhythmogenic effect of isoprenaline was reduced in a dose-dependent manner by SAN4825, a novel inhibitor of ADP-ribosyl-cyclases (ARCs), the enzymes thought to be responsible for the synthesis of both NAADP and the related messenger cyclic-ADP-ribose (cADPR). This confirmed previously-reported anti-arrhythmic properties of this drug, and a related compound SAN2589 (Kannt et al., 2012).

The same anti-arrhythmic effect of BZ194 was seen when it was infused with isoprenaline into live mice. Electrocardiograph monitoring was used to count the number of premature ventricular beats (PVBs), episodes of bigeminy and salves of ventricular tachycardia, all of which were increased by the infusion of isoprenaline. However, simultaneous exposure to BZ194 prevented this increase, and numbers of each event in the treatment group were not significantly increased compared with controls (Nebel et al., 2013). A possible toxic effect of

BZ194 was also suggested in these experiments; the authors noted that some mice treated with BZ194 in combination with isoprenaline developed reduced motor activity and an impaired general condition and that 50% of the animals died within four days of the experiments. This was not observed in animals that were not given BZ194. No such effect has been reported in mice lacking the TPC2 gene previously, and was not observed in populations of *Tpcn2*$^{-/-}$ mice used in experiments presented here.

In similar experiments performed elsewhere using isolated guinea pig ventricular cells, it took significantly longer for spontaneous action potentials to develop in response to isoprenaline (50 nM) when treated with bafilomycin-A1 compared with DMSO-treated controls (Bolton, 2014). Since the TPC2 protein is located primarily on the lysosomal membrane (Calcraft et al., 2009), this result is consistent with those presented in this chapter using *Tpcn2*$^{-/-}$ mice.

In other experiments, Capel et al. (2015) exposed wildtype and *Tpcn2*$^{-/-}$ mice to chronic infusions of isoprenaline for 14 days to induce cardiac hypertrophy. Hearts from *Tpcn2*$^{-/-}$ mice were significantly less hypertrophied and less susceptible to arrhythmias induced by burst pacing protocols compared with their wildtype counterparts. Whether this reduced susceptibility to arrhythmia was actually due to lack of TPC2 and therefore interruption of NAADP signalling *per se*, or due to the reduction in hypertrophy-related structural abnormalities was not addressed in those experiments. Although the mice were chronically exposed to isoprenaline, there was no isoprenaline present during the ex-vivo arrhythmia experiments, yet arrhythmias were still seen in wildtype hearts.

These results are therefore in contrast to those presented here, where burst pacing failed to provoke arrhythmias in wildtypes in the absence of isoprenaline. It is possible that chronic β-adrenergic stimulation results in constitutive activity in the NAADP/TPC2 pathway that is not present under baseline conditions. Further investigation is needed in order to elucidate the mechanisms responsible for this observation.

The mechanism by which activation of the β-adrenergic receptor is linked to the NAADP/TPC2 pathway is currently largely unknown, although it has been demonstrated that NAADP synthesis is increased when cardiac tissue is perfused with isoprenaline (Gul et al., 2016; Lewis et al., 2012; Macgregor et al., 2007). The generation of cAMP by adenylate cyclase occurs early in the β-adrenergic signalling pathway and can activate both Protein Kinase A (PKA) and the Exchange Protein Activated by cAMP (EPAC). Both PKA and EPAC go on to activate different enzyme signalling cascades. Nebel et al. (2013) used selective activators of these enzymes (6-BNZ-cAMP and 8-pCPT respectively) in an attempt to replicate the arrhythmias seen following isoprenaline exposure in isolated mouse cardiomyocytes. Selective activation of the EPAC pathway did not appear to cause arrhythmogenic events, which was in contrast to activation of the PKA pathway which resulted in after-depolarisations and associated spontaneous calcium transients. It is possible that the activity of ARC is increased due to phosphorylation by PKA, and this results in the generation of NAADP (and cADPR). Experiments using both 6-BNZ-cAMP and SAN4825 or BZ194 simultaneously were not performed. However, this hypothesis predicts that the

arrhythmogenic events caused by 6-BNZ-cAMP should be prevented by both SAN4825 and by BZ194.

The involvement of cAMP upstream of NAADP signalling has also been observed in extra-cardiac tissues. The increase in calcium concentration in salivary gland acinar cells caused by the muscarinic agonist carbachol was not affected by pre-treatment with bafilomycin-A1. An enhancement of the calcium response to carbachol was seen if the cells were also exposed to forskolin, an activator of adenyl cyclase, or if the cells were first treated with isoprenaline. However, this enhancement was reduced by 65% in the presence of bafilomycin-A1 (Imbery et al., 2016). Similarly, in the same set of experiments Ned-19 had no effect on the carbachol-induced increase in calcium concentration in the absence of β-adrenergic stimulation, but attenuated the enhancement caused by pre-treatment with isoprenaline.

Experiments by Rakovic et al. (1999) showed that pro-arrhythmic calcium mishandling events such as spontaneous action potentials, calcium waves and afterdepolarisations in response to isoprenaline stimulation or ouabain exposure could be prevented by using 8-amino-cADPR and 8-bromo-cADPR - both antagonists of cADPR, thought to act at ryanodine receptors of the SR. More recently, Gul et al. (2016) suggested that NAADP and cADPR may be sequentially produced by different ARCs in response to β-adrenergic stimulation in the heart. It was hypothesised that the action of NAADP stimulates the synthesis of cADPR, which then acts at the SR to regulate calcium release. These conclusions are consistent with observations here, although the exact events that lead to

arrhythmogenesis are unclear. However, it has been demonstrated that the increase in calcium transient that is observed following the photorelease of caged NAADP in both atrial and ventricular myocytes does not occur in the presence of inhibitors of CaMKII, such as KN93 and AIP (Capel et al., 2015). It is therefore tempting to speculate that this recently-discovered involvement of CaMKII in the NAADP/TPC2 pathway is also a contributing factor to arrhythmogenesis caused by β-adrenergic stimulation.

CaMKII, a holoenzyme that requires the binding of calcium and calmodulin for activation, has been implicated in the generation of cardiac arrhythmias (Hund et al., 2015; Mattiazzi et al., 2015; Vincent et al., 2014; Westenbrink et al., 2013). The phosphorylation of L-type calcium channels by CaMKII results in an enhanced calcium current and slowed inactivation, the so-called calcium-dependent I_{Ca} facilitation (Yuan et al., 1994). This may lead to an increase in depolarising current and consequently the possibility of developing EADs and DADs. However, the release of NAADP has been shown to have no effect on plasma membrane calcium current in either atrial or ventricular myocytes (Capel et al., 2015; Collins et al., 2011; Macgregor et al., 2007), suggesting that this mechanism is not likely. Conversely, CaMKII is known to phosphorylate phospholamban at threonine-17 (Stammers et al., 2015), relieving its inhibition of SERCA, and resulting in increased calcium loading of the SR. In contrast with its lack of effect on calcium current, NAADP does seem to cause an increase in SR calcium loading, as suggested by increased spark frequency and calcium release in response to caffeine (Macgregor et al., 2007). Additionally, CaMKII can phosphorylate the ryanodine receptor to increase open probability

(Westenbrink et al., 2013). Together, phosphorylation of both phospholamban and the ryanodine receptor may lead to spontaneous calcium release from the SR causing DADs and leading to arrhythmia. In chronic activation of CaMKII – and perhaps occurring in experiments by Capel et al. (2015) discussed above – expression of the sodium-calcium exchanger (NCX) and SERCA are altered – the former being increased and the latter reduced (Lu et al., 2011; Mani et al., 2010). This occurs during cardiac failure and changes the balance between calcium reuptake to the SR and calcium extrusion from the cell. This has two main effects: firstly, there is SR calcium depletion which contributes to cardiac failure, but secondly – and more importantly in the context of arrhythmias – there is a greater depolarising inward sodium current at the plasma membrane via NCX as more calcium is extruded from the cytoplasm via this route (Bers, 2006). This is likely to result in a prolongation of the action potential and arrhythmogenic triggers such as EADs and DADs. Prolongation of the action potential was not observed in the current experiments - possibly because the isoprenaline exposure, and therefore CaMKII activation – was acute and transient rather than chronic and prolonged and therefore there was insufficient time for altered protein expression. In addition to those discussed here, CaMKII also has the potential to be pro-arrhythmogenic via several other mechanisms, including modulation of sodium, potassium, and chloride channels in the plasma membrane (Hund et al., 2015).

In the failing heart, there is increased activation of CaMKII, and the threshold for inducing arrhythmias with adrenergic agonists such as noradrenaline is lowered. However, CaMKII inhibitors such as KN93 are able to suppress arrhythmias

under these conditions (Hoeker et al., 2016). The involvement of NAADP in this process was not investigated in this study, but given the evidence for the importance of CaMKII in NAADP signalling (Capel et al., 2015) it would be interesting to investigate how this pathway influences propensity to arrhythmia in the failing heart.

There is also evidence that suggests a role for NAADP signalling in the arrhythmias seen during ischaemia-perfusion injury. Rat cardiac myocytes subjected to 40 minutes of simulated ischaemia followed by reperfusion and reoxygenation suffered rapid periodic contractions and calcium oscillations as a consequence. These effects were reduced or eliminated if the cells had been pre-treated with the NAADP antagonist Ned-19 or its derivative Ned-K. Further investigation suggested that the opening of the mitochondrial permeability transition pore (mPTP) in response to ischaemia was indirectly prevented by these drugs, and this was a mechanism whereby the arrhythmic consequences of ischaemia-reperfusion were mitigated (Davidson et al., 2015).

In summary, there is now good evidence from several studies, including the data presented here, that implicates the NAADP/TPC2 system in cardiac arrhythmogenesis. However, many questions still remain regarding the mechanisms underlying these observations, and it remains to be seen whether CaMKII plays a significant role in this area. Results would suggest that the NAADP/TPC2 system may be a potential therapeutic target in the management of arrhythmias in the acute clinical setting.

4

Cardiac hypertrophy induced by chronic adrenergic stimulation: Involvement of NAADP

4.1 Introduction

In the last chapter, experiments were performed to further explore the role of NAADP and TPC2 signalling in the context of acute β-adrenergic stimulation. Here, the part played by this system in chronic activation of adrenergic receptors will be investigated.

As already discussed, there is now significant evidence suggesting that NAADP is an important part of the downstream signalling cascade that is initiated following acute β-adrenergic receptor stimulation. NAADP synthesis appears to be increased following exposure of the heart to isoprenaline (Gul et al., 2016; Lewis et al., 2012), and a large proportion of the positive inotropic and lusitropic responses that follow can be blocked by interruption of the NAADP signalling pathway, either pharmacologically or by genetic knockout of the putative NAADP receptor in the heart, TPC2 (Capel et al., 2015). Similarly, release of NAADP in cardiomyocytes mimics many of the effects of isoprenaline such as enhancement of the calcium transient (Macgregor et al., 2007).

Cardiac hypertrophy is an increase in the size of the heart or of individual cardiac myocytes in response to increased workload or other stimulus. This can be caused by a variety of physical or neurohumoral factors that may be physiological or pathological. Physiological, 'adaptive', hypertrophy is the normal growth pattern of the heart, and may also occur in response to cardiovascular training. It is a largely reversible state and is associated with maintained or enhanced cardiac performance. Adaptive hypertrophy is also stimulated in the

early stages of some pathological pressure-overload states such as essential hypertension or aortic valve stenosis. However, as these states persist or worsen hypertrophy becomes irreversible and associated with cardiac failure, foetal gene induction, fibrosis and cell death. This is known as pathological or 'maladaptive' hypertrophy (Maillet et al., 2013).

The long-term activation of adrenergic signalling pathways in the heart is known to be associated with maladaptive cardiac remodelling and hypertrophy, regardless of the underlying pathology (Osadchii, 2007; Scheuer, 1999). For example, hypertensive patients with hypertrophic hearts were found to have higher circulating noradrenaline levels (Strand et al., 2006), higher cardiac noradrenaline spillover (Kelm et al., 1996) and a higher peripheral sympathetic nerve discharge rate (Greenwood et al., 2001) compared to control hypertensive patients with similar blood pressures, but who lacked morphological cardiac changes. Similarly, in experiments designed to test whether a causal relationship exists, chronic (1 – 4 weeks) exposure of animals to levels of isoprenaline or noradrenaline that were too small to induce haemodynamic changes resulted in cardiac remodelling and hypertrophy in many species, including mouse, guinea pig, rabbit and dog (Osadchii, 2007).

Of adrenergic receptors found in adult rat cardiac muscle, the α1 subtype represents approximately 10%, while β1 makes up just over 70% and β2 the remainder (Cotecchia et al., 2015). β2 receptors may make up a higher proportion of the total (and may be more prevalent than β1) in neonatal rat cells (Morisco et al., 2001). Both α1 and β1 receptors have been implicated in causing

hypertrophy via complex and overlapping pathways (Cotecchia et al., 2015; Fu et al., 2012), and these are discussed in detail in the Introduction. However, one factor that is common to both pathways to varying degrees is calcium, which contributes to cardiac hypertrophy and remodelling in a process that has been dubbed excitation-transcription coupling (Mattiazzi et al., 2015)

In the α1 pathway, IP_3 is generated following hydrolysis of PIP_2 by phospholipase C (PLC). IP_3 targets specific receptors on the nuclear membrane and SR, causing calcium release. This calcium then binds to calmodulin and activates calcineurin, resulting in the dephosphorylation and nuclear translocation of the Nuclear Factor activated in T-cells (NFAT). In the nucleus, NFAT then acts as a transcription factor that influences the expression of genes involved in hypertrophy (Cotecchia et al., 2015). Similarly, in the β1 pathway, activation of PKA results in enhanced calcium entry into the cytoplasm during systolic depolarisation, via L-type calcium channels from the extracellular environment and via ryanodine receptors from the SR. This calcium, following binding to calmodulin, can also activate calcineurin and result in increased expression of hypertrophic genes by the same mechanism (Fu et al., 2012).

Calcium can also combine with calmodulin to activate CaMKII. Activated CaMKII phosphorylates some of the histone deacetylase (HDAC) family of enzymes. Unphosphorylated HDACs suppress the activity of the MEF transcription factors, which regulate expression of hypertrophic genes (Anderson et al., 2011; Mattiazzi et al., 2015). Therefore the activity of CaMKII at HDAC promotes hypertrophy by relieving the inhibition on MEF transcription factors. This is

significant from the point of view of NAADP signalling, since recent evidence suggests that CaMKII may become activated via this pathway (Capel et al., 2015).

There is some evidence for a role of NAADP and TPC2 in cardiac hypertrophy following β-adrenergic stimulation. Capel et al. (2015) showed that mice lacking the TPC2 gene were protected from cardiac hypertrophy induced by a chronic (two week) subcutaneous infusion of isoprenaline compared with wildtypes. Similarly, Gul et al. (2016) showed that knockout of CD38, an enzyme that is likely to be involved in the synthesis of NAADP and the related signalling molecule cADPR, also protected hearts against isoprenaline-induced hypertrophy. However, there have been no studies of pharmacological manipulation of this signalling system downstream of CD38 in the context of cardiac remodelling.

NAADP signalling via TPC2 has therefore been shown to play an important role in the transduction of acute β-adrenergic stimulation, and there is some evidence that CaMKII may be involved. In the context of recent studies suggesting the involvement of this pathway in the development of hypertrophy following chronic β-adrenergic activation, it was hypothesised that its pharmacological manipulation with Ned-19 or Bafilomycin-A1 may alter adrenergically-induced cardiac remodelling in cultured cardiomyocytes. This was tested in experiments presented in this chapter.

4.2 Results

4.2.1 Viability of cultured neonatal rat cardiomyocytes depends upon functioning lysosomes, but not on functioning NAADP signalling.

The viability of rat neonatal cardiomyocytes in culture was evaluated twice during the 48-hour period of this experiment. 24 hours following the addition of either DMSO 0.001%, Ned-19 10 μM, or Bafilomycin-A1 100 nM to the culture medium, there was no detectable difference in viability between these three groups ($P>0.05$, one-way ANOVA, $n=6$ for all groups). At 48 hours there was no significant reduction in the viability of cells treated with Ned-19, but Bafilomycin-A1 had caused viability to fall to 68±4% of DMSO viability at the same time point ($P=0.0001$, one-way ANOVA, $n=6$).

Mean data for cultured cell viability evaluation is shown in figure 4.2. Representative images of cells cultured with each of the three compounds for 48 hours is shown in figure 4.3.

4.2.2 Size of cultured neonatal rat cardiomyocytes is not affected by the presence of Ned-19, but is reduced by the presence of Bafilomycin-A1.

Cell size was estimated by measuring cross-sectional area after 48 hours in culture with DMSO, Ned-19 or Bafilomycin-A1. Two concentrations of Ned-19 (1

μM and 10 μM) had no effect on cell size compared with DMSO controls (P>0.05, Kruskal-Wallis test with Dunn correction).

In contrast, Bafilomycin-A1 caused a reduction in mean cell size to 71±3% (100 nM) and 71±5% (1 μM) of DMSO controls (P<0.0001 and P=0.0088 respectively, Kruskal-Wallis test with Dunn correction). There was no difference in the magnitude of the reduction between the two concentrations of Bafilomycin-A1 (P>0.05). Cells that were obviously non-viable were not included in this analysis.

Sample numbers were n=114 cells (DMSO), n=63 cells (Ned-19 1 μM), n=124 cells (Ned-19 100 nM), n=58 cells (Bafilomycin-A1 100 nM), and n=37 cells (Bafilomycin-A1 1 μM). Cells were harvested and measured in three separate cultures from a total of approximately 36 individuals. The number of cells measured from Bafilomycin cultures were smaller due to its apparent toxic effect.

The effect of Ned-19 and Bafilomycin-A1 is summarised in figures 4.4 and 4.5 respectively.

4.2.3 Noradrenaline is a more powerful stimulant of hypertrophy in cultured neonatal rat cardiomyocytes than isoprenaline.

Cell hypertrophy was induced by exposure of the cultured myocytes to isoprenaline 10 μM or noradrenaline 10 μM for 48 hours. Isoprenaline caused an

increase in cell size to 155±5% of DMSO controls (P<0.0001, Kruskal-Wallis test with Dunn correction). Noradrenaline had a more pronounced effect, causing an increase in size to 202±11% of DMSO control size (P<0.0001). The effect of noradrenaline was significantly greater than that of isoprenaline (P=0.0258) using these concentrations.

Figure 4.6 illustrates these effects.

4.2.4 Ned-19 is protective against isoprenaline-induced hypertrophy of cultured neonatal rat cardiomyocytes.

Myocytes were cultured with two concentrations of Ned-19 (1 μM and 10 μM), which were added to the culture medium at the same time as isoprenaline. The lower concentration of Ned-19 had no effect on the increase in cell size compared with DMSO controls caused by isoprenaline (P>0.05, Kruskal-Wallis test). However, addition of 10 μM Ned-19 to the culture medium resulted in complete prevention of the isoprenaline-induced hypertrophy, with no significant difference between the size of control cells cultured in DMSO and those cultured in isoprenaline and Ned-19 10 μM.

Mean data for these groups is shown in figure 4.7, and representative differential interference contrast (DIC) images of cells cultured in DMSO, isoprenaline and isoprenaline with Ned-19 10 μM are shown in figure 4.8.

A further test of the effect of Ned-19 on isoprenaline-induced hypertrophy, the expression of messenger RNA for marker proteins associated with changes in cell size was also measured. Expression of atrial natriuretic peptide (ANP) and α-actin were measured and normalised to the expression of glyceraldehyde-3-phosphate dehydrogenase (GAPDH) using quantitative polymerase chain reaction (qPCR).

ANP mRNA expression was increased 3±0.6 fold compared to DMSO controls by culture with isoprenaline 10 μM (P=0.0003, one-way ANOVA). Culture with Ned-19 10 μM alone had no effect on ANP mRNA levels. The combination of Ned-19 and isoprenaline prevented the increase seen with isoprenaline alone and expression only rose by 1.5±0.4 fold. This was not significantly different from control expression, but is less than that seen with isoprenaline alone (P=0.0061). These data are summarised in figure 4.9.

Similarly, cultures treated with isoprenaline increased α-actin expression by 4.8±0.9 fold compared with DMSO-treated controls (P<0.0001). This increase was not seen with Ned-19 alone, and was prevented when cells were cultured with both Ned-19 and isoprenaline in combination (P=0.0207). This data is shown in figure 4.10.

4.2.5 Ned-19 is protective against noradrenaline-induced hypertrophy of cultured neonatal rat cardiomyocytes.

Noradrenaline-induced hypertrophy was also prevented by Ned-19 10 μM ($P<0.0001$, Kruskal-Wallis test with Dunn correction). There was no significant difference in the size of cells treated with the combination of noradrenaline 10 μM and Ned-19 10 μM when compared with control cells treated with DMSO alone.

These data are summarised in figure 4.11.

Again, in order to test the anti-hypertrophic effect of Ned-19 on noradrenaline-induced hypertrophy, expression of mRNA for ANP and αActin was measured.

Culture with noradrenaline resulted in ANP mRNA expression being increased by 7.6±1.8 fold compared with DMSO controls ($P=0.0003$, one-way ANOVA, $n=5$), while culture with noradrenaline and Ned-19 together caused significantly less of an increase (2.4±0.9 fold, $P=0.0051$). There was no difference caused by Ned-19 alone. Figure 4.12 shows this data.

αActin expression was increased by noradrenaline alone by 5.1±0.5 fold. However, the addition of Ned-19 10 μM to cultures alongside noradrenaline reduced the effect so that the expression was only 3±1 fold higher than DMSO controls, and significantly less than that seen with noradrenaline alone ($P=0.0163$). Again, Ned-19 alone had no effect on αActin expression. This data is shown in figure 4.13.

4.2.6 Bafilomycin may have a protective effect against isoprenaline-induced hypertrophy of cultured neonatal rat cardiomyocytes.

Bafilomycin-A1 may have a preventative effect on isoprenaline-induced hypertrophy of rat neonatal cardiomyocytes in culture. The addition of either 100 nM or 1 μM bafilomycin prevented the hypertrophic effect of isoprenaline 10 μM (figure 4.14, $P<0.0001$, Kruskal-Wallis test with Dunn correction). There was no dose-dependence in the range tested, and no difference was detected in responses between the two doses.

However, this result should be interpreted in the context of the effect of bafilomycin on cells not exposed to isoprenaline. It may be that the apparent prevention of isoprenaline-induced hypertrophy by bafilomycin was due to toxicity.

Indeed, the total yield of RNA from cultures containing bafilomycin (both concentrations treated as a single group) was lower than that of other cultures – perhaps suggesting that overall transcription was reduced (see figure 4.15).

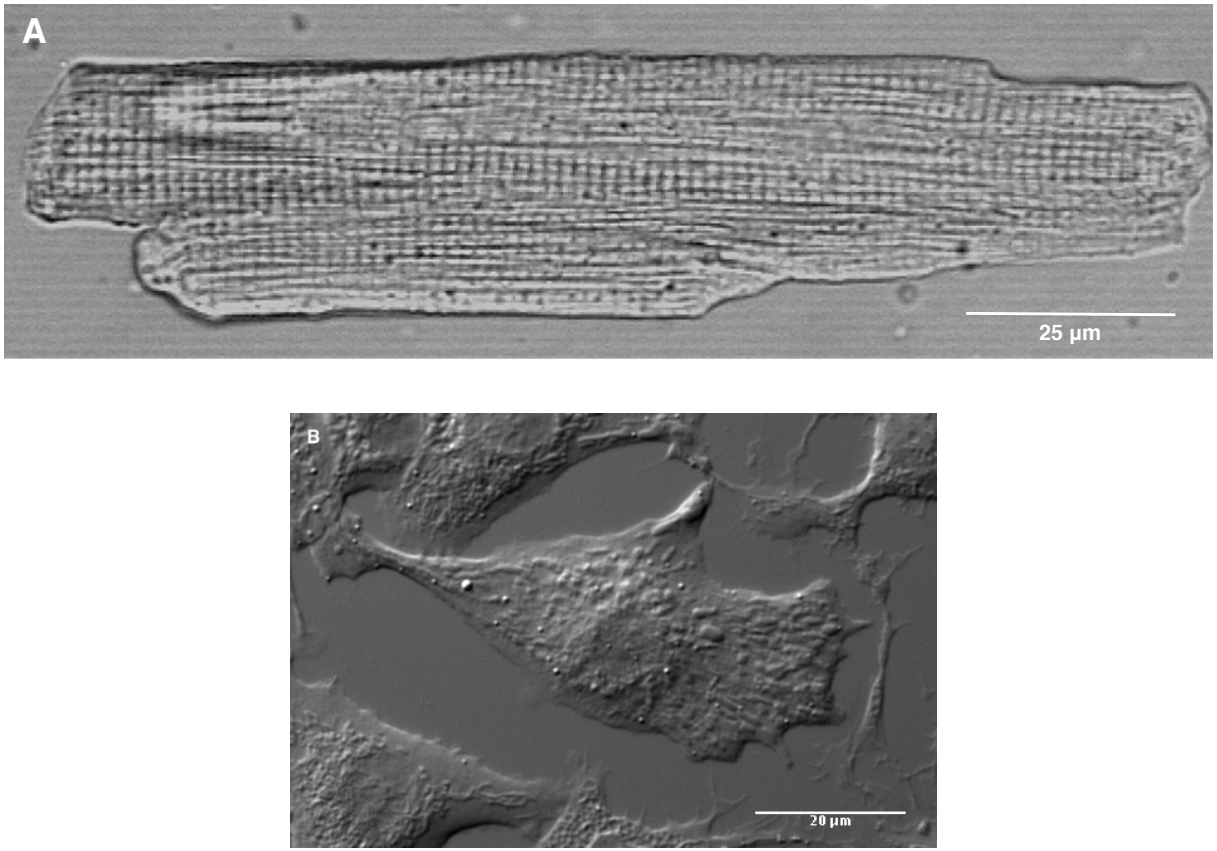


Figure 4.1: Typical appearance of cardiomyocytes. Image A (reproduced with permission from Loughrey et al. (2004)) shows an isolated adult cardiomyocyte while image B shows a typical neonatal rat cardiomyocyte in cell culture. The adult cell is a regular shape with a noticeably more organised structure and visible striations in comparison with the cultured neonatal cell.

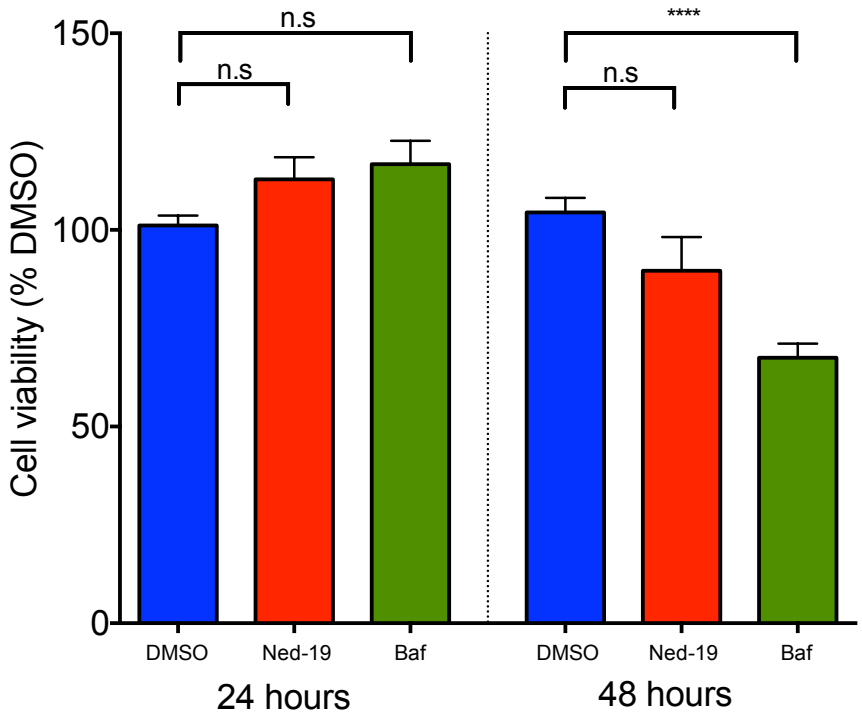


Figure 4.2: Viability of cultured neonatal rat cardiomyocytes exposed to Ned-19 10 µM or Bafilomycin-A1 100 nM over time. Cell viability was measured at 24 hours and 48 hours after addition of Ned-19 or Bafilomycin-A1 to the culture plates. There was no significant reduction in cell viability at 24 hours compared with cells treated with DMSO alone. However, at 48 hours there was a significant reduction in the viability of cells exposed to Bafilomycin-A1 (P=0.0001, one-way ANOVA, n=6 for all groups).

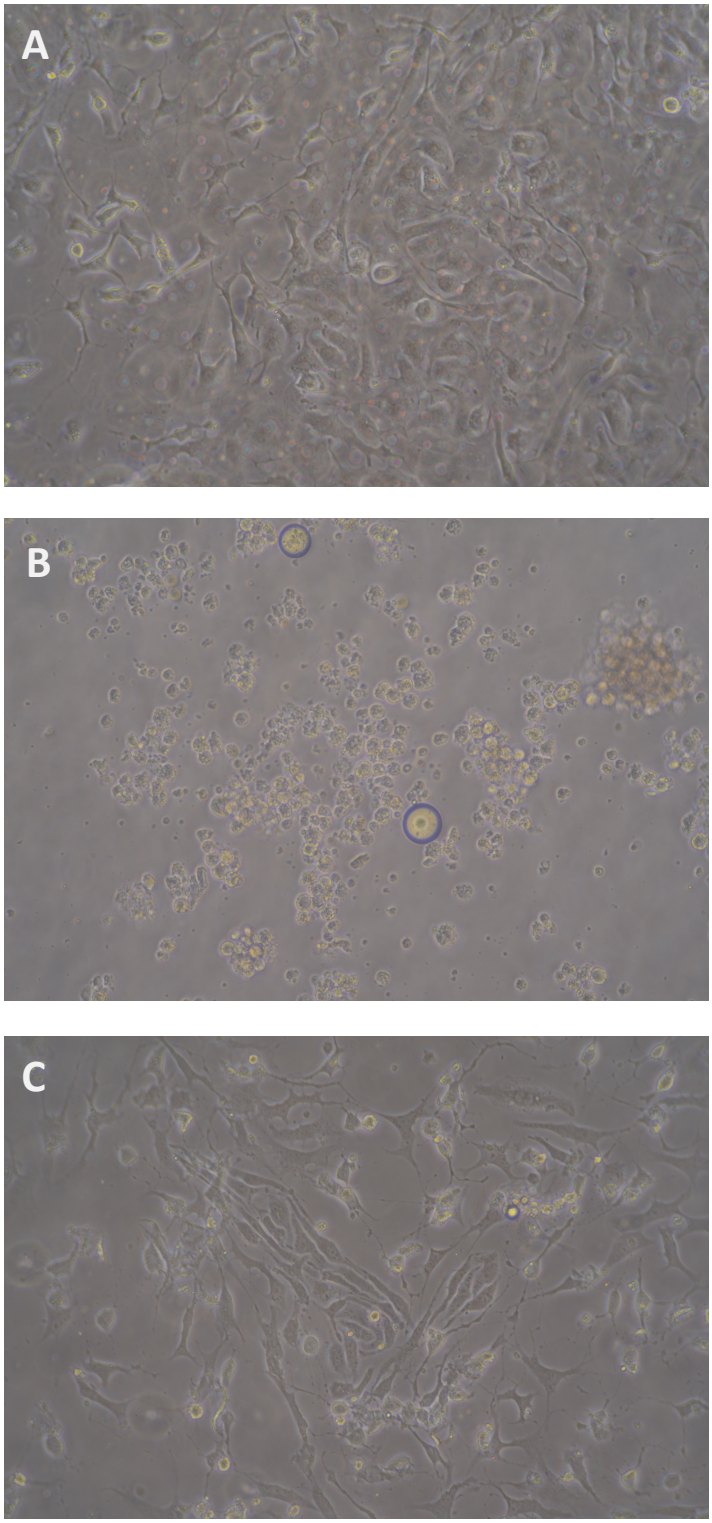


Figure 4.3: The toxic effect of Bafilomycin-A1. Cells in culture were exposed to A, DMSO 0.01% B, Bafilomycin-A1 100 nM or C, Ned-19 10 μM for 48 hours. Typical low magnification images are shown above and illustrate an extensive toxic effect seen with Bafilomycin-A1 in comparison with DMSO or Ned-19. Although significant, the toxicity was not 100%, and enough cells maintained normal morphology to be able to measure.

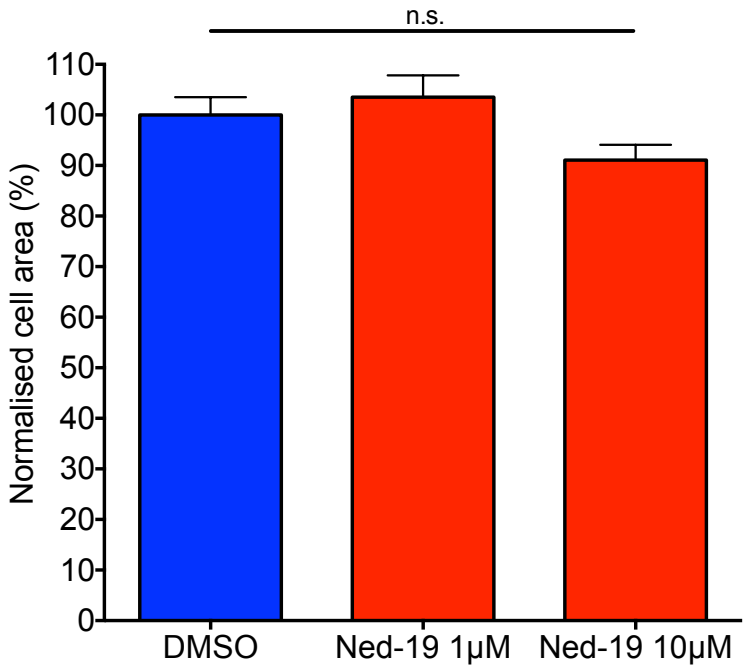


Figure 4.4: The effect of Ned-19 on the size of neonatal rat cardiomyocytes after 48 hours. Neither 1 μM nor 10 μM Ned-19 had a significant effect on the mean size of cultured cardiomyocytes after 48 hours in comparison with DMSO alone ($P>0.05$, Kruskal-Wallis test with Dunn correction for multiple comparisons, n=114 cells (DMSO group), n=63 (Ned-19 1 μM group), n=124 (Ned-19 10 μM group). Cells taken from three separate cultures (approximately 36 individuals)).

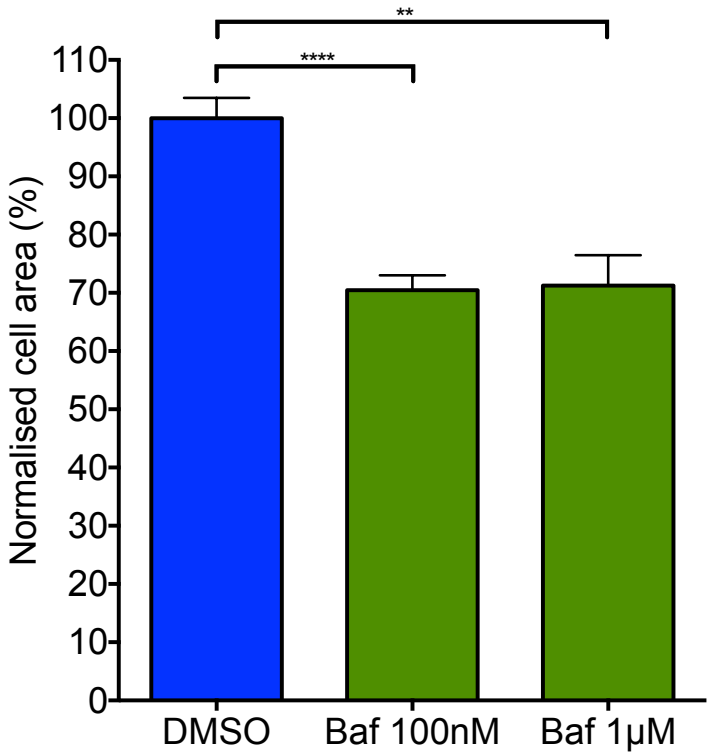


Figure 4.5: The effect of Bafilomycin-A1 on the size of neonatal rat cardiomyocytes after 48 hours. Both 100 nM and 1 µM Bafilomycin-A1 caused a significant reduction in the size of cultured cardiomyocytes in comparison with DMSO alone. A large proportion of cells in cultures exposed to Bafilomycin-A1 died, and it may be that the effect summarised above is due to toxicity of this drug at these concentrations ($P<0.0001$ and $P=0.0088$ for Bafilomycin-A1 100nM and 1 µM respectively, Kruskal-Wallis test with Dunn correction for multiple comparisons, n=114 for DMSO and n=58 and 37 for Bafilomycin-A1 100 nM and 1 µM respectively. There was no difference in effect between the two doses of Bafilomycin-A1, $P>0.05$)).

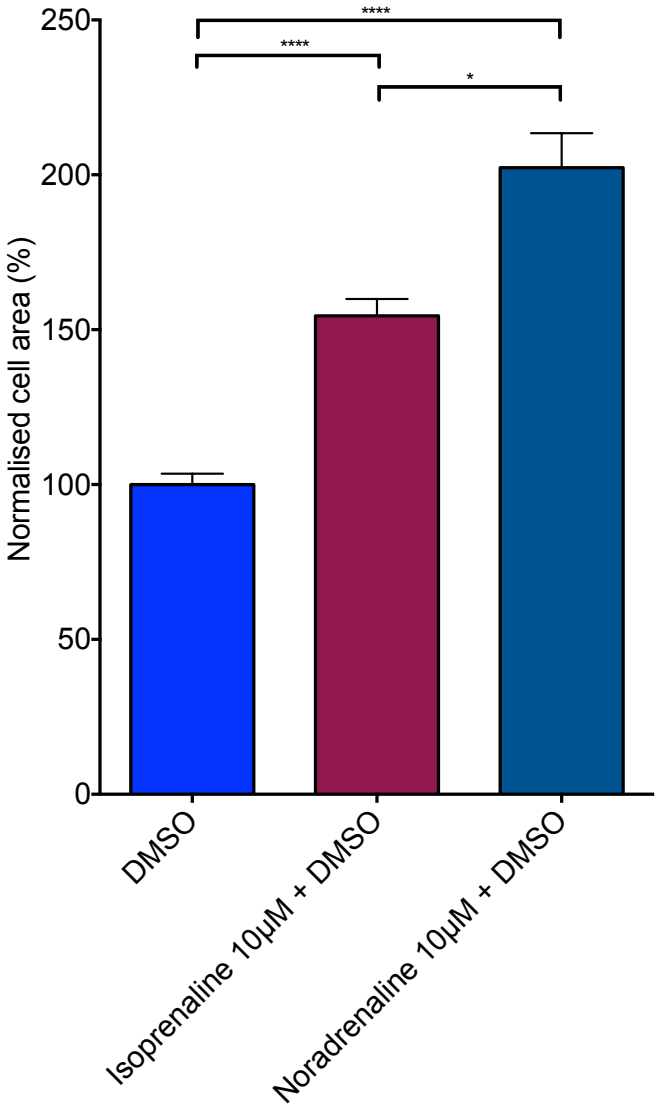


Figure 4.6: Hypertrophic effect of isoprenaline 10 μM compared with that of noradrenaline 10 μM. Noradrenaline had a more marked effect on cell size than isoprenaline at these concentrations (202% ± 11 vs 155% ± 5). Above, * and **** indicates P=0.0258 and P<0.0001 respectively. Data were analysed using a Kruskal-Wallis test with Dunn correction for multiple comparisons, n= 114, 101 and 27 cells from 3 cultures (approximately 36 individuals) for DMSO, Iso 10 μM and noradrenaline 10 μM groups respectively.

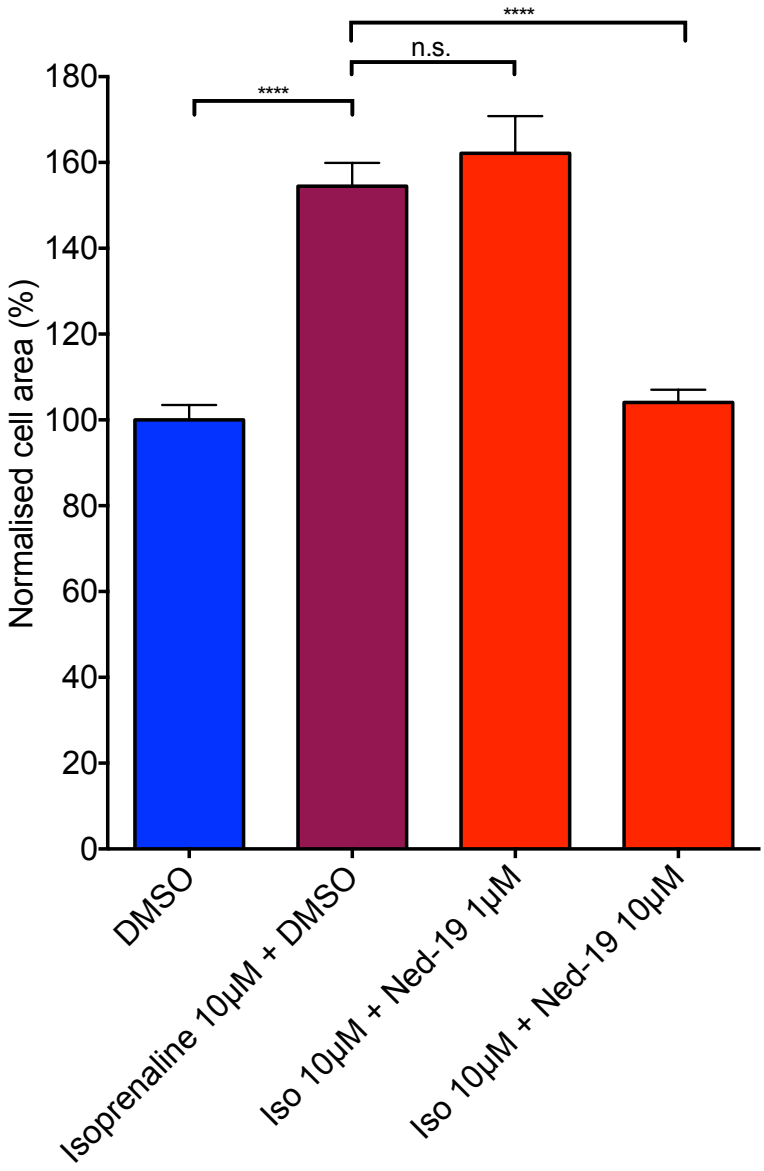


Figure 4.7: Isoprenaline-induced hypertrophy of cells and the effect of Ned-19. Cultured neonatal myocytes exposed to isoprenaline 10 μM for 48 hours became hypertrophied in comparison with DMSO-exposed controls. Cells treated with isoprenaline increased in size to 155% of controls (SEM 5.41). Cells cultured with both Ned-19 10 μM and isoprenaline 10 μM were protected against this effect and did not increase in size compared with controls. A lower concentration of Ned-19 (1 μM) had no protective effect. Above, **** indicates P<0.0001, data were analysed using a Kruskal-Wallis test with Dunn correction for multiple comparisons, n= 114, 101, 44, and 187 cells from 3 cultures (approx 36 individuals) for the DMSO, Isoprenaline 10 μM, Iso + Ned-19 1 μM, and Iso + Ned-19 10 μM groups respectively.

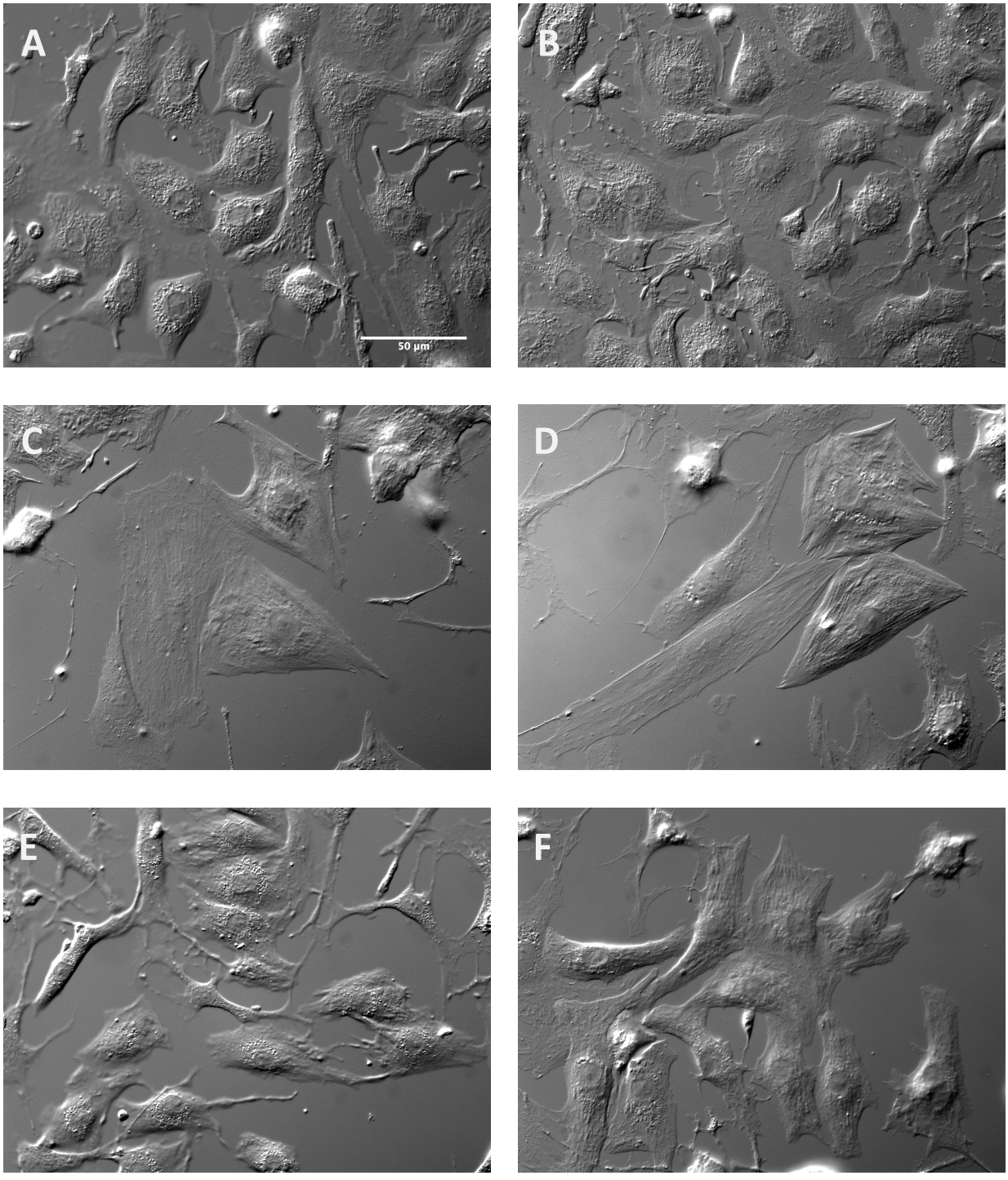


Figure 4.8: Differential Interference Contrast (DIC) images of cultured neonatal rat cardiomyocytes illustrating the effect of isoprenaline and Ned-19. Panels A & B show control cells cultured with DMSO 0.01% alone. Panels C & D show hypertrophied cells as a result of culture with isoprenaline 10 µM and panels E and F show the protective effect of Ned-19 10 µM when added to culture medium containing isoprenaline 10 µM. The scale of panels B to F is identical to that shown on panel A.

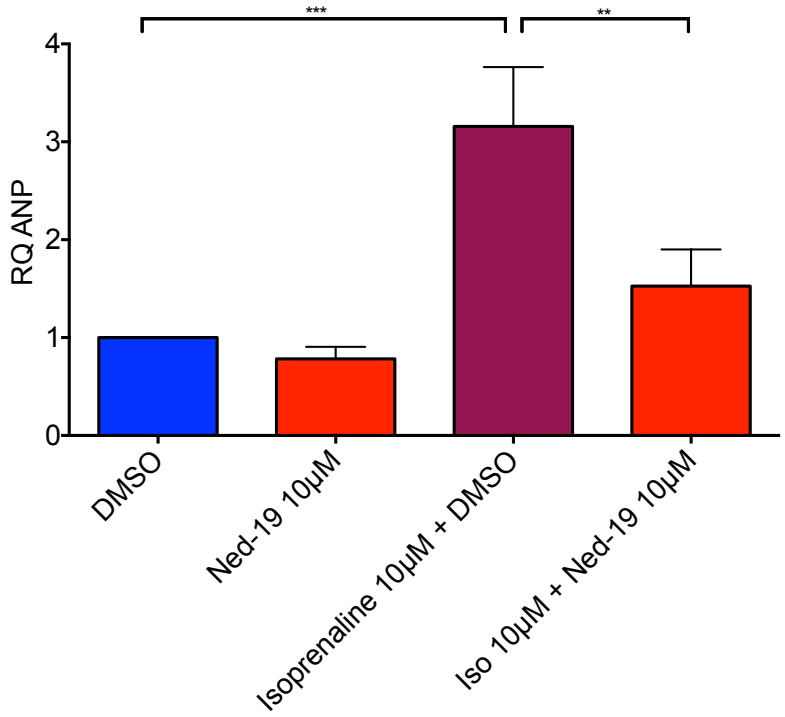


Figure 4.9: Atrial Natriuretic Peptide (ANP) mRNA expression in neonatal rat cardiomyocyte cultures exposed to isoprenaline 10 μM after 48 hours. ANP mRNA was measured using real-time polymerase chain reaction (rtPCR) and normalised to expression of GAPDH mRNA as a marker of cell hypertrophy. Cells treated with isoprenaline 10 μM demonstrated a 3.2±0.6-fold increase in ANP mRNA expression compared with DMSO controls. This effect was prevented by the inclusion of Ned-19 10 μM in the culture medium. Above, *** and ** indicate P=0.0003 and P=0.0061 respectively (one-way ANOVA, n=5).

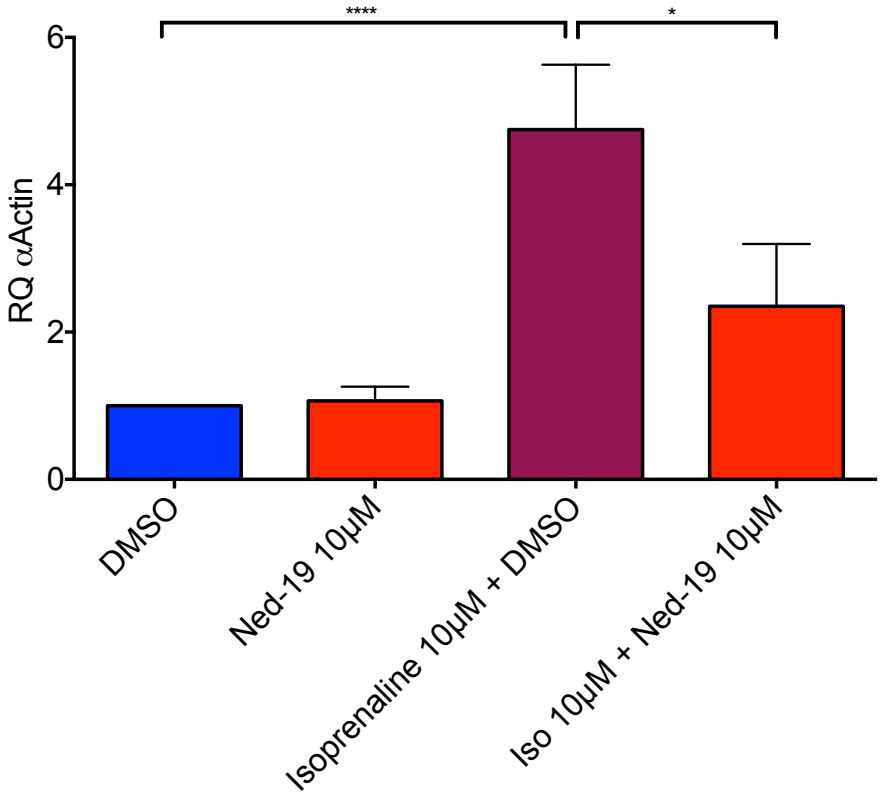


Figure 4.10: α-Actin mRNA expression in neonatal rat cardiomyocyte cultures exposed to isoprenaline 10 μM after 48 hours. α-Actin mRNA was measured using real-time polymerase chain reaction (rtPCR) and normalised to expression of GAPDH mRNA as a marker of cell hypertrophy. Cells treated with isoprenaline 10 μM demonstrated a 4.8±0.9-fold increase in ANP mRNA expression compared with DMSO controls. This effect was significantly reduced by the inclusion of Ned-19 10 μM in the culture medium. Above, **** and * indicate P=<0.0001 and P=0.0207 respectively (one-way ANOVA, n=5).

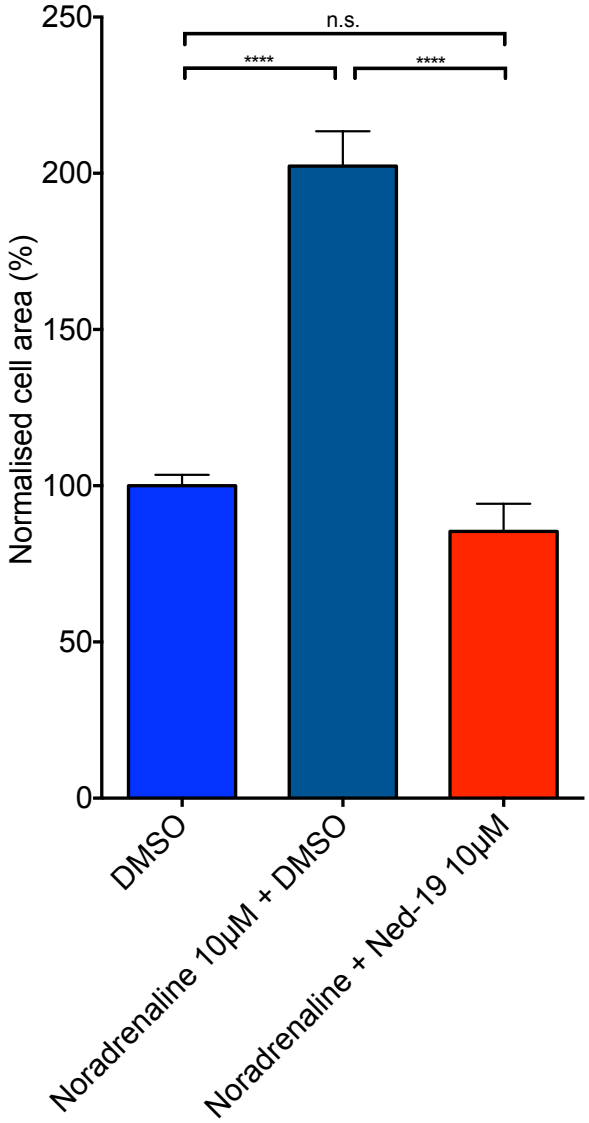


Figure 4.11: Hypertrophic effect of noradrenaline on cultured neonatal rat cardiomyocytes and protective effect of Ned-19 10 µM. Noradrenaline increased cell size by 202±11%, but no significant change in size was observed when Ned-19 10 µM was included with noradrenaline in the culture medium. Above, **** indicates P<0.0001. Data analysed with Kruskal-Wallis test, n=114, 27 and 27 cells from 3 cultures (approximately 36 individuals) for DMSO, Noradrenaline 10 µM and Noradrenaline 10 µM + Ned-19 10 µM groups respectively.

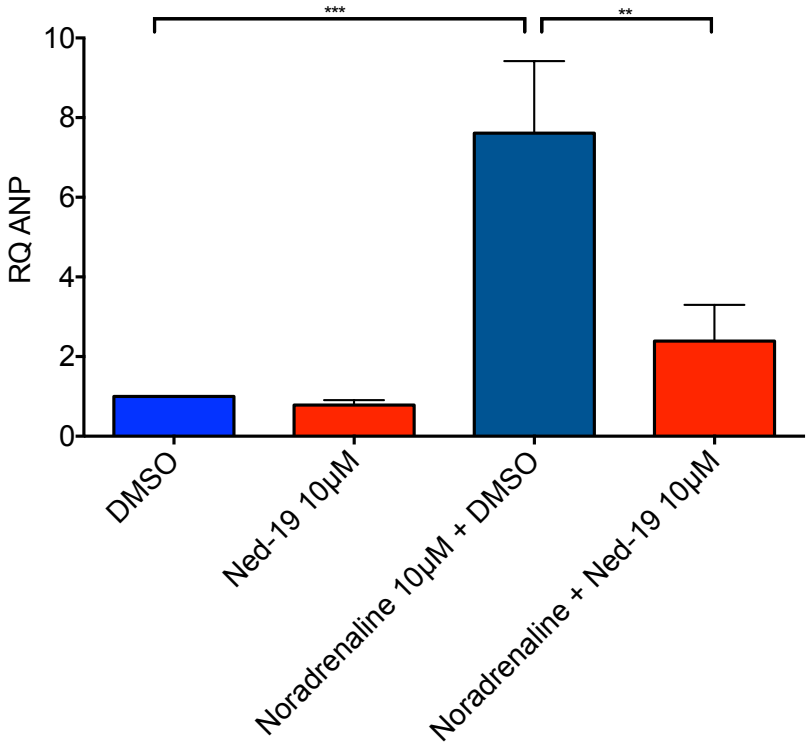


Figure 4.12: Atrial Natriuretic Peptide (ANP) expression in neonatal rat cardiomyocytes cultures exposed to noradrenaline after 48 hours. ANP mRNA was measured using real-time polymerase chain reaction (rtPCR) and normalised to expression of GAPDH mRNA as a marker of cell hypertrophy. Cells treated with noradrenaline 10 μM demonstrated a 7.6±1.8-fold increase in ANP mRNA expression compared with DMSO controls. This effect was prevented by the inclusion of Ned-19 10 μM in the culture medium. Above, *** and ** indicate P=0.0003 and P=0.0051 respectively (one-way ANOVA, n=5).

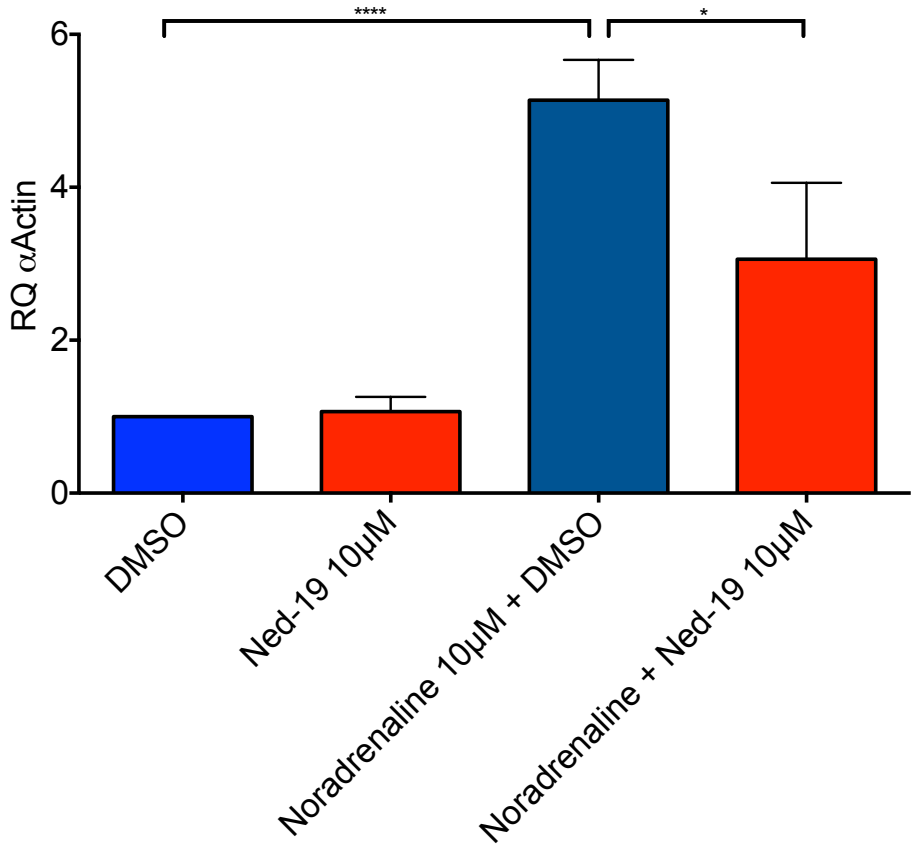


Figure 4.13: αActin expression in neonatal rat cardiomyocyte cultures exposed to noradrenaline after 48 hours. αActin mRNA was measured using real-time polymerase chain reaction (rtPCR) and normalised to expression of GAPDH mRNA as a marker of cell hypertrophy. Cells treated with noradrenaline 10 μM demonstrated a 5.1±0.5-fold increase in αActin mRNA expression compared with DMSO controls. This effect was prevented by the inclusion of Ned-19 10 μM in the culture medium. Above, **** and * indicate $P<0.0001$ and $P=0.0163$ respectively (one-way ANOVA, n=5).

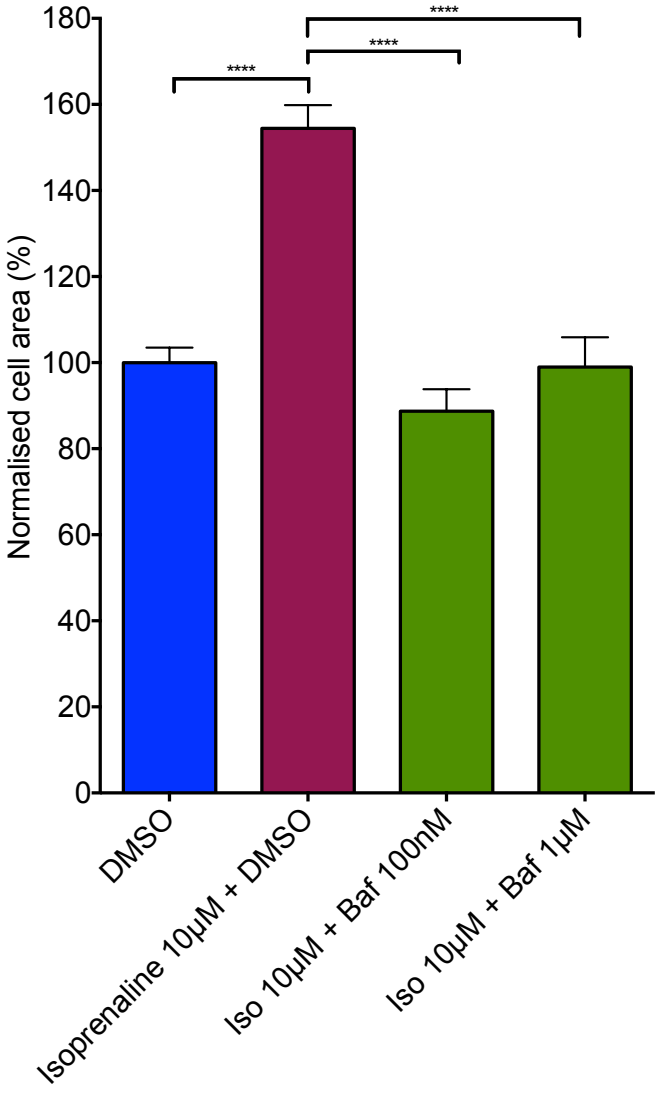


Figure 4.14: Isoprenaline-induced hypertrophy of cells and the effect of Bafilomycin-A1. Cultured neonatal myocytes exposed to isoprenaline 10 μM for 48 hours became hypertrophied in comparison with DMSO-exposed controls. Cells cultured with both Bafilomycin-A1 and isoprenaline 10 μM did not increase in size, and this effect was present regardless of which concentration of Bafilomycin-A1 was used, and both concentrations had the same effect size. It is possible that this finding may reflect toxicity of Bafilomycin-A1 at these concentrations. Above, **** indicates $P<0.0001$, data were analysed using a Kruskal-Wallis test with Dunn correction for multiple comparisons, n= 114, 101, 46 and 45 cells from 3 cultures (approx 36 individuals) for the DMSO, Isoprenaline, Iso + Baf 100 nM, and Iso + Baf 1 μM groups respectively.

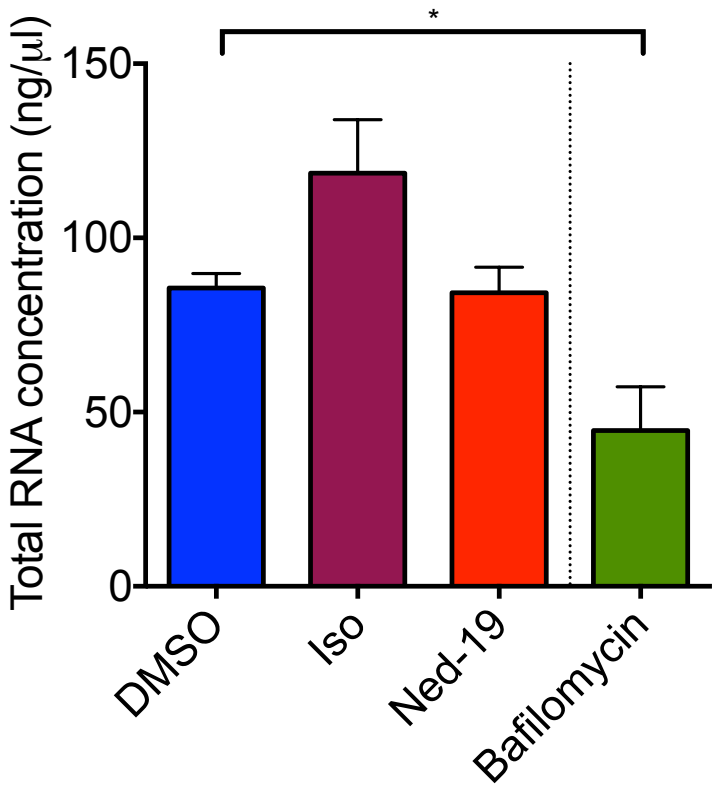


Figure 4.15: Mean total RNA yields from cultures of neonatal rat cardiomyocytes treated with different drugs. Each culture was seeded with approximately equal numbers of cells. Due to the low 'n' of the bafilomycin group, both concentrations were treated as a single group. There were no significant differences between any group and DMSO controls except bafilomycin, which was significantly lower (P=0.0384, one-way ANOVA). There was an expected – although non-significant in this set of experiments – increase in total RNA yield with isoprenaline exposure.

4.3 Conclusion

The results presented in this chapter suggest a role for NAADP in both isoprenaline- and noradrenaline-induced cardiac hypertrophy. Both of these agents provoked a hypertrophic response in cultured neonatal rat cardiomyocytes that could be seen using both cell cross-sectional area measurements and quantitative PCR for transcription of the hypertrophic marker genes, αActin and ANP. The addition of Ned-19 prevented or attenuated these responses, suggesting the involvement of NAADP in the hypertrophy process. Ned-19 had no effect on cells without the prior addition of an adrenergic agonist, suggesting that the NAADP system is dormant in unstimulated cells. On first inspection, the addition of bafilomycin-A1 did appear to reduce the size of cells both in the absence and the presence of adrenergic agonists. However, although no cells that were obviously non-viable were included in the analysis, the number of dead or dying cells was much higher in the cultures exposed to bafilomycin-A1. This was confirmed using a viability assay, which revealed a toxic effect of bafilomycin-A1 at the concentrations used.

The culture of cardiomyocytes with bafilomycin-A1 has not been previously reported. However, bafilomycin-A1 toxicity was observed in cell cultures of a variety of human and mouse derived cell lines (Kinoshita et al., 1996; Nakashima et al., 2003; Nishihara et al., 1995), where it induced apoptosis characterised by DNA fragmentation at concentrations of 10 – 50 nM. The mechanism was not investigated in these studies. Ned-19 had no such toxic effect in the present experiments, and knockout of the putative NAADP receptors TPC1 and TPC2

(either individually or simultaneously) has not been reported to have toxic effects (Ruas et al., 2015). This suggests that the mechanism of bafilomycin-A1 toxicity probably does not involve the NAADP signalling pathway *per se*, but rather depends on long-term attenuation of lysosomal function.

Hypertrophy of cardiac myocytes was observed following culture with both noradrenaline and isoprenaline. The cross sectional area of myocytes exposed to isoprenaline was approximately 150% of controls. This is comparable to the increase of approximately 180% of controls seen in cardiac weight to tibial length ratio by Capel et al. (2015) in wildtype mice when exposed to isoprenaline via subcutaneous mini-pump for fourteen days. However, in the present set of experiments, all markers of hypertrophy were increased to a greater degree by noradrenaline compared with isoprenaline. This may be explained by the relative selectivity of these compounds; noradrenaline has activity at both α and β receptors, whereas isoprenaline is relatively inactive at α receptors. Therefore, exposure of cells to noradrenaline may lead to activation of both Gs and Gq signalling pathways – perhaps conferring a stronger hypertrophic stimulus than if one were activated alone. It has also been noted previously that the β-mediated hypertrophic response desensitizes, which may lead to an overall smaller effect (Simpson et al., 1991). Experiments were not conducted in the presence of selective α or β blockers in order to dissect the effect of blocking one or other of these receptors in the presence of noradrenaline. It is possible that the blockade of α receptors would have attenuated the increase in hypertrophy markers stimulated by noradrenaline to levels more comparable to those stimulated by isoprenaline.

Interestingly, Simpson (1983) demonstrated that noradrenaline-induced hypertrophy of rat neonatal cardiomyocytes was blocked by phentolamine and prazosin but not by propranolol or yohimbine, suggesting that the hypertrophic response to noradrenaline was entirely due to its action at α1 receptors. However, in the same study this group was unable to elicit any hypertrophy using isoprenaline – lending further weight to their argument that β receptors play little role in this response. One reason for this may have been that isoprenaline was used at a concentration of 0.2μM – significantly less than that used in the present experiments and that used by other groups (Gul et al., 2016; Morisco et al., 2001). A modest (10-20%) increase in cell size was later detected using this low concentration of isoprenaline and it was suggested that at least part of the isoprenaline-induced hypertrophy of myocytes may occur as an indirect effect via the small population of non-myocyte cells in the culture induced to release growth factors such as $TGF\beta_3$ as a result of isoprenaline exposure and that this then caused hypertrophy of the myocytes (Long et al., 1993).

Larger concentrations of isoprenaline (2 – 10 μM) were found to induce myocyte hypertrophy in culture. This response could be inhibited using propranolol and betaxolol but not by ICI 118551 (a selective β2 antagonist) or by prazosin. Similarly, the selective β2 agonist zinterol failed to induce hypertrophy in this model. Taken together these results suggest that the hypertrophic response to isoprenaline is due to its action at β1 receptors (Morisco et al., 2001). It has also been suggested that following β1 stimulation, cardiomyocyte hypertrophy in

response to isoprenaline may be due to the upregulation and activation of the exchange protein directly activated by cAMP (EPAC) and not a result of PKA activation (Metrich et al., 2008; Morel et al., 2005). In keeping with this, EPAC has also been shown to be involved with excitation-transcription coupling and can also lead to CaMKII activation (Pereira et al., 2007; Pereira et al., 2012) – an enzyme shown to be important in NAADP signalling (Capel et al., 2015). These observations are in contrast to the results of experiments looking at the development of ventricular arrhythmias in response to β-adrenergic stimulation instead of hypertrophy, when EPAC did not appear to play a role but PKA did (Nebel et al., 2013).

Despite these possible differences in mechanism between isoprenaline and noradrenaline, the addition of Ned-19 to cultures completely prevented the development of hypertrophy in response to either drug. This has important implications for the NAADP signalling system, and there are several explanations. It is possible that both α and β transduction cascades converge on the NAADP system and that it functions in a similar way to that hypothesised during acute adrenergic stimulation. However, it is also possible that NAADP functions as a more widespread signalling molecule in the heart than previously thought – at least in the context of chronic adrenergic exposure. There is a possibility that NAADP signalling is not only coupled to β receptors, but also independently to α receptors. Furthermore, while the synthesis of NAADP is thought to be coupled to the activation of an ADP-ribosyl cyclase (ARC) following PKA activation (Gul et al., 2016), it is also possible that EPAC is an upstream component of the pathway that leads to NAADP production.

Bafilomycin-A1 also significantly attenuated the hypertrophic effect of isoprenaline. However, due to the results discussed above that suggest reduced viability of cells treated with this drug, it is difficult to say whether this observation is really due to an anti-hypertrophic effect or just a result of toxicity.

In experiments where isoprenaline was infused into *Tpcn2*$^{-/-}$ mice for two weeks, there was a reduction in the hypertrophic response compared to wildtype animals (Capel et al., 2015). The subtype of receptor being stimulated in these experiments was not explored. However, these results are in keeping with those presented here and together suggest that NAADP acts at TPC2 to initiate a chain of events leading to a hypertrophic response.

Also in keeping with a role for the NAADP system in adrenergic-induced hypertrophy, Gul et al. (2016) performed similar experiments using mice lacking the gene for CD38. Like the *Tpcn2*$^{-/-}$ animals these mice were protected from the effects of chronic infusion of isoprenaline compared with wildtypes which developed hypertrophy, fibrosis and impaired cardiac function. However, Gul et al. also presented data suggesting that while CD38 seems to synthesise cADPR, another ARC is responsible for NAADP production in the heart. This conclusion is supported by data showing that CD38 and CD157 can be stimulated by zinc ions, but cardiac ARC is inhibited (Kannt et al., 2012; Xie et al., 2005). These findings may indicate a role for both NAADP and cADPR in the development of hypertrophy.

In summary, the data presented in this chapter show that inhibition of NAADP signalling prevents the development of hypertrophy in response to both chronic α- and β- adrenergic stimuli. This suggests that NAADP may be involved in the downstream signalling pathways of more than one subtype of adrenergic receptor in the heart.

5

The association of lysosomes with sarcomeric structures in ventricular muscle: Light microscopy

5.1 Introduction

Despite the significance of NAADP signalling in excitation-contraction coupling and β-adrenergic signalling in the heart (Capel et al., 2015; Macgregor et al., 2007), little is known about the relevant ultrastructural organisation of cardiomyocytes to this pathway. However, functional studies suggest clues that allow hypotheses to be made.

Release of NAADP into cardiomyocytes results in an enhancement of the calcium transient and a positive inotropic effect. Conversely, inhibition of NAADP signalling causes a blunting of the increase in calcium transient and of the positive inotropic effect that are usually seen following exposure to β-adrenergic agonists such as isoprenaline (Capel et al., 2015).

It is widely accepted that NAADP acts at lysosomes to cause calcium release (Calcraft et al., 2009; Churchill et al., 2002; Galione, 2006). However, the link between lysosomal calcium release and enhanced whole-cell calcium transient has not been definitively established. On first consideration, the simplest answer would seem to be that lysosomal calcium and calcium released from the SR are additive, such that extra calcium released from the lysosome contributes to that released from the SR and results in an increased whole-cell calcium transient amplitude. However, it is likely that the mechanism is less straightforward than this. In most cell types, the total lysosomal volume represents a small fraction of the volume of the S/ER; for example, in hepatocytes, the ER occupies approximately 15% of the total cell volume, whereas the cumulative lysosomal

volume is approximately 1% (Alberts, 2015 p. 643.). Therefore, depending on buffering capacity, it is likely that lysosomes contain only a small percentage of whole-cell calcium. In addition to this, there are several pieces of evidence that suggest that an amplification mechanism exists.

The 'trigger' hypothesis has been suggested as a mechanism by which lysosomal calcium release is amplified (Cancela et al., 1999; Guse et al., 2008; Morgan et al., 2011). The hypothesis states that the relatively small local release of calcium from the lysosome in response to NAADP stimulates a much larger, global calcium release from the SR. This is most likely to occur by direct stimulation of SR ryanodine receptors by lysosomal calcium, causing calcium-induced calcium release (CICR). An alternative is that the small amount of calcium released from the lysosome is taken up by SERCA, and although this does not alter the absolute mass of SR calcium by a significant degree, the small change in luminal calcium concentration is sufficient to prime ryanodine receptors so that calcium release is enhanced (Morgan et al., 2011). It has recently been suggested that calcium release caused by NAADP leads to the synthesis of the related calcium signalling molecule, cADPR and it is this that acts at the ryanodine receptor (Gul et al., 2016).

There is considerable evidence for the trigger hypothesis in non-cardiac cells. For example, in pulmonary artery smooth muscle cells (PASMCs), introduction of NAADP into the cell evoked a global increase in calcium concentration that disappeared if the cells had been pre-incubated with thapsigargin (an inhibitor of SERCA), and ryanodine (which blocks calcium release from the SR). However,

although the global calcium increase was abolished under these conditions, smaller localised calcium 'bursts' were still visible. This suggested that the initial localised increase in calcium that was induced by NAADP was responsible for (and amplified to produce) the global rise in calcium seen subsequently. Calcium responsible for the global rise appeared to be released from the SR, but the initial localised calcium was from a thapsigargin and ryanodine-insensitive store (Boittin et al., 2002; Kinnear et al., 2004).

In the heart, given the regular cyclical release and reuptake of calcium from the SR, the concept of a calcium 'trigger' could be replaced by a more fluid calcium 'modulator' that may function in a similar way; calcium is released from and taken up by the SR during every cardiac cycle, but the amount released and taken up again can be altered – under the influence of lysosomal calcium released in response to NAADP.

Evidence is already accumulating that is consistent with this hypothesis. Enhanced calcium loading of the SR in cardiomyocytes has been demonstrated following application of NAADP (Macgregor et al., 2007), and the increase in calcium transient that occurs following application of NAADP in these cells can be blocked by inhibitors of type-II calmodulin-dependent protein kinase (CaMKII) – suggesting that this enzyme is required for the regulation of the calcium transient amplitude following NAADP stimulation (Capel et al., 2015).

It is therefore possible that the calcium released from the lysosome in response to NAADP may activate CaMKII to cause phosphorylation of targets that enhance

calcium loading of the SR, and therefore enhance the calcium transient. An obvious target to consider is phospholamban (PLB), which binds to SERCA and exerts an inhibitory effect – acting as a 'brake' on the activity of the pump. Phosphorylation of PLB relieves this inhibition and allows enhanced loading of the SR with calcium (Bers, 2002; Stammers et al., 2015).

The possibility that this mechanism works alongside that described earlier cannot be ruled out; calcium could still cause CICR via the ryanodine receptor at the same time as CaMKII acts at SERCA via phospholamban. It is also possible that CaMKII could phosphorylate the ryanodine receptor to enhance calcium conductance, resulting in increased calcium release. There are known phosphorylation targets for CaMKII on the ryanodine receptor that enhance activity (Guo et al., 2006; Kockskamper et al., 2006).

If the calcium trigger/modulator hypothesis is correct, an intimate spatial relationship between lysosome and SR is prerequisite (Morgan et al., 2011). Furthermore, it may be that a close association between the lysosome and particular SR structures such as the ryanodine receptor or phospholamban are also required. To date, there is no evidence of such a relationship in cardiac tissue. However, in vascular smooth muscle cells, when lysosomes were fluorescently labelled with lysotracker red at the same time as ryanodine binding sites were labelled with BODIPY-ryanodine, there was a close association between the two signals (Kinnear et al., 2004). Similarly, using the same tissue, another study found co-localisation of the type-1 lysosome-associated membrane protein (LAMP-1) and type-3 ryanodine receptor (RyR3) in the

perinuclear region of these cells, along with the finding that NAADP preferentially invoked calcium bursts in the same region (Kinnear et al., 2004; Kinnear et al., 2008). This strongly suggests that these structures are closely associated in order to facilitate an amplification mechanism for calcium signalling.

If all lysosomes in the heart were associated with SR structures, then it would be reasonable to assume that labelling them using a technique such as immunocytochemistry would reveal a striated appearance in cardiomyocytes. However, this is known not to be the case (Endo et al., 2015). However, in addition to the hypothesised function described above, lysosomes are known to be highly heterogeneous, and also have a well-established role in cellular degradation processes such as autophagy (Alberts, 2015, p.726). It may be that only a subpopulation of lysosomes are involved in calcium signalling, and only this subpopulation that are associated with SR proteins such as ryanodine receptor and phospholamban.

This aim of experiments in this chapter is to test this hypothesis using immunocytochemical techniques and labelling of live cardiomyocytes to directly visualise lysosomes in relation to SR-associated structures and proteins. In addition, the location of NAADP binding sites will be identified using the fluorescent NAADP antagonist, Ned-19.

Recent experiments have also implicated NAADP signalling in the mechanism of ischaemia-reperfusion injury in the heart (Davidson et al., 2015), and a possible

link to mitochondrial function in this context. Observations were therefore made to evaluate the possibility that there might also be a close spatial relationship between lysosomes and mitochondria in the heart.

5.2 Results

5.2.1 Labelling of lysosomes with LAMP-2 or lysotracker green in rabbit ventricular cardiomyocytes reveals a punctate distribution.

Labelling of lysosomes in rabbit ventricular cardiomyocytes was performed using two different techniques. In the first method, primary antibodies against the type-2 lysosome-associated membrane protein (LAMP-2) were used in fixed cells and then labelled with a fluorescent secondary antibody. The second method involved using lysotracker green or red to stain acidic compartments in live cells. In both techniques, a confocal microscope was used to obtain images.

Both techniques revealed a punctate pattern of labelling seen throughout the cell. The labelling seen with LAMP-2 in fixed cells appeared to indicate that lysosomes were more numerous than when labelled with lysotracker green in live cells, but (on first inspection), lysosomes appeared to be numerous and randomly distributed using both labelling techniques. Labelling of LAMP-2 also revealed fluorescence in the nucleus, which was not seen with lysotracker green stains (figure 5.1, panel A).

Typical patterns of staining using these techniques can be seen in figures 5.1 and 5.2.

5.2.2 A subpopulation of lysosomes labelled with LAMP-2 were found to be distributed through rabbit cardiomyocytes with a similar periodicity to sarcomeric proteins such as ryanodine receptor-2 and phospholamban.

In contrast with the pattern of staining seen using LAMP-2 immunocytochemistry, that seen when primary antibodies against type-2 ryanodine receptor (RyR2) or phospholamban (PLB) were used revealed the well-recognised regular striated appearance. Both of these labels were seen as striations running across the width of the cell, perpendicular to its long axis. The distance between each striation for RyR2 and PLB was 1.82±0.04 μm and 1.79±0.04 μm respectively (n=6 cells in each group).

When the pattern of LAMP-2 labelling was inspected more closely, there appeared to be a subpopulation of lysosomes that were distributed along the long axis of the cell with a regular periodicity. These areas were deliberately chosen and the frequency of the labelling measured by plotting fluorescence intensity against distance. The mean distance between LAMP-2 labels was 1.87±0.07 μm (n=6 cells).

Typical examples of these measurements can be seen in figure 5.3 and mean data is shown in figure 5.4. The frequency of the fluorescence signals for RyR2, PLB and LAMP-2 was not significantly different using these techniques ($P>0.05$, one-way ANOVA).

In order to evaluate whether this relationship held true throughout cells labelled with LAMP-2 and not just in areas deliberately chosen for analysis, a broader analysis technique was employed. Images of cells that had been co-labelled with both RyR2 and LAMP-2 using different secondary antibodies were orientated so that the RyR2 striations were seen vertically. The sum of the fluorescence intensities for each column of pixels in the image was then measured and plotted against horizontal distance. With the cell in the same orientation, column fluorescence intensity plots were also constructed using the LAMP-2 labelling. The intensity plots against distance for the two labels were overlaid (an example is shown in figure 5.5, panel C). The intensity for each column in the RyR2 channel was also plotted against the intensity for each column in the LAMP-2 channel (see figure 5.5, panel D) in order to give a correlation.

The waveforms obtained by plotting fluorescence intensity against distance for both RyR2 and LAMP2 were then subjected to Fourier analysis to reveal their individual frequency components. An example of this analysis is shown in Figure 5.5 panels E and F. In this particular cell, the dominant frequency of the RyR2 signal is 0.560 striations per micron, corresponding to one striation every 1.79 μm. Although the LAMP-2 signal was much more complicated, Fourier analysis revealed a dominant frequency peak in this cell at 0.555 signals per micron, or one LAMP-2 signal every 1.80 μm.

This analysis was also performed in the same way using cells co-labelled with PLB and LAMP2. See figure 5.6 for an example – in this cell, both the PLB signal

and the LAMP-2 signal have a dominant frequency of 0.574 signals per micron, or one signal every 1.74 μm.

In total, 22 cells (18 RyR2 vs LAMP-2 and 4 PLB vs LAMP-2) were analysed in this way. The dominant frequency of the RyR2 or PLB in each cell was plotted against the dominant frequency of the LAMP-2 signal in the same cell. When all 22 cells were taken together, there was a positive correlation between the dominant frequencies of the two signals (r=0.72, figure 5.7).

This method of analysis is in broad agreement with the simpler method described earlier, and suggests that a subpopulation lysosomes may be distributed across the cell with a similar periodicity to that of RyR2 and PLB.

5.2.3 A subpopulation of lysosomes labelled with LAMP2 were found in close proximity with ryanodine-receptor-2 and with phospholamban.

The fact that LAMP-2 and RyR2 or PLB seem to be distributed across the length of the cell with a very similar periodicity does not in itself mean that these proteins are necessarily located in close proximity with each other. The question of whether this is the case was addressed next.

Ryanodine receptor and phospholamban are both proteins found associated with the SR and are concerned with calcium release and reuptake respectively. As expected, in cells that had been co-labelled with antibodies against both LAMP-2

and either RyR2 or PLB, there was little overt co-localisation. The Pearson correlation co-efficients for RyR2 vs LAMP-2 and PLB vs LAMP-2 using the column fluorescence intensity method described above were 0.35 and 0.22 respectively. However, in both groups of cells there were subpopulations where the labelling of the two proteins did come into very close proximity. This is illustrated by the white arrows in figures 5.8 and 5.9. There was no cross-reactivity detected between antibodies (data not shown).

The proximity of RyR2 or PLB to LAMP-2 was studied in more detail using the pixel column fluorescence intensity data obtained from the co-labelled cells as described above. When the intensity-distance plots of the two labels were overlaid, the phase offset between the signals could be estimated to evaluate the mean distance between an RyR2 or PLB signal and the nearest LAMP-2 signal (an example is shown in figure 5.10). These distances were estimated to be 0.27±0.03 μm (n=16) and 0.22±0.05 μm (n=3) respectively. See figure 5.11.

5.2.4 Binding sites for Ned-19 are highly co-localised with lysosomes labelled with lysotracker red.

Ned-19 is a recently synthesised compound that has a structure very similar to that of NAADP and in many contexts has been found to act as its antagonist (Naylor et al., 2009). It is therefore reasonable to hypothesise that Ned-19 and NAADP may bind to the same receptor and act as antagonist and agonist respectively (Rosen et al., 2009).

There is considerable evidence suggesting that NAADP acts on the lysosomal membrane (Galione, 2006), and we therefore hypothesised that Ned-19 would also bind here. In order to visualise any association between Ned-19 and the lysosome, we performed experiments using Ned-19 (which is itself fluorescent) and lysotracker red.

Live isolated rabbit ventricular cardiomyocytes were incubated with Ned-19 and lysotracker red and then observed with a confocal microscope. There was a high degree of co-localisation between the signals ($r=0.84\pm0.022$, $n=6$, shown in figure 5.12). Some areas were stained with lysotracker red but did not co-label with Ned-19. These were seen most frequently adjacent to the nucleus, and it is possible that these represent Golgi apparatus rather than lysosomes. This can be seen in panel C in figure 5.12, and is highlighted by the white arrow.

There was no optical bleed-through detected between fluorescence channels that might explain this high degree of co-localisation (see appendix A).

5.2.5 Lysosomes labelled with lysotracker green appear in close proximity with T-tubules labelled with di-8-anepps in rabbit ventricular cardiomyocytes.

It is well established that ryanodine receptors are found on the SR very closely apposed to L-type calcium channels on the T-tubules formed by the plasma membrane. These two proteins are found together and form a structure known

as the couplon (Asghari et al., 2012; Scriven et al., 2013). The plasma membrane can be labelled with the voltage-sensitive dye di-8-anepps. Cells were therefore co-labelled with this and lysotracker green to test whether there may be a spatial association between lysosomes and T-tubules (and therefore possibly between lysosomes and the couplon) in ventricular myocytes.

As expected, T-tubules were seen as striations when stained with di-8-anepps. These strongly resembled the appearance of cells labelled with RyR2 or PLB. The co-labelling of cells with lysotracker green appeared very similar to cells co-labelled with LAMP2 and RyR2: There were many examples where the lysosomes appeared in close proximity with the T-tubules. A typical image can be seen in figure 5.13.

5.2.6 Mitochondrial labelling produces diffuse staining of rabbit ventricular cardiomyocytes.

In similar experiments, mitochondria were labelled with tetramethylrhodamine ethyl ester (TMRE) at the same time as lysosomes were labelled with lysotracker green.

Due to the high energy demands of cardiomyocytes, mitochondria are densely packed. Consequently, TMRE staining was diffuse with only narrow dark bands indicating a striated mitochondrial organisation.

Lysotracker green also produced its characteristic punctate appearance. However, due to the density of TMRE labelling, it is difficult to comment on the association between lysosomes and mitochondria using this technique. A typical cell co-labelled with TMRE and lysotracker green is shown in figure 5.14.

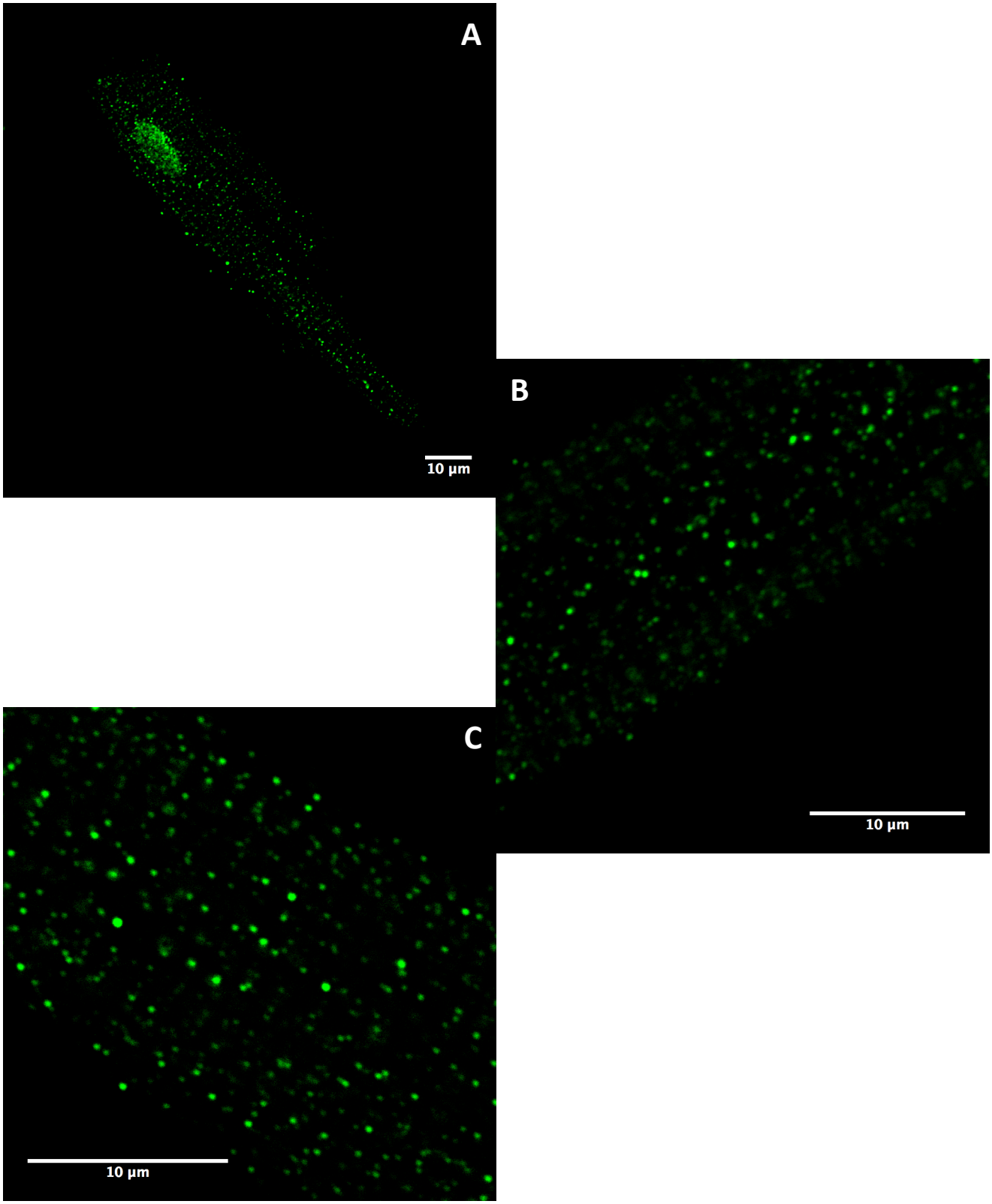


Figure 5.1: Typical distribution of LAMP2 in a rabbit ventricular cardiomyocyte using fluorescent immunocytochemistry. Panels A, B and C show progressively increasing magnification of whole rabbit ventricular cardiomyocytes. The punctate distribution of LAMP2 labelling is typical, and similar to that seen with lysosomal labelling using lysotracker green. However, the density of labelling is higher with LAMP2 and it is possible that this may represent trafficking of the LAMP2 protein as well as that found on lysosomal membranes.

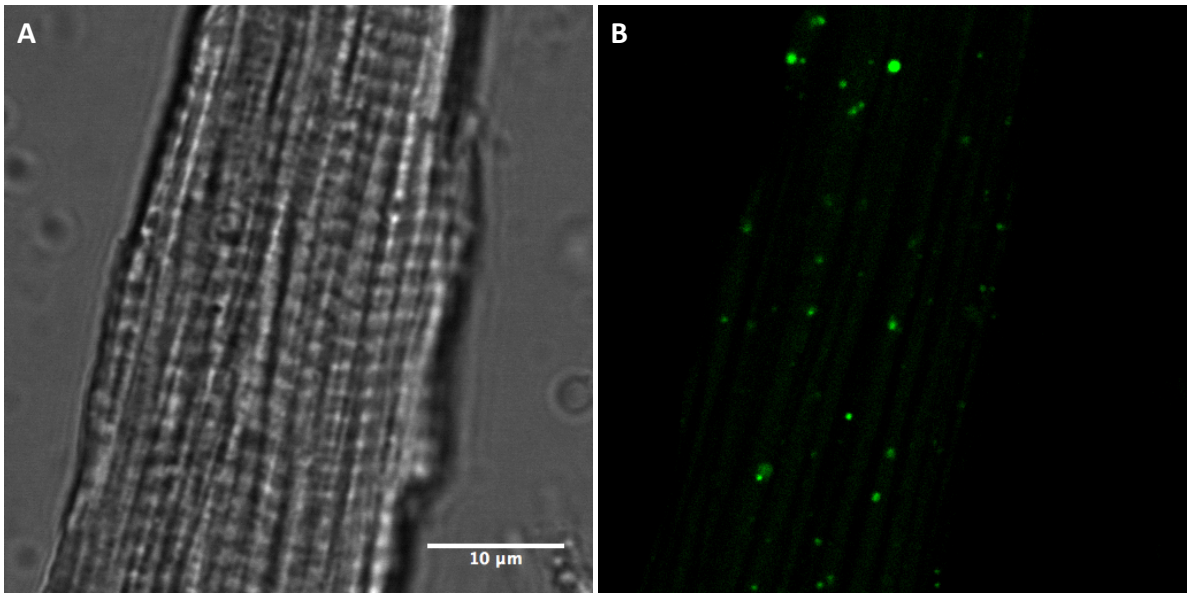


Figure 5.2: Typical distribution of lysosomes labelled with lysotracker green in a rabbit ventricular cardiomyocyte. Panels A and B show the brightfield microscope image and the fluorescence from lysotracker green respectively. The punctate distribution of lysotracker is typical, and similar to that seen with LAMP2 labelling, although it is less dense.

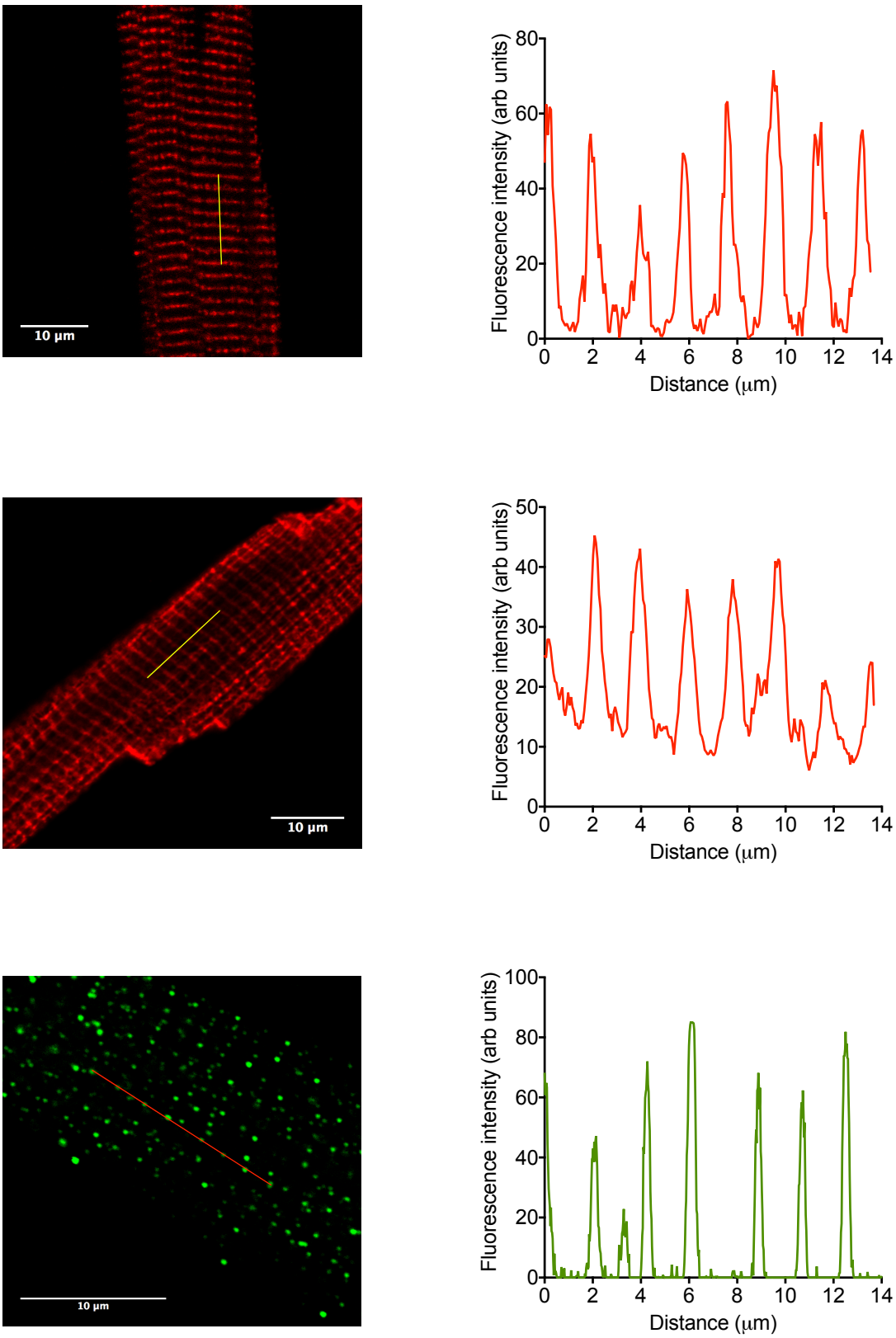


Figure 5.3: Representative measurements of fluorescence intensity across rabbit ventricular cardiomyocytes. Cells were labelled using fluorescent immunocytochemistry to show type-2 ryanodine receptor (top panel), phospholamban (middle) and LAMP2 (bottom). Using the intensity plot, the frequency of the wave could be calculated, and compared between the different protein labels.

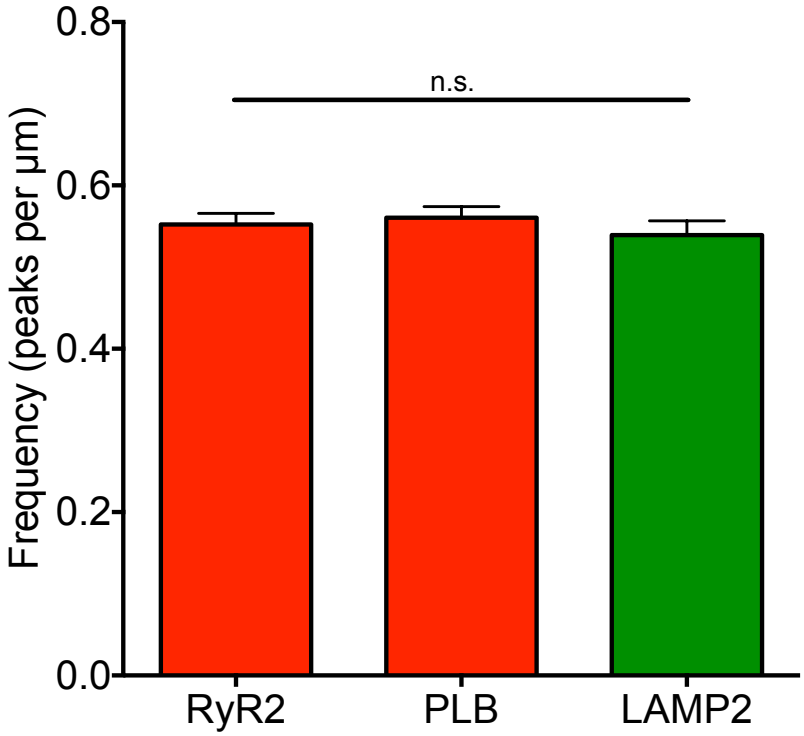


Figure 5.4: Frequency of fluorescence intensity plots for type-2 ryanodine receptor (RyR2), phospholamban (PLB) and LAMP2 in rabbit ventricular cardiomyocytes. No significant difference was seen between frequencies of these proteins (P>0.05, one-way ANOVA, n=6). This finding may suggest that some lysosomes are organised in association with sarcomeric structures.

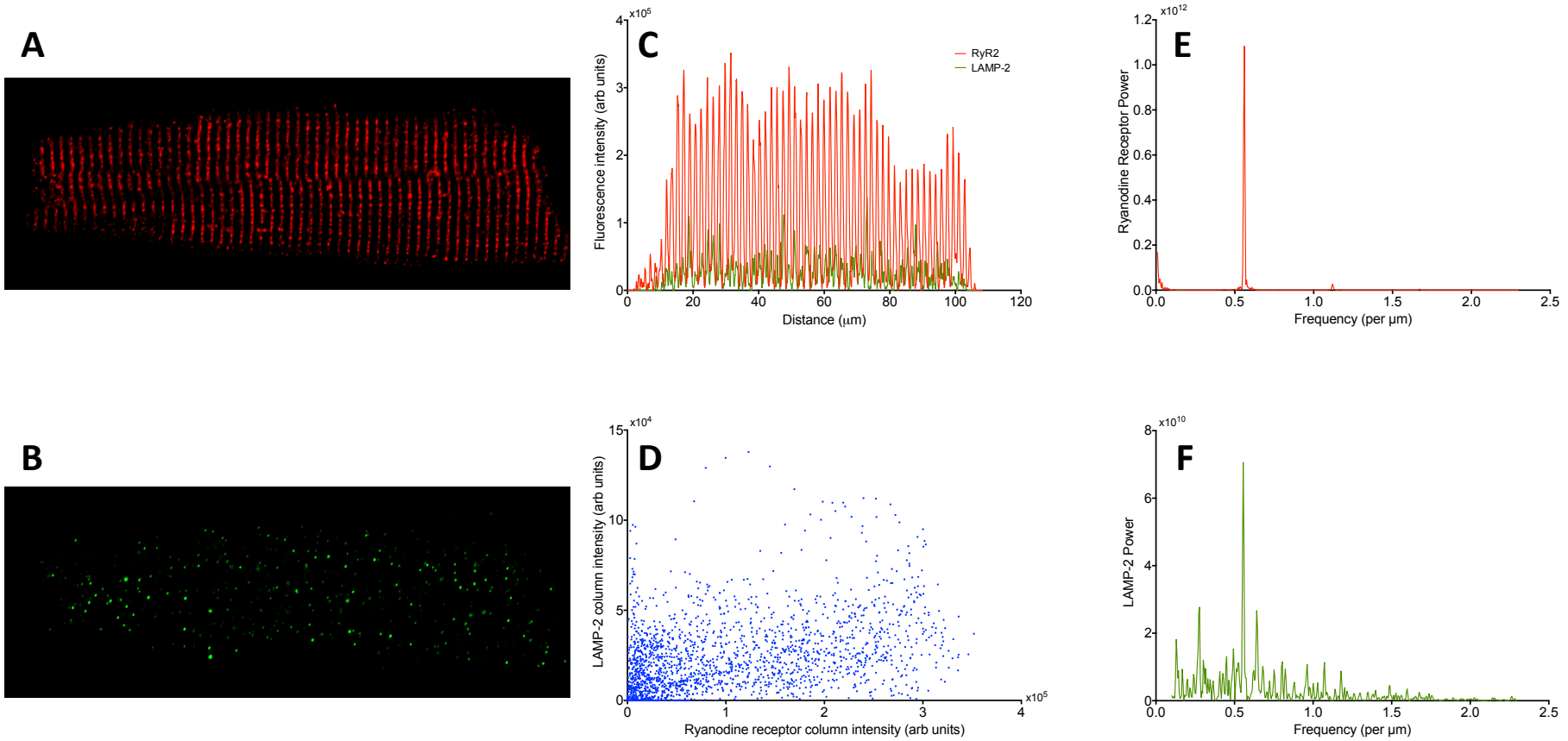


Figure 5.5: A representative example of a more sophisticated method for analysis of immunocytochemistry of cells co-labelled with antibodies against RyR2 and LAMP-2. Panels A and B show the same cell labelled with RyR2 and LAMP-2 respectively. The cell has been orientated so that the striations of RyR2 run vertically. The sum of the fluorescence intensity of each column in the image was then calculated and plotted against distance along the cell (shown in panel C). The sum of fluorescence intensities of RyR2 was also plotted against the sum of intensities of LAMP-2 (panel D). Fourier analysis was performed on each of the waveforms to derive the dominant frequencies. These are plotted in panels E (RyR2) and F (LAMP-2). Despite the apparent randomness of the LAMP-2 labelling, the dominant frequency is almost identical to that seen in RyR2 labelling (0.560 RyR2 signals per μm, corresponding to one striation every 1.79 μm versus 0.555 LAMP-2 signals per μm, corresponding to one LAMP-2 signal every 1.80 μm in this image).

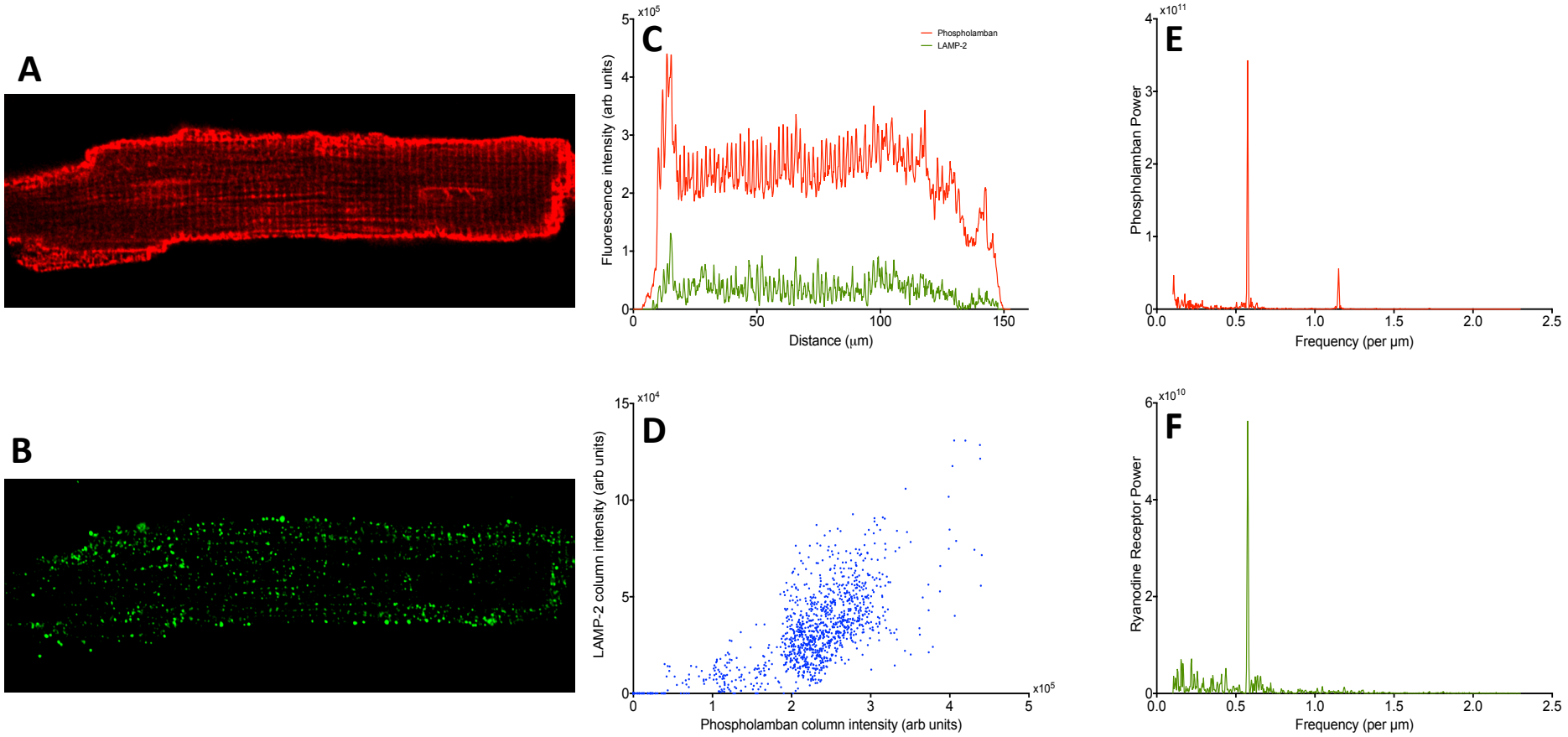


Figure 5.6: A representative example of a more sophisticated method for analysis of immunocytochemistry of cells co-labelled with antibodies against phospholamban (PLB) and LAMP-2. Cells co-labelled with antibodies against PLB and LAMP-2 were analysed in the same way as those co-labelled with antibodies against RyR2 and LAMP-2. Panels A and B show the same cell labelled with PLB and LAMP-2 respectively. The cell has been orientated so that the striations of PLB run vertically. The sum of fluorescence intensities of each column in each image was then calculated and plotted against distance along the cell (shown in panel C). The sum of fluorescence intensities of PLB was also plotted against those of LAMP-2 (panel D). Fourier analysis was performed on each of the waveforms to derive the dominant frequencies. These are plotted in panels E (PLB) and F (LAMP-2). In this image, the dominant frequency seen in the PLB waveform is identical to that seen in that from PLB (0.574 signals per μm, corresponding to one striation or one LAMP-2 signal every 1.74 μm).

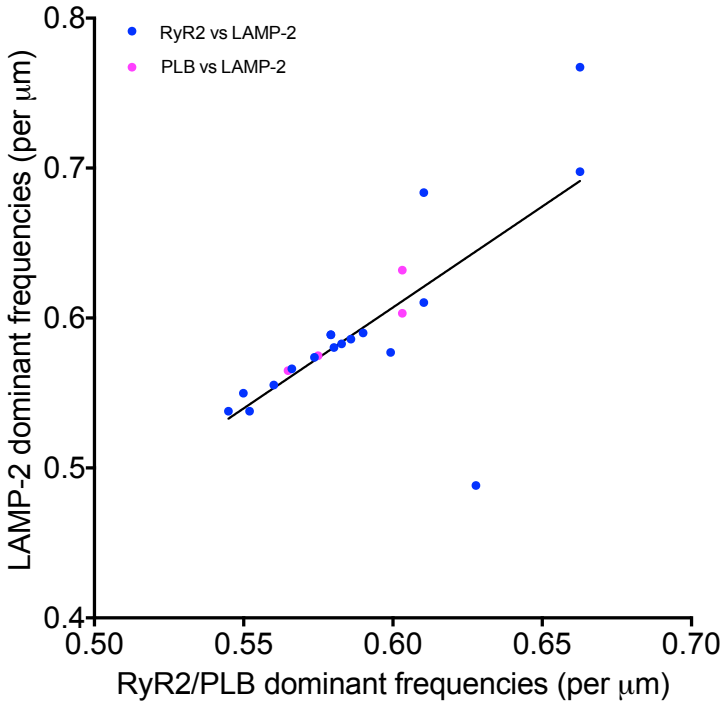


Figure 5.7: Correlation between dominant frequencies of RyR2/PLB and LAMP-2 images. The dominant frequencies found in the fluorescence intensity waveforms from images of RyR2 or PLB labelling were plotted against those from LAMP-2 labelling in the same cell. The Pearson product-moment correlation coefficient (r) = 0.72, n=22 cells (n=18 for RyR2 vs LAMP-2 (blue) and n=4 for PLB vs LAMP-2 (pink)).

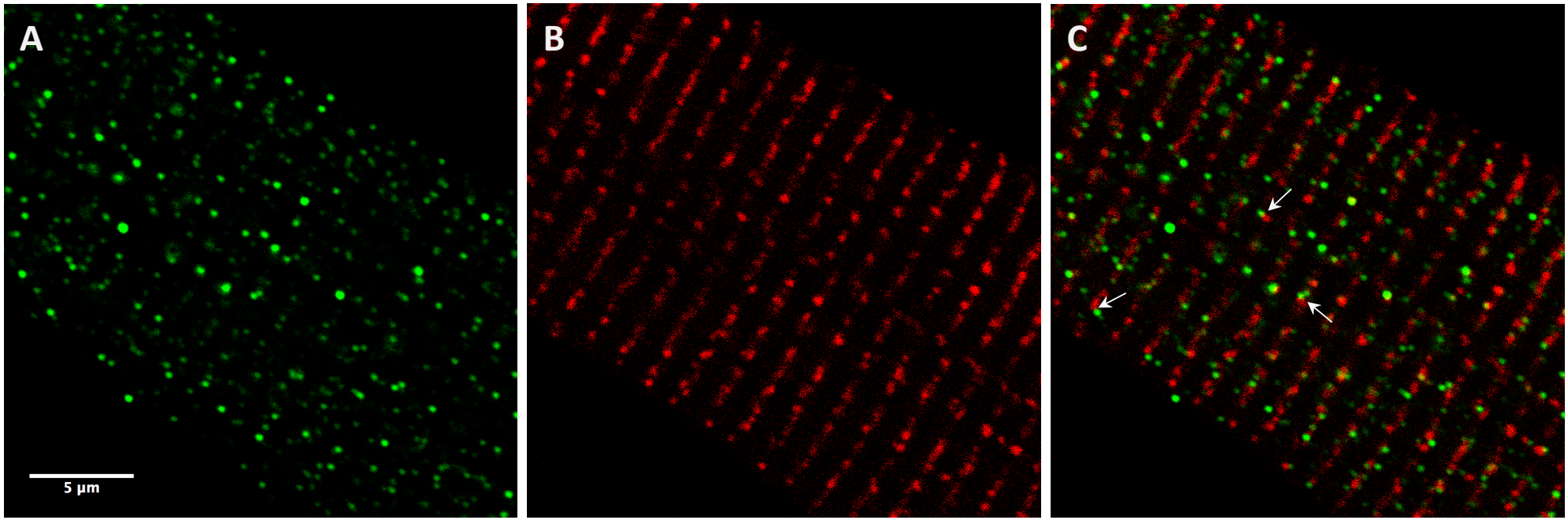


Figure 5.8: Co-labelling of LAMP2 and type-2 ryanodine receptor (RyR2) using fluorescent immunocytochemistry in a rabbit ventricular cardiomyocyte. Panel A and B show LAMP2 labelling and RyR2 labelling respectively, and these images are merged in panel C. LAMP2 had a punctate distribution while RyR2 was striated. There was no overt co-localisation, but in many places LAMP2 was seen in very close proximity to RyR2 (white arrows, panel C).

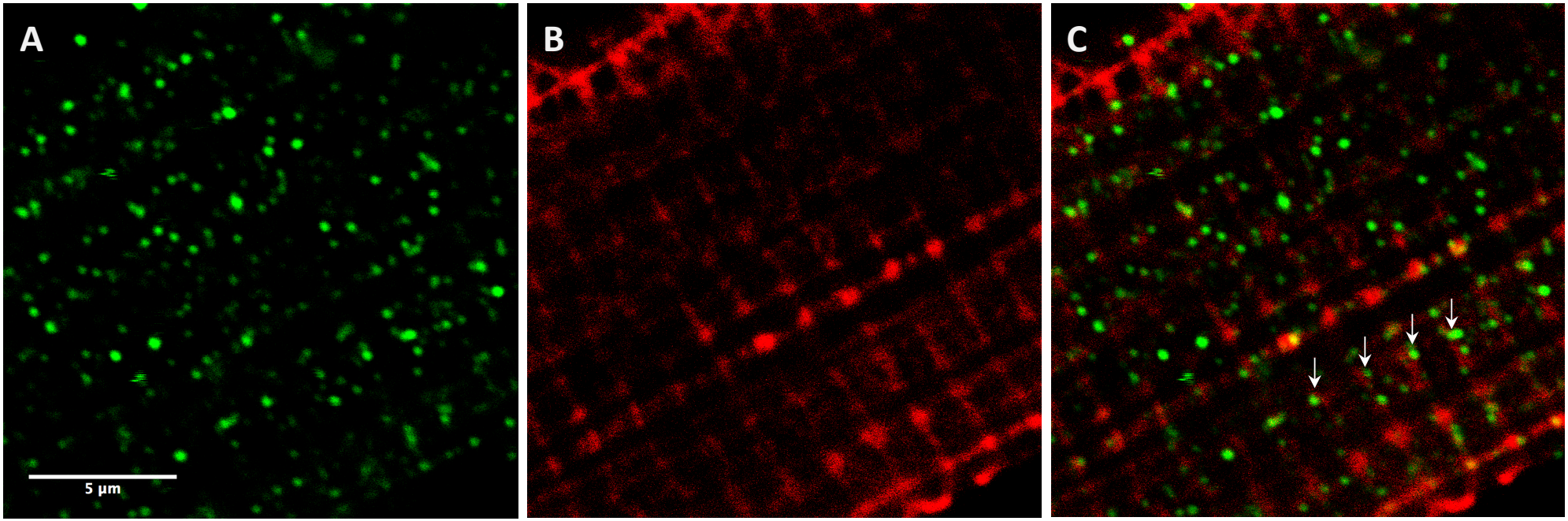


Figure 5.9: Co-labelling of LAMP2 and phospholamban (PLB) using fluorescent immunocytochemistry in a rabbit ventricular cardiomyocyte. Panel A and B show LAMP2 and PLB labelling respectively, and these images are merged in panel C. Although there was no overt co-localisation, many places can be seen where these two proteins are in close proximity and in some areas they appear to be distributed with a regular periodicity (white arrows, panel C).

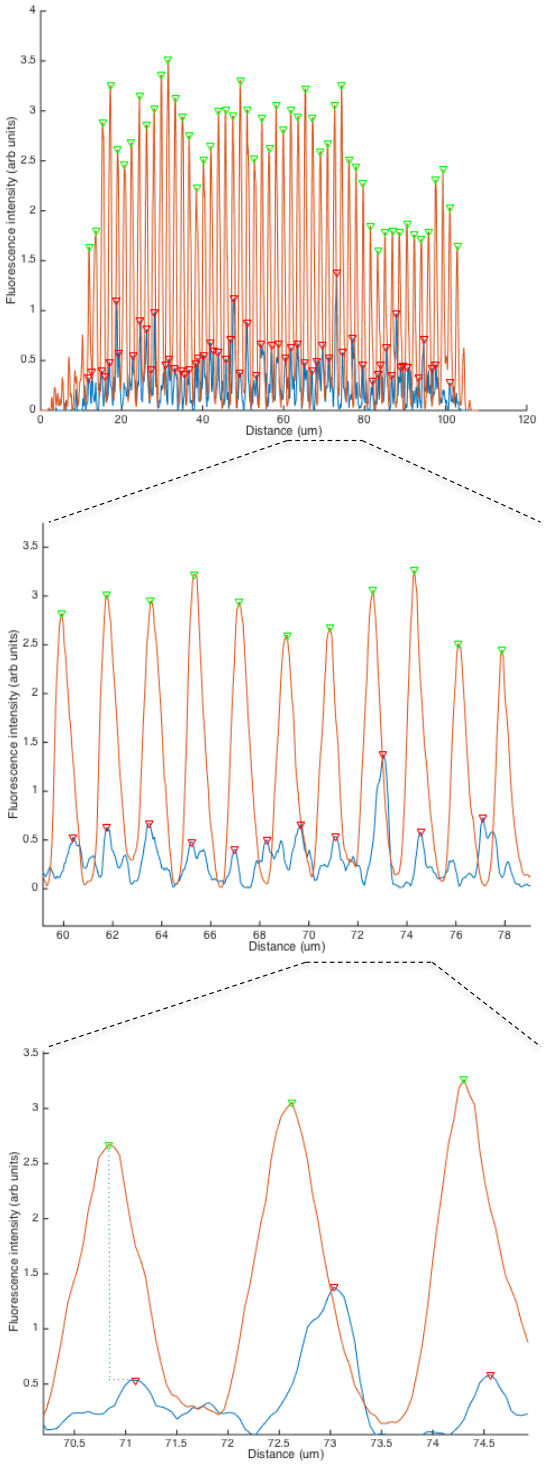


Figure 5.10: Estimating mean proximity between RyR2 and LAMP-2. The top graph is the sum of the fluorescence intensity for the each pixel column in the image plotted against distance across the cell for RyR2 (red line) and LAMP-2 (blue line). Peaks have been labelled on both waveforms with a 'v'. The middle graph is a zoomed-in section of the top, and the bottom is a zoomed-in section of the middle. The distance between RyR2 peaks and LAMP-2 peaks could be calculated and the mean found over many peaks in several different cells (n=16). The same method was used to find the mean PLB-LAMP-2 distance.

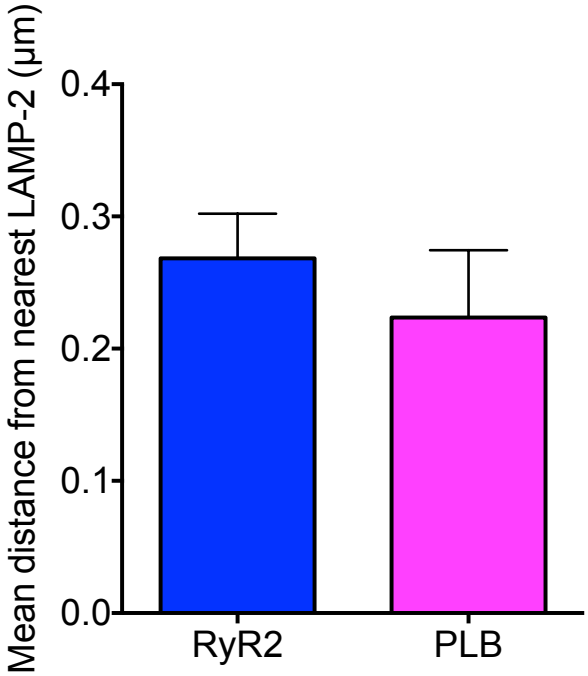


Figure 5.11: Proximity of RyR2 or PLB to LAMP-2. The mean distance from the peak RyR2 or PLB signal to the nearest LAMP-2 signal was calculated using the offset of superimposed fluorescence intensity plots for the two labels. The mean distance from RyR2 or PLB to the nearest LAMP-2 was 0.268±0.034 µm and 0.224±0.051 µm respectively.

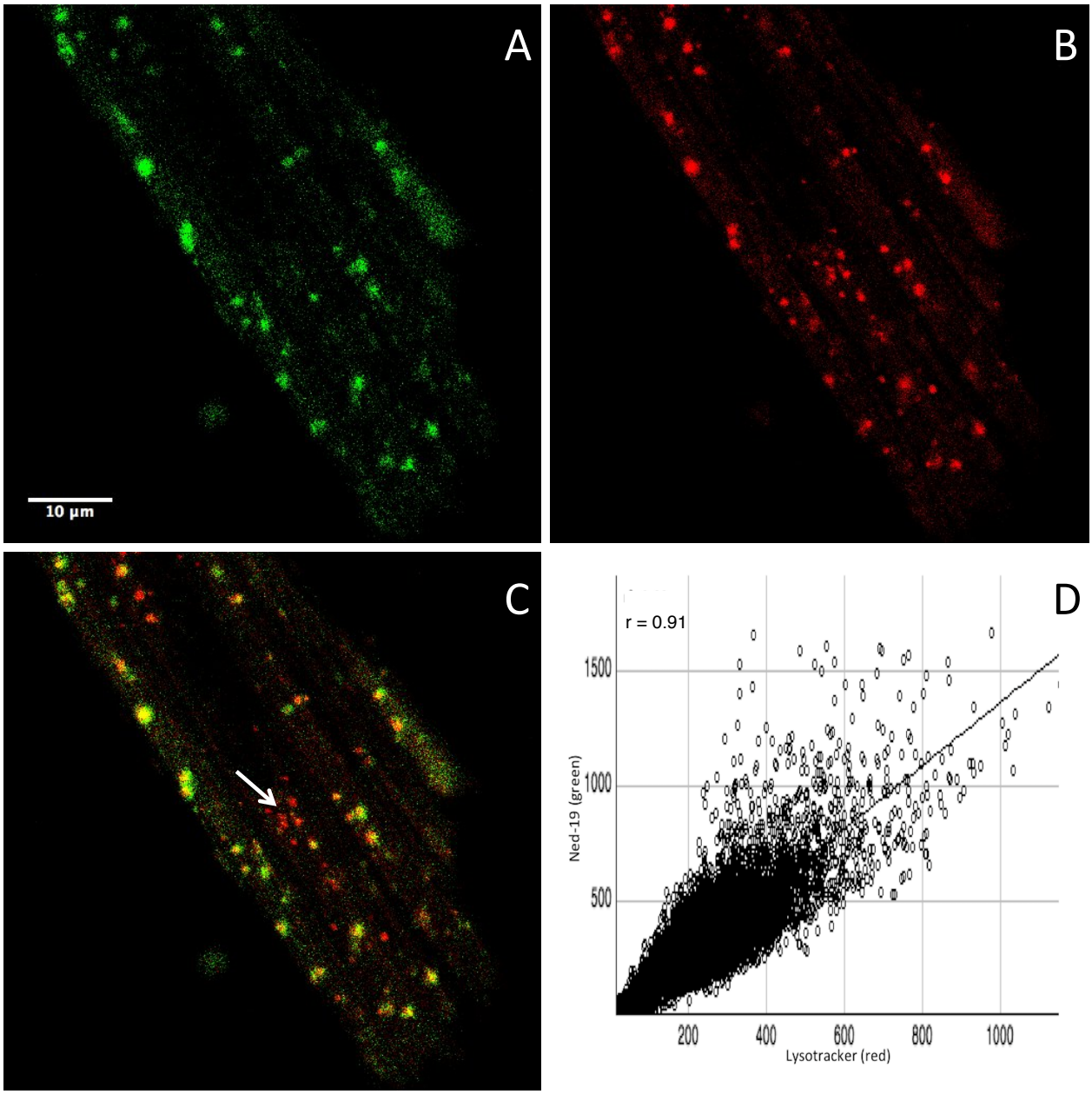


Figure 5.12: Co-labelling of Ned-19 binding sites with Ned-19 and lysosomes using lysotracker red. The binding distribution of the fluorescent NAADP antagonist Ned-19 and lysotracker red labelling can be seen in panels A and B respectively and these images are merged in panel C. A high degree of co-localisation was found between Ned-19 binding sites and lysosomes. A correlation plot for this image can be seen in panel D, and shows a Pearson correlation coefficient (r) of 0.91. Overall, correlation coefficient was 0.84±0.022, n=6. Some areas labelled with lysotracker red did not co-label with Ned-19 (white arrow, panel C). It is thought that these areas may represent Golgi apparatus.

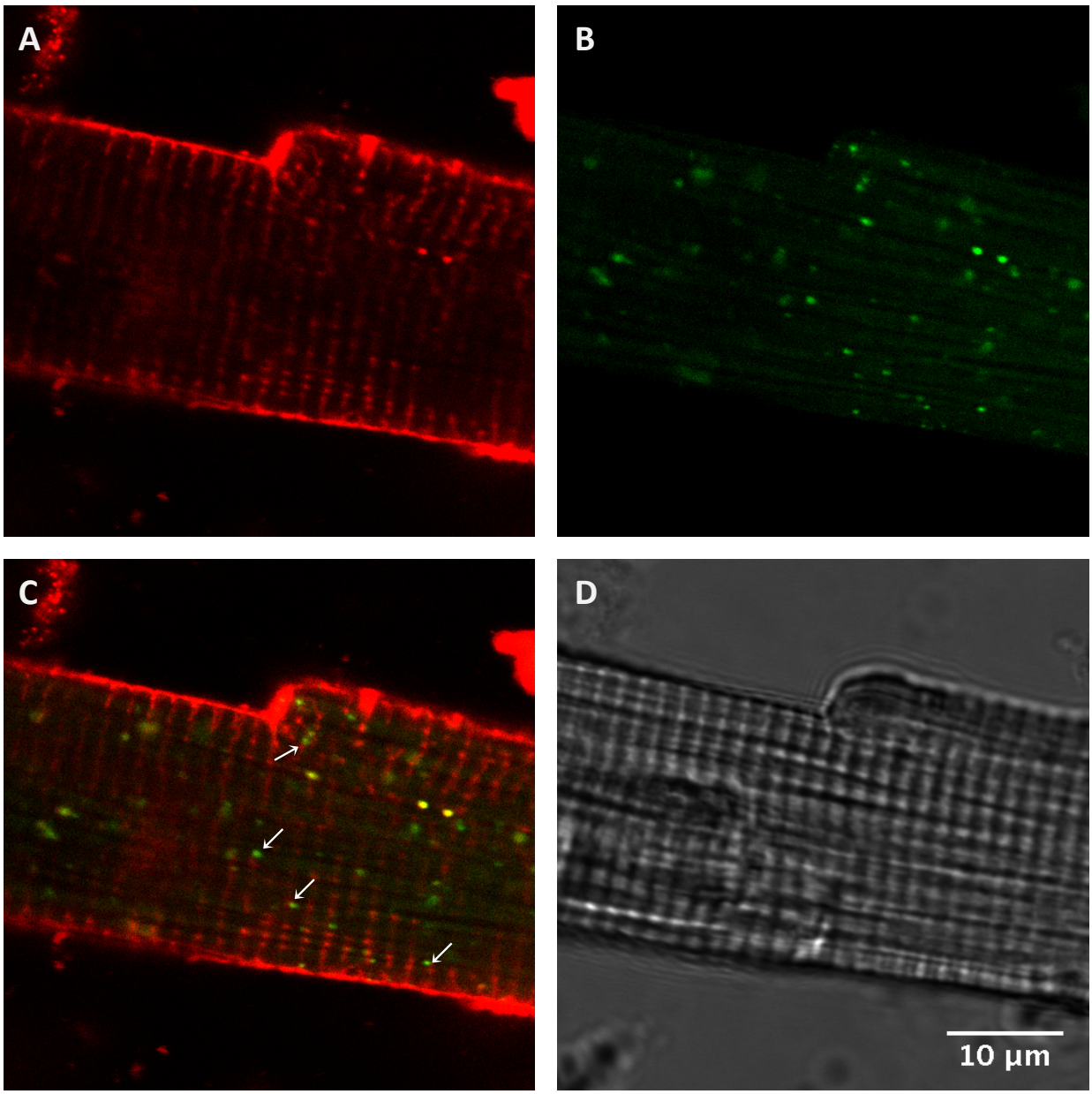


Figure 5.13: Co-labelling of t-tubules using the voltage-sensitive fluorescent dye di-8-anepps and lysosomes using lysotracker green. Panels A and B show labelling of t-tubules and lysosomes respectively while panel C shows these images merged. The brightfield is shown in panel D. The punctate distribution of the lysosomes contrasts with the striated pattern of the t-tubules. There is no overt colocalisation, although some lysosomes can be seen in close association with t-tubules (white arrows in panel C).

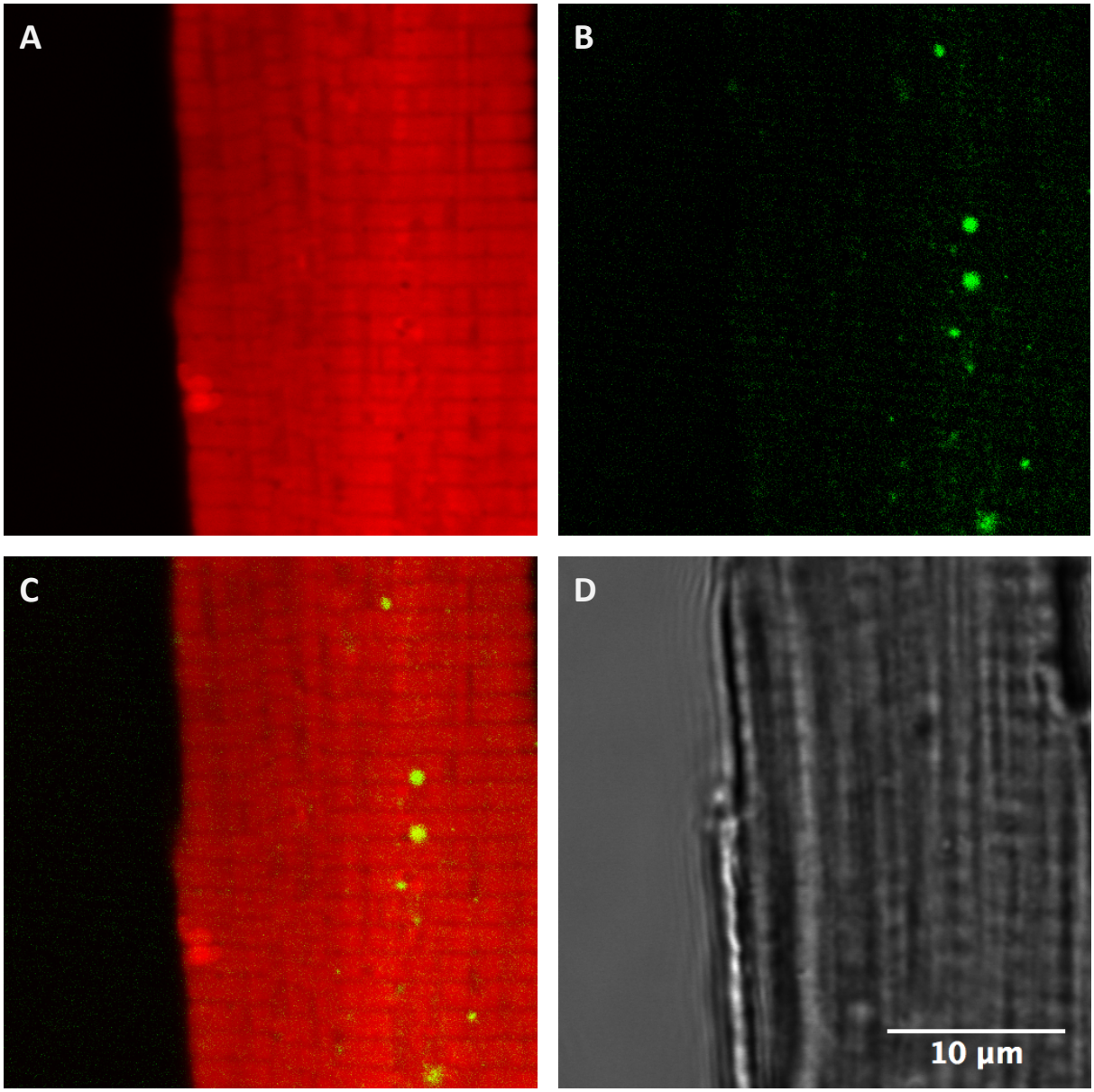


Figure 5.14: Co-labelling of mitochondria using tetramethylrhodamine ethyl ester (TMRE) and lysosomes using lysotracker green in a rabbit ventricular cardiomyocyte. Panels A and B show labelling of mitochondria and lysosomes respectively while panel C shows these images merged. The brightfield is shown in panel D. Mitochondria are densely packed into cardiomyocytes, and this is reflected in the TMRE labelling. However, darker bands can be seen indicating that mitochondrial distribution has a striated organisation. Lysotracker green labelling can be seen with a punctate distribution, although due to the density of TMRE labelling it is difficult to comment on the association between lysosomes and mitochondria using this technique.

5.3 Conclusion

The observations presented in this chapter suggest a novel relationship between lysosomes and SR structures in cardiomyocytes. The results lend further weight to the hypothesis that communication between lysosomes and other structures – particularly the SR – play a key role in NAADP-mediated calcium signalling in the heart. Furthermore, although no functional data are presented, the structural observations are consistent with the concept that calcium released from the lysosome in response to NAADP stimulation modulates the release of calcium from the SR.

Ned-19 is a fluorescent antagonist of NAADP. The structure of the two molecules is very similar, suggesting that they may bind to the same site. Indeed, Ned-19 has been shown to prevent binding of NAADP to its receptor, and to prevent the release of calcium in response to NAADP (Rosen et al., 2009). There was a high degree of co-localisation of Ned-19 binding and lysotracker red labelling in cardiomyocytes, suggesting that Ned-19 (and therefore NAADP) binds to and acts at lysosomes in these cells. The correlation between Ned-19 binding and lysotracker red was very high, but not perfect; some areas were stained with lysotracker red but did not co-label with Ned-19. These areas were seen most frequently adjacent to the nucleus, and it is possible that they represent Golgi apparatus rather than lysosomes (figure 5.12, panel C, white arrow). In order to visualise Ned-19 fluorescence, a concentration of 100 μM was required. This is in contrast to the 1 – 10 μM commonly used for functional experiments and therefore there is the possibility that non-specific binding formed a component

of the fluorescence signal. However, the high correlation with lysotracker labelling and the absence of a striated pattern in the Ned-19 labelling is reassuring in this respect. Additional data is also presented in appendix B (figure B3) that shows the results of the same experiment performed in the presence of another (non-fluorescent) antagonist of NAADP, BZ194. Under these conditions, the localization of Ned-19 to lysosomes was abolished in 16 of 19 cells tested, and substantially reduced in the remaining 3. This suggests that BZ194 is able to prevent the binding of Ned-19, and is important for two reasons: First, the possibility of non-specific binding due to the high concentration of Ned-19 is made unlikely, but secondly it also rules out the possibility that Ned-19 was seen to accumulate in lysosomes as part of their degradative and 'recycling' function. The results of these experiments strongly suggest that Ned-19 binds to a specific binding site on the lysosome. The relationship between lysotracker labelling and Ned-19 binding has been investigated before in rat astrocytes (Barcelo-Torns et al., 2011), where a strong correlation was also found.

Previous observations of vascular smooth muscle cells have detected a spatial relationship between lysosomes and the ryanodine receptor using confocal microscopy (Kinnear et al., 2004; Kinnear et al., 2008). Although the subcellular organisation of a cardiomyocyte differs substantially to that of a smooth muscle cell, the data presented here are certainly consistent with a similarly-close spatial relationship. After analysis, there was a striking association between lysosomes, as labelled by LAMP-2, and SR structures such as the ryanodine receptor and phospholamban. Although the distribution of LAMP-2 at first glance appears to be random, there was a strong association in periodicity between the

LAMP-2 and RyR signals on Fourier analysis. Given the known sarcomeric distribution of RyR, this suggests that a subpopulation of LAMP-2 (and therefore lysosomes) are also distributed in an organised fashion around the sarcomere. This relationship also held strongly for images co-labelled with LAMP-2 and PLB.

One explanation for the apparent sarcomeric spacing between lysosomes may be the density of the myofilaments. Since the primary function of these cells is the generation of contractile force, the proportion of the cell taken up with contractile apparatus is high. It may be that the sarcomeric distribution of lysosomes is simply a result of the constraints on space imposed by the myofilaments. However, lysosomal formation involves the fusion of endosomes, formed at the cell surface membrane with prelysosomal vesicles formed at the trans-Golgi apparatus (Kornfeld et al., 1989). It would therefore seem unlikely that the movement and distribution of lysosomes is limited by the contractile apparatus when their formation depends upon the movement and union of components from different parts of the cell.

In addition to the finding that a subset of lysosomes is distributed across the cell in fashion very reminiscent of sarcomeric structures, an estimate for the distance between the ryanodine receptor or phospholamban and the nearest LAMP-2 marker could be made by estimating the phase offset between the two fluorescence signals. This suggested that, on average, LAMP-2 is separated from RyR or PLB by 268 nm and 224 nm respectively. This distance is far too large to constitute a microdomain, however since the point-spread function of fluorescence cannot be guaranteed to centre exactly on the part of the lysosomal

membrane that is closest to the SR, the measured distance is likely to represent an average of the distances from the SR to the nearest and furthest membrane of the lysosome. Given that the minimum width of a lysosome is approximately 200 nm, the association between LAMP-2 and RyR or PLB observed here is intriguing. The width of a microdomain (approximately 20 nm) is also an order of magnitude below the minimum theoretical limit of resolution for standard light microscopy (approximately 200 nm, Schermelleh et al. (2010)), and therefore cannot be seen using techniques used in this chapter.

The ryanodine receptor has been implicated in lysosomal calcium signalling previously. In pancreatic acinar cells from TPC2 knockout (*Tpcn2*$^{-/-}$) mice, calcium release in response to NAADP was reduced by 64% compared with wildtypes. However, if an inhibitory antibody against RyR1 was also included, the calcium release was reduced by 86%. Similarly, in *RyR3*$^{-/-}$ mice, the calcium released in response to NAADP was reduced by 50%, unless the RyR1 antibody was also used, then it was reduced by 90% (Gerasimenko et al., 2015). TPC1 was also found to be responsive to NAADP in these experiments, although antibodies against RyR2 had little or no effect on NAADP calcium responses in this tissue; the relative importance of RyR isoforms is likely to vary from one tissue to another. The authors of this study concluded that both TPCs and RyRs are required for a normal calcium response to NAADP in pancreatic acinar cells, and that calcium initially released from the lysosomal TPC was then amplified by the RyR on the ER. Allowing for differences in RyR isoforms between pancreatic and cardiac tissue, these findings would be consistent with the structural results presented here.

There are no previous reports of an association between lysosomal calcium signalling and phospholamban. However, the combined observations that NAADP release causes increased SR calcium loading in the heart (Macgregor et al., 2007), and that CaMKII is required for the increase in cardiac calcium transient amplitude in response to NAADP (Capel et al., 2015) is circumstantial evidence, and more investigation of this area is required.

Although LAMP-2 immunocytochemistry and lysotracker fluorescent labelling of lysosomes revealed the same general punctate pattern of distribution across cells, the labelling with LAMP-2 was far more dense than that seen with lysotracker. There are several possible explanations for this: First, it is possible that lysotracker underestimates the number of lysosomes, and does not label all of them. This may be a characteristic of lysotracker, or a methodological problem in these experiments that led to imperfect penetration of lysotracker into cells and lysosomes.

Alternatively, it is possible that LAMP-2 labelling overestimates the number of lysosomes. On a simple level, it may be that a single lysosome can be labelled more than once. Individual lysosomes may be up to 0.5 μm in diameter, and up to 50% of their membrane protein may be LAMP (Winchester, 2001). Therefore, it is possible that a single lysosome may be labelled by more than one primary antibody and that more than one label would be visible using optical microscopic techniques. However, another reason may be due to LAMP-2 trafficking. It is known that LAMP-2 is manufactured in the rough endoplasmic reticulum (rER),

and is transported to the lysosome by either a 'direct' or 'indirect' pathway (Braulke et al., 2009; Kornfeld, 1987). In the former, LAMP-2 is transported from the rER via the Golgi apparatus and Trans-Golgi Network (TGN) onto vesicles that then fuse with late endosomes and lysosomes (Kornfeld et al., 1989). If LAMP-2 undergoes direct trafficking, it therefore does not appear at the cell membrane. Indirect trafficking is thought to be the route taken by the majority of LAMP-2, and instead of fusing with endosomes or lysosomes directly, vesicles fuse with the plasma membrane. LAMP-2 is therefore temporarily expressed on the cell surface until endocytosis occurs and a new endosome is formed, incorporating LAMP-2 in its membrane. The endosome then matures, and finally becomes a lysosome (Hunziker et al., 1996).

It is therefore possible that LAMP-2 is labelled by primary antibodies during the trafficking process, and that some LAMP-2 labels do not indicate lysosomes, but Golgi, rER, vesicles, or endosomes. The relative proportions of LAMP-2 in the lysosome membrane compared with that within the trafficking pathway in mammalian cardiomyocytes is not known. However, the avian version of LAMP-1, LEP-100 (Andrejewski et al., 1999), was found to be distributed in fibroblast cultures with 90% of the molecules in the lysosome, 5-8% in endosomes and 2-3% in the plasma membrane or elsewhere (Lippincott-Schwartz et al., 1986; Lippincott-Schwartz et al., 1987). In another study using murine fibroblast cultures, LAMP-1 was found to be 96-98% intracellular as opposed to at the cell membrane (Gough et al., 1997), although the cell membrane only accounts for part of the trafficking pathway. These studies provide some reassurance that the majority of LAMP-2 labels seen here represent true lysosomes, although the

definitive reason for the discrepancy between the number of labels seen with LAMP-2 versus the number seen with lysotracker remains unclear.

Observations of lysotracker labelling alongside di-8-anepps provided further qualitative support for the hypothesis that lysosomes are located near SR structures. Di-8-anepps is a voltage-sensitive dye that labels the plasma membrane. In cardiomyocytes it therefore labels the T-tubules, which are continuous with the plasma membrane, and the appearance is very similar to that of RyR labelling. It is reasonable to assume that, if lysosomes are closely associated with RyR, then they would also be associated with T-tubules. This is because L-type calcium channels are abundant in the T-tubule, forming couplons with RyR in the adjacent SR. The images obtained from these experiments do indicate a likely association between lysosomes and T-tubules, although no quantitative analysis was possible.

Observations of mitochondria and lysosomes were also attempted by labelling with tetramethylrhodamine ethyl ester (TMRE) and lysotracker respectively. Mitochondrial labelling was diffuse, due to the large population of these organelles in cardiomyocytes. An element of striated organisation of mitochondria could be seen, but due to the density of TMRE labelling, few conclusions can be drawn from these images.

In summary, the evidence presented in this chapter indicates that lysosomes in cardiomyocytes have a close spatial relationship with the SR. Furthermore, a novel association between lysosomes and the SR proteins RyR and PLB has been

revealed. These findings are consistent with the hypothesis that a calcium trigger/modulator effect governed by NAADP may function in the heart.

6

The association of lysosomes with sarcomeric structures in ventricular muscle: Electron microscopy

6.1 Introduction

In chapter 5, light microscopy was used with fluorescent markers of lysosomal and SR proteins. Evidence was presented that suggests a relationship between these structures. However, they are both below the resolution of light microscopy and so could not be observed directly. In this chapter, transmission electron microscopy is used to further investigate whether a relationship between lysosomes and the SR exists in the cardiac ventricle.

Lysosomes have previously been studied in the heart, although never in relation to NAADP function. Initially, cardiomyocytes were thought to be devoid of lysosomes (Marjomaki et al., 1990), and the low levels of lysosomal enzymes that had been detected in homogenates of heart muscle were assumed to be of non-myocyte origin (Romeo, 1966). However, the first images of cardiac lysosomes obtained using electron microscope were published by Hibbs et al. (1965). Granules that were very similar in appearance to the lysosomes previously described in liver and kidney cells were seen and stained positive for acid phosphatase. It was noted that the cardiac lysosomes were not as numerous as those observed in these other cell types and appeared to be concentrated in the perinuclear region. Even so, it was also observed that although lysosome numbers were low in normal cardiac tissue, stimuli such as ischaemia, starvation, or exposure to β-adrenergic agonists increased their numbers considerably (Decker et al., 1980; Hibbs et al., 1965; Maruffo, 1967). No differences were seen in lysosomes from ventricles compared with those from the atria (Hibbs et al., 1965), and there was no intimate relationship noted

between lysosomes and any other organelle (Maruffo, 1967). It was later suggested that lysosomes were also present in more peripheral regions of the cardiomyocyte (Decker et al., 1980; Topping et al., 1974), and relationships between the lysosome and the SR and mitochondria have been noted in extra-cardiac tissues (Lam et al., 2013), although this has not yet been specifically studied in cardiomyocytes.

Close spatial relationships between two organelles have been described in many contexts. Functional signalling microdomains or nanojunctions occur at structural membrane contact sites (MCS) where the organellar membranes are typically separated by no more than 30 nm (Helle et al., 2013; Penny et al., 2015). The microdomain contains the molecular apparatus required to generate a signal, as well as the target for that signal (Asghari et al., 2012). In the context of calcium signalling, this allows the release of a small amount of calcium to result in a locally high concentration and leads to rapid and efficient signalling. It also allows the signal to be highly localised and can depend on the enzymes present in a particular junction.

One of the best studied examples of a microdomain is that formed at the MCS between the ryanodine receptor on the SR membrane and the L-type calcium channel on the plasma membrane. The functional coupling where clusters of ryanodine receptors come into close contact with calcium channels is known as a couplon. These are found in cardiac muscle in the dyads, where a T-tubule is flanked by a solitary terminal cisternae SR membrane. In the analogous structure found more commonly in skeletal muscle, the T-tubule is flanked by two SR

cisternae (one on either side) and it is therefore known as a triad (Asghari et al., 2012; Scriven et al., 2013). In cardiac muscle, the opening of the calcium channel allows local movement of calcium from the extracellular space into the cell, where it can activate the SR ryanodine receptors and cause a global calcium release (Bers, 2002). The microdomain therefore allows local communication between the plasma membrane and the SR. There is also evidence that communication occurs in the opposite direction, allowing an increase in L-type channel activity if the SR calcium content is too low. This is known as 'store-operated' calcium entry (Soboloff et al., 2012). Other microdomains are known to exist in extra-cardiac tissues, including those between S/ER and mitochondria and S/ER and lysosomes (Lam et al., 2013).

Evidence is accumulating that the S/ER - lysosome microdomain may be involved in the NAADP signalling pathway. As discussed in the previous chapter, it has been hypothesised that NAADP stimulates local calcium release from the lysosome, and this 'triggers' global calcium release from the SR (Cancela et al., 1999; Guse et al., 2008). When NAADP is released into smooth muscle cells loaded with fluorescent calcium dyes, a biphasic calcium response is observed. The large global calcium rise is preceded by smaller localised calcium bursts. The differing sensitivities of these calcium phases to bafilomycin-A1, thapsigargin and ryanodine implies an amplification mechanism (Boittin et al., 2002; Kinnear et al., 2004). Enhanced calcium loading of the SR has also been observed following release of NAADP (Macgregor et al., 2007), and functioning CaMKII is required in the amplification of the NAADP signal (Capel et al., 2015). This amplification appears to fail if TPC2 is redirected from the lysosome to the

plasma membrane (Brailoiu et al., 2010). Furthermore, studies using light microscopy and fluorescent labelling of lysosomes with lysotracker red and RyR with BODIPY-ryanodine showed a close association between the signals (Kinnear et al., 2004). Co-labelling of LAMP-1 and RyR3 in smooth muscle cells indicated co-localisation in a perinuclear region where NAADP preferentially caused bursts of calcium release (Kinnear et al., 2008).

However, although functional studies and structural observations using optical microscopy techniques can provide clues regarding the nature of microdomains, the only method that allows their direct visualisation is electron microscopy (EM).

Although no studies have previously been conducted that examined the Lysosome-Sarcoplasmic Reticulum (L-SR) relationship in the heart, the L-SR MCS was found to exist in smooth muscle by investigators using EM. The mean L-SR distance was 16 nm, and modelling suggested that the number and arrangement of these junctions were sufficient to produce the observed calcium signals seen in these cells following release of NAADP (Fameli et al., 2014). Endosome-ER and multi-vesicular body (MVB)-ER MCS were also found in cultured cell lines (Eden et al., 2010; Rocha et al., 2009). In cultured human fibroblasts, 82% of lysosomes were found to have an MCS with the ER, and many appeared to be physically tethered (Kilpatrick et al., 2013).

Tethering between endosomes and the S/ER has been observed previously and the molecular interactions that govern tethering and lysosomal movement along

cytoskeletal components have been extensively investigated (Johansson et al., 2007; Jordens et al., 2001; Kaiser et al., 2005; Rocha et al., 2009).

No studies have yet used EM to specifically look at the L-SR junction in the context of NAADP signalling in the cardiac ventricle, and this is the primary aim of experiments in this chapter. In addition, the relationship between the lysosome and other subcellular structures is examined. The hypothesis that lysosomes need to be close to RyR on the SR in order for efficient calcium signalling might also imply that lysosomes should be close to T-tubules, since there is a well-established relationship between the SR RyR and the L-type calcium channel found on the T-tubule membrane. Similarly, T-tubules are often associated with Z-lines (Soeller et al., 1999; Trafford et al., 2013) and so lysosomes may be more likely to be found with this sarcomeric distribution.

In addition to the association between lysosomes and the SR, there is also evidence of a link between lysosomes and mitochondria. Autophagic processes may explain some of these interactions as it is well known that mitochondria are recycled by the endolysosomal system at the end of their useful life (Alberts, 2015 p. 726.). However, the lysosome-mitochondrial interaction may have a function unrelated to autophagy that concerns ischaemia/reperfusion injury and involves NAADP signalling. Hearts subjected to ischaemia/reperfusion were protected from injury if they were simultaneously exposed to the NAADP antagonist Ned-19 or a chemical varient, Ned-K. Similarly, hearts from *Tpcn1*$^{-/-}$ animals were also protected (Davidson et al., 2015). Calcium signalling is known to occur between mitochondria and the S/ER (Eisner et al., 2013; Naon et al.,

2014) and mitochondria-SR microdomains have been observed using EM in cardiac muscle (Sharma et al., 2000). It is possible that lysosome-mitochondrial microdomains also exist and facilitate functional interactions between these organelles. Experiments in this chapter also allowed investigation of this relationship.

6.2 Results

6.2.1 The general subcellular morphology of rabbit ventricular cardiomyocytes as seen on transmission electron microscopy

The extremely high resolution achieved by transmission electron microscopy (TEM) allows identification of structures not visible using the highest resolution optical microscopy. These include the lysosome, SR, T-tubules and contractile apparatus.

While striations can be identified using light microscopy, the detailed structure of the sarcomere becomes clear using TEM. Figure 6.1 shows an annotated image of a single sarcomere in a rabbit ventricular cardiomyocyte. It is bounded by the Z-lines and is a little under 2 μm in length. The bands and zones are formed by the overlapping of the thick myosin and thin actin filaments, as described in the main introduction.

The sarcomere is the fundamental functional unit of contractile apparatus in the heart, and many can be seen arranged in series along the length of a cell. Figure 6.2 shows four low-magnification TEM images illustrating this organisation. Between the sarcomeres, densely-packed mitochondria are present. There are also many T-tubules, cut in transverse section, that can often be seen at the end of a Z-line. The membrane forming these T-tubules is continuous with the cell plasma membrane and contains L-type calcium channels. Together with the

ryanodine receptors (RyR) on nearby sarcoplasmic reticulum (SR) these form the couplons. The SR membrane is too small to be clearly seen with the magnification used to obtain the images in figure 6.2.

Using higher magnification, several organelles relevant to the study of NAADP signalling can visualised in detail (see figure 6.3). The lysosome is a highly heterogeneous structure and several different forms can be identified. The typical immature lysosome can be seen in panel A of figure 6.3. It is circular / oval in section with a single delimiting membrane (in contrast with mitochondria, which are characterised by a double membrane, and lipid droplets (figure 6.3, panel F) which are not enclosed by a membrane at all) and a uniform luminal matrix that is a little more electron dense than the cytoplasm. A mature lysosome is seen in panel B, and is approximately the same as the immature lysosome in appearance, with the important exception that its matrix is significantly more electron dense and is less uniform. The mature lysosome has had debris delivered to it via phagosomes, autophagosomes, or endosomes for destruction, whereas the immature lysosome has not.

Multi-vesicular bodies (MVB), like that shown in panel C of figure 6.3 are related to lysosomes and endosomes. These are of similar appearance to lysosomes, except they contain small vesicles in their lumen. These are formed by inward 'budding' of the MVB membrane and allow the delivery of membrane-bound proteins to the lysosome.

T-tubules appear as single-membrane bound structures with a lumen that is uniformly less electron dense than the cytoplasm. Their shape varies from almost perfectly circular in section to bizarre irregular shapes. They can often be found associated with the sarcomere at the end of a Z-line. Examples are shown in panel D of figure 6.3.

Panel E of figure 6.3 shows an autophagosome (AP). This is a single-membrane bound organelle that has enveloped a cellular structure that needs to be recycled (e.g. a mitochondrion). Because of this, it often appears to have two or even three membranes if the membranes of the enveloped structure are still intact. The size, shape, and luminal appearance of APs vary considerably depending on what structure has been enveloped and whether fusion with a lysosome and degradation has begun.

SR membrane can be seen in panels B and C of figure 6.3, adjacent to the lysosome and MVB respectively.

6.2.1 The morphology of lysosomes in rabbit ventricular cardiomyocytes as seen on transmission electron microscopy.

A total of 69 lysosomes were identified in TEM images of rabbit ventricle. Their appearance was heterogeneous, but they could be identified by their characteristic features: A luminal matrix bounded by a single bilayer membrane. The luminal matrix was sometimes uniform and only slightly more electron

dense than the cytoplasm, and in other cases there was a significant difference in density and uniformity. These two distinct lysosomal appearances are shown in panels A and B of figure 6.3. Overall, the numbers of immature (pale) to more mature (dark coloured) lysosomes in this series was approximately equal.

Lysosomes were measured, and found to have a median long axis of 383 nm (306 – 580 nm) and a mean short axis of 290 nm (220 – 455 nm, n=69). This was in broad agreement with previous studies that had investigated lysosomes in pulmonary artery smooth muscle cells (Fameli et al., 2014). It has been suggested that differentiation between small lysosomes and endosomes is difficult and that a "cut-off" or threshold diameter of greater than 200 nm should be used to define lysosomes. If this criteria is applied to the data here, the median long axis becomes 414 nm (325 – 598 nm) and the median short axis becomes 320 nm (248 – 483 nm, n=61).

A histogram showing the distribution of lysosomal dimensions (including those with a short axis less than 200 nm) can be seen in figure 6.4.

6.2.2 The distribution of lysosomes in rabbit ventricular cardiomyocytes as seen in transmission electron microscopy: Association with SR

Previous experiments have shown that the inhibition of Calmodulin-dependent protein Kinase 2 (CaMKII) prevents the increase in calcium transient that would normally occur following intracellular release of NAADP (Capel et al., 2015). This

led to the hypothesis that calcium released from the lysosome in response to NAADP stimulation activates CaMKII. This enzyme is known to phosphorylate phospholamban and relieve its inhibition of the Sarco-Endoplasmic Reticulum Calcium ATPase (SERCA) pump. Therefore, calcium re-uptake into the SR is enhanced causing an increase in the peak of the calcium transient and in the rate of its decline.

There are also CaMKII phosphorylation sites known to exist on the ryanodine receptor. Therefore, the possibility that the NAADP pathway increases the calcium transient via a direct enhancement of SR calcium release from RyR cannot be ruled out.

If these hypotheses were correct, it would be reasonable to assume that lysosomes must have a close spatial relationship with the SR.

TEM images of rabbit ventricle demonstrate that many lysosomes are closely associated with SR membrane. The median distance between the lysosome and the closest piece of visible SR was 20.0 nm (13 – 24 nm), n=56. The histogram of this data is shown in figure 6.5.

Figure 6.6 shows a typical image of a lysosome within a few nanometers of SR membrane and adjacent to a T-tubule. The lysosome is also surrounded by circular structures that may be membrane-associated proteins. Another example is shown in figure 6.7.

Figure 6.8 shows another lysosome closely associated with SR membrane and a T-tubule. However, in this image some of the circular protein-like structures appear to span the gap between the lysosome and the SR, raising the possibility that some lysosomes may be physically tethered to the SR. An alternative explanation for this appearance may be that the proteins are directly involved in lysosome-SR communication (e.g. ryanodine receptors or SERCA).

6.2.3 The distribution of lysosomes in rabbit ventricular cardiomyocytes as seen in transmission electron microscopy: Association with T-tubules and Z-lines.

If the above hypothesis was correct, it might also be expected that lysosomes would be located near areas of SR associated with calcium re-uptake, and with areas associated with its release. The RyR on the SR membrane is known to form couplons with the L-type calcium channel on the T-tubule. Therefore, it would be consistent with the hypothesis if lysosomes were associated with SR near T-tubules and could have a function relating to RyR modulation. Similarly, it is possible that those lysosomes found some distance from T-tubules may be functionally related to calcium re-uptake, perhaps involving phospholamban and SERCA.

The distances from lysosomes to T-tubules and Z-lines were measured. The median distance from lysosome to nearest T-tubule was 163 nm (123 – 870 nm), n=24, while the median distance from lysosome to nearest Z-line was 318 nm

(176 – 529 nm), n=45. These distances are not dissimilar to the RyR2 or PLB to LAMP-2 distances calculated in the last chapter (0.268±0.034 μm and 0.224±0.051 μm respectively).

This data is presented using histograms in figures 6.9 and 6.10. While neither distance was bimodally distributed, as might be expected if all lysosomes were either very close or very distant from T-tubules and Z-lines, the distributions were positively skewed – suggesting that while some lysosomes lie a considerable distance from T-tubules and Z-lines, the majority were relatively close.

Figure 6.11 shows a low-magnification electron micrograph of part of a rabbit ventricular cardiomyocyte with several lysosomes. There are several that can be seen immediately adjacent to T-tubules and Z-lines, but there are also some that are relatively isolated from these structures.

Similarly in figure 6.12, higher magnification images show a lysosome very close to a T-tubule and Z-line in panel A, but another that is further away from these structures in panel B. Both lysosomes are very close to SR.

6.2.4 Lysosomes in rabbit ventricle may form membrane contact sites with mitochondria.

As well as being in close proximity with SR membrane, there were many examples where lysosomes were seen in contact with mitochondria.

The distances from lysosomes to the nearest mitochondrion varied considerably; some were so close that it was not possible to resolve the lysosomal membrane from the mitochondrial membrane. The minimum measurable distance was 7.1 nm. However, the maximum distance was 1419 nm indicating that while some lysosomes appear to be in direct physical contact with mitochondria, there are also some lysosomes that are isolated from them.

The majority of lysosomes in this data set appeared to belong to the former group, since only seven measured distances were over 75 nm. When these values were removed, the median lysosome-mitochondrial distance was 16 nm (13 – 24 nm), n=44.

Examples of lysosomes close to mitochondria are shown in figure 6.13. In panel A, two lysosomes can be seen that have a region of membrane that cannot be resolved from the adjacent mitochondrial membrane. Panel B shows a lysosome very close to adjacent mitochondria with structures that may be individual protein complexes on its surface. As seen in some images of lysosomes close to SR (e.g. figure 6.8), these structures appear to span the gap between the lysosome and one of the mitochondria, raising the possiblilty of tethering proteins or structures involed in signalling between these organelles.

The lysosome-mitochondrial distance data is shown as histograms in figure 6.14.

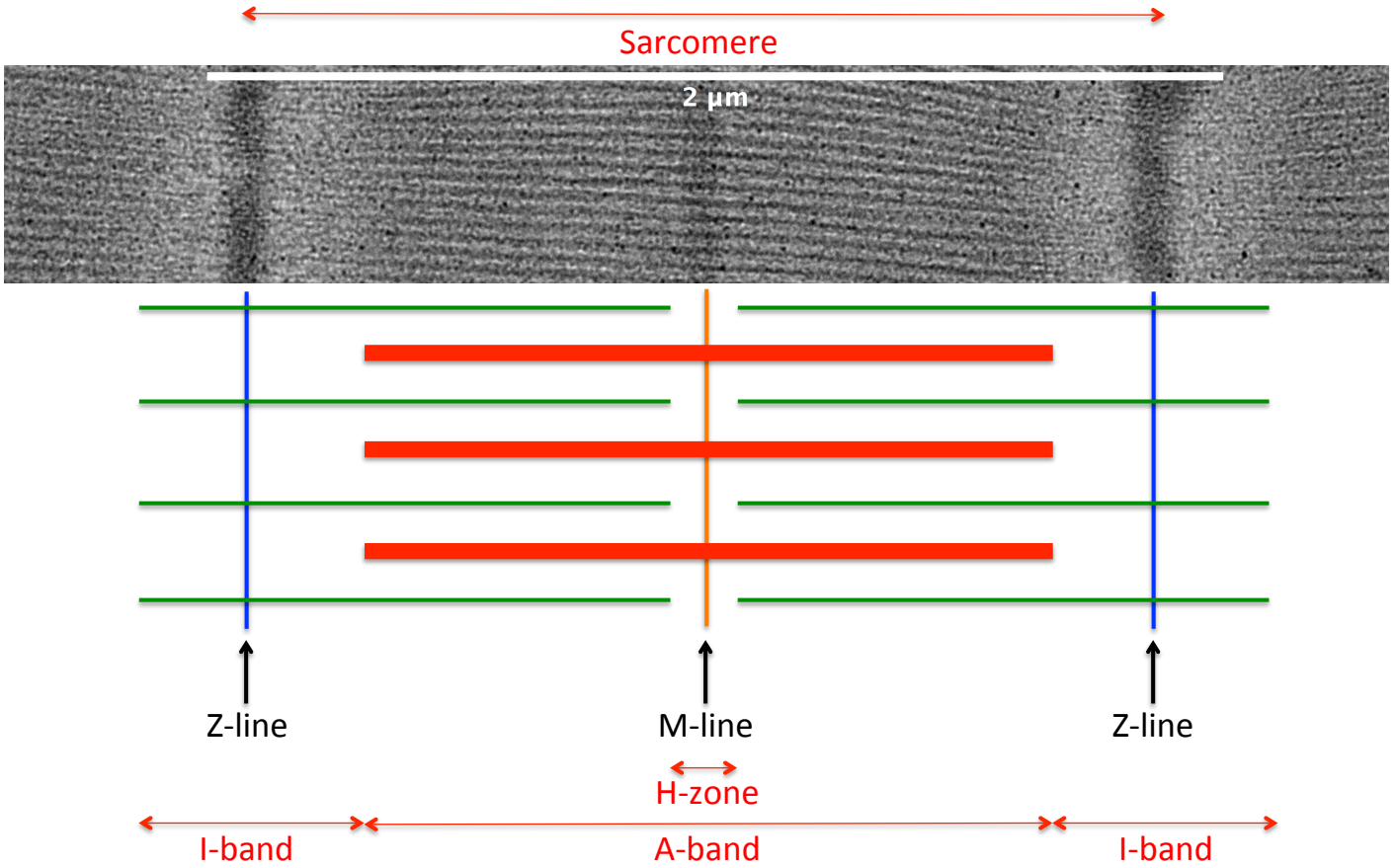


Figure 6.1: Annotated transmission electron micrograph of a single sarcomere in a rabbit ventricular cardiomyocyte. The Z-lines (composed of α-actinin) define the boundaries of a single sarcomere, and the distance between them is approximately 2 µm. 'Thin' actin filaments are anchored to α-actinin at the Z-line, and interlace with the 'thick' myosin filaments to form the bands and zones. The M-line is found at the centre of the sarcomere, equidistant between two Z-lines, and is formed from myomesin. Many other important proteins are found in the sarcomere, but are not shown above. Tropomyosin wraps around the actin filaments, and in turn has troponin bound to it. Titin extends from the Z-line to the myosin filament, and then runs along it to the M-line.

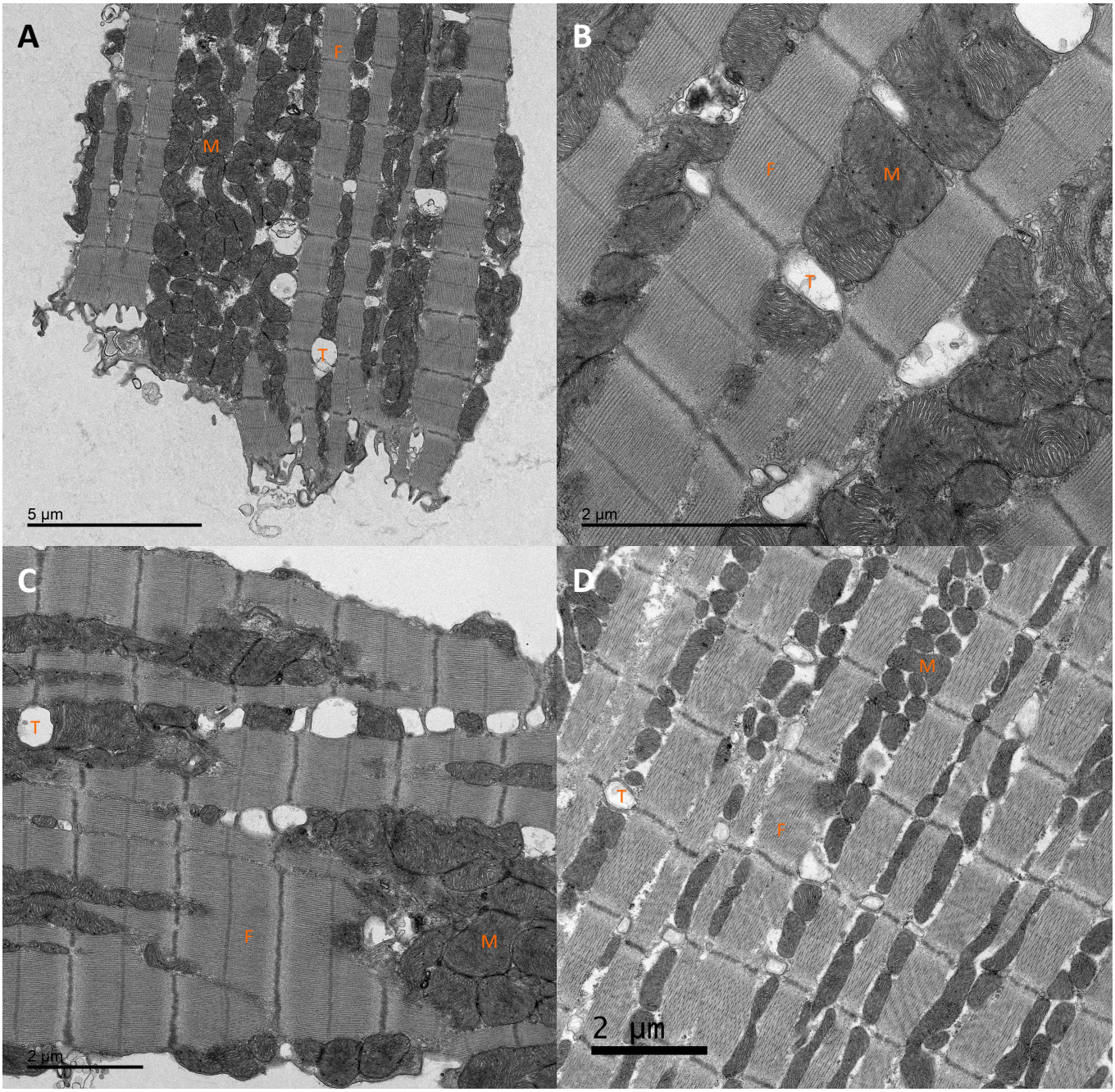


Figure 6.2: Low magnification transmission electron microscopy of rabbit ventricular cardiomyocytes. Several structures can easily be identified, including contractile filaments arranged into sarcomeres (F), mitochondria (M), and transverse-tubules (T). Mitochondria are often arranged in bands between the contractile filaments and supply energy for contraction in the form of adenosine triphosphate (ATP) . The t-tubules are often visible at the ends of sarcomeric Z-lines, and allow L-type calcium channels to form couplons with the ryanodine receptors on the sarcoplasmic reticulum (SR, not easily seen at these magnifications) deep within the cell.

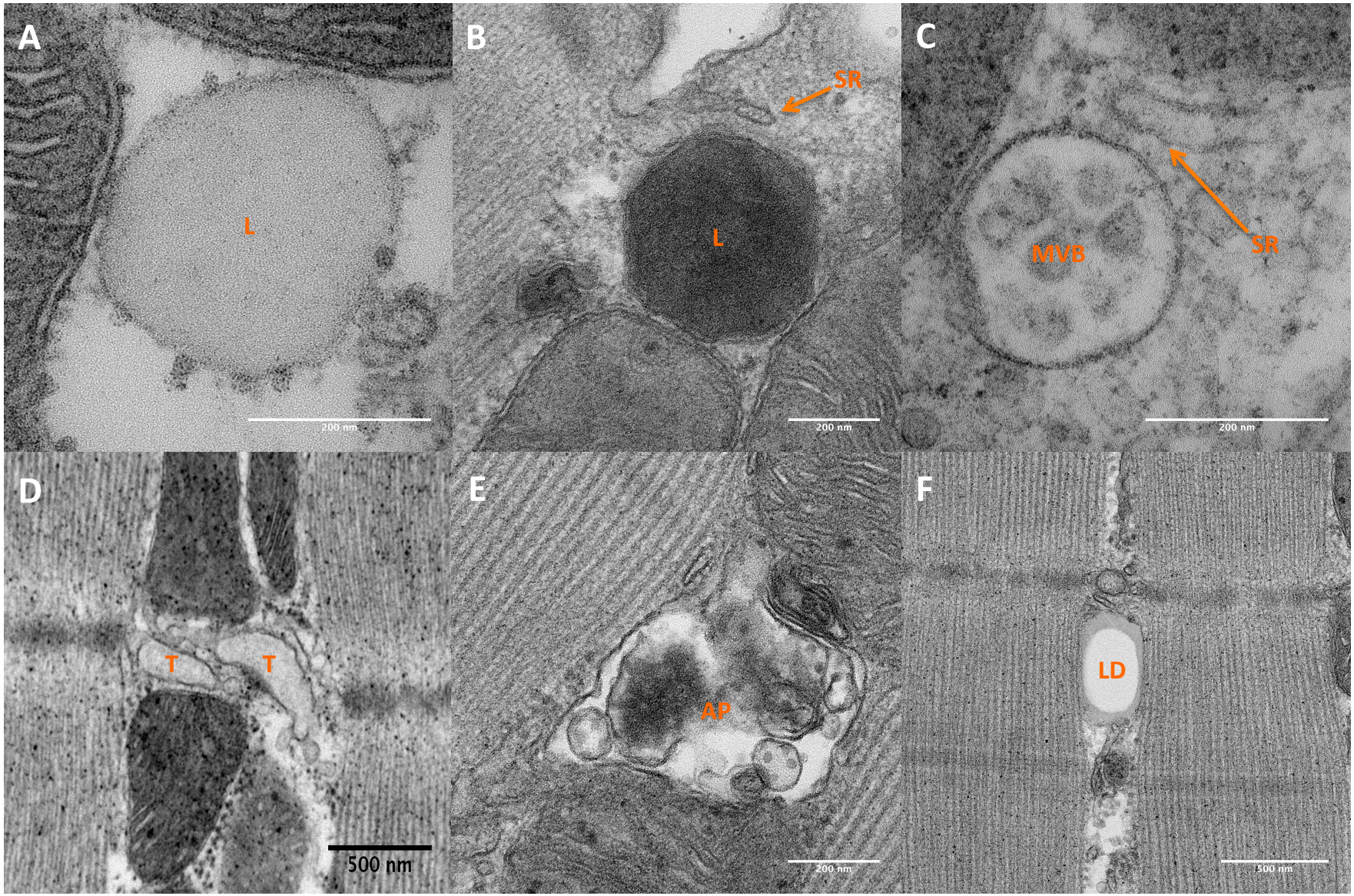

A
L
200 nm
B
SR
L
200 nm
C
MVB
SR
200 nm
D
T
T
500 nm
E
AP
200 nm
F
LD
300 nm

Figure 6.3: Typical examples of different organelles seen in rabbit ventricular cardiomyocytes with transmission electron microscopy. Panel A shows a typical immature lysosome (L). Note the single membrane (in contrast to the double membrane of the nearby mitochondrion) and that the interior is of approximately uniform appearance that is slightly more electron-dense than the surrounding cytoplasm. Circular structures on the edge of the of the lysosome may be membrane-bound proteins. In panel B, a more mature lysosome (L) can be seen. It is significantly more electron dense than its counterpart in panel A, and has a slightly more homogenous and less uniform appearance. Sarcoplasmic reticulum (SR) membrane can be seen nearby. Panel C shows a multi-vesicular body (MVB). These structures are related to endosomes and lysosomes. They are also enclosed by a single membrane, but discrete vesicular structures can be seen in their interior. Again, SR is nearby. Panel D shows two transverse tubules (t-tubules, T). These are often seen at the ends of sarcomeric Z-lines and are deep invaginations of the cell membrane into the interior of the cell which allow uniform spread of the cardiac action potential. An autophagosome (AP), an integral part part of the autophagy pathway, can be seen in panel E. It contains debris or structures that require degradation and will fuse with a lysosome. Finally, panel F shows a cardiac lipid droplet. Note that it is not membrane bound, unlike other organelles and that its circumference is more electron dense than its centre.

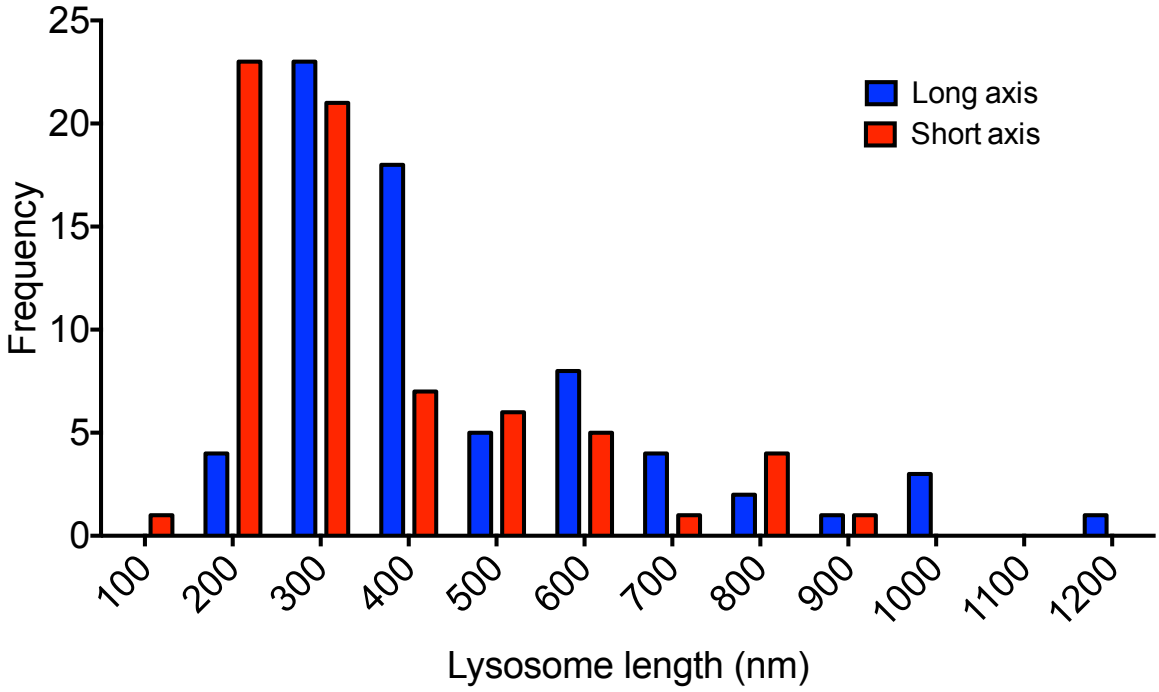


Figure 6.4: The size of cardiac lysosomes found in rabbit ventricle. The median long and short axis lengths were 383 nm (306 – 580 nm) and 290 nm (220 – 455 nm) respectively (n=69).

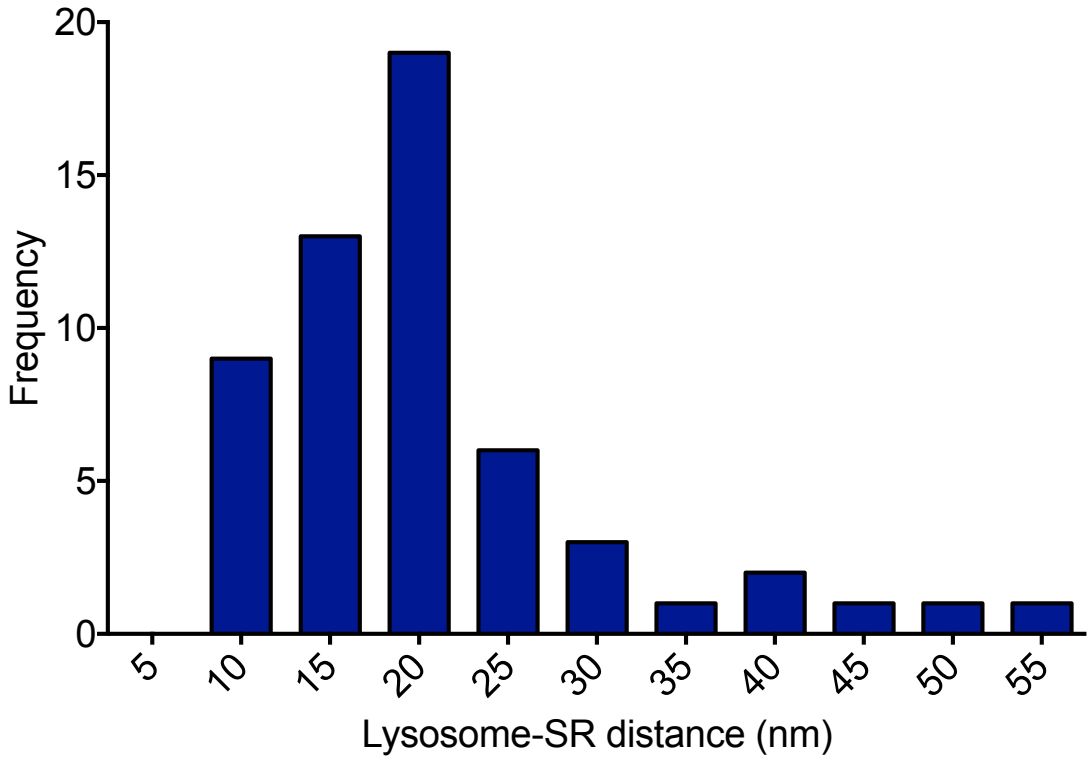


Figure 6.5: The distance from the lysosome to the sarcoplasmic reticulum (SR) in rabbit ventricular cardiomyocytes. The median distance was 20.0 nm (IQR = 13 – 24 nm), n=56. This is thought to be close enough to function as a microdomain for calcium signalling between these structures.

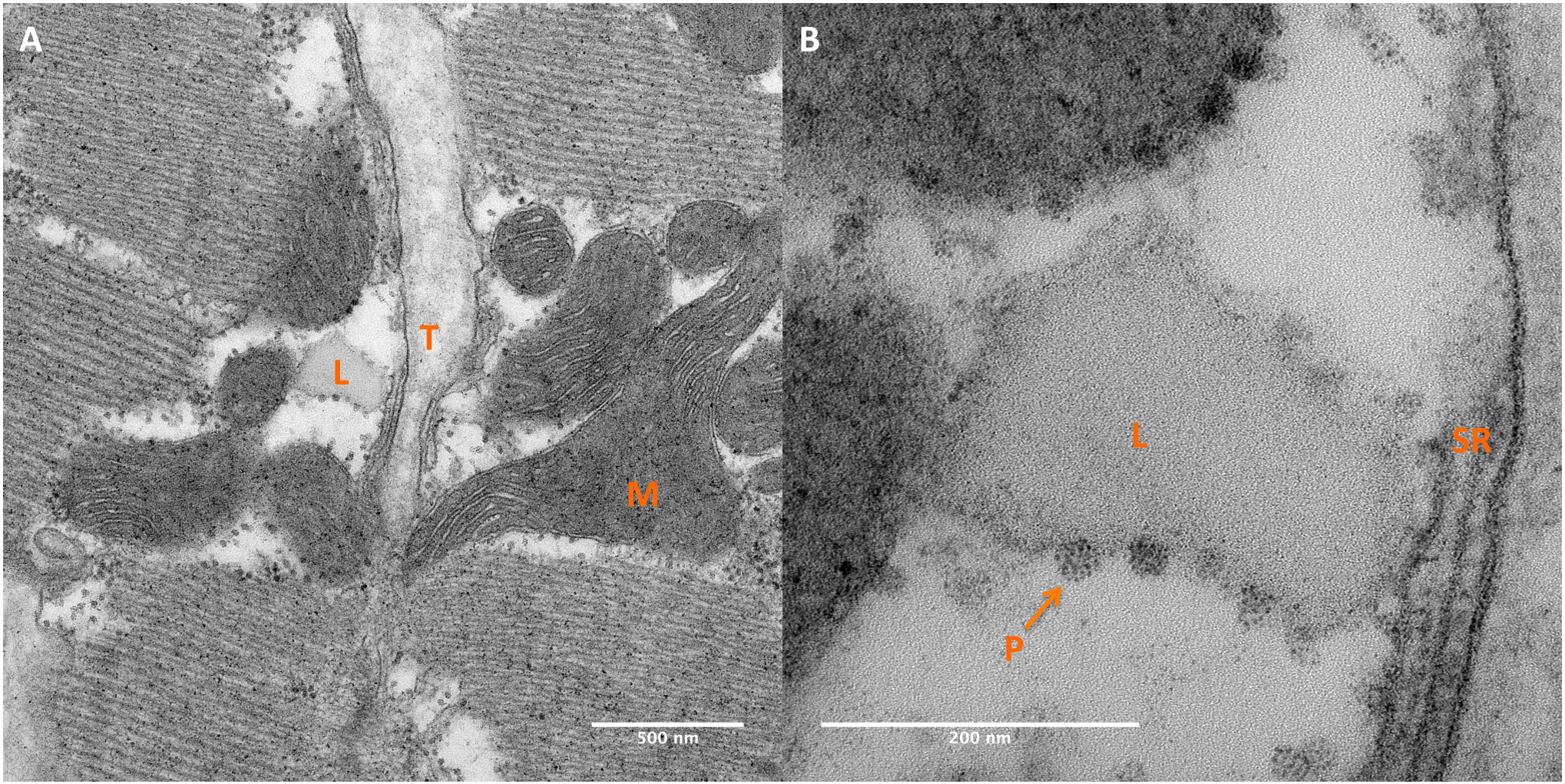


Figure 6.6: Proximity of lysosomes to sarcoplasmic reticulum (SR) and transverse (t-) tubules seen in rabbit ventricular cardiomyocytes on transmission electron microscopy. Panel A shows a lysosome (L) adjacent to a t-tubule (T) cut in longitudinal section. Between them lies SR membrane. Mitochondria (M) can also be seen nearby. Panel B shows the same lysosome at higher magnification, allowing more detailed examination of the SR. The L-SR distance in this image is 10.7 nm (measurement not shown). Circular structures seen on the outside of the lysosome may be membrane proteins (P).

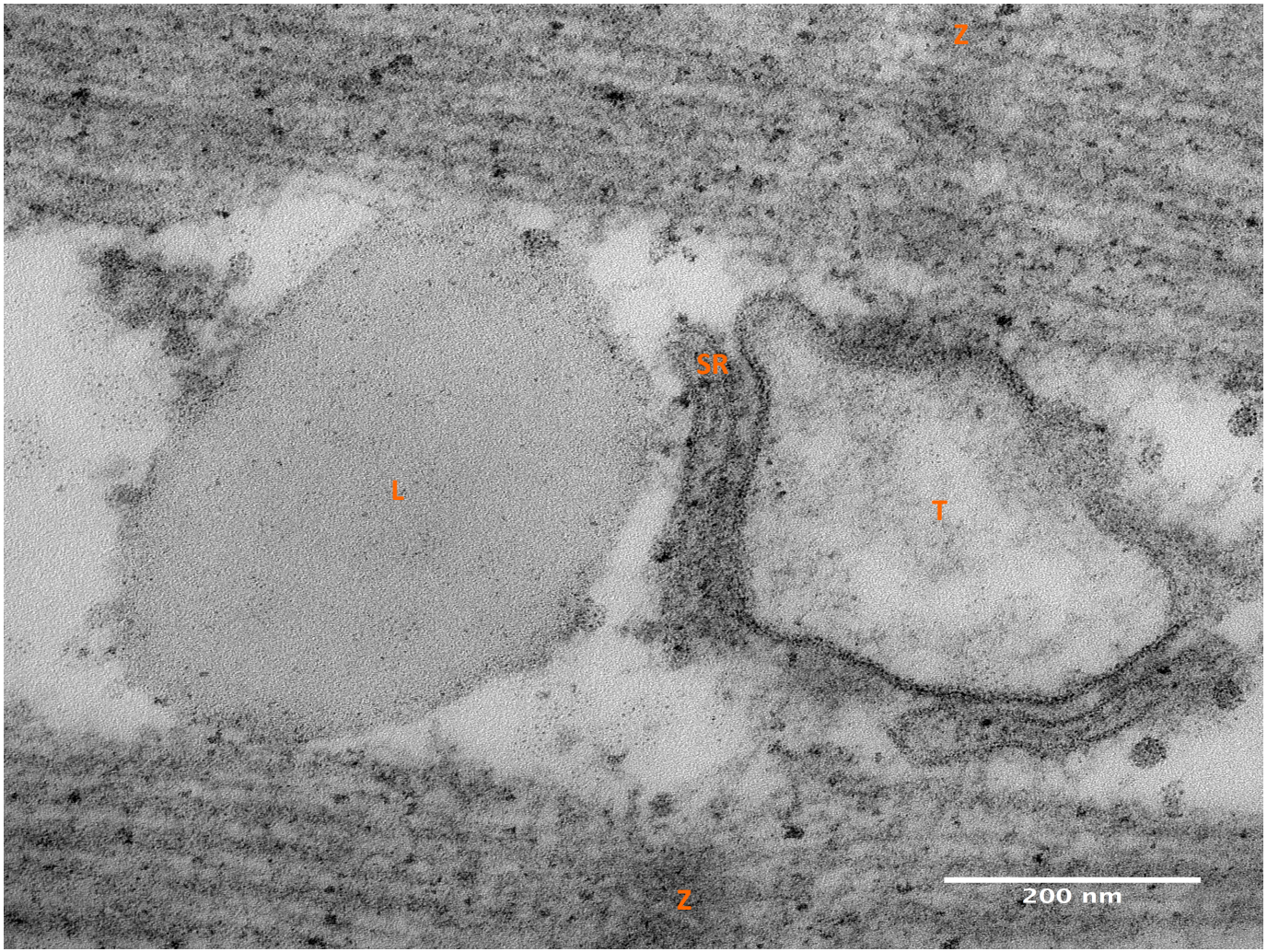


Figure 6.7: Proximity of lysosomes to sarcoplasmic reticulum (SR) and transverse (t-) tubules seen in rabbit ventricular cardiomyocytes on transmission electron microscopy. This image shows another example of the proximity of lysosomes with SR and t-tubules. The lysosome (L) is 24.1 nm from the SR membrane that lies between it and the t-tubule (T) in this image (measurement not shown). The end of a Z-line can also be seen at the bottom of the image (Z). The t-tubule is flanked by two terminal SR cisternae membranes and is therefore a triad.

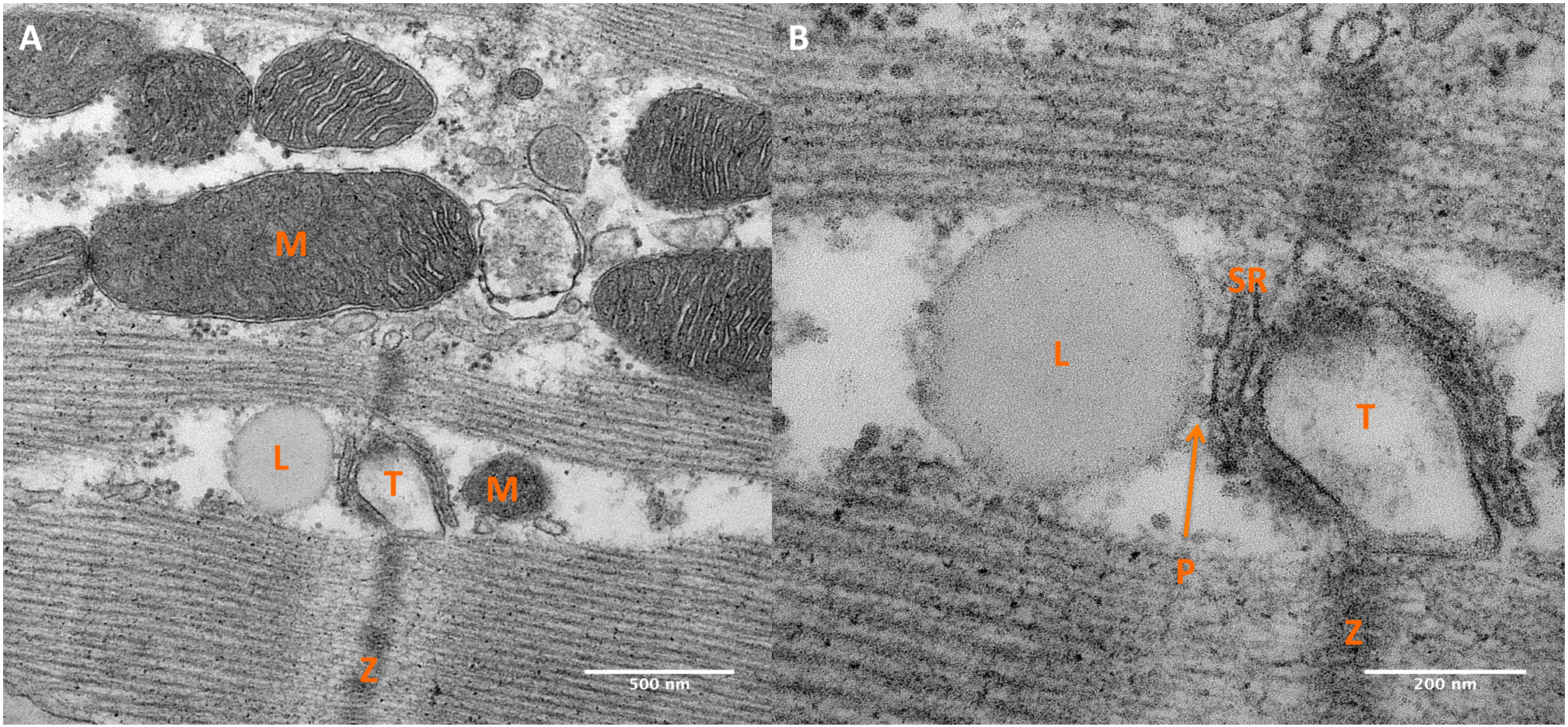


Figure 6.8: Possible tethering of lysosome to sarcoplasmic reticulum (SR) membrane seen in rabbit ventricular cardiomyocytes on transmission electron microscopy. Possible tethering proteins (P) are seen between the lysosome (L) membrane and SR. A t-tubule and a Z-line are also seen in close proximity and mitochondria (M) can also be seen.

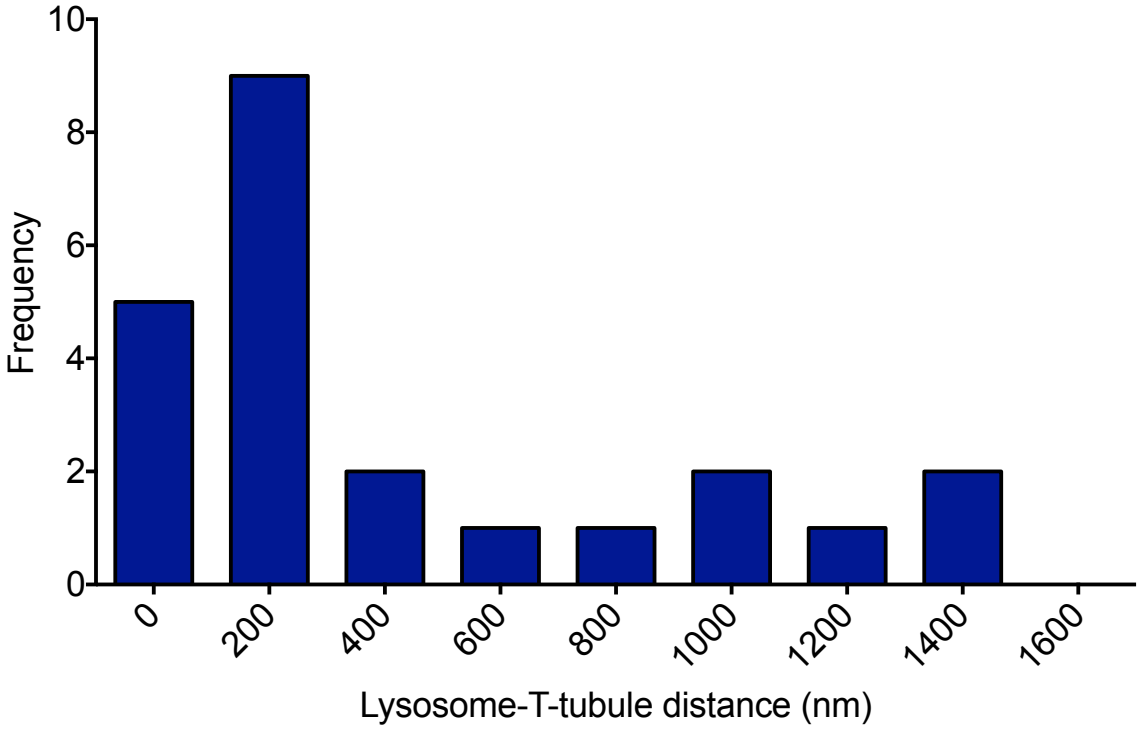


Figure 6.9: The distance from lysosomes to the nearest t-tubule in rabbit ventricular cardiomyocytes. The median distance was 163 nm (IQR = 123 – 870 nm), n=24. Note the positive skew of the distribution – suggesting that although lysosomes can be distant from t-tubules, it is more common to find them nearby.

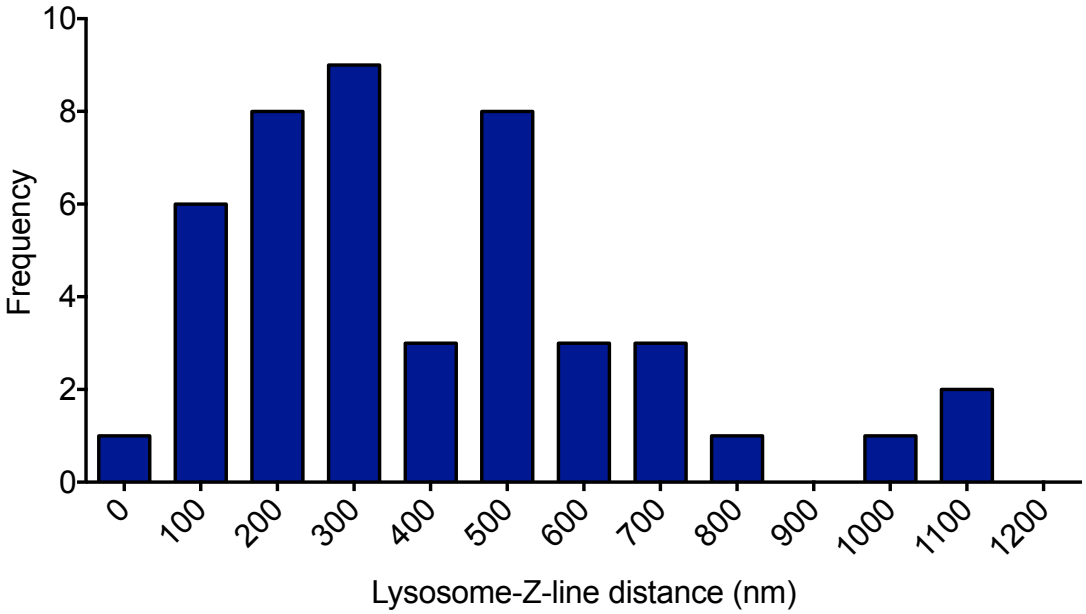


Figure 6.10: The distance from lysosomes to the nearest z-line in rabbit ventricular cardiomyocytes. The median distance was 318 nm (IQR = 176 – 529 nm), n=45. Note the positive skew of the distribution / distant outliers, suggesting that although lysosomes can be some distance from z-lines, they are more likely to be nearby.

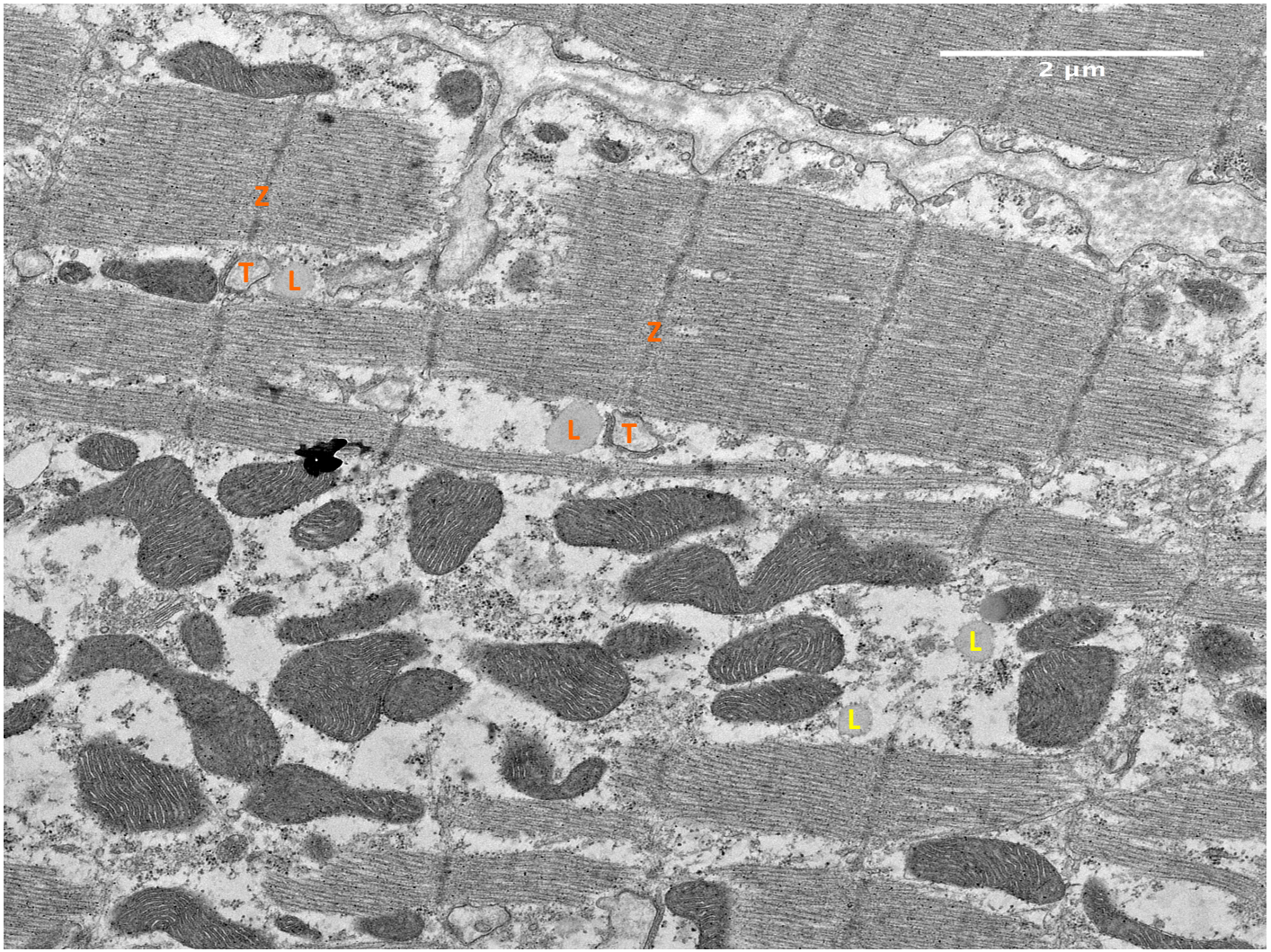


Figure 6.11: A wide-view image of a rabbit ventricular cardiomyocyte. Some lysosomes are in close proximity with Z-lines and t-tubules while others are more distant. The lysosomes (L) labelled in orange are close to t-tubules and Z-lines and SR membrane can also be seen. However, the lysosomes labelled in yellow appear much more distant from these structures.

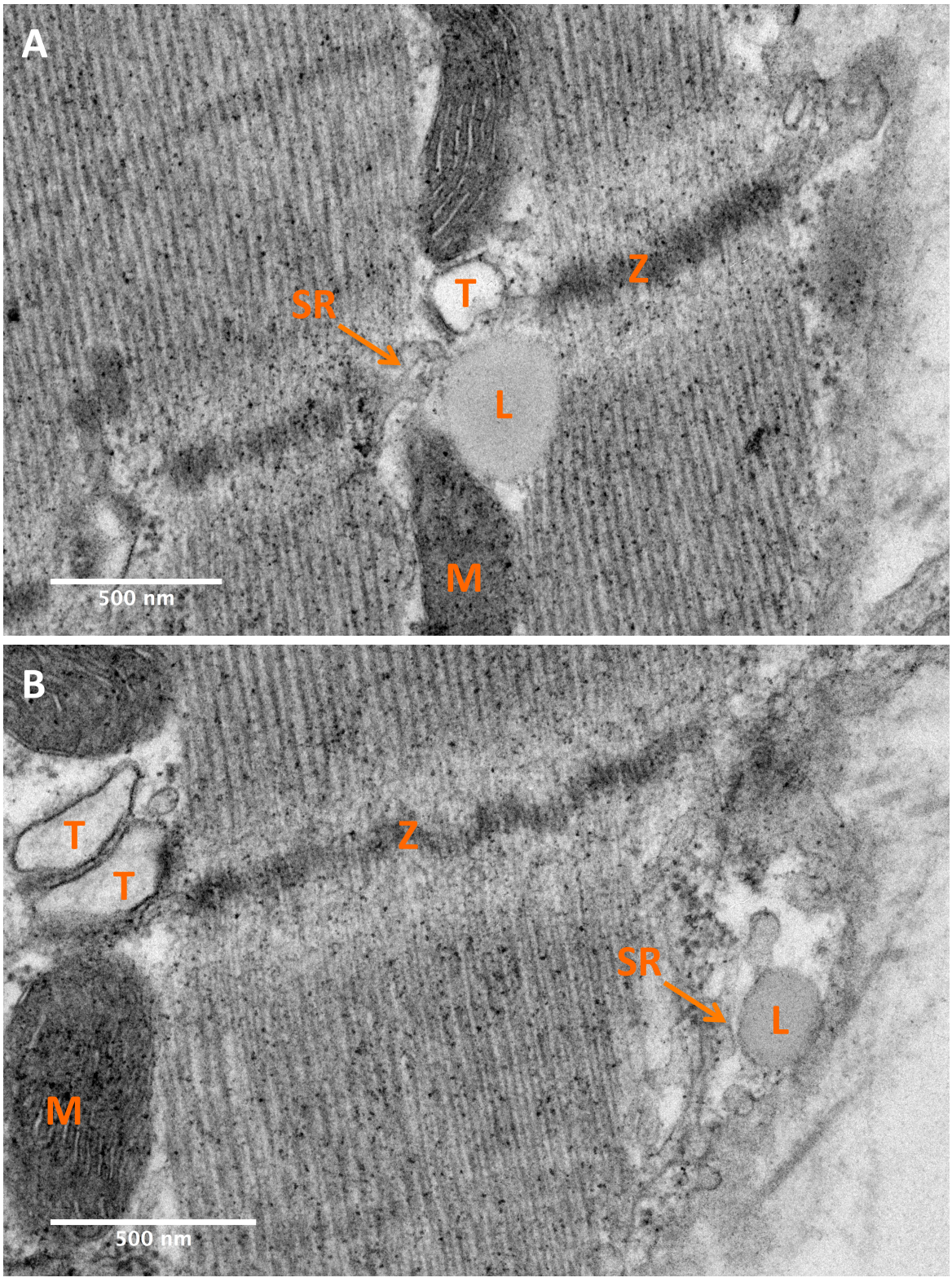


Figure 6.12: Lysosomal distribution in a rabbit ventricular cardiomyocyte seen on transmission electron microscopy. Panel A shows a lysosome (L) in close proximity with a T-tubule (T) and a Z-line (Z) in contrast to panel B where a lysosome can be seen distant from these structures. Both lysosomes are close to SR. Mitochondria (M) can also be seen.

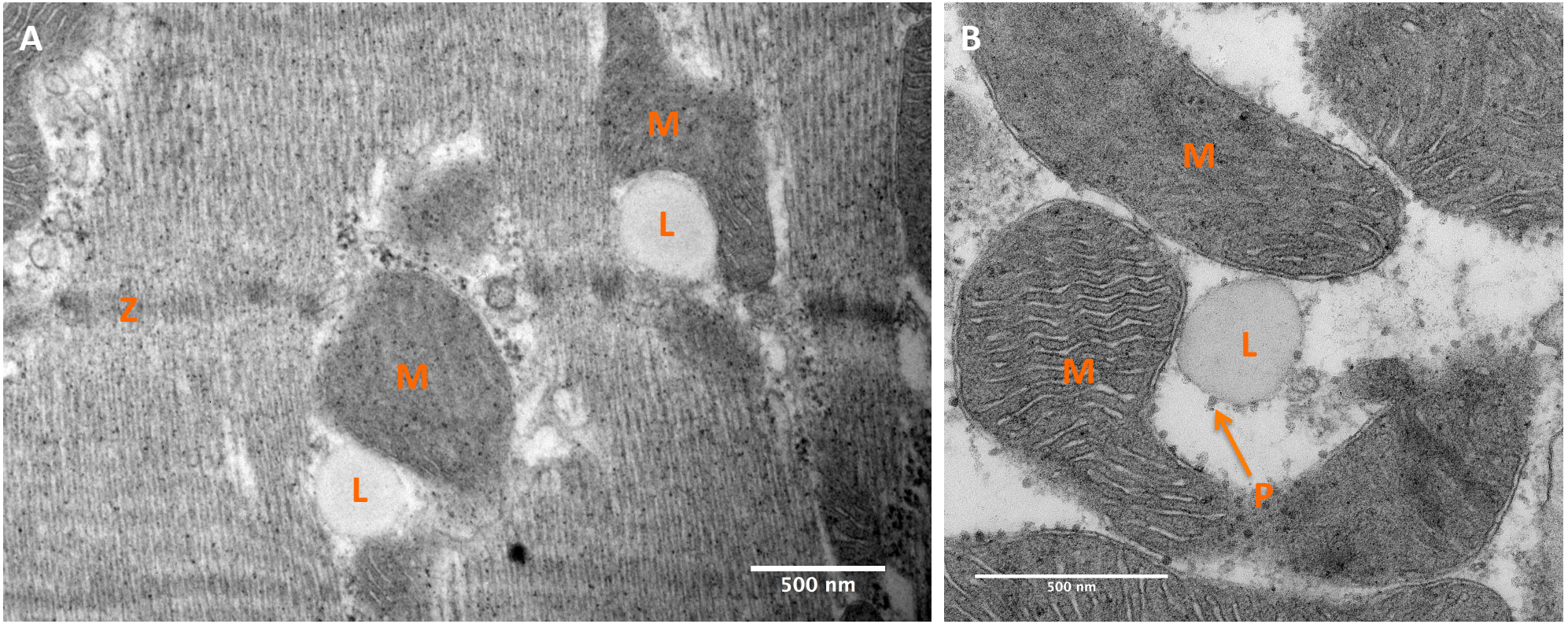


Figure 6.13: Lysosomes in close proximity with mitochondria in rabbit ventricular cardiomyocytes seen on transmission electron microscopy. Many lysosomes can be seen having membrane contact sites with mitochondria. Panel A shows two lysosomes (L) abutting adjacent mitochondria (M). A Z-line (Z) is also seen. Panel B illustrates another lysosome in close contact with mitochondria. In this image proteins on the lysosome surface (P) may form tethers or other communications between the two structures.

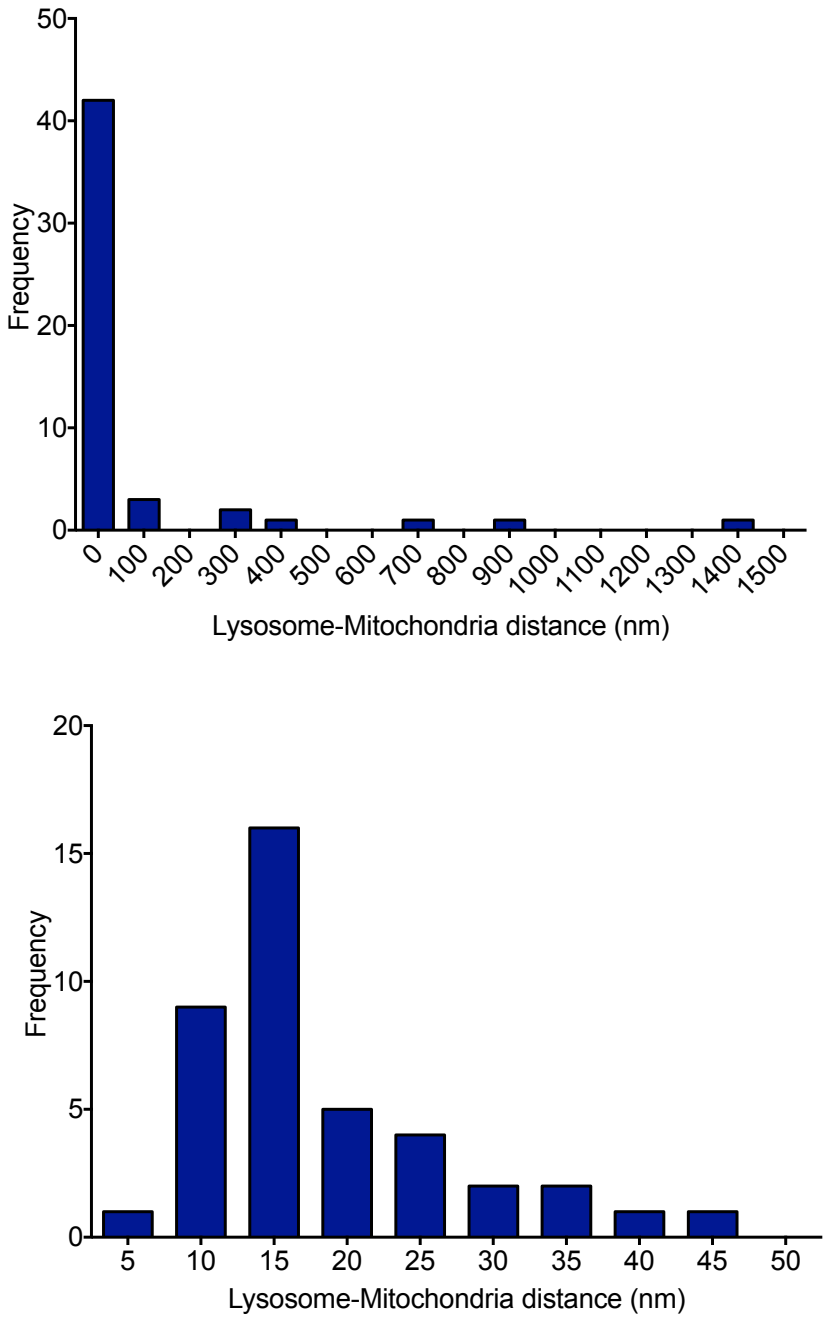


Figure 6.14: The distance from the lysosome to the nearest mitochondrion in rabbit ventricular cardiomyocytes. All but seven distances were less than 75 nm. The complete data set is shown in the top panel, while the bottom panel shows the data without the outliers. The median distance of the data in the bottom panel is 16 nm (IQR = 13 – 24 nm), n=44.

6.3 Conclusion

The observations described in this chapter show for the first time that cardiac lysosome-SR membrane contact sites exist in the ventricle, and that lysosomes are often located in association with sarcomeric structures such as T-tubules and Z-lines. This data is consistent with the trigger/modulator hypothesis of lysosomal calcium signalling in response to NAADP stimulation. Furthermore, an MCS between lysosomes and mitochondria was also observed, suggesting that communication between these organelles may also occur.

The size and morphology of lysosomes were generally consistent with those seen in most previous studies (Bandyopadhyay et al., 2014; Fameli et al., 2014; Junqueira et al., 1983 p. 39; Zhou et al., 2013), although it is acknowledged that their appearance is very heterogeneous (Alberts, 2015 p. 723.). The lysosomes seen here were smaller than those described by Hibbs et al. (1965), who reported cardiac lysosomes ranging in size from 0.1 – 2.0 μm with an average of approximately 1.0 μm. The reason for this difference is not apparent.

The age of the animals used for the experiments may influence the ratio of immature to mature lysosomes seen. The latter have a much darker coloured and less homogenous matrix due to fusion with (auto-)phagosomes and due to lipofuscin pigment accumulation with age (Brunk et al., 2002; Schmucker et al., 2002; Terman et al., 2005) Mature lysosomes may be considered to represent a more classical appearance of this organelle, although the paler-coloured immature lysosomes are well recognized (Neiss, 1983; Schmucker et al., 2002).

The animals used in the present investigation were young rabbits (6 – 8 weeks old) and therefore had a higher ratio of immature to mature lysosomes, and only a small amount of lipofuscin accumulation.

Few other studies have used EM to specifically focus on the lysosome-SR (L-SR) junction. One was recently performed using pulmonary artery smooth muscle cells (Fameli et al., 2014). The mean width of the L-SR junction observed in that study was 15 nm with a lateral extension of approximately 300 nm. According to computer modelling, these parameters were sufficient to allow the calcium concentration in the junction to reach the required threshold to trigger calcium-induced calcium release from ryanodine receptors. The median L-SR distance observed in experiments here (20 nm) is consistent with that reported by Fameli *et al*.

Additional data is presented in appendix B (table B1 and figure B1) that shows measurements of the L-SR junction using three-dimensional reconstructions of electron tomographs. In two dimensional images, the distance measured between two objects is accurate in the plane of the section, but no information is available about the separation of the objects in other planes. Therefore, measurements were also made in three dimensions to account for this. The median L-SR distance in these reconstructions was 3.3 nm, confirming that L-SR MCS do indeed exist, and that measurements in two-dimensions underestimate the intimacy of the relationship between these structures.

Other studies have examined the relationship between late endosomes and the SR. Although late endosomes are functionally and structurally distinct from lysosomes, they are closely related (Alberts, 2015; Phillips et al., 2015; Raiborg et al., 2015). One study that examined the late endosome-ER microdomain using EM in HeLa cells measured the mean distance as 8.3 nm (Alpy et al., 2013) and another, also using HeLa cells, observed late endosome-ER distances of less than 20 nm, although an average distance was not reported (Eden et al., 2010).

Distances between the lysosome and T-tubules (L-TT) and Z-lines (L-Z) were also measured. The distance estimated in the last chapter between LAMP-2 and RyR2 immunofluorescence signals is a good surrogate marker for the L-TT distance measured on EM, since LAMP-2 is found in the lysosome membrane and RyR2 is mostly found on SR adjacent to L-type calcium channels in the T-tubules (the dyads). Similarly, since most T-tubules are found in association with Z-lines, the L-TT and L-Z distances should not be dissimilar. The distance between LAMP-2 and RyR2 estimated using immunofluorescence (268 nm) is of the same order as the L-TT and L-Z distances measured on EM (163 nm and 318 nm respectively). Similarly, the distance from LAMP-2 to the nearest PLB signal was also comparable at 224 nm.

In three dimensions, the median L-TT and L-Z distances were 99 nm and 232 nm respectively, which are not dissimilar to the two dimensional measurements (see table B1).

The distributions of L-TT and L-Z distances were positively skewed. This indicates that while most lysosomes appear to be associated with T-tubules or Z-lines, there are some that are isolated and distant from these structures. It is possible, although this cannot be confirmed using the current data, that the lysosomes close to the T-tubules and Z-lines are associated with RyR2 and are therefore involved in stimulating calcium release from the SR, whereas those lysosomes that are distant from the T-tubules and Z-lines (but still close to SR) are associated with PLB and SERCA and are involved in stimulating calcium re-uptake by the SR. If this is correct, then different subpopulations of L-SR junctions might have different functions depending on the target for lysosomal calcium. This concept will require further investigation; for example the use of immunogold labelling of RyR2 and SERCA or PLB on future EM studies, or colabelling of RyR2 and PLB using immunocytochemistry. In light of the discovery that CaMKII is required for the action of NAADP on the calcium transient, it is interesting to note that CaMKII showed a high degree of colocalisation with RyR2 in both ventricular and atrial cardiomyocytes (Collins, 2009). The relative locations of CaMKII and PLB have not been elucidated in the heart.

Lysosomes are known to switch between being mobile organelles that move along cytoskeletal filaments such as microtubules to being immobile and tethered to other structures such as the SR (Lam et al., 2013). Physical linkage between lysosomes and the SR occurs via many different protein complexes that vary depending on the organism (Helle et al., 2013; Prinz, 2014). In mammals, examples of lysosomal proteins include ORP1L, StARD3 and EGRF and these bind

to VAP-A/RILP, other VAPs and PTP1B on the S/ER respectively. The transformation of the lysosome from mobile to tethered is governed by cholesterol binding to ORP1L and resulting in an alteration in conformational state (Lam et al., 2013; Rocha et al., 2009). Such tethering complexes have been visualised using EM in cultured HeLa cells (Eden et al., 2010), but never in cardiomyocytes.

Some images obtained here appeared to show structures that may be proteins spanning the width of the MCS between the lysosome and the SR. It is possible that these may represent tethering proteins, although further investigation will be required before this can be suggested with any degree of certainty. Immunogold labelling of the known mammalian tethering proteins may help to further define these structures. Although it is currently unclear how these proteins influence calcium signalling between lysosomes and the SR, their presence may indicate that important communication is likely to occur between these structures, and this would support the trigger/modulator hypothesis.

Although microdomains have been previously studied between mitochondria and the SR (Kohlhaas et al., 2013; Lam et al., 2013), few studies have examined the relationship between mitochondria and lysosomes outside the context of autophagy. Observations here demonstrated a subpopulation of lysosomes were closely associated with mitochondria. An MCS could sometimes be measured (with a median distance of 16 nm) between these organelles, although in some cases the distance was too small to measure. There were also some lysosomes that did not appear to be associated with mitochondria. When some images were

reconstructed in three dimensions, the median distance from a lysosome to the nearest mitochondrion was 6 nm, suggesting an over-estimation of the distance between these organelles using two dimensional imaging.

It is possible that where these MCS did exist they may have a function related to ischaemia/reperfusion injury. A recent investigation by Davidson et al. (2015) demonstrated that hearts subjected to ischaemia-reperfusion injury were protected if simultaneously exposed to Ned-19 or a more recently synthesised chemical varient, Ned-K. Similarly, hearts from *Tpcn1*$^{-/-}$ mice were also protected. It was hypothesised that protection was due to prevention of calcium oscillations that occur during ischaemia/reperfusion injury that cause opening of the mitochondrial mPTP channel. Opening of this channel is known to be related to cell death during ischaemia/reperfusion (Ong et al., 2015). It is possible that calcium released from lysosomes in response to NAADP communicates with mitochondria via microdomains to influence mPTP opening.

7

The structure and function of cardiac atrial tissue in the context of NAADP signalling

7.1 Introduction

Responses of atrial and ventricular myocytes to NAADP are very similar; both display positive inotropic effects, increased calcium transient amplitude and enhanced loading of the SR in response to NAADP (Collins et al., 2011; Macgregor et al., 2007). The response to β-adrenergic stimulation of both cell types appears to partially depend on an intact NAADP signalling pathway, as responses to isoprenaline are blunted in cells from *Tpcn2*$^{-/-}$ mice or in hearts exposed to Bafilomycin-A1 or Ned-19 (Bolton, 2014; Capel et al., 2015). In addition, functional CaMKII is required for NAADP-mediated calcium signalling in both cell types, and inhibition of this enzyme prevents the increase in calcium transient observed following NAADP release in both atria and ventricles (Bolton, 2014; Capel et al., 2015).

However, the basal 'tone' of the NAADP system may be higher in the atrium than in the ventricle. When 1 μM bafilomycin-A1 was applied to guinea pig ventricular cells in the absence of β-adrenergic stimulation the calcium transient fell by 20% (Macgregor et al., 2007). When the same experiment was performed using atrial myocytes and a ten-fold reduction in bafilomycin-A1 dose (100 nM), the calcium transient fell by at least the same amount as with 1 μM bafilomycin-A1 (19%, Bolton (2014)), and up to more than twice as much (47%, Collins et al. (2011)).

Structural explanations for the differences in response to blockade of the NAADP/TPC2 system under basal conditions between atrial and ventricular muscle may lie in the relative numbers or morphology of lysosomes, or -

especially in small mammals such as the rodents used here – in the T-tubule / transverse/axial tubule (TAT) network.

The TAT network is known to be extensively developed in ventricular cells (Trafford et al., 2013). However, in atrial cells the prevailing view had been until recently that it was only rudimentary and less-well developed. This remains the view in the case of small laboratory mammals such as mouse, rat, guinea pig and rabbit but recently evidence suggests that the TAT network is well developed in the atria of larger mammals such as cow, horse and human (Dibb et al., 2013; Trafford et al., 2013).

The absence of a well-developed T-tubules in the atria of small mammals means that the action potential and calcium transient does not spread uniformly across the cell. Instead, the cell interior lags behind the periphery, since T-tubules are not present to conduct the depolarisation deep into the cell (Dibb et al., 2013; Trafford et al., 2013). L-type calcium channels on the plasma membrane are restricted to the cell surface and are uncoupled from the RyR on the SR inside. However, the RyR are still found adjacent to Z-lines in the atrium despite the lack of T-tubules (Chen-Izu et al., 2006) meaning - in contrast to the ventricle - there is little or no co-localisation of RyR and L-type calcium channels in the atria (Schulson et al., 2011; Smyrnias et al., 2010).

Despite this, there is still dependence of the NAADP pathway on the presence of a functional SR and RyR in the atria. In atrial myocytes exposed to ryanodine and thapsigargin, NAADP had a negligible effect on calcium transient amplitude, and

the addition of bafilomycin-A1 to these cells had no additional effect (Collins et al., 2011). The necessity that both lysosomes and the SR remain functional in order that NAADP has an effect on calcium handling in the atria implies communication between the two structures, and is again consistent with the trigger/modulator hypothesis described earlier: Locally released calcium from the lysosome in response to NAADP could influence the SR either via direct CICR at the RyR, and/or by causing enhanced SR calcium loading – perhaps via a mechanism involving CaMKII and phospholamban. Similarly, the possibility that CaMKII could also phosphorylate the RyR to influence its activity cannot be excluded. RyR and CaMKII are known to co-localise in both atrial and ventricular myocytes (Collins, 2009). All of these mechanisms are likely to require a microdomain.

If lysosomes form microdomains with the SR in atrial muscle this may mean that a subpopulation of atrial RyR are under the influence of calcium released in response to NAADP, but not under the influence of calcium from the L-type channel. Therefore, an inhibition of lysosomal function with bafilomycin-A1 might be expected to have a more dramatic effect on the resting calcium transient since a higher percentage of the input to the RyR is being disrupted. Furthermore, during β-adrenergic stimulation increased levels of NAADP may result in increased activity in these RyR, contributing to the observed increase in calcium transient amplitude.

This putative role of lysosomes in the atria may prove important, since the threshold for provoking and maintaining atrial fibrillation (AF) in small

mammals without extensive T-tubules is high, but in larger mammals such as humans it is much lower (Dibb et al., 2013). It is possible that the NAADP/TPC2 system may prove a useful therapeutic target in this respect, especially as an involvement in ventricular arrhythmias has already been demonstrated in chapter 3 and elsewhere (Nebel et al., 2013).

The ultrastructure of the rabbit left atrium is examined using TEM in this chapter. Any differences in morphology, size and distribution between lysosomes seen in the atria compared with those in the ventricle will be noted. In addition, given the observed association between lysosomes and mitochondria seen in the ventricle, this relationship will be examined in atrial tissue as well.

Additional structures that should be expected in the atria that are not seen in EM studies of the ventricle include atrial-specific granules. These structures are now known to contain atrial-natriuretic peptide, which is a hormone released to cause vasodilatation and salt and water excretion in response to increased atrial stretch as one of the physiological controls of blood pressure and fluid balance (de Bold, 2011; de Bold et al., 1983; Flynn et al., 1983). However, these granules superficially resemble lysosomes (Otsuka et al., 1969; Tomisawa, 1969), are acidic and contain calcium (Somlyo et al., 1988). Unlike lysosomes, they do not stain positive for acid phosphatase enzymes and are found in dense clusters (Tomisawa, 1969). To date, no association has been identified between these granules and the NAADP/TPC2 signalling pathway.

In addition to electron microscopic examination of atrial tissue, experiments are presented in this chapter testing the effect of manipulation of the NAADP signalling pathway both pharmacologically (with Ned-19 and bafilomycin-A1) and genetically (using atria from *Tpcn2*$^{-/-}$ mice) on responses to β-adrenergic stimulation. Although these manipulations have been tested in isolated atrial myocytes in the past (Bayliss, 2014; Collins et al., 2011) and have been shown to have a similar effect on the calcium transient to that seen in the ventricle, their effects have not been tested on contraction or in intact atrial tissue. Therefore, experiments were undertaken to test whether the intact atrium behaves in the same way as isolated atrial myocytes in the presence of these manipulations.

7.2 Results

Electron Microscopy

7.2.1 Transmission electron microscopy reveals the ultrastructure of rabbit atrial cardiomyocytes, including the presence of a limited number of T-tubules.

The organisation of the subcellular structure of atrial tissue had some similarities and some differences to ventricular tissue when seen on TEM. The most striking difference was lack of well-defined sarcomeres. However, this difference is likely to have been due to the atrial tissue sample being unintentionally sliced in a different orientation compared with the ventricular samples during preparation. Although the contractile filaments can be seen, the individual filaments often appear in transverse section ('end-on') instead of in longitudinal section that allows easy visualisation of the sarcomeric structure.

In keeping with this, T-tubules were seen in longitudinal section, and not in cross ('end on') section as they were in the ventriclar tissue. However, it should be noted that the transverse tubules in the ventricle also have axial branches that should still be visible in cross section in these samples, despite the orientation of the slicing. It is noteworthy that these tubules appear to be absent, indicating that the TAT network is likely to be less-well developed in the atria than in the ventricles, consistent with previous data (Dibb et al., 2013; Trafford et al., 2013)

Figure 7.1 shows these features in a low-magnification TEM image.

7.2.2 The morphology of lysosomes in rabbit atria as seen on transmission electron microscopy.

A total of 18 lysosomes were measured in TEM images of rabbit atrium. This was fewer than analysed in the ventricle due to the smaller number of images, and not because lysosomes were less commonly seen. Although numbers of lysosomes between the two tissues were not formally quantified, subjectively there was no difference in the abundance of lysosomes between the two tissues.

The overall morphology of lysosomes seen in the atria was identical to those seen in the ventricle, although their dimensions were slightly smaller (the median long axis was 253 nm (217 – 319 nm) and mean short axis was 204 nm (175 – 253 nm), $P<0.0001$ and $P=0.0012$ respectively compared with their ventricular counterparts, one-way ANOVA with Bonferroni multiple comparisons correction). Even if those lysosomes with a dimension less than 200 nm were excluded from both groups in order to attempt to ensure the exclusion of endosomes from the data (Fameli et al., 2014), this difference was still present, although the difference between the groups was smaller. There was a higher number of lysosomes with a dimension less than 200 nm in the atrial group than in the ventricular group.

The histograms of atrial dimensions are shown in figure 7.2, and the mean atrial lysosomal dimensions are compared with those from the ventricle in figure 7.3.

7.2.3 Lysosomes are not obviously more numerous in rabbit atrial cardiomyocytes compared with ventricular cardiomyocytes, although clusters of lysosome-like structures are exclusive to the atria.

Figure 7.4 shows an example of a cluster of many lysosome-like structures in a rabbit atrial cardiomyocyte. They are densely packed into a small area, and other structures – particularly SR membrane can be seen between them. The cluster is surrounded by several mitochondria. This organisational appearance was not observed in the ventricle. The size and general morphology of the structures appears virtually identical to lysosomes seen elsewhere in the atria and ventricles. However, their distribution is strikingly different, being densely clustered. It is possible that these structures are atrial-specific granules rather than lysosomes.

Figure 7.5 shows approximately five lysosomes in a distribution more similar to those seen in the ventricle, and this pattern was also the rule in the atria.

7.2.4 Lysosomes in rabbit atrium form membrane contact sites with sarcoplasmic reticulum.

In contrast with the lysosomal dimensions, there was no difference in the distance to SR membrane between atrial and ventricular lysosomes. The median

distance was 17 nm (13 – 22 nm), n=13. The histogram of this data is shown in figure 7.6.

Figure 7.7 shows TEM images of atrial lysosomes in close proximity with SR membrane.

7.2.5 Lysosomes in rabbit atrium may form membrane contact sites with mitochondria.

As in ventricular tissue, it was common to see lysosomes in close contact with mitochondria in the atrium. Although some lysosomes were some distance from mitochondria, a larger number were closely associated and some appeared to be in physical contact with no discernable distance between them. The minimum measurable distance was 7.8 nm and the maximum distance with 398.3 nm. The median lysosome-mitochondrial distance was 13 nm (10 – 63 nm), n=13 (no outliers removed).

Figure 7.8 shows the histograms of this data, and example images of lysosomes in close association with mitochondria are shown in figure 7.9.

Atrial contraction measurements

7.2.6 Atria taken from wildtype mice have a higher baseline contraction amplitude than atria taken from *Tpcn2*$^{-/-}$ mice.

Baseline atrial contraction amplitudes of wildtype and *Tpcn2*$^{-/-}$ mice are shown in figure 7.10. The force of contraction in atria from knockout animals was 74±6% of that seen in the wildtype (P=0.015, Student's unpaired t-test, n=10 in wildtype group and n=9 in knockout group).

7.2.7 There was no difference in contractile or rate responses to isoprenaline in isolated atria from wildtype and *Tpcn2*$^{-/-}$ mice.

Figure 7.11 shows the developed tension dose-response curves for isoprenaline in paced isolated left atria from wildtype and *Tpcn2*$^{-/-}$ knockout mice. No significant difference was detected between responses in these two groups (P>0.05, two-way ANOVA, n=9).

Similarly, the dose-response curves for spontaneous beating rate in isolated right atria from wildtype and *Tpcn2*$^{-/-}$ mice are shown in figure 7.12. No significant differences in response to isoprenaline were detected (P>0.05, two-way ANOVA, n=7).

7.2.8 Neither bafilomycin-A1 or Ned-19 had an effect on baseline atrial contraction in the absence of isoprenaline

Prior to the addition of isoprenaline, atria were allowed to equilibrate with inhibitors for 60 minutes. There was a small (< 10%) reduction in the baseline contraction amplitude in all groups including DMSO controls. However, there was no significant difference between control and drug-treated tissues ($P>0.05$, one-way ANOVA, n=6). This data is shown in figure 7.13.

7.2.9 Ned-19 reduced the contractile response of isolated atria to isoprenaline

In the presence of Ned-19 10 μM, the contractile response to isoprenaline was significantly blunted compared with DMSO controls. The maximum increase in developed tension in the control group was 97±10 mg and this was reduced to 47±5 mg in the Ned-19 group ($P=0.0008$, two-way ANOVA, n=6).

Mean data are shown in figure 7.14.

7.2.10 Bafilomycin-A1 reduced the contractile response of isolated atria to isoprenaline

Similarly, in the presence of bafilomycin-A1 10 μM the contractile response to isoprenaline was significantly blunted compared with DMSO controls. The maximum increase in developed tension with bafilomycin was 51±6 mg (P=0.0008, two-way ANOVA, n=6). This data is shown in figure 7.15.

Figure 7.16 shows representative traces of raw data from control hearts, along with hearts treated with Ned-19 or Bafilomycin-A1.

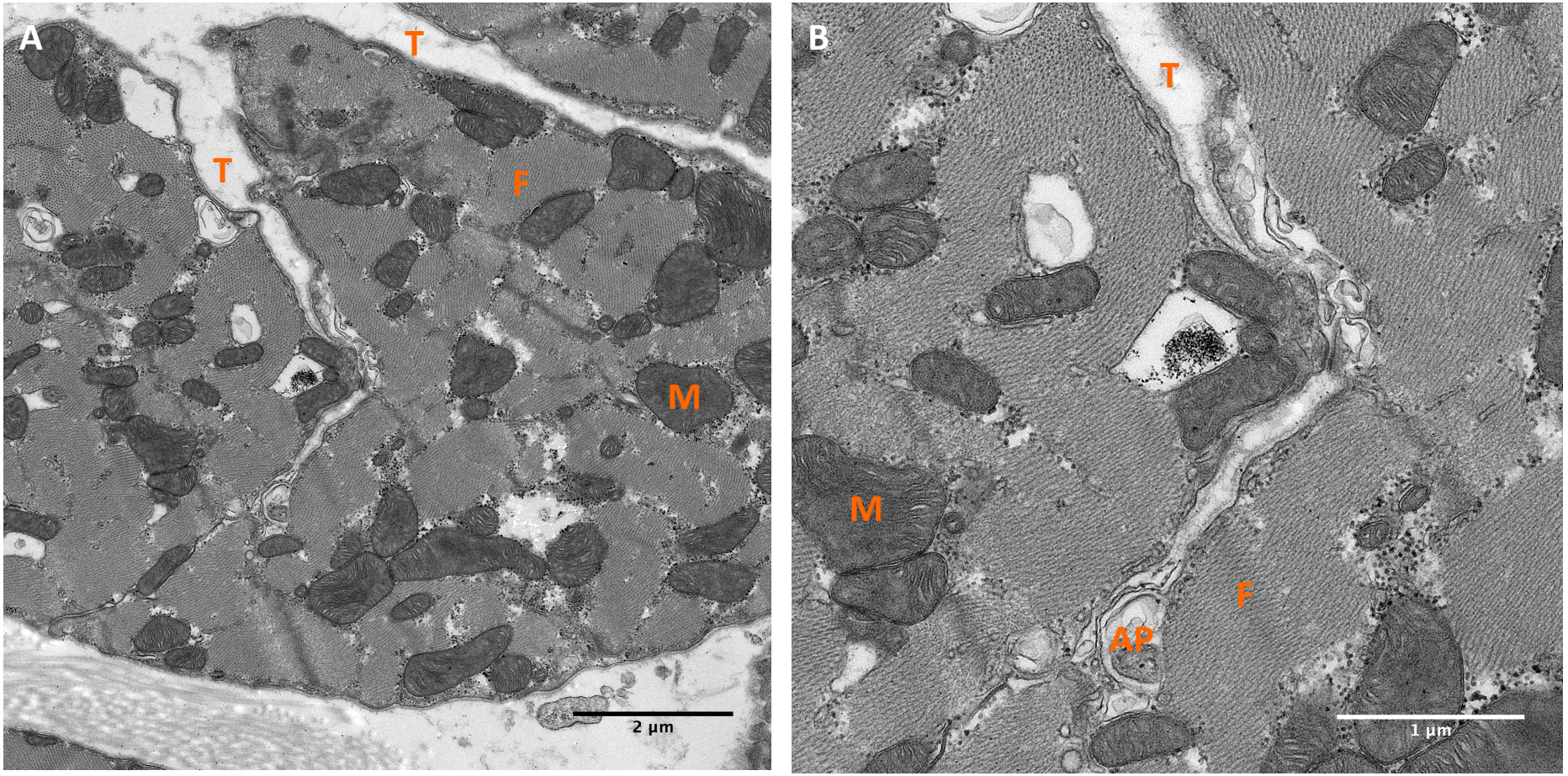


Figure 7.1: Low magnification transmission electron microscopy of rabbit atrial cardiomyocytes. Mitochondria (M), contractile filaments (F) and autophagosomes (AP) can easily be identified – as they were in ventricular tissue. However, note that the sarcomeres are less-well defined. There are also transverse (T-) tubules (T) clearly seen in these samples.

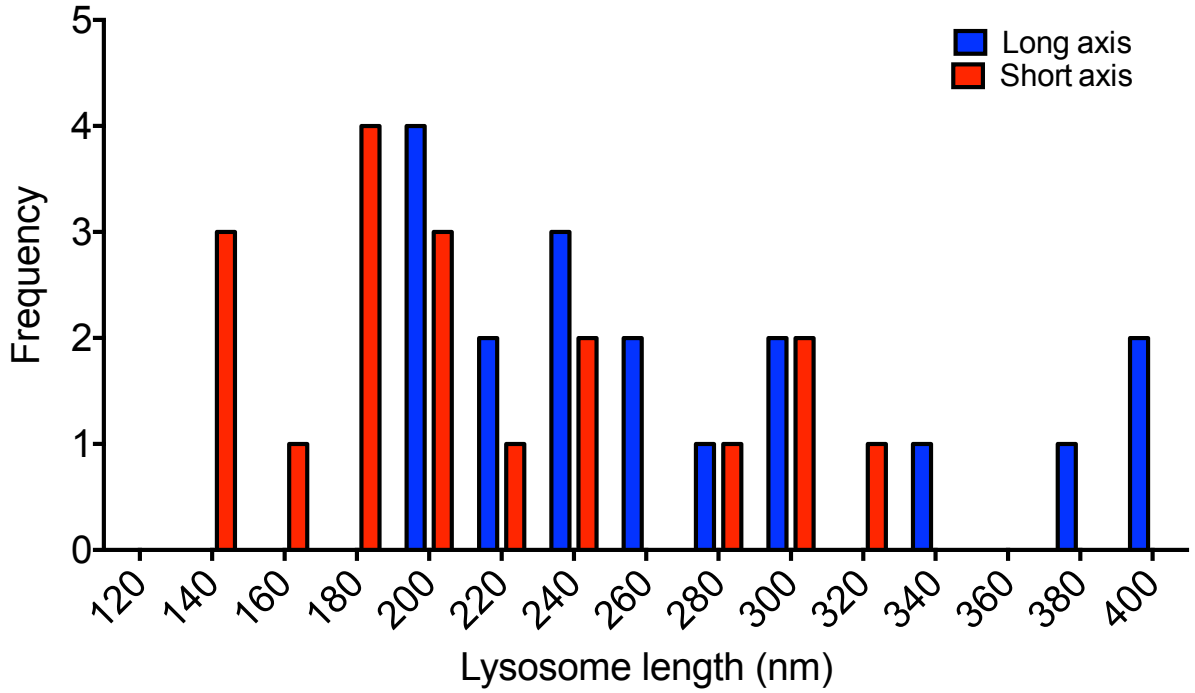


Figure 7.2: The size of cardiac lysosomes found in rabbit atria. The median long and short axis lengths were 253 nm (217 – 319 nm) and 204 nm (175 – 253 nm) respectively (n=18).

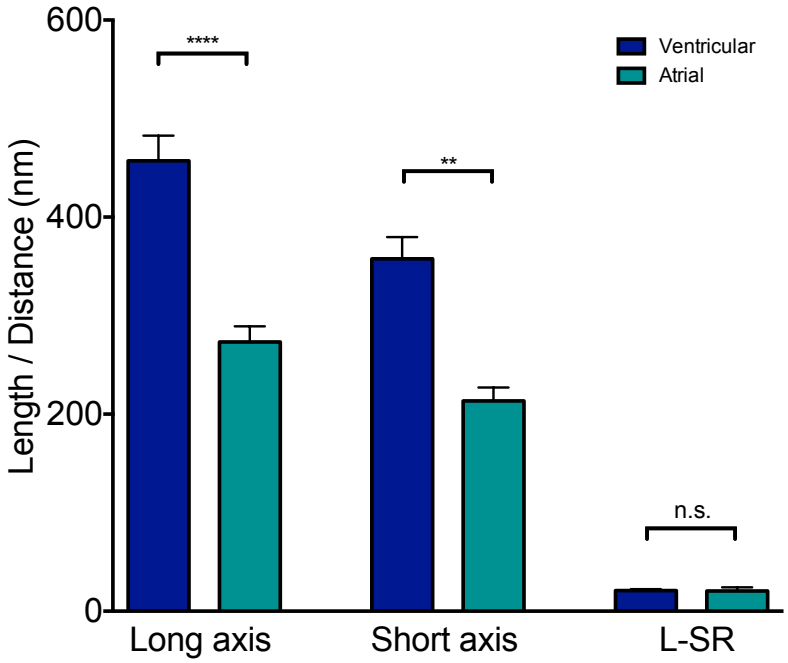


Figure 7.3: Dimensions and distance to SR of atrial and ventricular lysosomes compared. Above, **** and ** indicate P<0.0001 and P=0.0012 respectively. There was no significant difference in the distances measured between lysosomes and the SR (one-way ANOVA with Bonferroni correction).

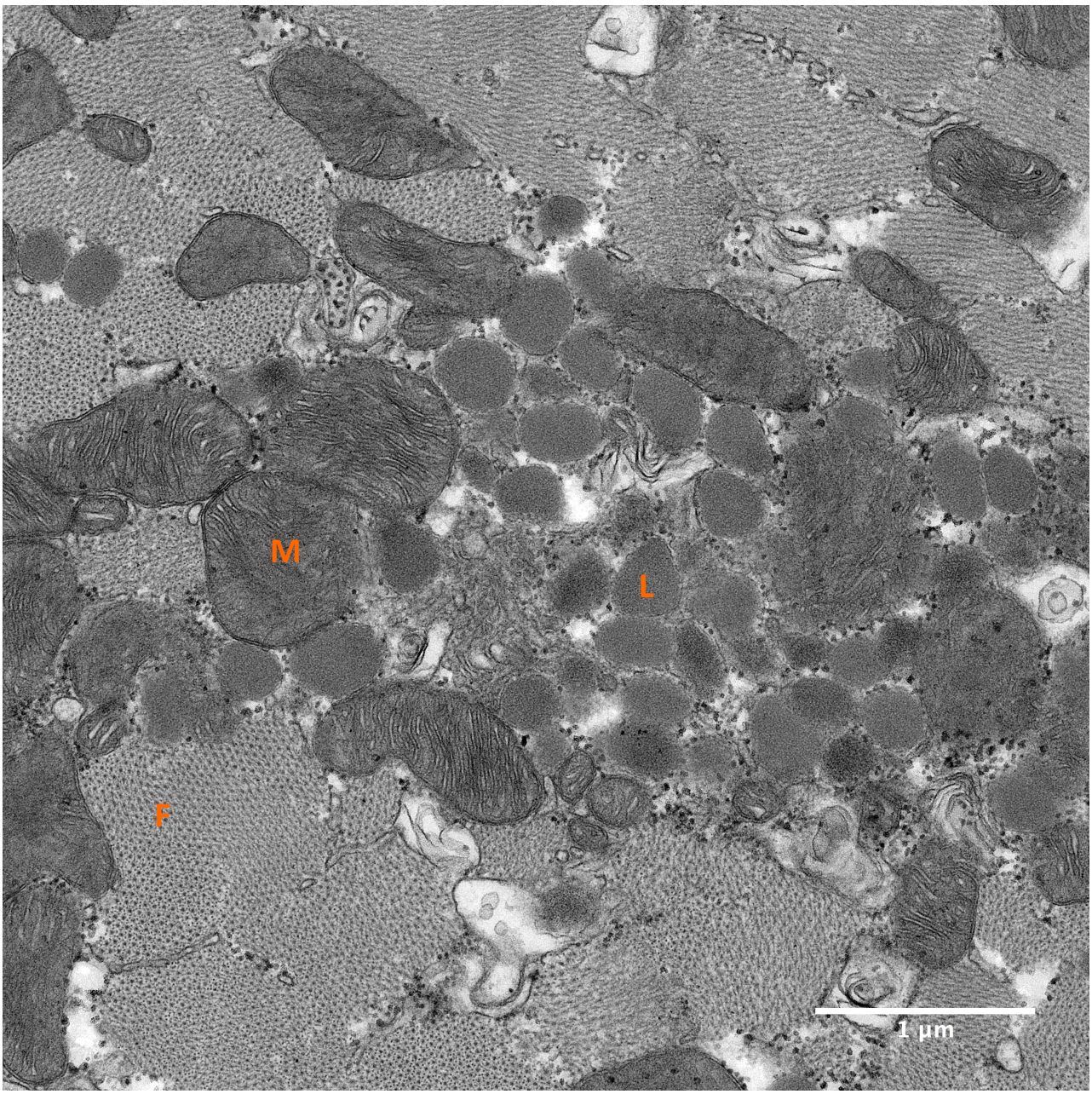


Figure 7.4: Dense clusters of lysosome-like structures in a cardiomyocyte from rabbit atrium. This image shows many lysosomes-like structures (L) clustered together in a small space. Mitochondria (M) and contractile filaments (F) can also be seen. These clusters were not found in ventricular tissue.

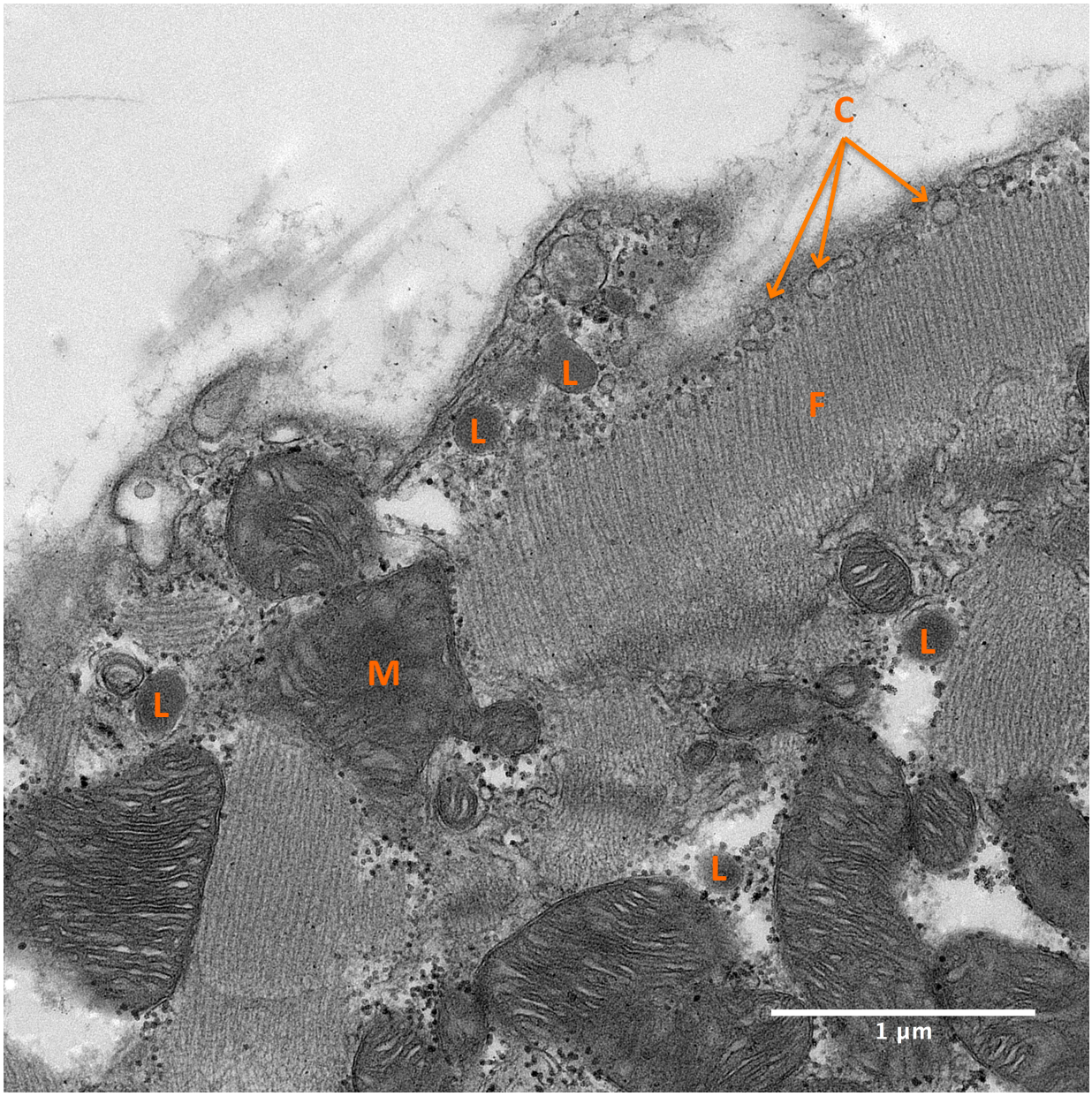


Figure 7.5: Transmission electron micrograph showing a low magnification view of the submembrane region in a rabbit atrial cardiomyocyte. At least five lysosomes (L) can be seen, along with mitochondria (M) and contractile filaments (F). Small submembranous vesicles that may be caveolae (C) can also be seen.

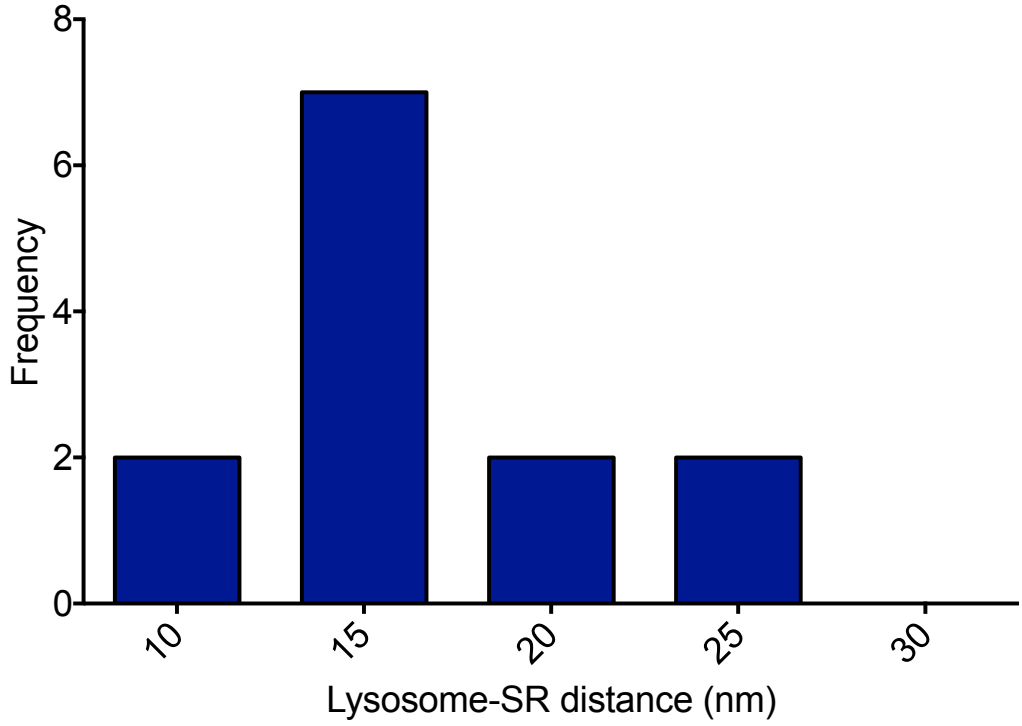


Figure 7.6: The distance from the lysosome to the sarcoplasmic reticulum (SR) in rabbit atrial cardiomyocytes. The median distance was 17 nm (13 – 22 nm), n=13.

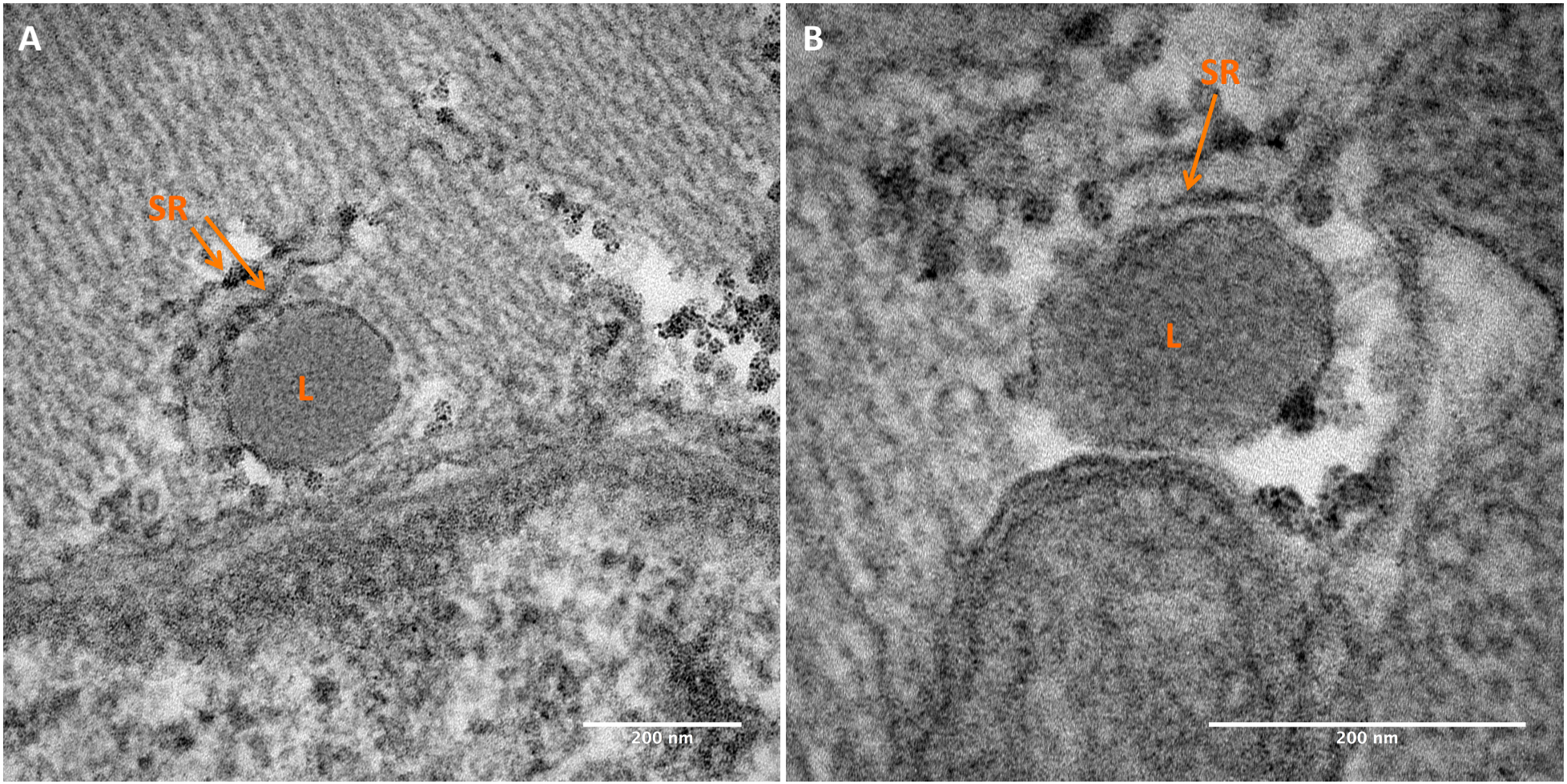


Figure 7.7: Lysosomes in rabbit atrial cardiomyocytes shown lying in close proximity with sarcoplasmic reticulum (SR). The distance between lysosome and SR membrane in panel B is 12.9 nm (measurement not shown). Circular structures that may be lysosomal membrane proteins can also be seen.

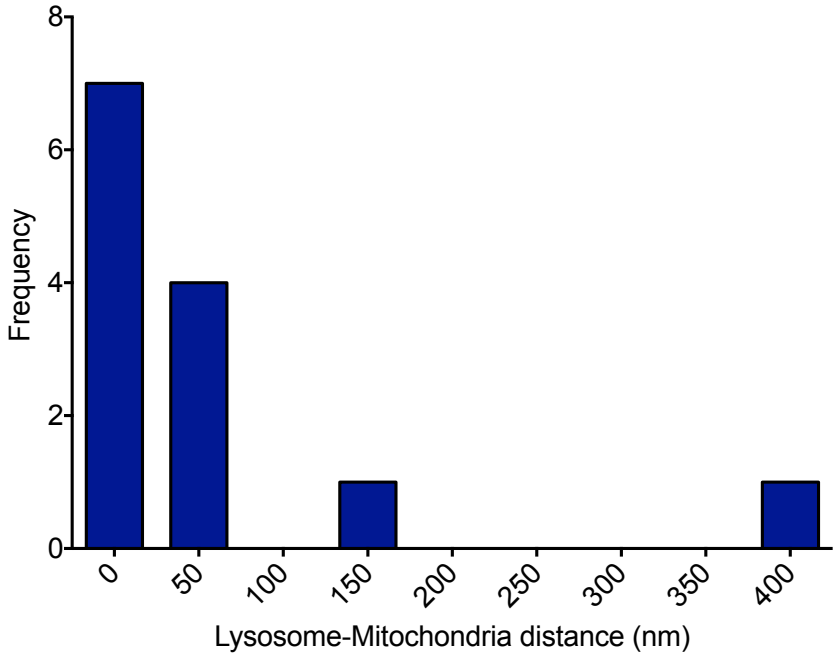


Figure 7.8: The distance from the lysosome to the nearest mitochondrion in rabbit atrial cardiomyocytes. The median distance is 13 nm (10 – 63 nm), n=13.

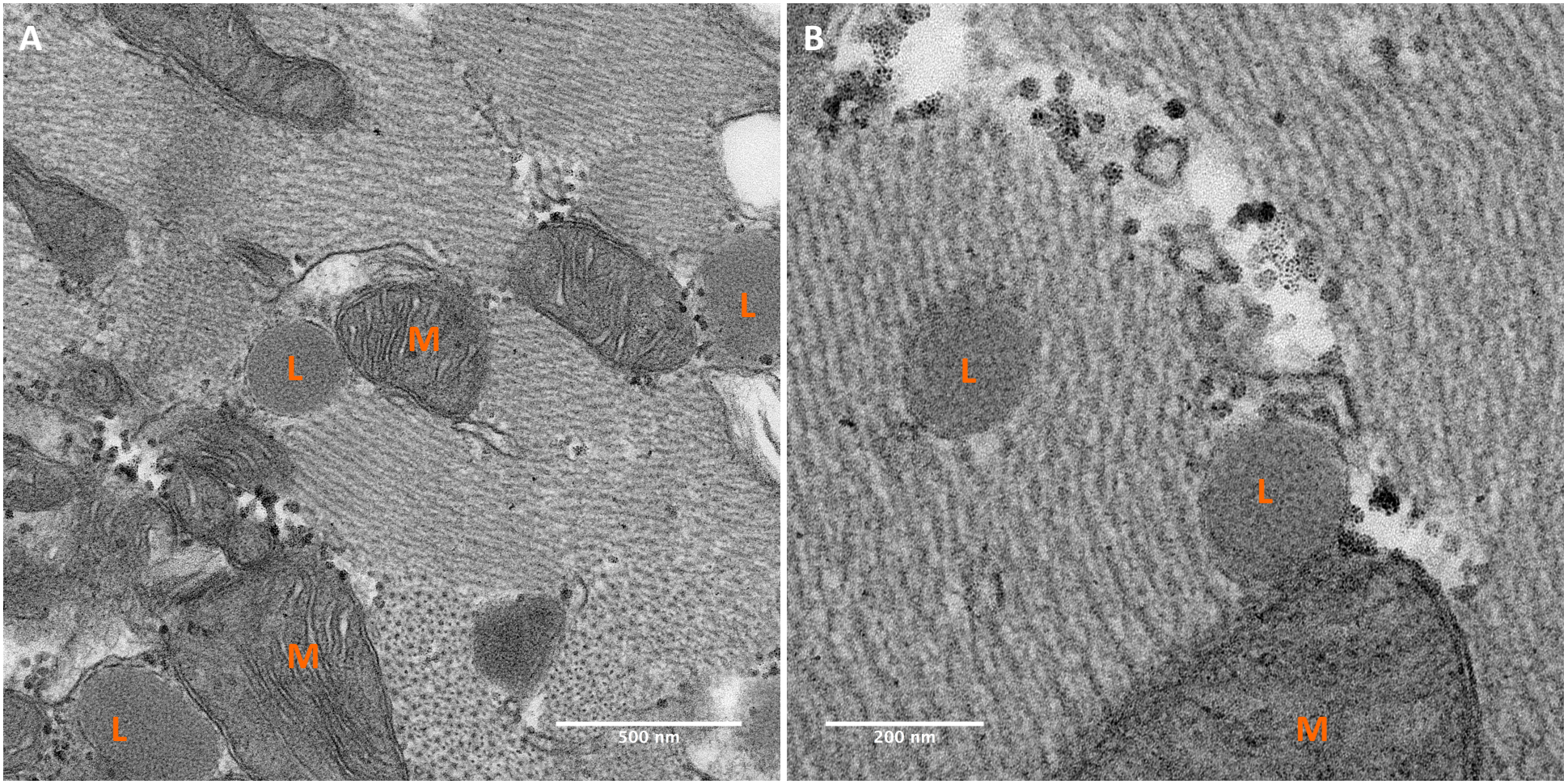


Figure 7.9: Lysosomes (L) lying in close proximity with mitochondria (M) in rabbit atrial cardiomyocytes. The membranes of these organelles are close enough to become almost unresolvable. This is seen especially in panel B.

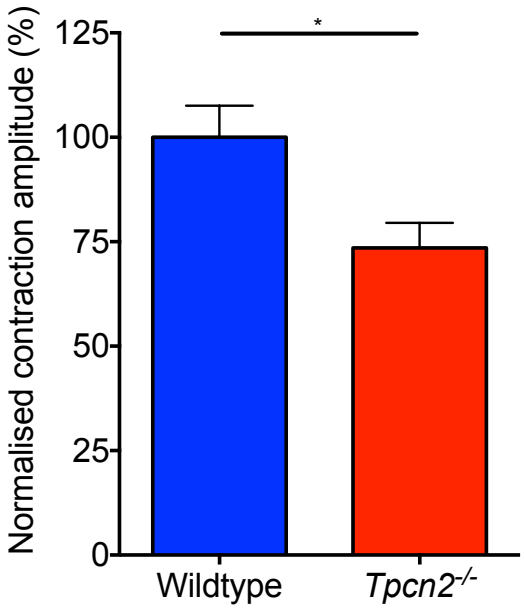


Figure 7.10: Comparison of baseline atrial contraction amplitudes between *Tpcn2*$^{-/-}$ and wildtype mice. Left atria were isolated and allowed to settle in an organ bath with baseline diastolic tension set at 0.3 grams. Contraction amplitude was then measured. Contractile force in atria from *Tpcn2*$^{-/-}$ mice was 74±6% of that in the wildtype (P=0.015, Student's unpaired t-test, n=10 in wildtype group and n=9 in *Tpcn2*$^{-/-}$ group).

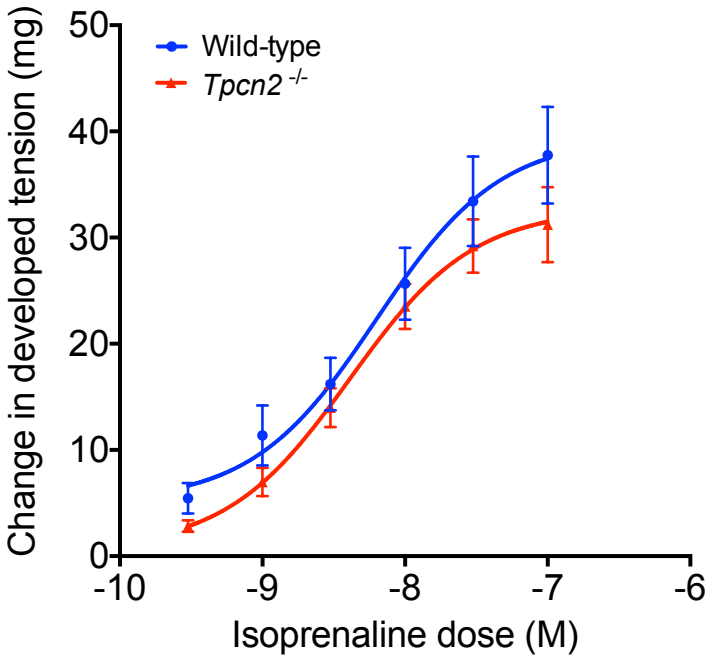


Figure 7.11: Contractile response of isolated left atria from wildtype and *Tpcn2*$^{-/-}$ mice to isoprenaline. No significant difference in responses between these genotypes was detected (P>0.05, 2-way ANOVA, n=9).

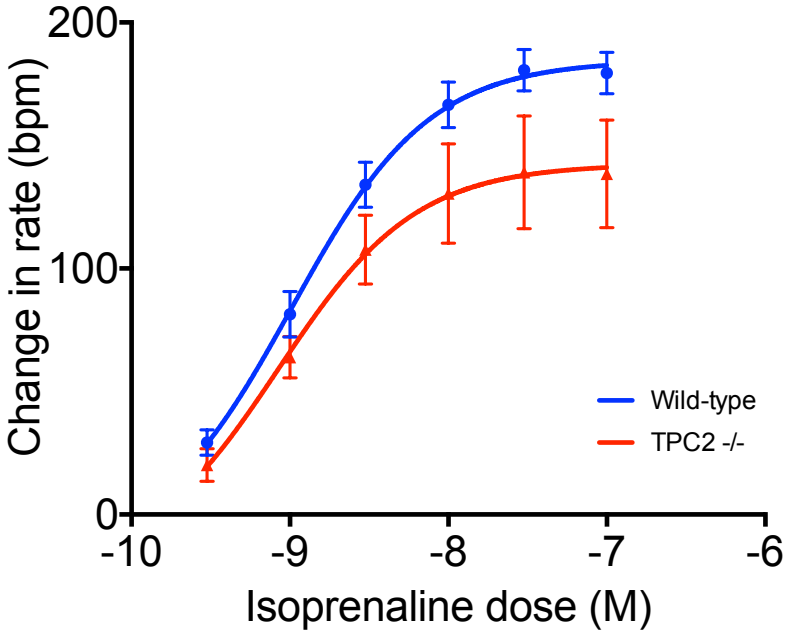


Figure 7.12: Rate response of isolated right atria from wildtype and *Tpcn2*$^{-/-}$ mice to isoprenaline. No significant difference in responses between these genotypes was detected (P>0.05, 2-way ANOVA, n=7).

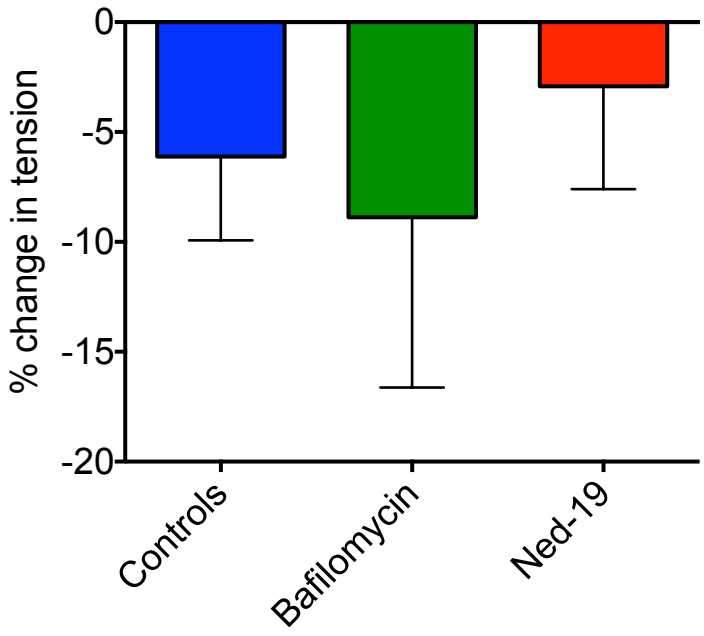


Figure 7.13: Effect of drugs on left atrial contraction amplitude. Isolated atria were allowed to equilibrate with drugs (DMSO 0.01%, Bafilomycin-A1 1μM, or Ned-19 10 μM) for 60 minutes before dose-response curves to isoprenaline were generated. The effect of these drugs on basal contraction amplitude before treatment with isoprenaline is shown. There was no significant difference between these groups ($P>0.05$, one-way ANOVA, n=6).

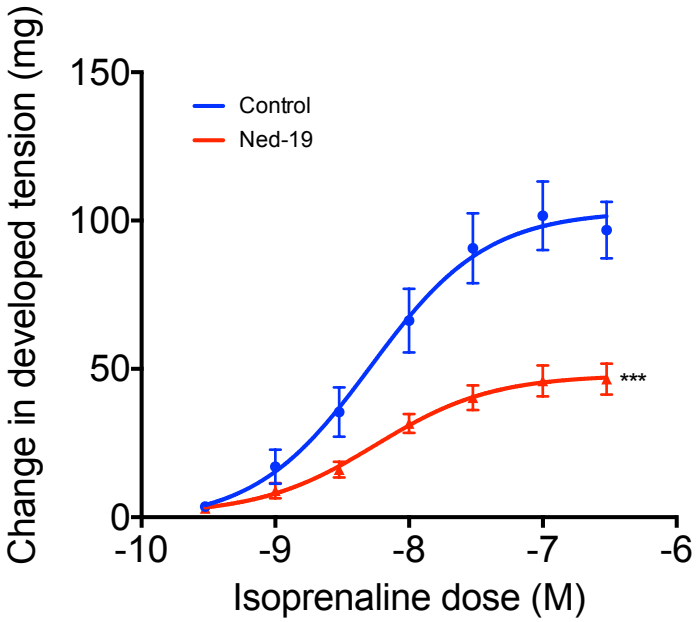


Figure 7.14: Contractile response of isolated murine left atria to isoprenaline or isoprenaline + Ned-19 10 µM. Atria were electrically stimulated at 5 Hz, and a dose-response curve to isoprenaline was elicited. In the presence of Ned-19 the maximum change in developed tension was reduced from 97±10 mg to 47±5 mg (P=0.0008, two-way ANOVA, n=6).

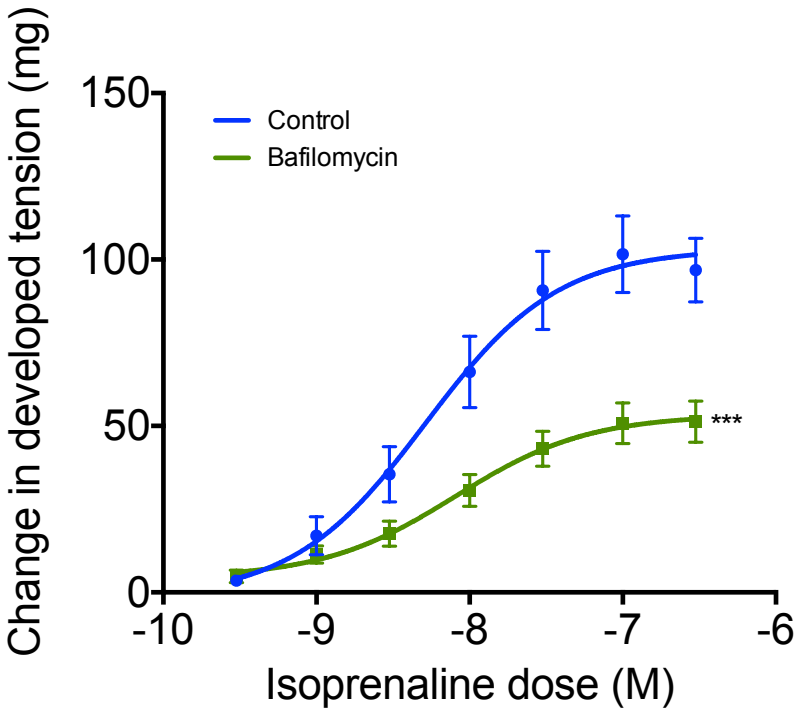


Figure 7.15: Contractile response of isolated murine left atria to isoprenaline or isoprenaline + Bafilomycin-A1 1 µM. Atria were electrically stimulated at 5 Hz, and a dose-response curve to isoprenaline was elicited. In the presence of Bafilomycin-A1 the maximum change in developed tension was reduced from 97±10 mg to 51±6 mg (P=0.0008, two-way ANOVA, n=6).

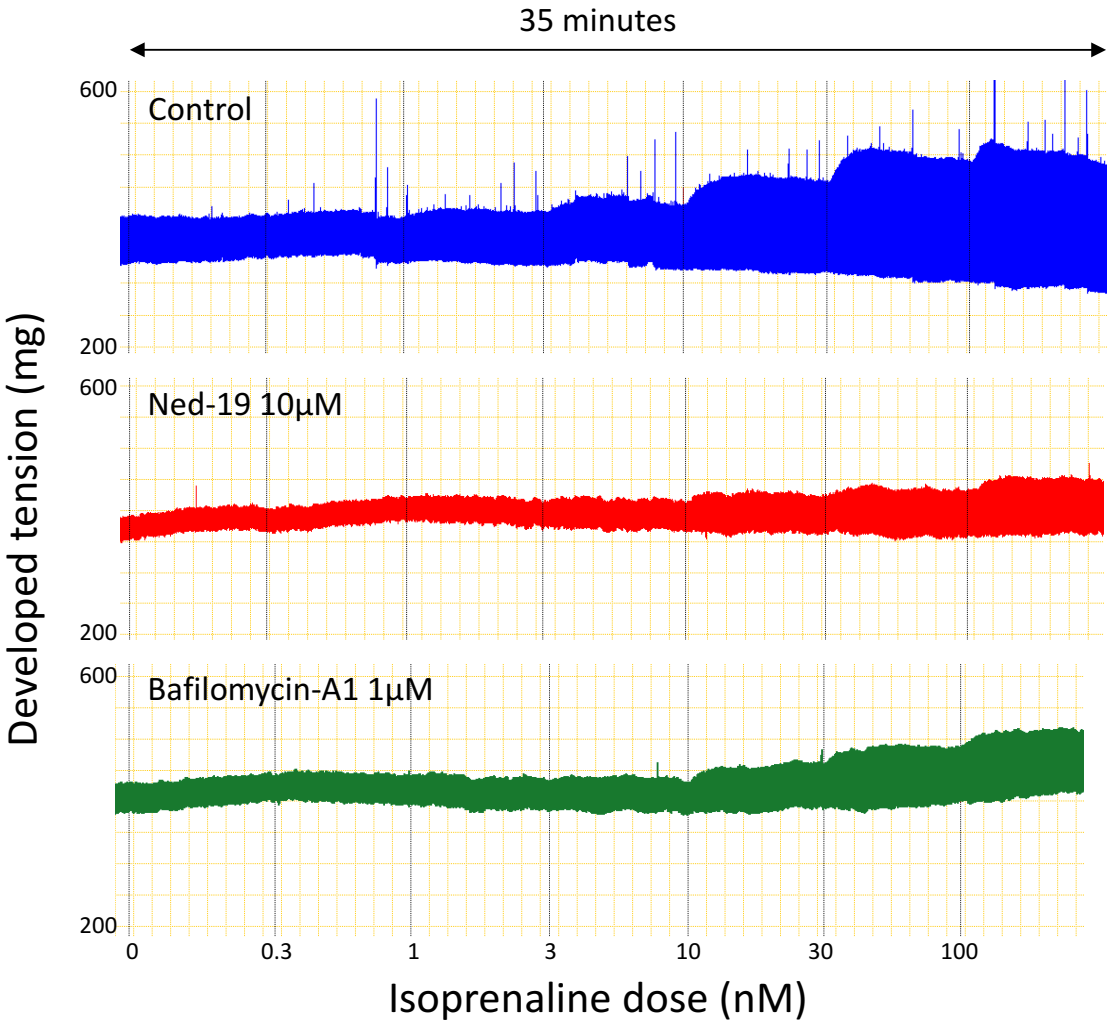


Figure 7.16: Representative recordings of atrial contraction in response to isoprenaline. Atria were electrically paced at 5 Hz, and the mean contraction amplitude was measured over five minutes at each isoprenaline dose interval. This was performed in the presence of DMSO 0.01% (top trace), Ned-19 10µM (middle trace) or Bafilomycin-A1 1 µM (bottom trace).

7.3 Conclusion

Electron Microscopy

The data presented in this chapter suggests the existence of lysosome-SR MCS in atrial cardiomyocytes. Lysosomes in the atria were broadly similar in terms of morphology as seen in the ventricles. However, they appeared to be smaller and this difference persisted even if all lysosomes with a dimension less than 200nm were removed from both groups. The difference in size may be due to confounding factors such as the existence of clusters of lysosome-like structures in the atrium that were not seen in the ventricle. Differentiation between these structures and true lysosomes was difficult and it may be that experiments need to be repeated using specific lysosomal labels to confirm their identity. The distribution of lysosomes in the atria appeared comparable to that in the ventricles, although due to the orientation of the tissue slices it was not possible to measure parameters such as L-Z distance that were ascertained in ventricular samples.

The L-SR distance in the atria was not different to that measured in the ventricles, indicating that this relationship does not differ between these tissues and that a functional calcium signalling microdomain is possible.

There were several issues relating to the orientation of the atrial slices. In the ventricular experiments, slices were made in the same axis as the sarcomeres, so that the sarcomere itself along with related structures could easily be seen. The

atrial slices were unintentionally made in an axis almost perpendicular to the sarcomere, and consequently it was not possible to measure parameters such as L-Z distance since the Z-lines could not easily be seen. The T-tubules could be seen in longitudinal section, but there were few tubules seen in transverse section. This may have been another consequence of the orientation of the slices, but if the TAT network is well-developed, tubules should run in several axes through the tissue, and this was not obviously apparent in the images obtained. Therefore, it is likely that – as expected – the TAT network in the rabbit atrium is less well developed than in the ventricle (Dibb et al., 2013; Trafford et al., 2013).

Vesicular structures that appeared similar in size and morphology to lysosomes were observed. However, their distribution was dissimilar to that of lysosomes, being densely clustered together. This distribution is very similar to descriptions and observations of atrial-specific granules (ASG) that contain atrial natriuretic peptide (ANP) (de Bold, 2011; de Bold et al., 1983). SR membrane could be seen running around and between these structures, although distances were not measured. One definitive method of determining the nature of these structures (and to differentiate them from true lysosomes) would be to use immunogold staining for ANP and labelling of acid phosphatase enzyme, to confirm ASG or lysosomes respectively (although as discussed earlier, membrane to membrane distances could not be accurately measured using this technique).

There is little structural evidence from this data to explain the apparent difference in basal 'tone' in the NAADP system observed in functional experiments. Subjectively, there did not appear to be a greater number of

lysosomes in the atria compared with the ventricles. In the future, it would be interesting to ascertain whether bafilomycin-A1 has the same effect on the basal calcium transient in atrial tissue from large mammals with an extensive TAT network. It is possible that due to the absence of a significant TAT network in small mammals (Dibb et al., 2013; Trafford et al., 2013), the lack of association of RyR with L-type calcium channels (Schulson et al., 2011; Smyrnias et al., 2010) leads to a relatively greater input at RyR from lysosomal calcium released in response to NAADP. Therefore, lysosomal dysfunction induced by bafilomycin-A1 leads to a greater loss of input to the RyR than in the ventricle, leading to a greater reduction in calcium transient. The current data cannot support or contradict this hypothesis and further work will be needed to investigate the structure-function relationship of lysosomes and NAADP in the cardiac atria. Additionally, the fact that the work establishing a possible higher basal tone of NAADP in the atria was performed using guinea pig tissue, whereas the present data is from mouse and rabbit experiments should also be considered.

As in the ventricle, mitochondrial-lysosome MCS were also observed in the atria. Some lysosomes were distant from mitochondria, but many were very close, and in some cases there was no measurable distance between them – implying they were physically in contact. The association between mitochondria and lysosomes in cardiac atria has been noted previously in an investigation into the formation of lipofuscin following lysosomal degradation of mitochondria (Skepper et al., 1987). At that time, lysosomes were not considered to be important in calcium signalling. It is obviously likely that some mitochondrion-lysosome contacts will be explained by autophagic processes, however in light of evidence of the

involvement of the NAADP pathway in ischaemia/reperfusion injury in the ventricle (Davidson et al., 2015) it is possible that mitochondrial-lysosome interactions also have another function in the atria. The nature of this function is currently unclear, although the possible modulation of the mitochondrial mPTP channel by the NAADP pathway that was uncovered by studies of ischaemia/reperfusion in the ventricle, may also occur in the atrium for reasons currently unknown. Further investigation into this possibility is required.

Atrial contraction

Data obtained from atrial contraction experiments presented in this chapter show several differences compared with similar experiments performed in isolated atrial myocytes (Bayliss, 2014; Collins et al., 2011).

In the present experiments, atria were allowed to equilibrate with drugs for 60 minutes before isoprenaline responses were measured. While there was a small (less than 10%) reduction in the contraction amplitude over this period, it was no greater in the tissues treated with bafilomycin-A1 or Ned-19 than it was in DMSO controls. In contrast, the reduction in calcium transient seen in ventricular myocytes with 1μM bafilomycin-A1 was 20% (Macgregor et al., 2007), and the reduction seen in atrial myocytes using only 100 nM bafilomycin-A1 was 19-47% (Bayliss, 2014; Collins et al., 2011). As discussed above, this apparent difference between atrial and ventricular myocytes led to the hypothesis that there may be a higher basal level of NAADP activity in the atria than in the ventricles. However, this effect could not be reproduced in the present set of

experiments; either the reduction in calcium transient did not occur, or its reduction was not translated into a reduced contraction amplitude. This difference is difficult to explain. One possibility is that, despite the long incubation period, the drugs were still not able to penetrate intact atrial tissue as efficiently as they can isolated myocytes. The obvious counter-argument to this is that the increase in contraction force mediated by isoprenaline was significantly reduced by both bafilomycin-A1 and Ned-19 in these experiments. It is possible that the addition of isoprenaline to intact tissues in some way facilitates the entry of these drugs into cells, although there have been no reports offering evidence in favour of this idea. Another possibility is that the basal level of NAADP activity is reduced in intact tissues compared with isolated myocytes, since the experiments that detected it used the latter preparation. Why this should be the case in the atria and not in the ventricles (since isolated ventricular myocytes did not demonstrate the same reduction in resting calcium transient amplitude following exposure to bafilomycin-A1) also remains unknown.

The attenuation of the increase in contractile force due to isoprenaline seen with Ned-19 or bafilomycin-A1 in intact atria is in keeping with previous experiments in both atrial and ventricular cells: In atrial cells, the increase in calcium transient seen following application of isoprenaline was blunted by these drugs (Bayliss, 2014; Collins et al., 2011). Similarly, in ventricular myocytes bafilomycin-A1 and Ned-19 attenuated both the increase in calcium transient and the increase in contractile force caused by isoprenaline (Bolton, 2014; Capel et al., 2015), although in intact hearts perfused by Langendorff apparatus, no

significant effect of Ned-19 could be elicited (Bolton, 2014). The latter observation does suggest that although Ned-19 is cell-permeant, it may be less successful at penetrating intact tissues.

In all, these observations are consistent with previous findings suggesting that acidic stores such as the lysosome and NAADP are involved in responses to β-adrenergic stimulation in the cardiac atria. However, it was not possible to reproduce results suggesting an increased basal activity in this system.

In contrast, experiments using atria from *Tpcn2*$^{-/-}$ and wildtype mice showed the opposite pattern. There was a difference in baseline left atrial contraction amplitude, with atria from *Tpcn2*$^{-/-}$ mice generating only 74±6% of the force seen in the wildtype. However, there was no detectable difference in either the contractile response or rate response to isoprenaline. Taken together, these observations are hard to explain.

8

General Discussion

8.1 General Discussion

Accumulated evidence has established NAADP as one of the three primary calcium signalling molecules in a wide variety of tissues from different species, along with IP_3 and cADPR. In the heart there is now significant evidence showing that NAADP has an important effect in the modulation of the amplitude of the calcium transient, and that the endogenous production and action of NAADP follows activation of the β-adrenergic receptor pathway (Capel et al., 2015; Macgregor et al., 2007). Additionally, there are strong reasons to accept the view that TPC2 on the lysosomal membrane is a likely receptor for NAADP (Ruas et al., 2015).

Although previous studies have demonstrated a role for NAADP and lysosomes in cardiac arrhythmogenesis (Bolton, 2014; Nebel et al., 2013), the data presented in chapter three are the first to specifically show that arrhythmias generated in the presence of acute β-adrenergic stimulation are dependent on TPC2. Hearts from mice lacking the TPC2 protein were significantly less likely to experience ventricular arrhythmias in response to burst pacing in the presence of isoprenaline than their wildtype counterparts. This protective effect of TPC2 knockout is consistent with the anti-arrhythmic effects of the NAADP antagonist BZ194 seen by Nebel et al. and with the increased time taken for myocytes to develop arrhythmias following stimulation by isoprenaline if they were simultaneously exposed to bafilomycin-A1 reported by Dr Bolton.

In chapter four, the presented evidence suggests a role for NAADP signalling in chronic β-adrenergic stimulation, as the NAADP antagonist Ned-19 prevents the development of hypertrophy in response to isoprenaline in cultured neonatal rat cardiomyocytes. Similar

evidence from experiments using *Tpcn2*$^{-/-}$ mice has also demonstrated that disruption of this pathway abrogates the hypertrophic effect of chronic isoprenaline exposure in vivo (Capel et al., 2015). However, the data in chapter four are the first to show this effect in cultured myocytes using an NAADP antagonist. Interestingly, Ned-19 was also able to completely prevent the hypertrophy induced by chronic exposure of noradrenaline - a compound that has previously been shown to cause hypertrophy via its action at α-adrenergic receptors (Simpson, 1983). This finding requires more in depth investigation, but tentatively suggests a novel role for NAADP signalling in the α-adrenergic pathway in the heart.

Chapters five and six presented ultrastructural studies of the position of lysosomes in rabbit ventricular myocytes relative to other organelles, particularly the SR. There were several interesting and novel findings presented; under confocal microscopy, the apparently random pattern of distribution of lysosomes through the myocyte was shown to be at least partially non-random with a subpopulation that were distributed across the cell with the same frequency as other important sarcomeric structures such as the ryanodine receptor (and therefore SR). Indeed, analysis of electron micrographs of ventricular myocytes supported the hypothesis that functional calcium signalling microdomains are present between lysosomes and the SR in this tissue: MCS were frequently observed between these structures with a median lysosome-SR distance compatible with a functioning microdomain.

MCS between lysosomes and the SR have been observed in pulmonary artery smooth muscle cells (Fameli et al., 2014) and in fibroblasts (Kilpatrick et al., 2013), but never in cardiac muscle until now. One possible criticism of the data presented in chapter six is

that it is limited to two dimensions, meaning that there is no depth axis to confirm the reported lysosome-SR measurements. Although the tissue sections were very thin (80 nm), it is still possible that two objects that are closely apposed in two dimensions may be significantly separated in the third dimension. Therefore, in addition to the 2-dimensional electron micrographs shown in chapter six, complimentary work carried out in conjunction with the present study demonstrated that the lysosome-SR MCS could also be visualised using EM tomography and 3-dimensional reconstructions. Indeed, following analysis of these additional images the median distance was reduced to just 3 nm (see appendix B), lending further weight to the suggestion that functional microdomains exist between lysosomes and the SR in the heart.

Although the morphological identification of lysosomes is well accepted (Alegre-Abarrategui et al., 2009; Fernandes et al., 2016), another possible criticism of the data in chapter six is that no labelling technique was employed to ensure that these structures were correctly recognised. One possible method of specifically labelling lysosomes on electron microscopy is to use the same LAMP-2 primary antibody used in chapter five followed by a secondary gold conjugate. Gold particles are highly electron dense and are manufactured with a fixed diameter and can be readily identified on the electron micrograph. In order to do this, a different tissue fixative must be used that does not contain glutaraldehyde since this destroys protein antigenicity and prevents recognition of specific epitopes by antibodies. However, the lack of glutaraldehyde results in poor preservation of lipid membranes, the visualisation of which is essential for the measurement of inter-organelle distances and accurate identification of MCS. In order to demonstrate that the identification of lysosomes was correct, some electron micrographs were prepared using a low-glutaraldehyde fixative and labelled using antibodies against

LAMP-2 and immunogold, but no measurements were made using these images and they were not included in the dataset used to identify a lysosome-SR MCS. They are also included in the appendix B.

MCS were also observed between lysosomes and mitochondria. It is possible that this relationship may be related to the autophagic functions of the lysosome, although recent evidence also suggests a role for NAADP signalling in cardiac ischaemia-reperfusion injury which may require communication between these organelles (Davidson et al., 2015). Antagonists of NAADP reduced arrhythmias, volume of infarcted tissue and prevented opening of the mPTP channel following ischaemia-reperfusion. The possibility that the MCS between lysosomes and mitochondria observed in electron micrographs might function as a calcium signalling microdomain cannot be ruled out, and further investigation into how NAADP signalling affects mitochondrial calcium handling is required.

Additional evidence that Ned-19 binds to lysosomes was also presented in chapter five using confocal microscopy images. The fluorescence of this compound allowed visualisation of its binding sites, which were highly correlated with the position of lysosomes as demonstrated by another fluorescent compound, lysotracker. However, since lysosomes are the common end-point of the cellular degradation pathway, it is possible that Ned-19 was deposited here as a result of this, rather than due to specific receptor binding. Further experiments have been performed which demonstrate that Ned-19 localisation at lysosomes is prevented in the presence of another (non-fluorescent) NAADP antagonist, BZ194 (see appendix B). This suggests that the spatial

correlation between the fluorescence of Ned-19 and lysotracker is indeed due to its specific binding, and not part of the lysosomal degradation pathway.

Finally, in chapter seven, preliminary data showing electron micrographs of atrial tissue was presented along with evidence of a functional role for the NAADP pathway in response to β-adrenergic stimulation in this tissue. MCS between lysosomes and the SR and between lysosomes and mitochondria were also identified in these experiments. Functional data was not entirely consistent with that from isolated atrial myocytes, but did demonstrate that Ned-19 and bafilomycin-A1 caused a reduction in contractile response to isoprenaline.

In summary, the data presented in this thesis demonstrate that the ultrastructural organisation of cardiac myocytes is consistent with functional evidence of a role for NAADP signalling in the heart. The hypothesis that NAADP acts at specific lysosomal receptors such as TPC2 to cause release of calcium into a functional microdomain between the lysosome and the SR is supported by these data. Moreover, release of lysosomal calcium in response to β-adrenergic stimulation and the action of NAADP may then influence pathways that lead acutely to arrhythmogenesis or chronically to hypertrophy. The possibility that NAADP signalling also occurs as part of chronic α-adrenergic stimulation cannot be ruled out.

9

Appendices

Appendix A
Uncropped images of western blots
Control images of immunocytochemistry
Control images of live-cell confocal microscopy

Appendix B
Electron micrograph tomography and 3D reconstructions of lysosome-SR MCS
Immunogold labelling of lysosomes
Ned-19 vs lysotracker fluorescence in presence of BZ194

Appendix C
Matlab code for performing Fourier analysis of immunocytochemistry images

9.1 Appendix A

9.1.1 Western blot raw data

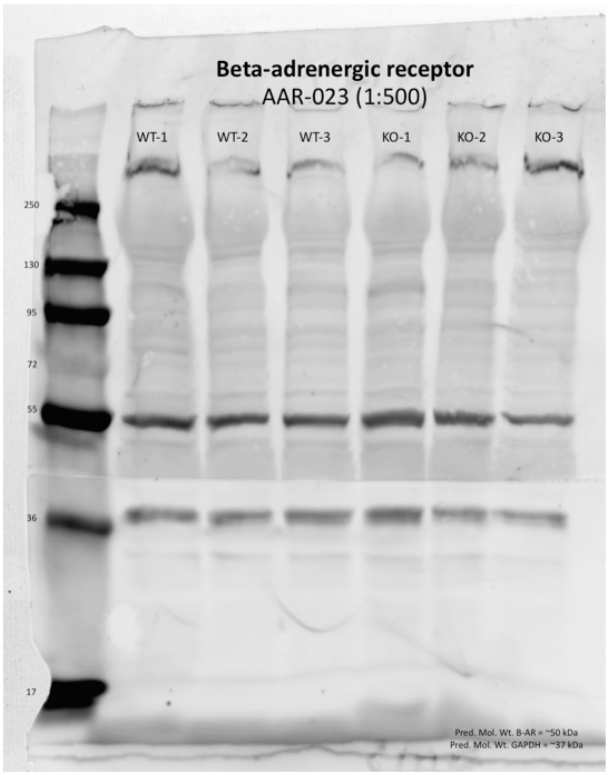
The following images are unedited scans of western blot membranes used to generate data in chapter 3 (section 3.2.1), showing the levels of expression of the β1-adrenergic receptor in wildtype and *Tpcn2*$^{-/-}$ mice. After electrophoresis and transfer, each membrane was divided between the 36 and 55 kDa molecular weight markers, so that antibodies could be incubated separately. The two halves were then re-positioned next to each other for scanning, and are shown in the images in this appendix.

The raw scans of the membranes are on the left of each panel, while the graphs on the right are fluorescence intensity plots of each blot lane (y-axis is fluorescence intensity and x-axis is distance along the lane from top to bottom).

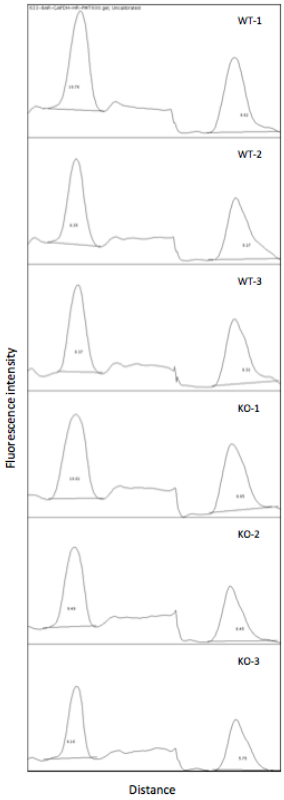
Samples from each animal were blotted twice to measure protein expression. Membranes A1a and A1b are first and second blots of wildtype (WT) mice 1-3 and *Tpcn2*$^{-/-}$ (KO) mice 1-3 respectively. Membranes A1c and A1d are first and second blots of WT mice 4-6 and KO mice 4-6 respectively.

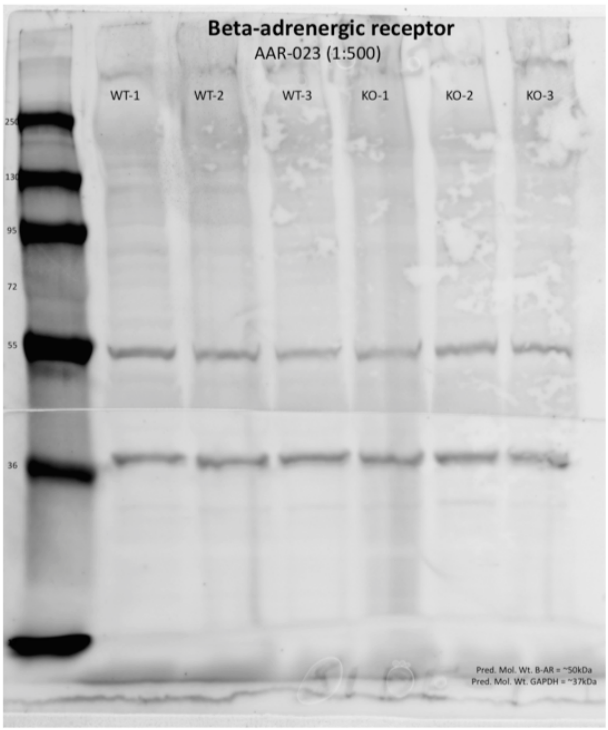
Membrane A1e contains blots of WT mice 1-3 and KO mice 1-3. This membrane was incubated with antibodies in the same fashion as membranes A and B, but in the presence of a blocking peptide against the β1-AR antibody.

Membrane A1f shows a blot of a sample from a WT mouse in the absence of primary antibody (i.e. with secondary antibody alone).

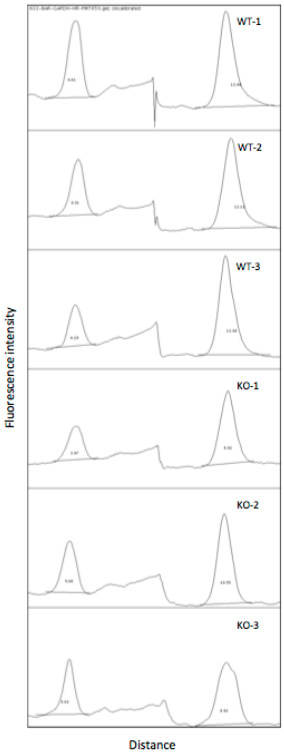

Beta-adrenergic receptor
AAR-023 (1:500)
WT-1
WT-2
WT-3
KO-1
KO-2
KO-3
250
130
95
72
55
36
17
Pred. Mol. Wt. B-AR = ~50 kDa
Pred. Mol. Wt. GAPDH = ~37 kDa

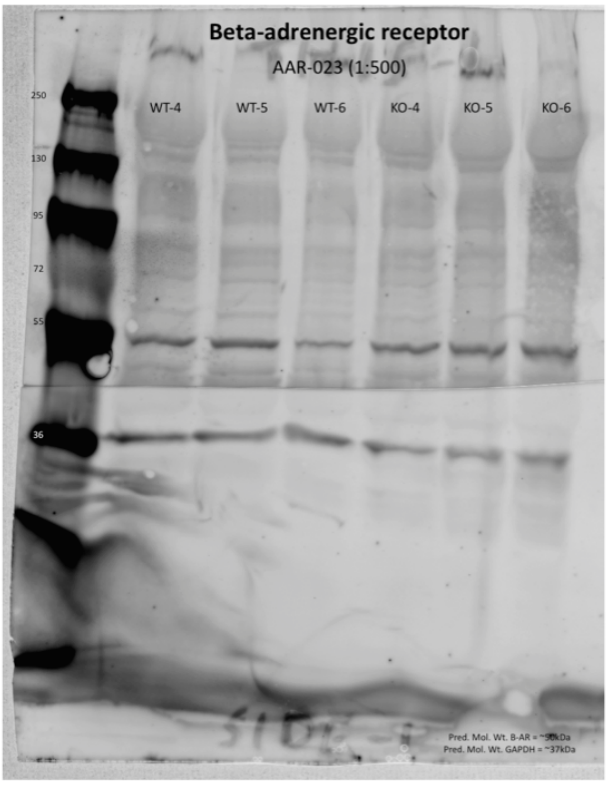
A1a


WT-1
WT-2
WT-3
KO-1
KO-2
KO-3
Fluorescence intensity
Distance

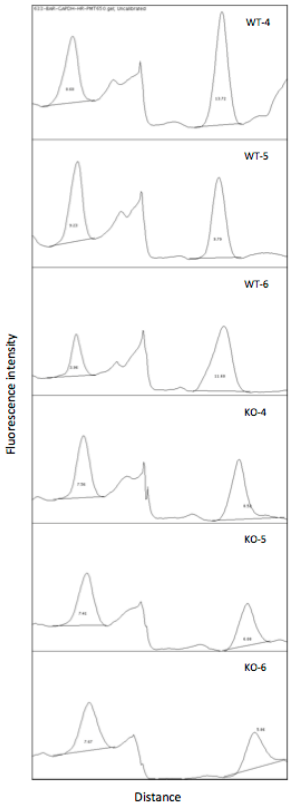

Beta-adrenergic receptor
AAR-023 (1:500)
WT-1
WT-2
WT-3
KO-1
KO-2
KO-3
250
130
95
72
55
36
Pred. Mol. Wt. B-AR = ~50kDa
Pred. Mol. Wt. GAPDH = ~37kDa

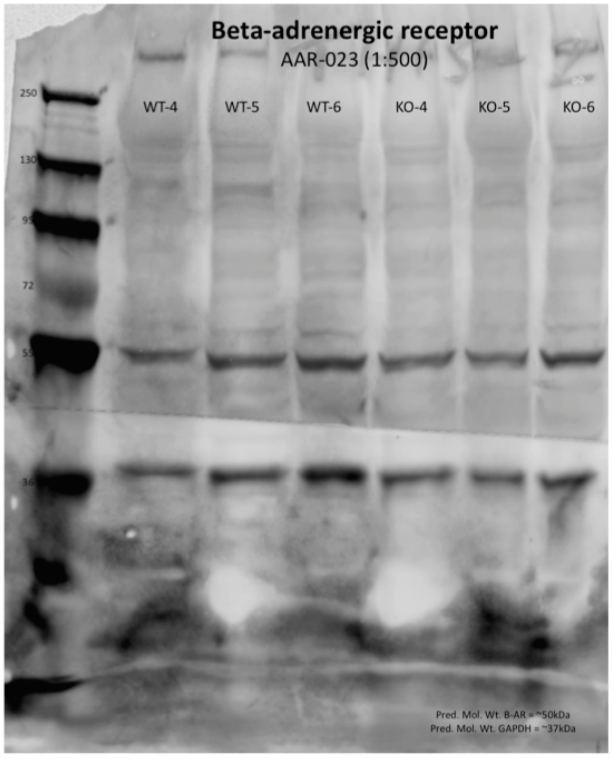
A1b


WT-1
WT-2
WT-3
KO-1
KO-2
KO-3
Fluorescence intensity
Distance

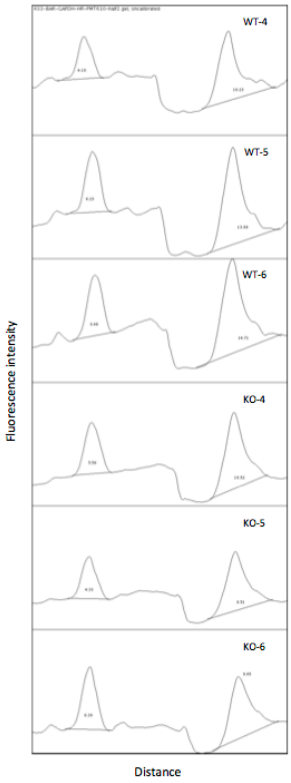

Beta-adrenergic receptor
AAR-023 (1:500)
WT-4
WT-5
WT-6
KO-4
KO-5
KO-6
250
130
95
72
55
36
Pred. Mol. Wt. B-AR = ~50kDa
Pred. Mol. Wt. GAPDH = ~37kDa

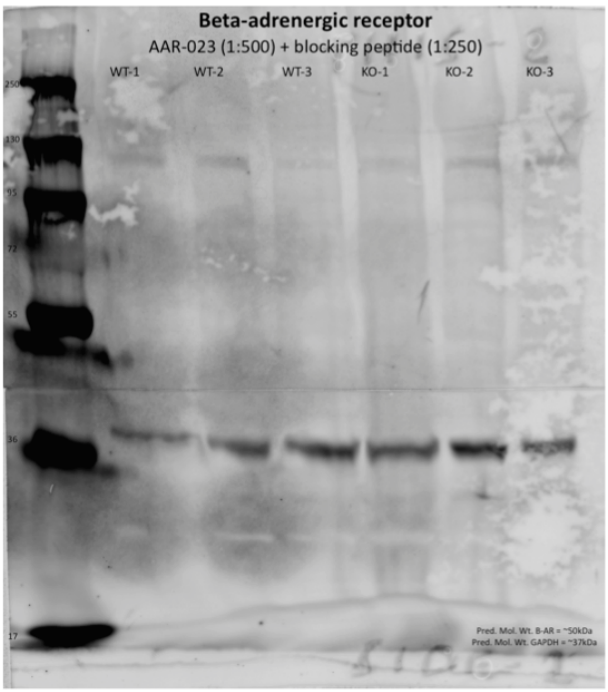
A1c


WT-4
WT-5
WT-6
KO-4
KO-5
KO-6
Fluorescence intensity
Distance

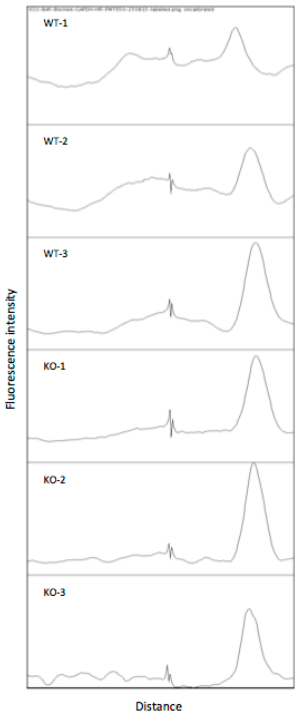

Beta-adrenergic receptor
AAR-023 (1:500)
WT-4
WT-5
WT-6
KO-4
KO-5
KO-6
250
130
72
55
36
Pred. Mol. Wt. B-AR = ~50kDa
Pred. Mol. Wt. GAPDH = ~37kDa

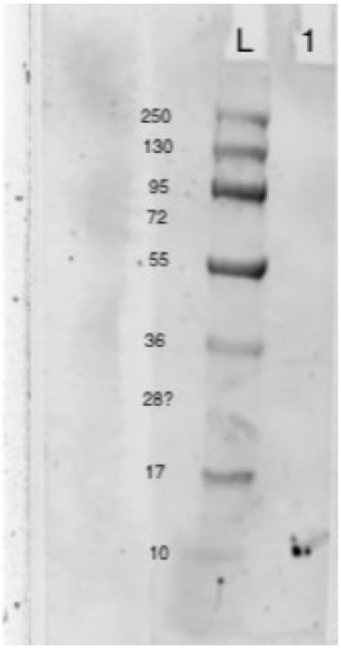
A1d


WT-4
WT-5
WT-6
KO-4
KO-5
KO-6
Fluorescence intensity
Distance


Beta-adrenergic receptor
AAR-023 (1:500) + blocking peptide (1:250)
WT-1
WT-2
WT-3
KO-1
KO-2
KO-3
Pred. Mol. Wt. β-AR = ~50kDa
Pred. Mol. Wt. GAPDH = ~37kDa

A1e


WT-1
WT-2
WT-3
KO-1
KO-2
KO-3
Fluorescence Intensity
Distance


L
1
250
130
95
72
55
36
28?
17
10

A1f

9.1.2 Immunocytochemistry control images

For immunocytochemistry experiments using fixed rabbit ventricular cells, primary antibodies against PLB or RyR2 (both raised in mouse) were used simultaneously with primary antibodies against LAMP-2 (raised in rabbit). Control images were obtained, either using the secondary antibodies alone (i.e. in the absence of a primary antibody), or using the primary antibody with the "wrong" secondary.

For each control, an image was taken using contrast settings that were used to obtain experimental data. The contrast was then enhanced to emphasize the presence of the cell. Finally, the enhanced image was merged with an image of the cell nucleus (stained with the fluorescent compound, DAPI).

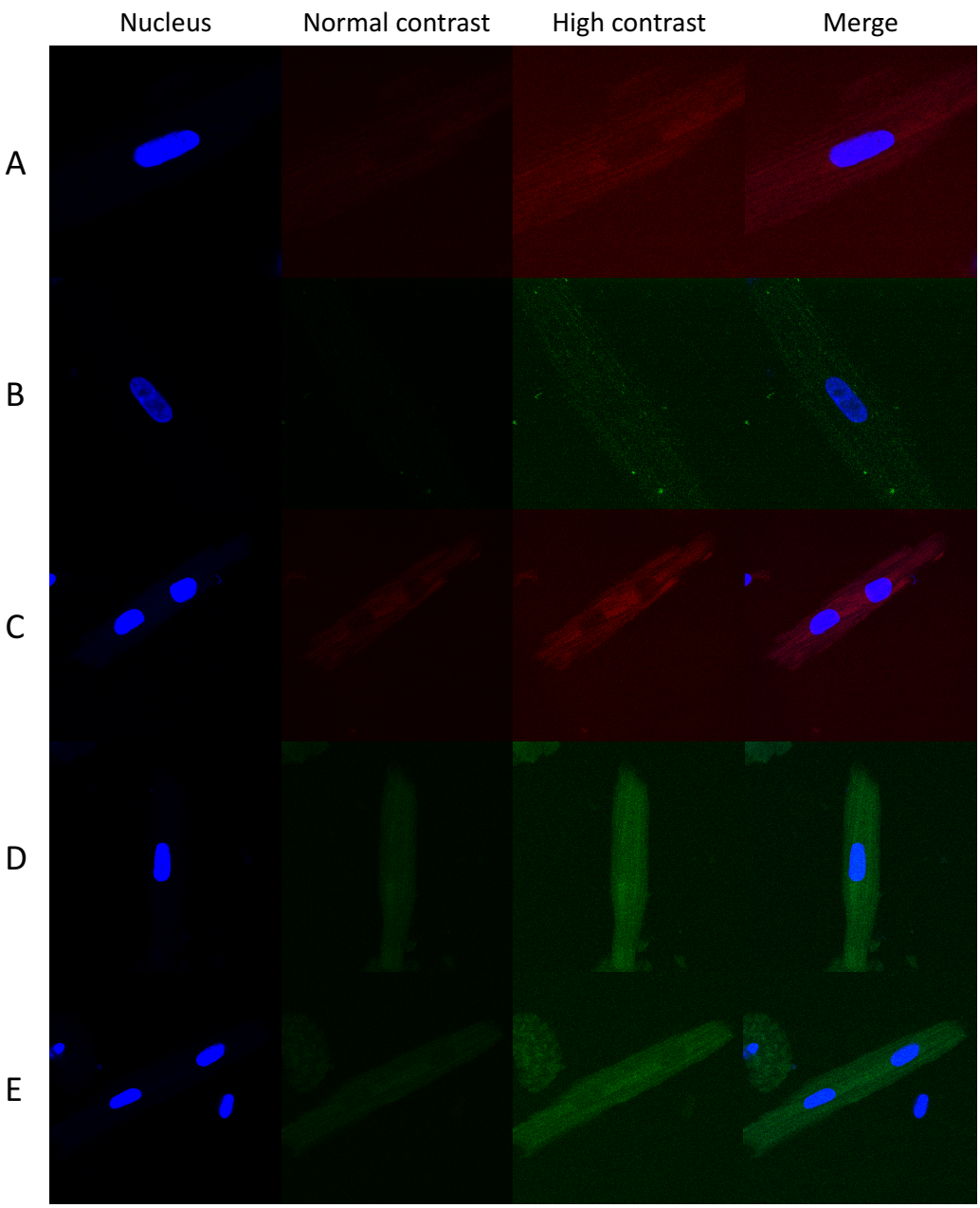


Figure A2: Control images for immunocytochemistry experiments. The rows represent the following controls: A) Dylight anti-mouse-555 nm secondary antibody alone. B) AlexaFluor-anti-rabbit-488 nm secondary antibody alone. C) LAMP-2 primary antibody (PA1-655) with Dylight anti-mouse-555 nm secondary D) PLB primary antibody (ab2865) with AlexaFluor-488 nm secondary and E) RyR2 primary antibody (ab2827) with AlexaFluor-488 nm secondary. All images are rabbit ventricular cardiomyocytes.

9.1.3 Live cell confocal microscopy control images

Cells simultaneously labelled with Ned-19 and lysotracker red to allow visualization of Ned-19 binding sites and lysosomes respectively were imaged using confocal microscopy. Results are shown in chapter five. Control images were also taken to ensure no bleed-through between channels.

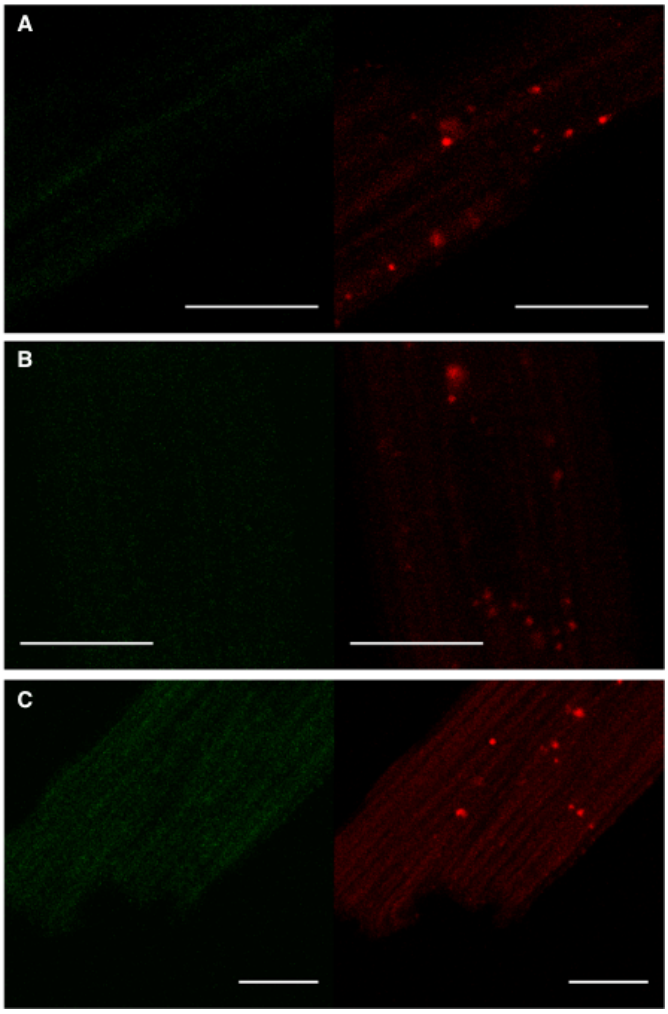


Figure A3: Live cell confocal control images: Panels A-C show control images obtained from the fluorescence emission channels of Ned-19 (on the left in each image) and lysotracker (on the right), when each cell was loaded with lysotracker alone (i.e. in the absence of Ned-19). These control images demonstrate that there is no bleed-through from the lysotracker channel into the Ned-19 channel. Scale bars all represent 10 μm.

9.2 Appendix B

The following data is complimentary to that presented in this thesis, and supports the conclusions made here. However, the majority of the work presented in this appendix was done by investigators other than myself.

9.2.1 Tomography and 3D reconstruction of electron micrographs

This data was provided by Dr Eva A Rog-Zielinska and Prof Peter Kohl of the National Heart and Lung Institute, Imperial College London, and the Institute for Experimental Cardiovascular Medicine, University Heart Centre Freiburg / Bad Krozingen, University Medical School, Freiburg, Germany and reproduced here with permission. Some text was taken from the submitted manuscript 'Aston et al., High resolution structural evidence suggests the Sarcoplasmic Reticulum forms microdomains with Acidic Stores (lysosomes) in the heart. SciRep. Submitted for publication 2016'.

The electron micrographs presented in this thesis are two-dimensional, and there is therefore a potential problem in measuring the lysosome-SR distance because no depth measurement is possible. This has been overcome by performing electron tomography and three-dimensional reconstruction of images.

Methods

Rabbit left ventricular tissue fragments (n=6 animals) were fixed via Langendorff perfusion in iso-osmotic (300 mOsm) Karnovsky's reagent (2.4% sodium cacodylate,

0.75% paraformaldehyde, 0.75% glutaraldehyde) and washed with 0.1 M sodium cacodylate before fixing in 1% OsO_4 for one hour. They were then dehydrated in graded acetone, and embedded in Epon-Araldite resin. Thick sections were cut (~275 nm, 3 sections per animal), transferred onto copper slot grids coated with 1% formvar and post-stained with 2% aqueous uranyl acetate, followed by Reynold's lead citrate. Colloidal gold particles (15 nm) were added to both surfaces of the sections to serve as fiducial markers for subsequent tilt series alignment. All sections were prepared and imaged at the Boulder Laboratory for 3D Electron Microscopy of Cells (University of Colorado, Boulder, CO) using an intermediate voltage electron microscope (Tecnai TF30; 4FEI-Company, Eindhoven, The Netherlands) operating at 300 kV with images captured on a charge-coupled device camera (UltraScan; Gatan, Pleasanton, CA) at a pixel size of 1.206 nm^2.

For dual-axis tomography, a series of tilted views were collected from +60° to -60° at 1° increments at 20,000x magnification. After the first tilt series was acquired, the specimen was rotated by 90° in the horizontal plane, and another +60° to -60° tilt series was taken. Images from each tilt-series were aligned by fiducial marker tracking and back-projected to generate two single full-thickness reconstructed volumes (tomograms), which were then combined to generate a high-resolution 3D reconstruction of the original volume of interest. Tomograms were processed and analysed using IMOD software, and used to segment and generate 3D models of the structures of interest. The models were smoothed and meshed to obtain a final 3D representation, in which spatial relationships of T-tubules, sarcoplasmic reticulum, and mitochondria with lysosomes can be visualised.

Results

Ten lysosomes were identified on 3D tomographs, and measurements were made of its dimensions as well as of distances between it and the SR, Z-lines, T-tubules and mitochondria. This data is presented in table B1, and representative reconstructed images are shown in figure B1.

Lysosome	Min Diameter	Max Diameter	Min distance to SR	Min distance to Z-line	Min distance to T-tubule	Min distance to mitochondrion
1	166.1	202.3	3.3	232	16.3	3.2
2	143.9	258.9	4.1	435.3	441.9	262.7§
3	146	233.1	1.1	145.6	145.1	28.4
4	187	315.5	5.4	n/a	n/a	1.7
5	467.5	528.2	5.4	455	n/a	69.1
6	291.1	386.1	2.2	76.8	52.4	5.1
7	204.6	380.4	15.6§	376.7	8.8	17.8
8	327.6	358.6	1.1	354.1	n/a	7.2
9	340.6	420.2	2.3	39.1	213.3	4.5
10	441.2	442.3	3.6	51.5	n/a	n/a
Median	**247.9**	**369.5**	**3.3**	**232**	**98.8**	**6.2**

Table B1: 3D tomography-based analysis of spatial interactions of lysosomes and other organelle membrane systems in rabbit left ventricular cells. Measurements were performed using IMOD software. n/a – no accurate measurement possible, § - indicates statistical outlier (ROUT analysis, Q=1%, GraphPad Prism 6). Medians are given after removal of statistical outliers, in keeping with the analysis of 2D EM measurements.

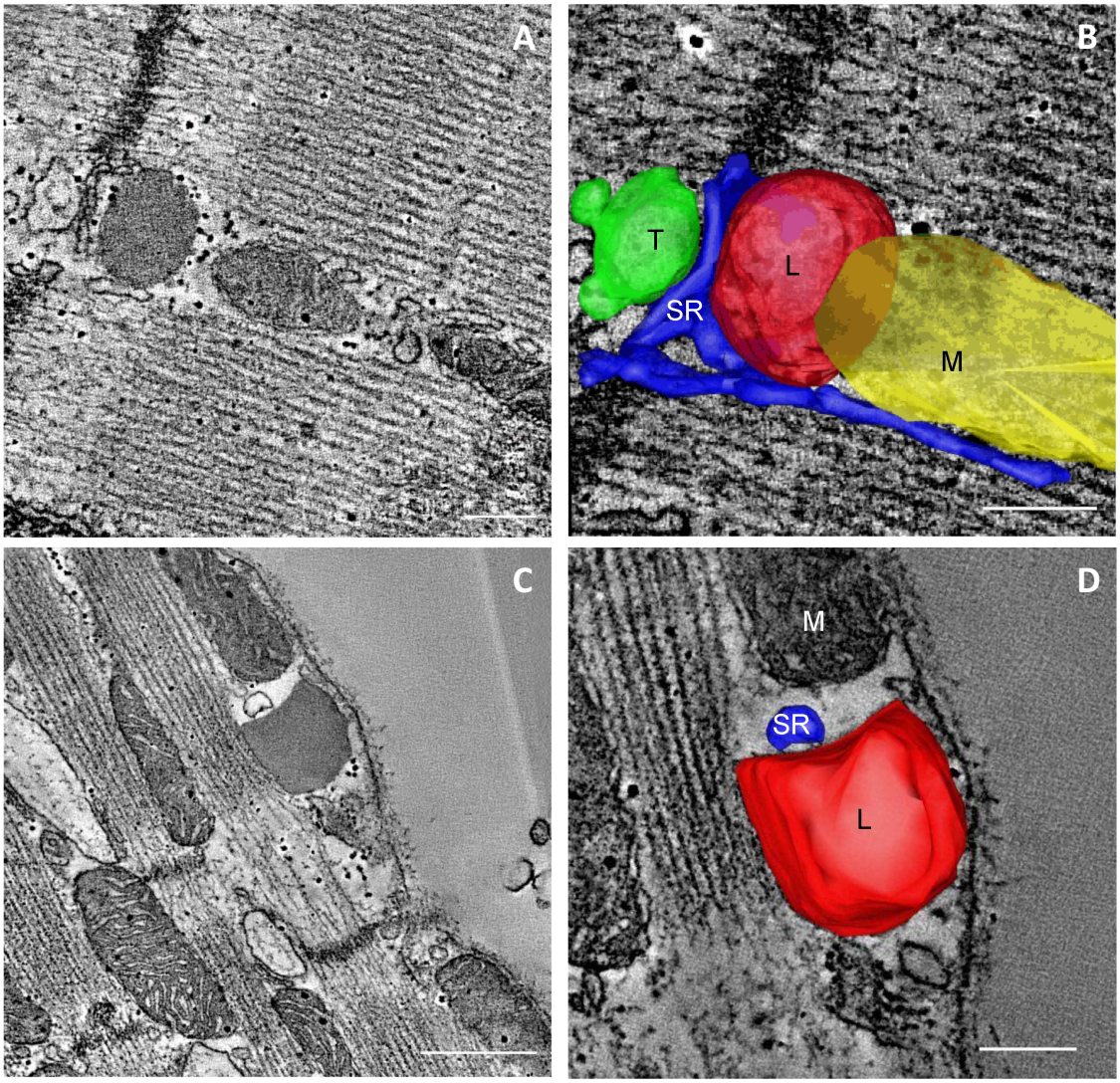


Figure B1: Electron tomography reconstruction of a lysosome with SR, T-tubules and mitochondria. This is a representative electron tomography image of a lysosome near calcium signalling organelles, including raw images (A&C) and reconstructed organelles in 3D (B&D). Dual-axis ET and IMOD software were used to image, reconstruct and model lysosomes (L, red), sarcoplasmic reticulum (SR, blue), mitochondria (M, yellow), and T-tubules (T, green) in 3D. Voxel size=1.206nm, Z-depth=275nm. Scale bars (A,B,D)=200nm and (C)=500nm.

9.2.2 Immunogold labelling of lysosomes

This data was provided by Dr Rebecca Burton of Oxford University and reproduced here with permission. Again, some text was taken from the submitted manuscript 'Aston et al., High resolution structural evidence suggests the Sarcoplasmic Reticulum forms microdomains with Acidic Stores (lysosomes) in the heart. SciRep. Submitted for publication 2016'.

In the electron microscopy techniques presented in this thesis, the preservation of intracellular lipid membranes was essential. This was so that accurate measurements of distances between lysosomes and other membrane-bound structures could be made. This preservation was achieved using a fixative that included 5% glutaraldehyde.

No immunological technique was employed to label lysosomes because this concentration of glutaraldehyde destroys the tertiary and quaternary structure of proteins, leading to loss of antigenicity. Therefore, antibody labelling was not possible. If glutaraldehyde had been excluded from the fixative, or used at a much lower concentration, immunocytochemical labelling techniques would have been possible but the loss of lipid membranes would have made accurate measurements difficult.

Therefore, in the experiments presented in this thesis, lysosomes were not immunologically labelled, but identified by their previously well-documented (e.g. Fameli et al. (2014)) appearance. They are single-membrane bound organelles with a matrix that is more electron dense than the surrounding cytoplasm.

However, in order to demonstrate that lysosomes were accurately identified, some specimens were fixed using a much lower concentration of glutaraldehyde and labelled with LAMP-2 primary antibody and gold particles. These images were not included in analysis of distance measurements due to the poor definition of lipid membranes.

Methods

Samples were prepared from chemically fixed intact mouse ventricular tissue. Approximately 1 mm^3 pieces of tissue from ventricles were chemically fixed (paraformaldehyde 4%, glutaraldehyde 0.1%, phosphate buffer, pH 7.4), embedded in LR White resin and cut into ultrathin sections. For staining sections were washed in distilled water followed by PBS/chicken egg albumin (EA) twice for 5 minutes and blocked in EA for 30 minutes. Sections were incubated in LAMP-2 (rabbit-anti-LAMP-2, Thermofisher PA1-655, Lot: PA189864) primary antibody made up in PBS/EA (2 hours) and washed several times in PBS/EA followed by incubation with protein A gold (1 hour, British Biocell). Finally, sections were washed in PBS/EA and distilled water several times. Prior to viewing the section under an electron microscope (TEM, Joel 1200EX II), sections were post-stained with uranyl acetate and lead citrate.

Results

Example electron micrographs labelled with a primary antibody against LAMP-2 are shown in figure B2.

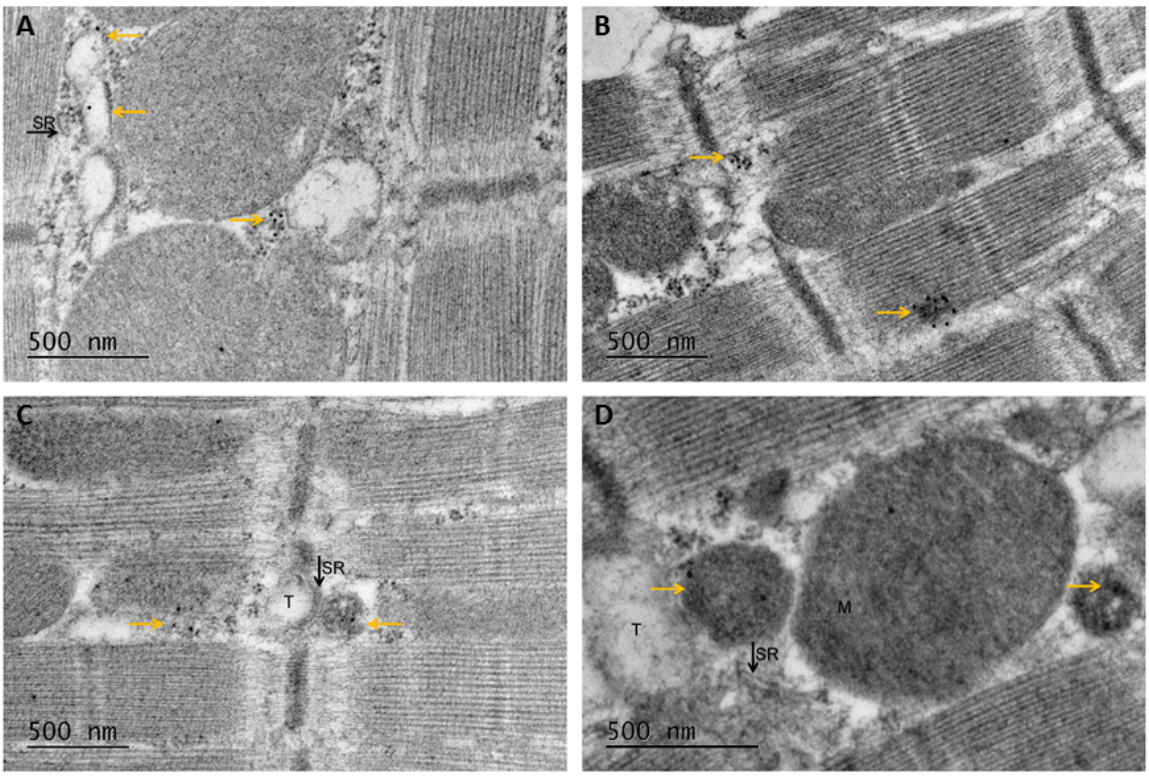


Figure B2: Immuno-gold staining of LAMP-2 in mouse ventricular tissue. A-D show LAMP-2 stained organelles (dense black dots are gold labelling, highlighted using arrows) are found in close proximity to organelles likely to be sarcoplasmic reticulum (SR), mitochondria (M) and T-tubules (T).

9.2.3 Ned-19 vs Lysotracker fluorescence in the presence of BZ194

This data was provided by Dr Kerrie Ford and Dr Rebecca Burton of Oxford University, and reproduced here with permission. Again, some text was taken from the submitted manuscript 'Aston et al., High resolution structural evidence suggests the Sarcoplasmic Reticulum forms microdomains with Acidic Stores (lysosomes) in the heart. SciRep. Submitted for publication 2016'.

In chapter five, data is presented that demonstrates that the fluorescent NAADP antagonist, Ned-19 has binding sites that are highly colocalised with the lysosomal marker Lysotracker red. However, it is possible that Ned-19 was found localized in lysosomes not due to specific binding, but as part of the lysosomal degradation pathway. In order to test this, the experiments with Ned-19 and Lysotracker were repeated in the presence of another (non-fluorescent) antagonist of NAADP, BZ194.

Methods

Isolated rabbit ventricular cardiomyocytes were incubated with BZ194 (100 μM, 1 h) and Ned-19 (100 μM, 40 minutes) at room temperature with addition of 500 nM LysoTracker red for the final 2 min. Cells were allowed to adhere to a glass coverslip and superfused with Tyrode's solution containing (in mM): 135 NaCl, 4.5 KCl, 11 glucose, 20 HEPES, 1 $MgCl_2$, 1.8 $CaCl_2$, pH 7.4 with NaOH. Ned-19 fluorescence was excited at 355 nm and detected at 415±30 nm, whilst LysoTracker red was excited at 514 nm and collected at 590-747 nm. Imaging was performed with a Leica SP5 inverted confocal microscope with a 63x oil-immersion objective.

Results

Ned-19 does not stain lysosomes or other acidic compartments after cells have been pre-incubated with BZ194, suggesting that Ned-19 is binding at the lysosomal membrane and not accumulating here as part of a degradative pathway. This data is shown in figure B3.

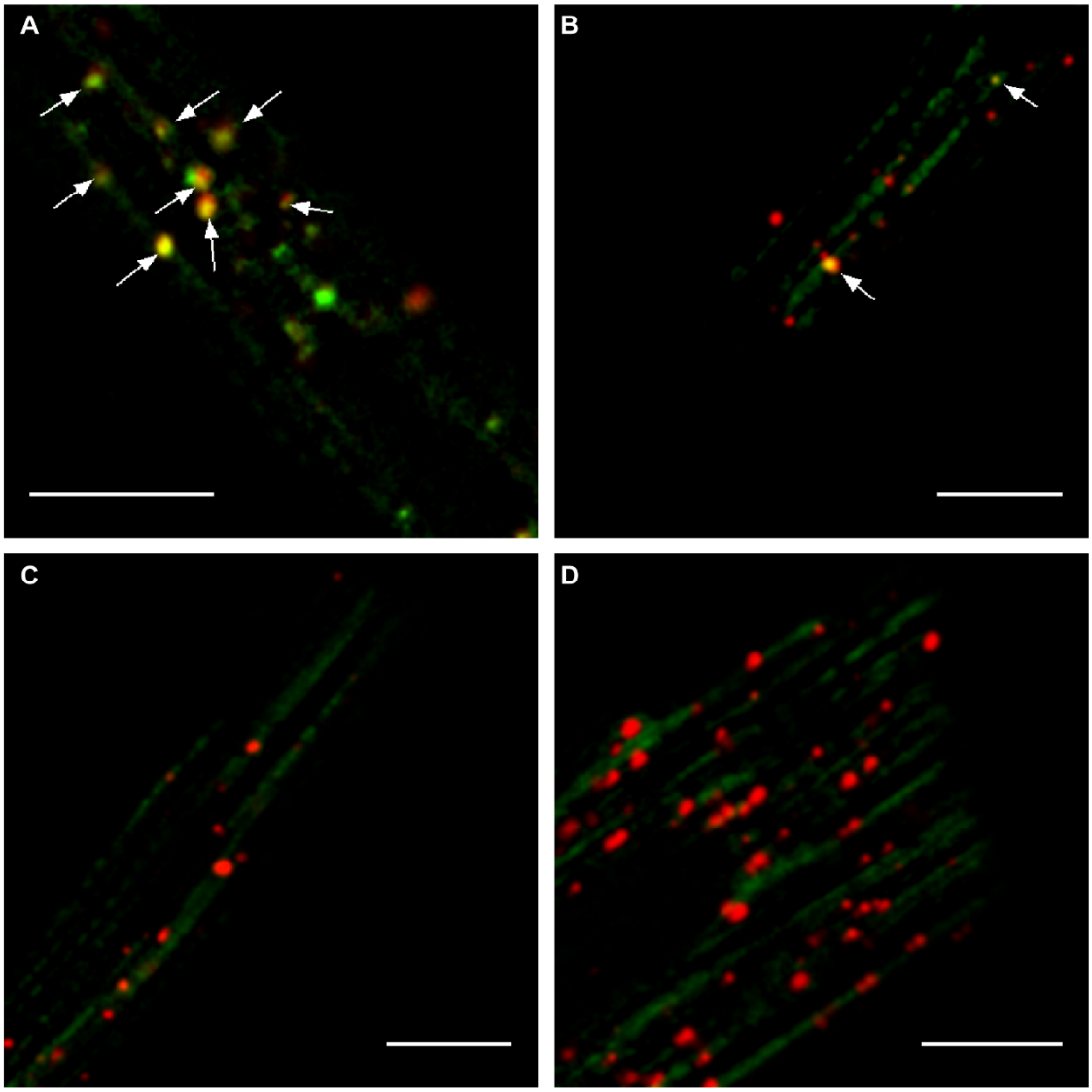


Figure B3: Specific binding of Ned-19 in live ventricular cardiomyocytes. All images in this figure are merged, with Ned-19 channel signals in green and Lysotracker red channel signals in red. Scale bars indicate 10 μm. A) Repeat of the Ned-19 and Lysotracker co-labelling experiment in chapter five. B&C) Ned-19 and Lysotracker loaded following pre-incubation with BZ194. Of 19 cells imaged in this data set, 3 cells exhibited the partial staining shown in B, whilst 16 exhibited no evidence of lysosomal Ned-19 as shown in C. Panel D) shows cells incubated with BZ194 and Lysotracker in the absence of Ned-19, demonstrating lack of fluorescence of BZ194 under these conditions.

9.3 Appendix C

9.3.1 Matlab script for analysis of confocal micrographs

This Matlab (Mathworks, Cambridge, UK) code was written by Dr Gary Mirams (Department of Computer Science, University of Oxford), and reproduced here with permission. It was used in chapter five to analyse confocal micrograph images of rabbit ventricular cells co-labelled with antibodies against LAMP-2 and either RyR2 or PLB. This code determines the dominant frequency of the fluorescent antibody signals across the cell using Fourier analysis.

Figure C1 (below): Matlab code for analysis of immunocytochemistry images.

```
clear all

% Bioformats Matlab Toolbox, downloaded on 4/11/15 from
% http://downloads.openmicroscopy.org/bio-formats/5.1.5/
addpath('bfmatlab')

file_names = {'1.oif','2.oib','3.oib','3.oib'};
folder_type = 'PLB';% Or
% folder_type = 'RyR';


for f = 1:length(file_names)
```

```
close all
    folder_name = ['ICC/' folder_type '_vs_LAMP/'];
    file_name = file_names{f};
    full_file_path = [folder_name file_name];

    data = bfopen(full_file_path)

    seriesCount = size(data, 1);
    series1 = data{1, 1};
    % etc
    nucleus_plane = series1{1, 1};
    nucleus_label = series1{1, 2};

    LAMP_plane = series1{2, 1};
    LAMP_label = series1{2, 2};

    RyR_plane = series1{3, 1};
    RyR_label = series1{3, 2};

    omeMeta = data{1, 4};
    stackSizeX = omeMeta.getPixelsSizeX(0).getValue(); % image width, pixels
    stackSizeY = omeMeta.getPixelsSizeY(0).getValue(); % image height, pixels
    stackSizeZ = omeMeta.getPixelsSizeZ(0).getValue(); % number of Z slices

    voxelSizeXdefaultValue = omeMeta.getPixelsPhysicalSizeX(0).value()           % returns
value in default unit
    voxelSizeXdefaultUnit = omeMeta.getPixelsPhysicalSizeX(0).unit().getSymbol() % returns
the default unit type
    voxelSizeX = omeMeta.getPixelsPhysicalSizeX(0).value(ome.units.UNITS.MICROM) % in Âµm
```

```
    voxelSizeXdouble = voxelSizeX.doubleValue()                                    % The
numeric value represented by this object after conversion to type double
    voxelSizeY = omeMeta.getPixelsPhysicalSizeY(0).value(ome.units.UNITS.MICROM) % in Âµm
    voxelSizeYdouble = voxelSizeY.doubleValue()                                    % The
numeric value represented by this object after conversion to type double
    voxelSizeZ = omeMeta.getPixelsPhysicalSizeZ(0).value(ome.units.UNITS.MICROM) % in Âµm
    voxelSizeZdouble = voxelSizeZ.doubleValue()                                    % The
numeric value represented by this object after conversion to type double

    figure
    subplot(1,3,1)
    imshow(nucleus_plane);
    max(max(nucleus_plane))
    title('DAPI - Nucleus')

    subplot(1,3,2)
    imshow(LAMP_plane, []);
    max(max(LAMP_plane))
    title('LAMP')

    subplot(1,3,3)
    imshow(RyR_plane, []);
    whos RyR_plane
    max(max(RyR_plane))
    title('RyR')
```

Work out a 'mask' that shows where cell is

```
    level = graythresh(uint8(RyR_plane));
    BW_RyR = im2bw(uint8(RyR_plane), level);

    figure
    subplot(3,1,1)
    imshow(RyR_plane, [0 max(max(RyR_plane))])
    % imshow(BW_RyR)
    % title('BW RyR')

    % Get rid of noisy isolated points
    se = strel('disk',2);
    BW_RyR = imerode(BW_RyR, se);
    %BW_RyR = imerode(BW_RyR, se);
    %BW_RyR = imerode(BW_RyR, se);

    % figure
    subplot(3,1,2)
    imshow(BW_RyR)
    title('BW RyR eroded')

    % Apply a mask to filter background noise out of RyR plane
    RyR_plane_masked = immultiply(RyR_plane,BW_RyR);
    subplot(3,1,3)
    imshow(RyR_plane_masked, [0 max(max(RyR_plane))])
    RyR_plane = RyR_plane_masked;
```

Work out a rough binary image for doing cropping later on.

```
    se = strel('disk',24);
    BW_whole_cell = imdilate(BW_RyR, se);
    BW_whole_cell = imfill(BW_whole_cell,'holes');

    % Remove smaller isolated objects
    BW_whole_cell = bwareaopen(BW_whole_cell, 5000);
```

Work out the orientation and get it aligned.

```
    angle = rotate_to_vertical_stripes_minimisation_powerspectrum(RyR_plane,
voxelSizeXdouble);

    if f==1
        % Fix for a troublesome case!
        angle = angle + 90.0;
    end
```

Show the angle of cell axis on figure

```
    figure(1)
    x0 = stackSizeX/2.0;
    y0 = stackSizeY/2.0;
    x_long = (stackSizeX/2.0)*cos(pi*(-angle/180.0))/2.0;
    y_long = (stackSizeY/2.0)*sin(pi*(-angle/180.0))/2.0;
    for i=1:3
        subplot(1,3,i)
        hold on
        plot(x0,y0,'r*')
        hold on
        % Beware! In images the x increases as you'd expect, but y is
        % measured top down, so these are not quite as expected...
        plot([x0-x_long x0+x_long],[y0+y_long y0-y_long],'b-*')
    end
```

Rotate all images to this orientation

```
    BW_whole_cell = imrotate(BW_whole_cell,angle,'bilinear');
    BW_RyR = imrotate(BW_RyR,angle,'bilinear');
    RyR_plane2 = imrotate(RyR_plane,angle,'bilinear');
    LAMP_plane2 = imrotate(LAMP_plane,angle,'bilinear');
    nucleus_plane2 = imrotate(nucleus_plane,angle,'bilinear');

    % Then crop down to slightly larger than the new bounding box
    stats_rotated = regionprops(BW_whole_cell,'Centroid',...
        'MajorAxisLength','MinorAxisLength','Orientation','BoundingBox');

    % If we didn't manage to select one whole cell, get biggest bit.
    if length(stats_rotated) > 1
        stats_rotated = stats_rotated(1);
    end

    border_size = 10;
    rectangle = [stats_rotated.BoundingBox(1) - border_size ...
```

```
                stats_rotated.BoundingBox(2) - border_size...
                stats_rotated.BoundingBox(3) + 2*border_size...
                stats_rotated.BoundingBox(4) + 2*border_size];

    % For the last image, we cut it into two and analyse twice.
    prop_y_in_first = 0.6;
    if f==3
        rectangle(4) = prop_y_in_first*stats_rotated.BoundingBox(4)+border_size;
        file_name = '3a.oib';
    elseif f==4
        rectangle(2) =
stats_rotated.BoundingBox(2)+prop_y_in_first*stats_rotated.BoundingBox(4) - border_size;
        rectangle(4) = (1-prop_y_in_first)*stats_rotated.BoundingBox(4) + border_size;
        file_name = '3b.oib';
    end


    BW_whole_cell = imcrop(BW_whole_cell,rectangle);
    BW_RyR = imcrop(BW_RyR, rectangle);
    RyR_plane2 = imcrop(RyR_plane2, rectangle);
    LAMP_plane2 = imcrop(LAMP_plane2, rectangle);
    nucleus_plane2 = imcrop(nucleus_plane2, rectangle);

    % figure
    % subplot(2,1,1)
    % whos RyR_plane2
    % imshow(RyR_plane2,[0 4096])
    % subplot(2,1,2)
    % imshow(LAMP_plane2,[0 4096])

    % Mask out the bits outside the cell
    RyR_plane2 = immultiply(RyR_plane2,BW_whole_cell);
    LAMP_plane2 = immultiply(LAMP_plane2,BW_whole_cell);
    nucleus_plane2 = immultiply(nucleus_plane2,BW_whole_cell);
```

Remove some of the background colour to emphasise the 'dots' you can visually see

```
    figure
    subplot(3,1,1)
    imshow(LAMP_plane2,[0 max(max(LAMP_plane2))])
    title('Full LAMP image')

    tmp = find(LAMP_plane2>0);
    non_zero_image = im2double(LAMP_plane2(tmp));
    mean_val = mean(non_zero_image)
    std_val = std(non_zero_image)

    BW_LAMP = logical(zeros(size(LAMP_plane2)));
    idx = find(im2double(LAMP_plane2(:))> mean_val);
    BW_LAMP(idx) = 1;

    se = strel('disk',2);
    BW_LAMP = imerode(BW_LAMP,se);
    LAMP_plane_masked = immultiply(LAMP_plane2,BW_LAMP);

    subplot(3,1,2)
    imshow(BW_LAMP)
```

```
title('Mask')

subplot(3,1,3)
imshow(LAMP_plane_masked,[0 max(max(LAMP_plane2))])
title('Masked LAMP image')

% Make the masked version the one we work with.
LAMP_plane2 = LAMP_plane_masked;
```

Apply same to nucleus DAPI stain for fairness

```
figure
subplot(3,1,1)
imshow(nucleus_plane2,[0 max(max(nucleus_plane2))])
title('Full DAPI image')

tmp = find(nucleus_plane2>0);
non_zero_image = im2double(nucleus_plane2(tmp));
mean_val = mean(non_zero_image);
std_val = std(non_zero_image);

BW_nucleus = logical(zeros(size(nucleus_plane2)));
idx = find(im2double(nucleus_plane2(:))> mean_val);
BW_nucleus(idx) = 1;

se = strel('disk',2);
BW_nucleus = imerode(BW_nucleus,se);
nucleus_plane_masked = immultiply(nucleus_plane2,BW_nucleus);

subplot(3,1,2)
imshow(BW_nucleus)
title('Mask')

subplot(3,1,3)
imshow(nucleus_plane_masked,[0 max(max(nucleus_plane2))])
title('Masked DAPI image')

% Make the masked version the one we work with.
nucleus_plane2 = nucleus_plane_masked;

%
% % Brightened just so we can see better
% figure
% subplot(3,1,1)
% imshow(RyR_plane2,[0 max(max(RyR_plane2))])
% xlabel('RyR')
% subplot(3,1,2)
% imshow(LAMP_plane2,[0 max(max(LAMP_plane2))])
% xlabel('LAMP')
% subplot(3,1,3)
% imshow(nucleus_plane2,[0 max(max(nucleus_plane2))])
% xlabel('Nucleus')
```

Try just collapsing down the image and looking at the 1D Fourier transform

height of image

```
height = size(RyR_plane2,1);
num_stripes = 1;
for i=1:num_stripes
```

```
    spacing = height/num_stripes;
    from_idx = floor(spacing*(i-1))+1;
    to_idx = floor(spacing*i);

    %figure
    %scatter(RyR_plane2(:),LAMP_plane2(:),'b.')
    mdl = LinearModel.fit(double(RyR_plane2(:)),double(LAMP_plane2(:)),'linear')

    sum_RyR = sum(RyR_plane2(from_idx:to_idx,:),1);
    sum_LAMP = sum(LAMP_plane2(from_idx:to_idx,:),1);
    sum_nucleus = sum(nucleus_plane2(from_idx:to_idx,:),1);

    % Look at frequencies
    [P1,f1] = periodogram(sum_RyR,[],[],1);
    [P2,f2] = periodogram(sum_LAMP,[],[],1);
    [P3,f3] = periodogram(sum_nucleus,[],[],1);

    figure1 = figure('PaperSize',[15 10]);
    set(gcf, 'PaperPositionMode', 'manual');
    set(gcf, 'PaperUnits', 'inches');
    set(gcf, 'PaperPosition', [0.5 0.5 14 9]); % last 2 are width/height.
```

First column raw images

```
    subplot(331)
    imshow(RyR_plane2,'DisplayRange',[0 max(max(RyR_plane2))])
    xlabel('RyR')
    title('Thresholded images')
    subplot(334)
    imshow(LAMP_plane2,[0 max(max(LAMP_plane2))])
    xlabel('LAMP')
    subplot(337)
    imshow(nucleus_plane2,[0 max(max(nucleus_plane2))])
    xlabel('Nucleus')
```

Second column, column totals

```
    t = (0:numel(sum_RyR)-1);
    subplot(332);
    plot(t*voxelSizeXdouble,sum_RyR,'k-');
    hold on
    plot(t*voxelSizeXdouble,sum_LAMP,'b-')
    ylabel('Sum of all intensities in this column');
    xlabel('Position (um)')
    legend('RyR','LAMP')
    grid on
    title('Series')

    subplot(335);
        scatter(sum_RyR,sum_LAMP,'b.')
    xlabel('RyR Column Intensity')
```

```
        ylabel('LAMP Column Intensity')

        subplot(338);
        plot(t*voxelSizeXdouble,sum_nucleus,'r-')
        ylabel('DAPI Sum of intensities in column');
        xlabel('Position (um)')
        grid on
```

Third column, Fourier analysis

```
        subplot(333);
        plot(f1./(voxelSizeXdouble),P1,'k-');
        ylabel('RyR');
        xlim([0.1 2.3])
        grid on;
        %axis tight
        title('Power Spectrum')
        xlabel('Frequency (per um)')

        subplot(336)
        plot(f2./(voxelSizeXdouble),P2,'b-');
        xlim([0.1 2.3])
        ylabel('LAMP');
        grid on;
        %axis tight
        xlabel('Frequency (per um)')

        subplot(339);

        plot(f3./(voxelSizeXdouble),P3,'r-');
        ylabel('DAPI');
        xlabel('Frequency (per um)')
        xlim([0.1 2.3])
        ylim([0 max(P1+10)])
        grid on;
        %axis tight

        %print(['FrequencyPlot_' file_name(1:end-4) '_' file_name(end-2:end) '.eps'],'-
depsc','-tiff')
        print(['FrequencyPlot_' folder_type '_' file_name(1:end-4) '_' file_name(end-2:end)
'.png'],'-dpng')

    %     figure
    %     plot(t*voxelSizeXdouble,sum_RyR,'k-');
    %     hold on
    %     plot(t*voxelSizeXdouble,sum_LAMP,'b-')
    %     ylabel('Sum of all intensities in this column');
    %     xlabel('Position (um)')
    %     legend('RyR','LAMP')
    %     xlim([80 90])

    end

end
```

10

Bibliography

AARHUS, R., DICKEY, D. M., GRAEFF, R. M., GEE, K. R., WALSETH, T. F. & LEE, H. C. 1996. Activation and inactivation of Ca2+ release by NAADP+. *J Biol Chem,* 271**,** 8513-6.

AARHUS, R., GRAEFF, R. M., DICKEY, D. M., WALSETH, T. F. & LEE, H. C. 1995. ADP-ribosyl cyclase and CD38 catalyze the synthesis of a calcium-mobilizing metabolite from NADP. *J Biol Chem,* 270**,** 30327-33.

ALBERTS, B. 2015. *Molecular biology of the cell,* New York, NY, Garland Science, Taylor and Francis Group.

ALEGRE-ABARRATEGUI, J., CHRISTIAN, H., LUFINO, M. M., MUTIHAC, R., VENDA, L. L., ANSORGE, O. & WADE-MARTINS, R. 2009. LRRK2 regulates autophagic activity and localizes to specific membrane microdomains in a novel human genomic reporter cellular model. *Hum Mol Genet,* 18**,** 4022-34.

ALEY, P. K., NOH, H. J., GAO, X., TICA, A. A., BRAILOIU, E. & CHURCHILL, G. C. 2010. A functional role for nicotinic acid adenine dinucleotide phosphate in oxytocin-mediated contraction of uterine smooth muscle from rat. *J Pharmacol Exp Ther,* 333**,** 726-35.

ALEY, P. K., SINGH, N., BRAILOIU, G. C., BRAILOIU, E. & CHURCHILL, G. C. 2013. Nicotinic acid adenine dinucleotide phosphate (NAADP) is a second messenger in muscarinic receptor-induced contraction of guinea pig trachea. *J Biol Chem,* 288**,** 10986-93.

ALPY, F., ROUSSEAU, A., SCHWAB, Y., LEGUEUX, F., STOLL, I., WENDLING, C., SPIEGELHALTER, C., KESSLER, P., MATHELIN, C., RIO, M. C., LEVINE, T. P. & TOMASETTO, C. 2013. STARD3 or STARD3NL and VAP form a novel molecular tether between late endosomes and the ER. *J Cell Sci,* 126**,** 5500-12.

ANDERSON, M. E., BROWN, J. H. & BERS, D. M. 2011. CaMKII in myocardial hypertrophy and heart failure. *J Mol Cell Cardiol,* 51**,** 468-73.

ANDREJEWSKI, N., PUNNONEN, E. L., GUHDE, G., TANAKA, Y., LULLMANN-RAUCH, R., HARTMANN, D., VON FIGURA, K. & SAFTIG, P. 1999. Normal lysosomal morphology and function in LAMP-1-deficient mice. *J Biol Chem,* 274**,** 12692-701.

APPELQVIST, H., WASTER, P., KAGEDAL, K. & OLLINGER, K. 2013. The lysosome: from waste bag to potential therapeutic target. *J Mol Cell Biol,* 5**,** 214-26.

ASGHARI, P., SCRIVEN, D. R., HOSKINS, J., FAMELI, N., VAN BREEMEN, C. & MOORE, E. D. 2012. The structure and functioning of the couplon in the mammalian cardiomyocyte. *Protoplasma,* 249 Suppl 1**,** S31-8.

BAINTON, D. F. 1981. The discovery of lysosomes. *J Cell Biol,* 91**,** 66s-76s.

BAK, J., BILLINGTON, R. A., TIMAR, G., DUTTON, A. C. & GENAZZANI, A. A. 2001. NAADP receptors are present and functional in the heart. *Curr Biol,* 11**,** 987-90.

BAK, J., WHITE, P., TIMAR, G., MISSIAEN, L., GENAZZANI, A. A. & GALIONE, A. 1999. Nicotinic acid adenine dinucleotide phosphate triggers Ca2+ release from brain

microsomes. *Curr Biol,* 9**,** 751-4.

BALSHAW, D. M., XU, L., YAMAGUCHI, N., PASEK, D. A. & MEISSNER, G. 2001. Calmodulin binding and inhibition of cardiac muscle calcium release channel (ryanodine receptor). *J Biol Chem,* 276**,** 20144-53.

BANDYOPADHYAY, D., CYPHERSMITH, A., ZAPATA, J. A., KIM, Y. J. & PAYNE, C. K. 2014. Lysosome transport as a function of lysosome diameter. *PLoS One,* 9**,** e86847.

BARCELO-TORNS, M., LEWIS, A. M., GUBERN, A., BARNEDA, D., BLOOR-YOUNG, D., PICATOSTE, F., CHURCHILL, G. C., CLARO, E. & MASGRAU, R. 2011. NAADP mediates ATP-induced Ca2+ signals in astrocytes. *FEBS Lett,* 585**,** 2300-6.

BARTH, E., STAMMLER, G., SPEISER, B. & SCHAPER, J. 1992. Ultrastructural quantitation of mitochondria and myofilaments in cardiac muscle from 10 different animal species including man. *J Mol Cell Cardiol,* 24**,** 669-81.

BASSANI, J. W., BASSANI, R. A. & BERS, D. M. 1994. Relaxation in rabbit and rat cardiac cells: species-dependent differences in cellular mechanisms. *J Physiol,* 476**,** 279-93.

BAUDHUIN, P., BEAUFAY, H. & DE DUVE, C. 1965. Combined biochemical and morphological study of particulate fractions from rat liver. Analysis of preparations enriched in lysosomes or in particles containing urate oxidase, D-amino acid oxidase, and catalase. *J Cell Biol,* 26**,** 219-43.

BAYLISS, R. A. 2014. *Actions of NAADP and other agents in cardiac myocytes.* DPhil DPhil, University of Oxford.

BEAN, B. P. 1989. Classes of calcium channels in vertebrate cells. *Annu Rev Physiol,* 51**,** 367-84.

BERG, I., POTTER, B. V., MAYR, G. W. & GUSE, A. H. 2000. Nicotinic acid adenine dinucleotide phosphate (NAADP(+)) is an essential regulator of T-lymphocyte Ca(2+)-signaling. *J Cell Biol,* 150**,** 581-8.

BERG, T. O., STROMHAUG, E., LOVDAL, T., SEGLEN, O. & BERG, T. 1994. Use of glycyl-L-phenylalanine 2-naphthylamide, a lysosome-disrupting cathepsin C substrate, to distinguish between lysosomes and prelysosomal endocytic vacuoles. *Biochem J,* 300 (Pt 1)**,** 229-36.

BERNARDO, B. C., WEEKS, K. L., PRETORIUS, L. & MCMULLEN, J. R. 2010. Molecular distinction between physiological and pathological cardiac hypertrophy: experimental findings and therapeutic strategies. *Pharmacol Ther,* 128**,** 191-227.

BERS, D. M. 2000. Calcium fluxes involved in control of cardiac myocyte contraction. *Circ Res,* 87**,** 275-81.

BERS, D. M. 2001. *Excitation-contraction coupling and cardiac contractile force,* Dordrecht ; Boston, Kluwer Academic Publishers.

BERS, D. M. 2002. Cardiac excitation-contraction coupling. *Nature,* 415**,** 198-205.

BERS, D. M. 2006. Cardiac ryanodine receptor phosphorylation: target sites and functional consequences. *Biochem J,* 396**,** e1-3.

BERS, D. M. 2012. Ryanodine receptor S2808 phosphorylation in heart failure: smoking gun or red herring. *Circ Res,* 110**,** 796-9.

BERS, D. M., POGWIZD, S. M. & SCHLOTTHAUER, K. 2002. Upregulated Na/Ca exchange is involved in both contractile dysfunction and arrhythmogenesis in heart failure. *Basic Res Cardiol,* 97 Suppl 1**,** I36-42.

BODI, I., MIKALA, G., KOCH, S. E., AKHTER, S. A. & SCHWARTZ, A. 2005. The L-type calcium channel in the heart: the beat goes on. *J Clin Invest,* 115**,** 3306-17.

BOGOYEVITCH, M. A., ANDERSSON, M. B., GILLESPIE-BROWN, J., CLERK, A., GLENNON, P. E., FULLER, S. J. & SUGDEN, P. H. 1996. Adrenergic receptor stimulation of the mitogen-activated protein kinase cascade and cardiac hypertrophy. *Biochem J,* 314 (Pt 1)**,** 115-21.

BOITTIN, F. X., GALIONE, A. & EVANS, A. M. 2002. Nicotinic acid adenine dinucleotide phosphate mediates Ca2+ signals and contraction in arterial smooth muscle via a two-pool mechanism. *Circ Res,* 91**,** 1168-75.

BOLTON, E. L. 2014. *Effects of endogenous cannabinoids and related substances on electrical activity and contraction in cardiac ventricular muscle.* DPhil DPhil, University of Oxford.

BRAILOIU, E., CHURAMANI, D., CAI, X., SCHRLAU, M. G., BRAILOIU, G. C., GAO, X., HOOPER, R., BOULWARE, M. J., DUN, N. J., MARCHANT, J. S. & PATEL, S. 2009. Essential requirement for two-pore channel 1 in NAADP-mediated calcium signaling. *J Cell Biol,* 186**,** 201-9.

BRAILOIU, E., RAHMAN, T., CHURAMANI, D., PROLE, D. L., BRAILOIU, G. C., HOOPER, R., TAYLOR, C. W. & PATEL, S. 2010. An NAADP-gated two-pore channel targeted to the plasma membrane uncouples triggering from amplifying Ca2+ signals. *J Biol Chem,* 285**,** 38511-6.

BRANDT, N. 1985. Identification of two populations of cardiac microsomes with nitrendipine receptors: correlation of the distribution of dihydropyridine receptors with organelle specific markers. *Arch Biochem Biophys,* 242**,** 306-19.

BRAULKE, T. & BONIFACINO, J. S. 2009. Sorting of lysosomal proteins. *Biochim Biophys Acta,* 1793**,** 605-14.

BRUNK, U. T. & TERMAN, A. 2002. The mitochondrial-lysosomal axis theory of aging: accumulation of damaged mitochondria as a result of imperfect autophagocytosis. *Eur J Biochem,* 269**,** 1996-2002.

BRUNK, U. T. & TERMAN, A. 2002. Lipofuscin: mechanisms of age-related accumulation

and influence on cell function. *Free Radic Biol Med,* 33**,** 611-9.

CALCRAFT, P. J., RUAS, M., PAN, Z., CHENG, X., ARREDOUANI, A., HAO, X., TANG, J., RIETDORF, K., TEBOUL, L., CHUANG, K. T., LIN, P., XIAO, R., WANG, C., ZHU, Y., LIN, Y., WYATT, C. N., PARRINGTON, J., MA, J., EVANS, A. M., GALIONE, A. & ZHU, M. X. 2009. NAADP mobilizes calcium from acidic organelles through two-pore channels. *Nature,* 459**,** 596-600.

CANCELA, J. M., CHURCHILL, G. C. & GALIONE, A. 1999. Coordination of agonist-induced Ca2+-signalling patterns by NAADP in pancreatic acinar cells. *Nature,* 398**,** 74-6.

CANG, C., ZHOU, Y., NAVARRO, B., SEO, Y. J., ARANDA, K., SHI, L., BATTAGLIA-HSU, S., NISSIM, I., CLAPHAM, D. E. & REN, D. 2013. mTOR regulates lysosomal ATP-sensitive two-pore Na(+) channels to adapt to metabolic state. *Cell,* 152**,** 778-90.

CAPEL, R. A., BOLTON, E. L., LIN, W. K., ASTON, D., WANG, Y., LIU, W., WANG, X., BURTON, R. A., BLOOR-YOUNG, D., SHADE, K. T., RUAS, M., PARRINGTON, J., CHURCHILL, G. C., LEI, M., GALIONE, A. & TERRAR, D. A. 2015. Two-pore Channels (TPC2s) and Nicotinic Acid Adenine Dinucleotide Phosphate (NAADP) at Lysosomal-Sarcoplasmic Reticular Junctions Contribute to Acute and Chronic beta-Adrenoceptor Signaling in the Heart. *J Biol Chem,* 290**,** 30087-98.

CARTER, S., COLYER, J. & SITSAPESAN, R. 2006. Maximum phosphorylation of the cardiac ryanodine receptor at serine-2809 by protein kinase a produces unique modifications to channel gating and conductance not observed at lower levels of phosphorylation. *Circ Res,* 98**,** 1506-13.

CATALUCCI, D., LATRONICO, M. V., CECI, M., RUSCONI, F., YOUNG, H. S., GALLO, P., SANTONASTASI, M., BELLACOSA, A., BROWN, J. H. & CONDORELLI, G. 2009. Akt increases sarcoplasmic reticulum Ca2+ cycling by direct phosphorylation of phospholamban at Thr17. *J Biol Chem,* 284**,** 28180-7.

CAZORLA, O., LUCAS, A., POIRIER, F., LACAMPAGNE, A. & LEZOUALC'H, F. 2009. The cAMP binding protein Epac regulates cardiac myofilament function. *Proc Natl Acad Sci U S A,* 106**,** 14144-9.

CHEN, L., SAMPSON, K. J. & KASS, R. S. 2016. Cardiac Delayed Rectifier Potassium Channels in Health and Disease. *Card Electrophysiol Clin,* 8**,** 307-22.

CHEN, W., WANG, R., CHEN, B., ZHONG, X., KONG, H., BAI, Y., ZHOU, Q., XIE, C., ZHANG, J., GUO, A., TIAN, X., JONES, P. P., O'MARA, M. L., LIU, Y., MI, T., ZHANG, L., BOLSTAD, J., SEMENIUK, L., CHENG, H., ZHANG, J., CHEN, J., TIELEMAN, D. P., GILLIS, A. M., DUFF, H. J., FILL, M., SONG, L. S. & CHEN, S. R. 2014. The ryanodine receptor store-sensing gate controls Ca2+ waves and Ca2+-triggered arrhythmias. *Nat Med,* 20**,** 184-92.

CHEN-IZU, Y., MCCULLE, S. L., WARD, C. W., SOELLER, C., ALLEN, B. M., RABANG, C., CANNELL, M. B., BALKE, C. W. & IZU, L. T. 2006. Three-dimensional distribution of ryanodine receptor clusters in cardiac myocytes. *Biophys J,* 91**,** 1-13.

CHENG, J., YUSUFI, A. N., THOMPSON, M. A., CHINI, E. N. & GRANDE, J. P. 2001. Nicotinic acid adenine dinucleotide phosphate: a new Ca2+ releasing agent in kidney. *J Am Soc Nephrol,* 12**,** 54-60.

CHERRY, E. M., FENTON, F. H. & GILMOUR, R. F., JR. 2012. Mechanisms of ventricular arrhythmias: a dynamical systems-based perspective. *Am J Physiol Heart Circ Physiol,* 302**,** H2451-63.

CHING, L. L., WILLIAMS, A. J. & SITSAPESAN, R. 2000. Evidence for Ca(2+) activation and inactivation sites on the luminal side of the cardiac ryanodine receptor complex. *Circ Res,* 87**,** 201-6.

CHINI, E. N., BEERS, K. W. & DOUSA, T. P. 1995. Nicotinate adenine dinucleotide phosphate (NAADP) triggers a specific calcium release system in sea urchin eggs. *J Biol Chem,* 270**,** 3216-23.

CHRISTENSEN, K. A., MYERS, J. T. & SWANSON, J. A. 2002. pH-dependent regulation of lysosomal calcium in macrophages. *J Cell Sci,* 115**,** 599-607.

CHURCHILL, G. C. & GALIONE, A. 2001. NAADP induces Ca2+ oscillations via a two-pool mechanism by priming IP3- and cADPR-sensitive Ca2+ stores. *EMBO J,* 20**,** 2666-71.

CHURCHILL, G. C., O'NEILL, J. S., MASGRAU, R., PATEL, S., THOMAS, J. M., GENAZZANI, A. A. & GALIONE, A. 2003. Sperm deliver a new second messenger: NAADP. *Curr Biol,* 13**,** 125-8.

CHURCHILL, G. C., OKADA, Y., THOMAS, J. M., GENAZZANI, A. A., PATEL, S. & GALIONE, A. 2002. NAADP mobilizes Ca(2+) from reserve granules, lysosome-related organelles, in sea urchin eggs. *Cell,* 111**,** 703-8.

CLAPHAM, D. E. 2007. Calcium signaling. *Cell,* 131**,** 1047-58.

CLAPPER, D. L., WALSETH, T. F., DARGIE, P. J. & LEE, H. C. 1987. Pyridine nucleotide metabolites stimulate calcium release from sea urchin egg microsomes desensitized to inositol trisphosphate. *J Biol Chem,* 262**,** 9561-8.

COLLINS, T. P. 2009. *Regulation of atrial myocyte calcium signalling by second messengers including cyclic AMP, Inositol trisphosphate and nicotinic acid adenine dinucleotide phosphate.* DPhil DPhil, University of Oxford.

COLLINS, T. P., BAYLISS, R., CHURCHILL, G. C., GALIONE, A. & TERRAR, D. A. 2011. NAADP influences excitation-contraction coupling by releasing calcium from lysosomes in atrial myocytes. *Cell Calcium,* 50**,** 449-58.

COLLINS, T. P. & TERRAR, D. A. 2012. Ca(2+)-stimulated adenylyl cyclases regulate the L-type Ca(2+) current in guinea-pig atrial myocytes. *J Physiol,* 590**,** 1881-93.

COPELLO, J. A., QI, Y., JEYAKUMAR, L. H., OGUNBUNMI, E. & FLEISCHER, S. 2001. Lack of effect of cADP-ribose and NAADP on the activity of skeletal muscle and heart ryanodine

receptors. *Cell Calcium,* 30**,** 269-84.

COSKER, F., CHEVIRON, N., YAMASAKI, M., MENTEYNE, A., LUND, F. E., MOUTIN, M. J., GALIONE, A. & CANCELA, J. M. 2010. The ecto-enzyme CD38 is a nicotinic acid adenine dinucleotide phosphate (NAADP) synthase that couples receptor activation to Ca2+ mobilization from lysosomes in pancreatic acinar cells. *J Biol Chem,* 285**,** 38251-9.

COTECCHIA, S., DEL VESCOVO, C. D., COLELLA, M., CASO, S. & DIVIANI, D. 2015. The alpha1-adrenergic receptors in cardiac hypertrophy: signaling mechanisms and functional implications. *Cell Signal,* 27**,** 1984-93.

CUI, Y., GALIONE, A. & TERRAR, D. A. 1999. Effects of photoreleased cADP-ribose on calcium transients and calcium sparks in myocytes isolated from guinea-pig and rat ventricle. *Biochem J,* 342 (Pt 2)**,** 269-73.

DAMMERMANN, W. & GUSE, A. H. 2005. Functional ryanodine receptor expression is required for NAADP-mediated local Ca2+ signaling in T-lymphocytes. *J Biol Chem,* 280**,** 21394-9.

DAMMERMANN, W., ZHANG, B., NEBEL, M., CORDIGLIERI, C., ODOARDI, F., KIRCHBERGER, T., KAWAKAMI, N., DOWDEN, J., SCHMID, F., DORNMAIR, K., HOHENEGGER, M., FLUGEL, A., GUSE, A. H. & POTTER, B. V. 2009. NAADP-mediated Ca2+ signaling via type 1 ryanodine receptor in T cells revealed by a synthetic NAADP antagonist. *Proc Natl Acad Sci U S A,* 106**,** 10678-83.

DAVIDSON, S. M., FOOTE, K., KUNUTHUR, S., GOSAIN, R., TAN, N., TYSER, R., ZHAO, Y. J., GRAEFF, R., GANESAN, A., DUCHEN, M. R., PATEL, S. & YELLON, D. M. 2015. Inhibition of NAADP signalling on reperfusion protects the heart by preventing lethal calcium oscillations via two-pore channel 1 and opening of the mitochondrial permeability transition pore. *Cardiovasc Res,* 108**,** 357-66.

DE BOLD, A. J. 2011. Thirty years of research on atrial natriuretic factor: historical background and emerging concepts. *Can J Physiol Pharmacol,* 89**,** 527-31.

DE BOLD, A. J. & FLYNN, T. G. 1983. Cardionatrin I - a novel heart peptide with potent diuretic and natriuretic properties. *Life Sci,* 33**,** 297-302.

DE DUVE, C. 2005. The lysosome turns fifty. *Nat Cell Biol,* 7**,** 847-9.

DE DUVE, C., PRESSMAN, B. C., GIANETTO, R., WATTIAUX, R. & APPELMANS, F. 1955. Tissue fractionation studies. 6. Intracellular distribution patterns of enzymes in rat-liver tissue. *Biochem J,* 60**,** 604-17.

DE ROOIJ, J., ZWARTKRUIS, F. J., VERHEIJEN, M. H., COOL, R. H., NIJMAN, S. M., WITTINGHOFER, A. & BOS, J. L. 1998. Epac is a Rap1 guanine-nucleotide-exchange factor directly activated by cyclic AMP. *Nature,* 396**,** 474-7.

DECKER, R. S., POOLE, A. R. & WILDENTHAL, K. 1980. Distribution of lysosomal cathepsin D in normal, ischemic, and starved rabbit cardiac myocytes. *Circ Res,* 46**,** 485-94.

DIAZ, E. & PFEFFER, S. R. 1998. TIP47: a cargo selection device for mannose 6-phosphate receptor trafficking. *Cell,* 93**,** 433-43.

DIBB, K. M., CLARKE, J. D., EISNER, D. A., RICHARDS, M. A. & TRAFFORD, A. W. 2013. A functional role for transverse (t-) tubules in the atria. *J Mol Cell Cardiol,* 58**,** 84-91.

DJERADA, Z. & MILLART, H. 2013. Intracellular NAADP increase induced by extracellular NAADP via the P2Y11-like receptor. *Biochem Biophys Res Commun,* 436**,** 199-203.

DJERADA, Z., PEYRET, H., DUKIC, S. & MILLART, H. 2013. Extracellular NAADP affords cardioprotection against ischemia and reperfusion injury and involves the P2Y11-like receptor. *Biochem Biophys Res Commun,* 434**,** 428-33.

DOBREV, D. & WEHRENS, X. H. 2014. Role of RyR2 phosphorylation in heart failure and arrhythmias: Controversies around ryanodine receptor phosphorylation in cardiac disease. *Circ Res,* 114**,** 1311-9; discussion 1319.

DONG, X. P., SHEN, D., WANG, X., DAWSON, T., LI, X., ZHANG, Q., CHENG, X., ZHANG, Y., WEISMAN, L. S., DELLING, M. & XU, H. 2010. PI(3,5)P(2) controls membrane trafficking by direct activation of mucolipin Ca(2+) release channels in the endolysosome. *Nat Commun,* 1**,** 38.

EDEN, E. R. 2016. The formation and function of ER-endosome membrane contact sites. *Biochim Biophys Acta,* 1861**,** 874-9.

EDEN, E. R., WHITE, I. J., TSAPARA, A. & FUTTER, C. E. 2010. Membrane contacts between endosomes and ER provide sites for PTP1B-epidermal growth factor receptor interaction. *Nat Cell Biol,* 12**,** 267-72.

EDES, I. & KRANIAS, E. G. 1990. Phospholamban and troponin I are substrates for protein kinase C in vitro but not in intact beating guinea pig hearts. *Circ Res,* 67**,** 394-400.

EICHHORN, E. J., HEESCH, C. M., BARNETT, J. H., ALVAREZ, L. G., FASS, S. M., GRAYBURN, P. A., HATFIELD, B. A., MARCOUX, L. G. & MALLOY, C. R. 1994. Effect of metoprolol on myocardial function and energetics in patients with nonischemic dilated cardiomyopathy: a randomized, double-blind, placebo-controlled study. *J Am Coll Cardiol,* 24**,** 1310-20.

EINSTEIN, A. 1905. Über die von der molekularkinetischen Theorie der Wärme geforderte Bewegung von in ruhenden Flüssigkeiten suspend- ierten Teilchen. *Annalan der Physik,* 17**,** 549 - 560.

EISNER, D. A. & LEDERER, W. J. 1985. Na-Ca exchange: stoichiometry and electrogenicity. *Am J Physiol,* 248**,** C189-202.

EISNER, V., CSORDAS, G. & HAJNOCZKY, G. 2013. Interactions between sarco-endoplasmic reticulum and mitochondria in cardiac and skeletal muscle - pivotal roles in Ca(2)(+) and reactive oxygen species signaling. *J Cell Sci,* 126**,** 2965-78.

EL-SHERIF, N. & TURITTO, G. 2011. Electrolyte disorders and arrhythmogenesis. *Cardiol J,* 18**,** 233-45.

ENDO, Y., FURUTA, A. & NISHINO, I. 2015. Danon disease: a phenotypic expression of LAMP-2 deficiency. *Acta Neuropathol,* 129**,** 391-8.

ESKELINEN, E. L. 2006. Roles of LAMP-1 and LAMP-2 in lysosome biogenesis and autophagy. *Mol Aspects Med,* 27**,** 495-502.

ESKELINEN, E. L., CUERVO, A. M., TAYLOR, M. R., NISHINO, I., BLUM, J. S., DICE, J. F., SANDOVAL, I. V., LIPPINCOTT-SCHWARTZ, J., AUGUST, J. T. & SAFTIG, P. 2005. Unifying nomenclature for the isoforms of the lysosomal membrane protein LAMP-2. *Traffic,* 6**,** 1058-61.

ESKELINEN, E. L., ILLERT, A. L., TANAKA, Y., SCHWARZMANN, G., BLANZ, J., VON FIGURA, K. & SAFTIG, P. 2002. Role of LAMP-2 in lysosome biogenesis and autophagy. *Mol Biol Cell,* 13**,** 3355-68.

ESKELINEN, E. L., TANAKA, Y. & SAFTIG, P. 2003. At the acidic edge: emerging functions for lysosomal membrane proteins. *Trends Cell Biol,* 13**,** 137-45.

FABIATO, A. 1983. Calcium-induced release of calcium from the cardiac sarcoplasmic reticulum. *Am J Physiol,* 245**,** C1-14.

FABIATO, A. 1985. Time and calcium dependence of activation and inactivation of calcium-induced release of calcium from the sarcoplasmic reticulum of a skinned canine cardiac Purkinje cell. *J Gen Physiol,* 85**,** 247-89.

FAMELI, N., OGUNBAYO, O. A., VAN BREEMEN, C. & EVANS, A. M. 2014. Cytoplasmic nanojunctions between lysosomes and sarcoplasmic reticulum are required for specific calcium signaling. *F1000Res,* 3**,** 93.

FARRELL, E. F., ANTARAMIAN, A., BENKUSKY, N., ZHU, X., RUEDA, A., GOMEZ, A. M. & VALDIVIA, H. H. 2004. Regulation of cardiac excitation-contraction coupling by sorcin, a novel modulator of ryanodine receptors. *Biol Res,* 37**,** 609-12.

FERNANDES, H. J., HARTFIELD, E. M., CHRISTIAN, H. C., EMMANOULIDOU, E., ZHENG, Y., BOOTH, H., BOGETOFTE, H., LANG, C., RYAN, B. J., SARDI, S. P., BADGER, J., VOWLES, J., EVETTS, S., TOFARIS, G. K., VEKRELLIS, K., TALBOT, K., HU, M. T., JAMES, W., COWLEY, S. A. & WADE-MARTINS, R. 2016. ER Stress and Autophagic Perturbations Lead to Elevated Extracellular alpha-Synuclein in GBA-N370S Parkinson's iPSC-Derived Dopamine Neurons. *Stem Cell Reports,* 6**,** 342-56.

FILL, M. & COPELLO, J. A. 2002. Ryanodine receptor calcium release channels. *Physiol Rev,* 82**,** 893-922.

FLYNN, T. G., DE BOLD, M. L. & DE BOLD, A. J. 1983. The amino acid sequence of an atrial peptide with potent diuretic and natriuretic properties. *Biochem Biophys Res Commun,*

117**,** 859-65.

FRANZINI-ARMSTRONG, C., PROTASI, F. & RAMESH, V. 1999. Shape, size, and distribution of Ca(2+) release units and couplons in skeletal and cardiac muscles. *Biophys J,* 77**,** 1528-39.

FREY, N., KATUS, H. A., OLSON, E. N. & HILL, J. A. 2004. Hypertrophy of the heart: a new therapeutic target? *Circulation,* 109**,** 1580-9.

FU, Y., XIAO, H. & ZHANG, Y. 2012. Beta-adrenoceptor signaling pathways mediate cardiac pathological remodeling. *Front Biosci (Elite Ed),* 4**,** 1625-37.

FUKUDA, M. 1991. Lysosomal membrane glycoproteins. Structure, biosynthesis, and intracellular trafficking. *J Biol Chem,* 266**,** 21327-30.

GABURJAKOVA, M., GABURJAKOVA, J., REIKEN, S., HUANG, F., MARX, S. O., ROSEMBLIT, N. & MARKS, A. R. 2001. FKBP12 binding modulates ryanodine receptor channel gating. *J Biol Chem,* 276**,** 16931-5.

GALIONE, A. 2006. NAADP, a new intracellular messenger that mobilizes Ca2+ from acidic stores. *Biochem Soc Trans,* 34**,** 922-6.

GALIONE, A. 2011. NAADP receptors. *Cold Spring Harb Perspect Biol,* 3**,** a004036.

GALIONE, A. 2015. A primer of NAADP-mediated Ca(2+) signalling: From sea urchin eggs to mammalian cells. *Cell Calcium,* 58**,** 27-47.

GALIONE, A., EVANS, A. M., MA, J., PARRINGTON, J., ARREDOUANI, A., CHENG, X. & ZHU, M. X. 2009. The acid test: the discovery of two-pore channels (TPCs) as NAADP-gated endolysosomal Ca(2+) release channels. *Pflugers Arch,* 458**,** 869-76.

GARRITY, A. G., WANG, W., COLLIER, C. M., LEVEY, S. A., GAO, Q. & XU, H. 2016. The endoplasmic reticulum, not the pH gradient, drives calcium refilling of lysosomes. *Elife,* 5.

GAUTEL, M. & GOULDING, D. 1996. A molecular map of titin/connectin elasticity reveals two different mechanisms acting in series. *FEBS Lett,* 385**,** 11-4.

GENAZZANI, A. A., EMPSON, R. M. & GALIONE, A. 1996. Unique inactivation properties of NAADP-sensitive Ca2+ release. *J Biol Chem,* 271**,** 11599-602.

GERASIMENKO, J. V., CHARLESWORTH, R. M., SHERWOOD, M. W., FERDEK, P. E., MIKOSHIBA, K., PARRINGTON, J., PETERSEN, O. H. & GERASIMENKO, O. V. 2015. Both RyRs and TPCs are required for NAADP-induced intracellular Ca(2)(+) release. *Cell Calcium,* 58**,** 237-45.

GERASIMENKO, J. V., MARUYAMA, Y., YANO, K., DOLMAN, N. J., TEPIKIN, A. V., PETERSEN, O. H. & GERASIMENKO, O. V. 2003. NAADP mobilizes Ca2+ from a thapsigargin-sensitive store in the nuclear envelope by activating ryanodine receptors. *J Cell Biol,* 163**,** 271-82.

GOUGH, N. R. & FAMBROUGH, D. M. 1997. Different steady state subcellular distributions of the three splice variants of lysosome-associated membrane protein LAMP-2 are determined largely by the COOH-terminal amino acid residue. *J Cell Biol,* 137**,** 1161-9.

GRAMOLINI, A. O., TRIVIERI, M. G., OUDIT, G. Y., KISLINGER, T., LI, W., PATEL, M. M., EMILI, A., KRANIAS, E. G., BACKX, P. H. & MACLENNAN, D. H. 2006. Cardiac-specific overexpression of sarcolipin in phospholamban null mice impairs myocyte function that is restored by phosphorylation. *Proc Natl Acad Sci U S A,* 103**,** 2446-51.

GRANGER, B. L., GREEN, S. A., GABEL, C. A., HOWE, C. L., MELLMAN, I. & HELENIUS, A. 1990. Characterization and cloning of lgp110, a lysosomal membrane glycoprotein from mouse and rat cells. *J Biol Chem,* 265**,** 12036-43.

GRANT, A. O. 2009. Cardiac ion channels. *Circ Arrhythm Electrophysiol,* 2**,** 185-94.

GREENWOOD, J. P., SCOTT, E. M., STOKER, J. B. & MARY, D. A. 2001. Hypertensive left ventricular hypertrophy: relation to peripheral sympathetic drive. *J Am Coll Cardiol,* 38**,** 1711-7.

GUL, R., PARK, D. R., SHAWL, A. I., IM, S. Y., NAM, T. S., LEE, S. H., KO, J. K., JANG, K. Y., KIM, D. & KIM, U. H. 2016. Nicotinic Acid Adenine Dinucleotide Phosphate (NAADP) and Cyclic ADP-Ribose (cADPR) Mediate Ca2+ Signaling in Cardiac Hypertrophy Induced by beta-Adrenergic Stimulation. *PLoS One,* 11**,** e0149125.

GUO, T., ZHANG, T., MESTRIL, R. & BERS, D. M. 2006. Ca2+/Calmodulin-dependent protein kinase II phosphorylation of ryanodine receptor does affect calcium sparks in mouse ventricular myocytes. *Circ Res,* 99**,** 398-406.

GUSE, A. H. & LEE, H. C. 2008. NAADP: a universal Ca2+ trigger. *Sci Signal,* 1**,** re10.

GUSE, A. H. & WOLF, I. M. 2016. Ca microdomains, NAADP and type 1 ryanodine receptor in cell activation. *Biochim Biophys Acta*.

GYORKE, I. & GYORKE, S. 1998. Regulation of the cardiac ryanodine receptor channel by luminal Ca2+ involves luminal Ca2+ sensing sites. *Biophys J,* 75**,** 2801-10.

HAGHIGHI, K., KOLOKATHIS, F., PATER, L., LYNCH, R. A., ASAHI, M., GRAMOLINI, A. O., FAN, G. C., TSIAPRAS, D., HAHN, H. S., ADAMOPOULOS, S., LIGGETT, S. B., DORN, G. W., 2ND, MACLENNAN, D. H., KREMASTINOS, D. T. & KRANIAS, E. G. 2003. Human phospholamban null results in lethal dilated cardiomyopathy revealing a critical difference between mouse and human. *J Clin Invest,* 111**,** 869-76.

HELLE, S. C., KANFER, G., KOLAR, K., LANG, A., MICHEL, A. H. & KORNMANN, B. 2013. Organization and function of membrane contact sites. *Biochim Biophys Acta,* 1833**,** 2526-41.

HIBBS, R. G., FERRANS, V. J., WALSH, J. J. & BURCH, G. E. 1965. Electron microscopic observations on lysosomes and related cytoplasmic components of normal and

pathological cardiac muscle. *Anat Rec,* 153**,** 173-85.

HOHENEGGER, M., SUKO, J., GSCHEIDLINGER, R., DROBNY, H. & ZIDAR, A. 2002. Nicotinic acid-adenine dinucleotide phosphate activates the skeletal muscle ryanodine receptor. *Biochem J,* 367**,** 423-31.

HOUSER, S. R. & MOLKENTIN, J. D. 2008. Does contractile Ca2+ control calcineurin-NFAT signaling and pathological hypertrophy in cardiac myocytes? *Sci Signal,* 1**,** pe31.

HOWARD, M., GRIMALDI, J. C., BAZAN, J. F., LUND, F. E., SANTOS-ARGUMEDO, L., PARKHOUSE, R. M., WALSETH, T. F. & LEE, H. C. 1993. Formation and hydrolysis of cyclic ADP-ribose catalyzed by lymphocyte antigen CD38. *Science,* 262**,** 1056-9.

HUIZING, M., HELIP-WOOLEY, A., WESTBROEK, W., GUNAY-AYGUN, M. & GAHL, W. A. 2008. Disorders of lysosome-related organelle biogenesis: clinical and molecular genetics. *Annu Rev Genomics Hum Genet,* 9**,** 359-86.

HUKE, S. & BERS, D. M. 2008. Ryanodine receptor phosphorylation at Serine 2030, 2808 and 2814 in rat cardiomyocytes. *Biochem Biophys Res Commun,* 376**,** 80-5.

HUNZIKER, W. & GEUZE, H. J. 1996. Intracellular trafficking of lysosomal membrane proteins. *Bioessays,* 18**,** 379-89.

HUXLEY, A. F. & NIEDERGERKE, R. 1954. Structural changes in muscle during contraction; interference microscopy of living muscle fibres. *Nature,* 173**,** 971-3.

HUXLEY, H. & HANSON, J. 1954. Changes in the cross-striations of muscle during contraction and stretch and their structural interpretation. *Nature,* 173**,** 973-6.

HUYNH, K. K., ESKELINEN, E. L., SCOTT, C. C., MALEVANETS, A., SAFTIG, P. & GRINSTEIN, S. 2007. LAMP proteins are required for fusion of lysosomes with phagosomes. *EMBO J,* 26**,** 313-24.

HWANG, P. M. & SYKES, B. D. 2015. Targeting the sarcomere to correct muscle function. *Nat Rev Drug Discov,* 14**,** 313-28.

IINO, S., CUI, Y., GALIONE, A. & TERRAR, D. A. 1997. Actions of cADP-ribose and its antagonists on contraction in guinea pig isolated ventricular myocytes. Influence of temperature. *Circ Res,* 81**,** 879-84.

IMBERY, J. F., BHATTACHARYA, S., KHUDER, S., WEISS, A., GOSWAMEE, P., IQBAL, A. K. & GIOVANNUCCI, D. R. 2016. cAMP dependent recruitment of acidic organelles for Ca2+ signaling in the salivary gland. *Am J Physiol Cell Physiol***,** ajpcell 00010 2016.

ITO, H., HOSOYA, Y., INANOBE, A., TOMOIKE, H. & ENDOH, M. 1995. Acetylcholine and adenosine activate the G protein-gated muscarinic K+ channel in ferret ventricular myocytes. *Naunyn Schmiedebergs Arch Pharmacol,* 351**,** 610-7.

JADOT, M., COLMANT, C., WATTIAUX-DE CONINCK, S. & WATTIAUX, R. 1984.

Intralysosomal hydrolysis of glycyl-L-phenylalanine 2-naphthylamide. *Biochem J,* 219**,** 965-70.

JANSE, M. J. & WIT, A. L. 1989. Electrophysiological mechanisms of ventricular arrhythmias resulting from myocardial ischemia and infarction. *Physiol Rev,* 69**,** 1049-169.

JAVADOV, S. & KARMAZYN, M. 2007. Mitochondrial permeability transition pore opening as an endpoint to initiate cell death and as a putative target for cardioprotection. *Cell Physiol Biochem,* 20**,** 1-22.

JOHANSSON, M., ROCHA, N., ZWART, W., JORDENS, I., JANSSEN, L., KUIJL, C., OLKKONEN, V. M. & NEEFJES, J. 2007. Activation of endosomal dynein motors by stepwise assembly of Rab7-RILP-p150Glued, ORP1L, and the receptor betalll spectrin. *J Cell Biol,* 176**,** 459-71.

JOHNSON, J. D. & MISLER, S. 2002. Nicotinic acid-adenine dinucleotide phosphate-sensitive calcium stores initiate insulin signaling in human beta cells. *Proc Natl Acad Sci U S A,* 99**,** 14566-71.

JORDENS, I., FERNANDEZ-BORJA, M., MARSMAN, M., DUSSELJEE, S., JANSSEN, L., CALAFAT, J., JANSSEN, H., WUBBOLTS, R. & NEEFJES, J. 2001. The Rab7 effector protein RILP controls lysosomal transport by inducing the recruitment of dynein-dynactin motors. *Curr Biol,* 11**,** 1680-5.

JUNQUEIRA, L. C. U. A., CARNEIRO, J. & CONTOPOULOS, A. N. 1983. Basic histology. *A Concise medical library for practitioner and student.* 2 ed. Los Altos, Calif. Norwalk, Conn. New York: Lange Medical Publications. Appleton & Lange. Lange Medical Books/McGraw Hill. McGraw Hill.

KADAMBI, V. J., PONNIAH, S., HARRER, J. M., HOIT, B. D., DORN, G. W., 2ND, WALSH, R. A. & KRANIAS, E. G. 1996. Cardiac-specific overexpression of phospholamban alters calcium kinetics and resultant cardiomyocyte mechanics in transgenic mice. *J Clin Invest,* 97**,** 533-9.

KAISER, S. E., BRICKNER, J. H., REILEIN, A. R., FENN, T. D., WALTER, P. & BRUNGER, A. T. 2005. Structural basis of FFAT motif-mediated ER targeting. *Structure,* 13**,** 1035-45.

KAMP, T. J. & HELL, J. W. 2000. Regulation of cardiac L-type calcium channels by protein kinase A and protein kinase C. *Circ Res,* 87**,** 1095-102.

KANNT, A., SICKA, K., KROLL, K., KADEREIT, D. & GOGELEIN, H. 2012. Selective inhibitors of cardiac ADPR cyclase as novel anti-arrhythmic compounds. *Naunyn Schmiedebergs Arch Pharmacol,* 385**,** 717-27.

KARNOVSKY, M. J. 1965. A formaldehyde-glutaraldehyde fixative of high osmolality for use in electron microscopy. *J Cell Biol,* 27**,** 137-8A.

KATZ, A. M. 2011. *Physiology of the heart,* Philadelphia, PA, Wolters Kluwer

Health/Lippincott Williams & Wilkins Health.

KELM, M., SCHAFER, S., MINGERS, S., HEYDTHAUSEN, M., VOGT, M., MOTZ, W. & STRAUER, B. E. 1996. Left ventricular mass is linked to cardiac noradrenaline in normotensive and hypertensive patients. *J Hypertens,* 14**,** 1357-64.

KEMI, O. J., CECI, M., WISLOFF, U., GRIMALDI, S., GALLO, P., SMITH, G. L., CONDORELLI, G. & ELLINGSEN, O. 2008. Activation or inactivation of cardiac Akt/mTOR signaling diverges physiological from pathological hypertrophy. *J Cell Physiol,* 214**,** 316-21.

KENTISH, J. C., TER KEURS, H. E., RICCIARDI, L., BUCX, J. J. & NOBLE, M. I. 1986. Comparison between the sarcomere length-force relations of intact and skinned trabeculae from rat right ventricle. Influence of calcium concentrations on these relations. *Circ Res,* 58**,** 755-68.

KILPATRICK, B. S., EDEN, E. R., SCHAPIRA, A. H., FUTTER, C. E. & PATEL, S. 2013. Direct mobilisation of lysosomal Ca2+ triggers complex Ca2+ signals. *J Cell Sci,* 126**,** 60-6.

KING, J. H., HUANG, C. L. & FRASER, J. A. 2013. Determinants of myocardial conduction velocity: implications for arrhythmogenesis. *Front Physiol,* 4**,** 154.

KINNEAR, N. P., BOITTIN, F. X., THOMAS, J. M., GALIONE, A. & EVANS, A. M. 2004. Lysosome-sarcoplasmic reticulum junctions. A trigger zone for calcium signaling by nicotinic acid adenine dinucleotide phosphate and endothelin-1. *J Biol Chem,* 279**,** 54319-26.

KINNEAR, N. P., WYATT, C. N., CLARK, J. H., CALCRAFT, P. J., FLEISCHER, S., JEYAKUMAR, L. H., NIXON, G. F. & EVANS, A. M. 2008. Lysosomes co-localize with ryanodine receptor subtype 3 to form a trigger zone for calcium signalling by NAADP in rat pulmonary arterial smooth muscle. *Cell Calcium,* 44**,** 190-201.

KINOSHITA, K., WARITANI, T., NOTO, M., TAKIZAWA, K., MINEMOTO, Y., NISHIKAWA, A. & OHKUMA, S. 1996. Bafilomycin A1 induces apoptosis in PC12 cells independently of intracellular pH. *FEBS Lett,* 398**,** 61-6.

KLEBER, A. G. & RUDY, Y. 2004. Basic mechanisms of cardiac impulse propagation and associated arrhythmias. *Physiol Rev,* 84**,** 431-88.

KOCKSKAMPER, J. & PIESKE, B. 2006. Phosphorylation of the cardiac ryanodine receptor by Ca2+/calmodulin-dependent protein kinase II: the dominating twin of protein kinase A? *Circ Res,* 99**,** 333-5.

KOCKSKAMPER, J., SEIDLMAYER, L., WALTHER, S., HELLENKAMP, K., MAIER, L. S. & PIESKE, B. 2008. Endothelin-1 enhances nuclear Ca2+ transients in atrial myocytes through Ins(1,4,5)P3-dependent Ca2+ release from perinuclear Ca2+ stores. *J Cell Sci,* 121**,** 186-95.

KOCKSKAMPER, J., ZIMA, A. V., RODERICK, H. L., PIESKE, B., BLATTER, L. A. & BOOTMAN, M. D. 2008. Emerging roles of inositol 1,4,5-trisphosphate signaling in cardiac myocytes.

J Mol Cell Cardiol, 45**,** 128-47.

KOHLHAAS, M. & MAACK, C. 2013. Calcium release microdomains and mitochondria. *Cardiovasc Res,* 98**,** 259-68.

KOMAZAKI, S., NISHI, M. & TAKESHIMA, H. 2003. Abnormal junctional membrane structures in cardiac myocytes expressing ectopic junctophilin type 1. *FEBS Lett,* 542**,** 69-73.

KORNFELD, S. 1987. Trafficking of lysosomal enzymes. *FASEB J,* 1**,** 462-8.

KORNFELD, S. & MELLMAN, I. 1989. The biogenesis of lysosomes. *Annu Rev Cell Biol,* 5**,** 483-525.

KWAKU, K. F. & JOSEPHSON, M. E. 2002. Typical AVNRT--an update on mechanisms and therapy. *Card Electrophysiol Rev,* 6**,** 414-21.

LAM, A. K. & GALIONE, A. 2013. The endoplasmic reticulum and junctional membrane communication during calcium signaling. *Biochim Biophys Acta,* 1833**,** 2542-59.

LANGHORST, M. F., SCHWARZMANN, N. & GUSE, A. H. 2004. Ca2+ release via ryanodine receptors and Ca2+ entry: major mechanisms in NAADP-mediated Ca2+ signaling in T-lymphocytes. *Cell Signal,* 16**,** 1283-9.

LEE, H. C. 1993. Potentiation of calcium- and caffeine-induced calcium release by cyclic ADP-ribose. *J Biol Chem,* 268**,** 293-9.

LEE, H. C. 1997. Mechanisms of calcium signaling by cyclic ADP-ribose and NAADP. *Physiol Rev,* 77**,** 1133-64.

LEE, H. C. 2001. Physiological functions of cyclic ADP-ribose and NAADP as calcium messengers. *Annu Rev Pharmacol Toxicol,* 41**,** 317-45.

LEE, H. C. 2002. *Cyclic ADP-Ribose and NAADP : structures, metabolism and functions,* Boston, Kluwer Academic Publishers.

LEE, H. C. & AARHUS, R. 1991. ADP-ribosyl cyclase: an enzyme that cyclizes NAD+ into a calcium-mobilizing metabolite. *Cell Regul,* 2**,** 203-9.

LEE, H. C. & AARHUS, R. 1995. A derivative of NADP mobilizes calcium stores insensitive to inositol trisphosphate and cyclic ADP-ribose. *J Biol Chem,* 270**,** 2152-7.

LEE, H. C. & AARHUS, R. 2000. Functional visualization of the separate but interacting calcium stores sensitive to NAADP and cyclic ADP-ribose. *J Cell Sci,* 113 Pt 24**,** 4413-20.

LEE, H. C., AARHUS, R., GEE, K. R. & KESTNER, T. 1997. Caged nicotinic acid adenine dinucleotide phosphate. Synthesis and use. *J Biol Chem,* 272**,** 4172-8.

LEE, H. C., AARHUS, R., GRAEFF, R., GURNACK, M. E. & WALSETH, T. F. 1994. Cyclic ADP

ribose activation of the ryanodine receptor is mediated by calmodulin. *Nature,* 370**,** 307-9.

LEE, H. C., AARHUS, R. & LEVITT, D. 1994. The crystal structure of cyclic ADP-ribose. *Nat Struct Biol,* 1**,** 143-4.

LEE, H. C., WALSETH, T. F., BRATT, G. T., HAYES, R. N. & CLAPPER, D. L. 1989. Structural determination of a cyclic metabolite of NAD+ with intracellular Ca2+-mobilizing activity. *J Biol Chem,* 264**,** 1608-15.

LEE, K. S., MARBAN, E. & TSIEN, R. W. 1985. Inactivation of calcium channels in mammalian heart cells: joint dependence on membrane potential and intracellular calcium. *J Physiol,* 364**,** 395-411.

LEHNART, S. E., WEHRENS, X. H., REIKEN, S., WARRIER, S., BELEVYCH, A. E., HARVEY, R. D., RICHTER, W., JIN, S. L., CONTI, M. & MARKS, A. R. 2005. Phosphodiesterase 4D deficiency in the ryanodine-receptor complex promotes heart failure and arrhythmias. *Cell,* 123**,** 25-35.

LEVITSKY, D. O., BENEVOLENSKY, D. S., LEVCHENKO, T. S., SMIRNOV, V. N. & CHAZOV, E. I. 1981. Calcium-binding rate and capacity of cardiac sarcoplasmic reticulum. *J Mol Cell Cardiol,* 13**,** 785-96.

LEVY, M. N. 1989. Role of calcium in arrhythmogenesis. *Circulation,* 80**,** IV23-30.

LEWIS, A. M., ALEY, P. K., ROOMI, A., THOMAS, J. M., MASGRAU, R., GARNHAM, C., SHIPMAN, K., PARAMORE, C., BLOOR-YOUNG, D., SANDERS, L. E., TERRAR, D. A., GALIONE, A. & CHURCHILL, G. C. 2012. beta-Adrenergic receptor signaling increases NAADP and cADPR levels in the heart. *Biochem Biophys Res Commun,* 427**,** 326-9.

LIPP, P., LAINE, M., TOVEY, S. C., BURRELL, K. M., BERRIDGE, M. J., LI, W. & BOOTMAN, M. D. 2000. Functional InsP3 receptors that may modulate excitation-contraction coupling in the heart. *Curr Biol,* 10**,** 939-42.

LIPPINCOTT-SCHWARTZ, J. & FAMBROUGH, D. M. 1986. Lysosomal membrane dynamics: structure and interorganellar movement of a major lysosomal membrane glycoprotein. *J Cell Biol,* 102**,** 1593-605.

LIPPINCOTT-SCHWARTZ, J. & FAMBROUGH, D. M. 1987. Cycling of the integral membrane glycoprotein, LEP100, between plasma membrane and lysosomes: kinetic and morphological analysis. *Cell,* 49**,** 669-77.

LLOYD-EVANS, E., MORGAN, A. J., HE, X., SMITH, D. A., ELLIOT-SMITH, E., SILLENCE, D. J., CHURCHILL, G. C., SCHUCHMAN, E. H., GALIONE, A. & PLATT, F. M. 2008. Niemann-Pick disease type C1 is a sphingosine storage disease that causes deregulation of lysosomal calcium. *Nat Med,* 14**,** 1247-55.

LONG, C. S., HARTOGENSIS, W. E. & SIMPSON, P. C. 1993. Beta-adrenergic stimulation of cardiac non-myocytes augments the growth-promoting activity of non-myocyte

conditioned medium. *J Mol Cell Cardiol,* 25**,** 915-25.

LOUGHREY, C. M., SMITH, G. L. & MACEACHERN, K. E. 2004. Comparison of Ca2+ release and uptake characteristics of the sarcoplasmic reticulum in isolated horse and rabbit cardiomyocytes. *Am J Physiol Heart Circ Physiol,* 287**,** H1149-59.

LU, Y., HAO, B. X., GRAEFF, R., WONG, C. W., WU, W. T. & YUE, J. 2013. Two pore channel 2 (TPC2) inhibits autophagosomal-lysosomal fusion by alkalinizing lysosomal pH. *J Biol Chem,* 288**,** 24247-63.

LUBKE, T., LOBEL, P. & SLEAT, D. E. 2009. Proteomics of the lysosome. *Biochim Biophys Acta,* 1793**,** 625-35.

LUO, W., GRUPP, I. L., HARRER, J., PONNIAH, S., GRUPP, G., DUFFY, J. J., DOETSCHMAN, T. & KRANIAS, E. G. 1994. Targeted ablation of the phospholamban gene is associated with markedly enhanced myocardial contractility and loss of beta-agonist stimulation. *Circ Res,* 75**,** 401-9.

LYON, R. C., ZANELLA, F., OMENS, J. H. & SHEIKH, F. 2015. Mechanotransduction in cardiac hypertrophy and failure. *Circ Res,* 116**,** 1462-76.

MACDONNELL, S. M., GARCIA-RIVAS, G., SCHERMAN, J. A., KUBO, H., CHEN, X., VALDIVIA, H. & HOUSER, S. R. 2008. Adrenergic regulation of cardiac contractility does not involve phosphorylation of the cardiac ryanodine receptor at serine 2808. *Circ Res,* 102**,** e65-72.

MACGREGOR, A., YAMASAKI, M., RAKOVIC, S., SANDERS, L., PARKESH, R., CHURCHILL, G. C., GALIONE, A. & TERRAR, D. A. 2007a. NAADP controls cross-talk between distinct Ca2+ stores in the heart. *J Biol Chem,* 282**,** 15302-11.

MACGREGOR, A. T., RAKOVIC, S., GALIONE, A. & TERRAR, D. A. 2007b. Dual effects of cyclic ADP-ribose on sarcoplasmic reticulum Ca2+ release and storage in cardiac myocytes isolated from guinea-pig and rat ventricle. *Cell Calcium,* 41**,** 537-46.

MACKENZIE, L., BOOTMAN, M. D., LAINE, M., BERRIDGE, M. J., THURING, J., HOLMES, A., LI, W. H. & LIPP, P. 2002. The role of inositol 1,4,5-trisphosphate receptors in Ca(2+) signalling and the generation of arrhythmias in rat atrial myocytes. *J Physiol,* 541**,** 395-409.

MACLENNAN, D. H. & KRANIAS, E. G. 2003. Phospholamban: a crucial regulator of cardiac contractility. *Nat Rev Mol Cell Biol,* 4**,** 566-77.

MACLEOD, K. 2014. *An essential introduction to cardiac electrophysiology,* London Singapore ; Hackensack, NJ, Imperial College Press. Distributed by World Scientific Publishing Co Pte. Ltd.

MAILLET, M., VAN BERLO, J. H. & MOLKENTIN, J. D. 2013. Molecular basis of physiological heart growth: fundamental concepts and new players. *Nat Rev Mol Cell Biol,* 14**,** 38-48.

MANDI, M., TOTH, B., TIMAR, G. & BAK, J. 2006. Ca2+ release triggered by NAADP in

hepatocyte microsomes. *Biochem J,* 395**,** 233-8.

MANE, S. M., MARZELLA, L., BAINTON, D. F., HOLT, V. K., CHA, Y., HILDRETH, J. E. & AUGUST, J. T. 1989. Purification and characterization of human lysosomal membrane glycoproteins. *Arch Biochem Biophys,* 268**,** 360-78.

MARJOMAKI, V. S., HUOVILA, A. P., SURKKA, M. A., JOKINEN, I. & SALMINEN, A. 1990. Lysosomal trafficking in rat cardiac myocytes. *J Histochem Cytochem,* 38**,** 1155-64.

MARUFFO, C. A. 1967. Fine structural study of myocardial changes induced by isoproterenol in rhesus monkeys. (Macaca mulatta). *Am J Pathol,* 50**,** 27-37.

MARX, S. O., GABURJAKOVA, J., GABURJAKOVA, M., HENRIKSON, C., ONDRIAS, K. & MARKS, A. R. 2001. Coupled gating between cardiac calcium release channels (ryanodine receptors). *Circ Res,* 88**,** 1151-8.

MARX, S. O., KUROKAWA, J., REIKEN, S., MOTOIKE, H., D'ARMIENTO, J., MARKS, A. R. & KASS, R. S. 2002. Requirement of a macromolecular signaling complex for beta adrenergic receptor modulation of the KCNQ1-KCNE1 potassium channel. *Science,* 295**,** 496-9.

MARX, S. O., REIKEN, S., HISAMATSU, Y., JAYARAMAN, T., BURKHOFF, D., ROSEMBLIT, N. & MARKS, A. R. 2000. PKA phosphorylation dissociates FKBP12.6 from the calcium release channel (ryanodine receptor): defective regulation in failing hearts. *Cell,* 101**,** 365-76.

MATTIAZZI, A., BASSANI, R. A., ESCOBAR, A. L., PALOMEQUE, J., VALVERDE, C. A., VILA PETROFF, M. & BERS, D. M. 2015. Chasing cardiac physiology and pathology down the CaMKII cascade. *Am J Physiol Heart Circ Physiol,* 308**,** H1177-H1191.

MCBRAYER, M. & NIXON, R. A. 2013. Lysosome and calcium dysregulation in Alzheimer's disease: partners in crime. *Biochem Soc Trans,* 41**,** 1495-502.

MCCALL, E., LI, L., SATOH, H., SHANNON, T. R., BLATTER, L. A. & BERS, D. M. 1996. Effects of FK-506 on contraction and Ca2+ transients in rat cardiac myocytes. *Circ Res,* 79**,** 1110-21.

MCDONALD, T. F., PELZER, S., TRAUTWEIN, W. & PELZER, D. J. 1994. Regulation and modulation of calcium channels in cardiac, skeletal, and smooth muscle cells. *Physiol Rev,* 74**,** 365-507.

MCMULLEN, J. R. & JENNINGS, G. L. 2007. Differences between pathological and physiological cardiac hypertrophy: novel therapeutic strategies to treat heart failure. *Clin Exp Pharmacol Physiol,* 34**,** 255-62.

METRICH, M., LUCAS, A., GASTINEAU, M., SAMUEL, J. L., HEYMES, C., MOREL, E. & LEZOUALC'H, F. 2008. Epac mediates beta-adrenergic receptor-induced cardiomyocyte hypertrophy. *Circ Res,* 102**,** 959-65.

MOJZISOVA, A., KRIZANOVA, O., ZACIKOVA, L., KOMINKOVA, V. & ONDRIAS, K. 2001.

Effect of nicotinic acid adenine dinucleotide phosphate on ryanodine calcium release channel in heart. *Pflugers Arch,* 441**,** 674-7.

MOREL, E., MARCANTONI, A., GASTINEAU, M., BIRKEDAL, R., ROCHAIS, F., GARNIER, A., LOMPRE, A. M., VANDECASTEELE, G. & LEZOUALC'H, F. 2005. cAMP-binding protein Epac induces cardiomyocyte hypertrophy. *Circ Res,* 97**,** 1296-304.

MORGAN, A. J. & GALIONE, A. 2007. NAADP induces pH changes in the lumen of acidic Ca2+ stores. *Biochem J,* 402**,** 301-10.

MORGAN, A. J. & GALIONE, A. 2013. Two-pore channels (TPCs): Current controversies. *Bioessays*.

MORGAN, A. J., PLATT, F. M., LLOYD-EVANS, E. & GALIONE, A. 2011. Molecular mechanisms of endolysosomal Ca2+ signalling in health and disease. *Biochem J,* 439**,** 349-74.

MORISCO, C., ZEBROWSKI, D. C., VATNER, D. E., VATNER, S. F. & SADOSHIMA, J. 2001. Beta-adrenergic cardiac hypertrophy is mediated primarily by the beta(1)-subtype in the rat heart. *J Mol Cell Cardiol,* 33**,** 561-73.

MOSCHELLA, M. C. & MARKS, A. R. 1993. Inositol 1,4,5-trisphosphate receptor expression in cardiac myocytes. *J Cell Biol,* 120**,** 1137-46.

MUSHTAQ, M., NAM, T. S. & KIM, U. H. 2011. Critical role for CD38-mediated Ca2+ signaling in thrombin-induced procoagulant activity of mouse platelets and hemostasis. *J Biol Chem,* 286**,** 12952-8.

MYLES, R. C., WANG, L., KANG, C., BERS, D. M. & RIPPLINGER, C. M. 2012. Local beta-adrenergic stimulation overcomes source-sink mismatch to generate focal arrhythmia. *Circ Res,* 110**,** 1454-64.

NAKAI, A., YAMAGUCHI, O., TAKEDA, T., HIGUCHI, Y., HIKOSO, S., TANIIKE, M., OMIYA, S., MIZOTE, I., MATSUMURA, Y., ASAHI, M., NISHIDA, K., HORI, M., MIZUSHIMA, N. & OTSU, K. 2007. The role of autophagy in cardiomyocytes in the basal state and in response to hemodynamic stress. *Nat Med,* 13**,** 619-24.

NAKASHIMA, S., HIRAKU, Y., TADA-OIKAWA, S., HISHITA, T., GABAZZA, E. C., TAMAKI, S., IMOTO, I., ADACHI, Y. & KAWANISHI, S. 2003. Vacuolar H+-ATPase inhibitor induces apoptosis via lysosomal dysfunction in the human gastric cancer cell line MKN-1. *J Biochem,* 134**,** 359-64.

NAON, D. & SCORRANO, L. 2014. At the right distance: ER-mitochondria juxtaposition in cell life and death. *Biochim Biophys Acta,* 1843**,** 2184-94.

NAYLOR, E., ARREDOUANI, A., VASUDEVAN, S. R., LEWIS, A. M., PARKESH, R., MIZOTE, A., ROSEN, D., THOMAS, J. M., IZUMI, M., GANESAN, A., GALIONE, A. & CHURCHILL, G. C. 2009. Identification of a chemical probe for NAADP by virtual screening. *Nat Chem Biol,* 5**,** 220-6.

NEBEL, M., SCHWOERER, A. P., WARSZTA, D., SIEBRANDS, C. C., LIMBROCK, A. C., SWARBRICK, J. M., FLIEGERT, R., WEBER, K., BRUHN, S., HOHENEGGER, M., GEISLER, A., HERICH, L., SCHLEGEL, S., CARRIER, L., ESCHENHAGEN, T., POTTER, B. V., EHMKE, H. & GUSE, A. H. 2013. Nicotinic acid adenine dinucleotide phosphate (NAADP)-mediated calcium signaling and arrhythmias in the heart evoked by beta-adrenergic stimulation. *J Biol Chem,* 288**,** 16017-30.

NEISS, W. F. 1983. The electron density of light and dark lysosomes in the proximal convoluted tubule of the rat kidney. *Histochemistry,* 77**,** 63-77.

NISHIHARA, T., AKIFUSA, S., KOSEKI, T., KATO, S., MURO, M. & HANADA, N. 1995. Specific inhibitors of vacuolar type H(+)-ATPases induce apoptotic cell death. *Biochem Biophys Res Commun,* 212**,** 255-62.

NISHINO, I. 2003. Autophagic vacuolar myopathies. *Curr Neurol Neurosci Rep,* 3**,** 64-9.
NOORMAN, M., VAN DER HEYDEN, M. A., VAN VEEN, T. A., COX, M. G., HAUER, R. N., DE BAKKER, J. M. & VAN RIJEN, H. V. 2009. Cardiac cell-cell junctions in health and disease: Electrical versus mechanical coupling. *J Mol Cell Cardiol,* 47**,** 23-31.

NOVIKOFF, A. B., BEAUFAY, H. & DE DUVE, C. 1956. Electron microscopy of lysosomerich fractions from rat liver. *J Biophys Biochem Cytol,* 2**,** 179-84.

OGUNBAYO, O. A., ZHU, Y., ROSSI, D., SORRENTINO, V., MA, J., ZHU, M. X. & EVANS, A. M. 2011. Cyclic adenosine diphosphate ribose activates ryanodine receptors, whereas NAADP activates two-pore domain channels. *J Biol Chem,* 286**,** 9136-40.

OLSHANSKY, B., SABBAH, H. N., HAUPTMAN, P. J. & COLUCCI, W. S. 2008. Parasympathetic nervous system and heart failure: pathophysiology and potential implications for therapy. *Circulation,* 118**,** 863-71.

ONG, S. B., SAMANGOUEI, P., KALKHORAN, S. B. & HAUSENLOY, D. J. 2015. The mitochondrial permeability transition pore and its role in myocardial ischemia reperfusion injury. *J Mol Cell Cardiol,* 78**,** 23-34.

OSADCHII, O. E. 2007. Cardiac hypertrophy induced by sustained beta-adrenoreceptor activation: pathophysiological aspects. *Heart Fail Rev,* 12**,** 66-86.

OTSU, K., WILLARD, H. F., KHANNA, V. K., ZORZATO, F., GREEN, N. M. & MACLENNAN, D. H. 1990. Molecular cloning of cDNA encoding the Ca2+ release channel (ryanodine receptor) of rabbit cardiac muscle sarcoplasmic reticulum. *J Biol Chem,* 265**,** 13472-83.

OTSUKA, N., OKAMOTO, H. & TOMISAWA, M. 1969. Electron and fluorescence microscopic study of specific granules in rat atrial muscle cells. *Arch Histol Jpn,* 30**,** 367-74.

PENNY, C. J., KILPATRICK, B. S., EDEN, E. R. & PATEL, S. 2015. Coupling acidic organelles with the ER through Ca microdomains at membrane contact sites. *Cell Calcium*.

PEREIRA, G. J., HIRATA, H., DO CARMO, L. G., STILHANO, R. S., URESHINO, R. P., MEDAGLIA, N. C., HAN, S. W., CHURCHILL, G., BINCOLETTO, C., PATEL, S. & SMAILI, S. S. 2014. NAADP-sensitive two-pore channels are present and functional in gastric smooth muscle cells. *Cell Calcium,* 56**,** 51-8.

PEREIRA, G. J., HIRATA, H., FIMIA, G. M., DO CARMO, L. G., BINCOLETTO, C., HAN, S. W., STILHANO, R. S., URESHINO, R. P., BLOOR-YOUNG, D., CHURCHILL, G., PIACENTINI, M., PATEL, S. & SMAILI, S. S. 2011. Nicotinic acid adenine dinucleotide phosphate (NAADP) regulates autophagy in cultured astrocytes. *J Biol Chem,* 286**,** 27875-81.

PEREIRA, L., METRICH, M., FERNANDEZ-VELASCO, M., LUCAS, A., LEROY, J., PERRIER, R., MOREL, E., FISCHMEISTER, R., RICHARD, S., BENITAH, J. P., LEZOUALC'H, F. & GOMEZ, A. M. 2007. The cAMP binding protein Epac modulates Ca2+ sparks by a Ca2+/calmodulin kinase signalling pathway in rat cardiac myocytes. *J Physiol,* 583**,** 685-94.

PEREIRA, L., RUIZ-HURTADO, G., MOREL, E., LAURENT, A. C., METRICH, M., DOMINGUEZ-RODRIGUEZ, A., LAUTON-SANTOS, S., LUCAS, A., BENITAH, J. P., BERS, D. M., LEZOUALC'H, F. & GOMEZ, A. M. 2012. Epac enhances excitation-transcription coupling in cardiac myocytes. *J Mol Cell Cardiol,* 52**,** 283-91.

PERIASAMY, M., BHUPATHY, P. & BABU, G. J. 2008. Regulation of sarcoplasmic reticulum Ca2+ ATPase pump expression and its relevance to cardiac muscle physiology and pathology. *Cardiovasc Res,* 77**,** 265-73.

PERIASAMY, M. & KALYANASUNDARAM, A. 2007. SERCA pump isoforms: their role in calcium transport and disease. *Muscle Nerve,* 35**,** 430-42.

PHILLIPS, M. J. & VOELTZ, G. K. 2015. Structure and function of ER membrane contact sites with other organelles. *Nat Rev Mol Cell Biol*.

PITT, S. J., FUNNELL, T. M., SITSAPESAN, M., VENTURI, E., RIETDORF, K., RUAS, M., GANESAN, A., GOSAIN, R., CHURCHILL, G. C., ZHU, M. X., PARRINGTON, J., GALIONE, A. & SITSAPESAN, R. 2010. TPC2 is a novel NAADP-sensitive Ca2+ release channel, operating as a dual sensor of luminal pH and Ca2+. *J Biol Chem,* 285**,** 35039-46.

PITT, S. J., REILLY-O'DONNELL, B. & SITSAPESAN, R. 2016. Exploring the biophysical evidence that mammalian two pore channels are NAADP-activated calcium-permeable channels. *J Physiol*.

POGWIZD, S. M., SCHLOTTHAUER, K., LI, L., YUAN, W. & BERS, D. M. 2001. Arrhythmogenesis and contractile dysfunction in heart failure: Roles of sodium-calcium exchange, inward rectifier potassium current, and residual beta-adrenergic responsiveness. *Circ Res,* 88**,** 1159-67.

POWELL, T., TERRAR, D. A. & TWIST, V. W. 1980. Electrical properties of individual cells isolated from adult rat ventricular myocardium. *J Physiol,* 302**,** 131-53.

PRINZ, W. A. 2014. Bridging the gap: membrane contact sites in signaling, metabolism, and organelle dynamics. *J Cell Biol,* 205**,** 759-69.

PROVEN, A., RODERICK, H. L., CONWAY, S. J., BERRIDGE, M. J., HORTON, J. K., CAPPER, S. J. & BOOTMAN, M. D. 2006. Inositol 1,4,5-trisphosphate supports the arrhythmogenic action of endothelin-1 on ventricular cardiac myocytes. *J Cell Sci,* 119**,** 3363-75.

PRYOR, P. R., REIMANN, F., GRIBBLE, F. M. & LUZIO, J. P. 2006. Mucolipin-1 is a lysosomal membrane protein required for intracellular lactosylceramide traffic. *Traffic,* 7**,** 1388-98.

RAH, S. Y., MUSHTAQ, M., NAM, T. S., KIM, S. H. & KIM, U. H. 2010. Generation of cyclic ADP-ribose and nicotinic acid adenine dinucleotide phosphate by CD38 for Ca2+ signaling in interleukin-8-treated lymphokine-activated killer cells. *J Biol Chem,* 285**,** 21877-87.

RAIBORG, C., WENZEL, E. M. & STENMARK, H. 2015. ER-endosome contact sites: molecular compositions and functions. *EMBO J,* 34**,** 1848-58.

RAKOVIC, S., CUI, Y., IINO, S., GALIONE, A., ASHAMU, G. A., POTTER, B. V. & TERRAR, D. A. 1999. An antagonist of cADP-ribose inhibits arrhythmogenic oscillations of intracellular Ca2+ in heart cells. *J Biol Chem,* 274**,** 17820-7.

REDDY, L. G., JONES, L. R., PACE, R. C. & STOKES, D. L. 1996. Purified, reconstituted cardiac Ca2+-ATPase is regulated by phospholamban but not by direct phosphorylation with Ca2+/calmodulin-dependent protein kinase. *J Biol Chem,* 271**,** 14964-70.

RESPRESS, J. L., VAN OORT, R. J., LI, N., ROLIM, N., DIXIT, S. S., DEALMEIDA, A., VOIGT, N., LAWRENCE, W. S., SKAPURA, D. G., SKARDAL, K., WISLOFF, U., WIELAND, T., AI, X., POGWIZD, S. M., DOBREV, D. & WEHRENS, X. H. 2012. Role of RyR2 phosphorylation at S2814 during heart failure progression. *Circ Res,* 110**,** 1474-83.

REYNOLDS, E. S. 1963. The use of lead citrate at high pH as an electron-opaque stain in electron microscopy. *J Cell Biol,* 17**,** 208-12.

RICHARDS, M. A., CLARKE, J. D., SARAVANAN, P., VOIGT, N., DOBREV, D., EISNER, D. A., TRAFFORD, A. W. & DIBB, K. M. 2011. Transverse tubules are a common feature in large mammalian atrial myocytes including human. *Am J Physiol Heart Circ Physiol,* 301**,** H1996-2005.

ROCHA, N., KUIJL, C., VAN DER KANT, R., JANSSEN, L., HOUBEN, D., JANSSEN, H., ZWART, W. & NEEFJES, J. 2009. Cholesterol sensor ORP1L contacts the ER protein VAP to control Rab7-RILP-p150 Glued and late endosome positioning. *J Cell Biol,* 185**,** 1209-25.

ROMEO, D. S., N. SOTTOCASA, G.L. PUGLIARELLO, M.C. DE BERNARD, B. VITTUR, F. 1966. Lysosomes in heart tissue. *Biochim Biophys Acta,* 130**,** 64.

ROSEN, D., LEWIS, A. M., MIZOTE, A., THOMAS, J. M., ALEY, P. K., VASUDEVAN, S. R., PARKESH, R., GALIONE, A., IZUMI, M., GANESAN, A. & CHURCHILL, G. C. 2009. Analogues of the nicotinic acid adenine dinucleotide phosphate (NAADP) antagonist Ned-19 indicate two binding sites on the NAADP receptor. *J Biol Chem,* 284**,** 34930-4.

RUAS, M., DAVIS, L. C., CHEN, C. C., MORGAN, A. J., CHUANG, K. T., WALSETH, T. F., GRIMM, C., GARNHAM, C., POWELL, T., PLATT, N., PLATT, F. M., BIEL, M., WAHL-SCHOTT, C., PARRINGTON, J. & GALIONE, A. 2015. Expression of Ca2+-permeable two-pore channels rescues NAADP signalling in TPC-deficient cells. *EMBO J*.

SAFTIG, P., BEERTSEN, W. & ESKELINEN, E. L. 2008. LAMP-2: a control step for phagosome and autophagosome maturation. *Autophagy,* 4**,** 510-2.

SAFTIG, P. & KLUMPERMAN, J. 2009. Lysosome biogenesis and lysosomal membrane proteins: trafficking meets function. *Nat Rev Mol Cell Biol,* 10**,** 623-35.

SAKMANN, B. & TRUBE, G. 1984. Conductance properties of single inwardly rectifying potassium channels in ventricular cells from guinea-pig heart. *J Physiol,* 347**,** 641-57.

SAKURAI, Y., KOLOKOLTSOV, A. A., CHEN, C. C., TIDWELL, M. W., BAUTA, W. E., KLUGBAUER, N., GRIMM, C., WAHL-SCHOTT, C., BIEL, M. & DAVEY, R. A. 2015. Ebola virus. Two-pore channels control Ebola virus host cell entry and are drug targets for disease treatment. *Science,* 347**,** 995-8.

SANCHEZ-TUSIE, A. A., VASUDEVAN, S. R., CHURCHILL, G. C., NISHIGAKI, T. & TREVINO, C. L. 2014. Characterization of NAADP-mediated calcium signaling in human spermatozoa. *Biochem Biophys Res Commun,* 443**,** 531-6.

SCHERMELLEH, L., HEINTZMANN, R. & LEONHARDT, H. 2010. A guide to super-resolution fluorescence microscopy. *J Cell Biol,* 190**,** 165-75.

SCHEUER, J. 1999. Catecholamines in cardiac hypertrophy. *Am J Cardiol,* 83**,** 70H-74H.

SCHMITT, J. P., KAMISAGO, M., ASAHI, M., LI, G. H., AHMAD, F., MENDE, U., KRANIAS, E. G., MACLENNAN, D. H., SEIDMAN, J. G. & SEIDMAN, C. E. 2003. Dilated cardiomyopathy and heart failure caused by a mutation in phospholamban. *Science,* 299**,** 1410-3.

SCHMUCKER, D. L. & SACHS, H. 2002. Quantifying dense bodies and lipofuscin during aging: a morphologist's perspective. *Arch Gerontol Geriatr,* 34**,** 249-61.

SCHULSON, M. N., SCRIVEN, D. R., FLETCHER, P. & MOORE, E. D. 2011. Couplons in rat atria form distinct subgroups defined by their molecular partners. *J Cell Sci,* 124**,** 1167-74.

SCOTT, C. C., VACCA, F. & GRUENBERG, J. 2014. Endosome maturation, transport and functions. *Semin Cell Dev Biol,* 31**,** 2-10.

SCRIVEN, D. R., ASGHARI, P. & MOORE, E. D. 2013. Microarchitecture of the dyad. *Cardiovasc Res,* 98**,** 169-76.

SCRIVEN, D. R., DAN, P. & MOORE, E. D. 2000. Distribution of proteins implicated in excitation-contraction coupling in rat ventricular myocytes. *Biophys J,* 79**,** 2682-91.

SHAN, J., KUSHNIR, A., BETZENHAUSER, M. J., REIKEN, S., LI, J., LEHNART, S. E.,

LINDEGGER, N., MONGILLO, M., MOHLER, P. J. & MARKS, A. R. 2010. Phosphorylation of the ryanodine receptor mediates the cardiac fight or flight response in mice. *J Clin Invest,* 120**,** 4388-98.

SHANNON, T. R., GUO, T. & BERS, D. M. 2003. Ca2+ scraps: local depletions of free [Ca2+] in cardiac sarcoplasmic reticulum during contractions leave substantial Ca2+ reserve. *Circ Res,* 93**,** 40-5.

SHARMA, V. K., RAMESH, V., FRANZINI-ARMSTRONG, C. & SHEU, S. S. 2000. Transport of Ca2+ from sarcoplasmic reticulum to mitochondria in rat ventricular myocytes. *J Bioenerg Biomembr,* 32**,** 97-104.

SHATTOCK, M. J., OTTOLIA, M., BERS, D. M., BLAUSTEIN, M. P., BOGUSLAVSKYI, A., BOSSUYT, J., BRIDGE, J. H., CHEN-IZU, Y., CLANCY, C. E., EDWARDS, A., GOLDHABER, J., KAPLAN, J., LINGREL, J. B., PAVLOVIC, D., PHILIPSON, K., SIPIDO, K. R. & XIE, Z. J. 2015. Na+/Ca2+ exchange and Na+/K+-ATPase in the heart. *J Physiol,* 593**,** 1361-82.

SHEN, D., WANG, X., LI, X., ZHANG, X., YAO, Z., DIBBLE, S., DONG, X. P., YU, T., LIEBERMAN, A. P., SHOWALTER, H. D. & XU, H. 2012. Lipid storage disorders block lysosomal trafficking by inhibiting a TRP channel and lysosomal calcium release. *Nat Commun,* 3**,** 731.

SHI, C. & SOLDATOV, N. M. 2002. Molecular determinants of voltage-dependent slow inactivation of the Ca2+ channel. *J Biol Chem,* 277**,** 6813-21.

SHIMIZU, I. & MINAMINO, T. 2016. Physiological and pathological cardiac hypertrophy. *J Mol Cell Cardiol,* 97**,** 245-62.

SIMMERMAN, H. K., COLLINS, J. H., THEIBERT, J. L., WEGENER, A. D. & JONES, L. R. 1986. Sequence analysis of phospholamban. Identification of phosphorylation sites and two major structural domains. *J Biol Chem,* 261**,** 13333-41.

SIMPSON, P. 1983. Norepinephrine-stimulated hypertrophy of cultured rat myocardial cells is an alpha 1 adrenergic response. *J Clin Invest,* 72**,** 732-8.

SIMPSON, P. 1985. Stimulation of hypertrophy of cultured neonatal rat heart cells through an alpha 1-adrenergic receptor and induction of beating through an alpha 1- and beta 1-adrenergic receptor interaction. Evidence for independent regulation of growth and beating. *Circ Res,* 56**,** 884-94.

SIMPSON, P. C., KARIYA, K., KARNS, L. R., LONG, C. S. & KARLINER, J. S. 1991. Adrenergic hormones and control of cardiac myocyte growth. *Mol Cell Biochem,* 104**,** 35-43.
SINGAL, T., DHALLA, N. S. & TAPPIA, P. S. 2004. Phospholipase C may be involved in norepinephrine-induced cardiac hypertrophy. *Biochem Biophys Res Commun,* 320**,** 1015-9.

SKEPPER, J. N. & NAVARATNAM, V. 1987. Lipofuscin formation in the myocardium of juvenile golden hamsters: an ultrastructural study including staining for acid phosphatase. *J Anat,* 150**,** 155-67.

SMYRNIAS, I., MAIR, W., HARZHEIM, D., WALKER, S. A., RODERICK, H. L. & BOOTMAN, M. D. 2010. Comparison of the T-tubule system in adult rat ventricular and atrial myocytes, and its role in excitation-contraction coupling and inotropic stimulation. *Cell Calcium,* 47**,** 210-23.

SOBOLOFF, J., ROTHBERG, B. S., MADESH, M. & GILL, D. L. 2012. STIM proteins: dynamic calcium signal transducers. *Nat Rev Mol Cell Biol,* 13**,** 549-65.

SOELLER, C. & CANNELL, M. B. 1999. Examination of the transverse tubular system in living cardiac rat myocytes by 2-photon microscopy and digital image-processing techniques. *Circ Res,* 84**,** 266-75.

SOLARO, R. J. & RARICK, H. M. 1998. Troponin and tropomyosin: proteins that switch on and tune in the activity of cardiac myofilaments. *Circ Res,* 83**,** 471-80.

SOMLYO, A. V., BRODERICK, R., SHUMAN, H., BUHLE, E. L., JR. & SOMLYO, A. P. 1988. Atrial-specific granules in situ have high calcium content, are acidic, and maintain anion gradients. *Proc Natl Acad Sci U S A,* 85**,** 6222-6.

SONG, E. K., LEE, Y. R., KIM, Y. R., YEOM, J. H., YOO, C. H., KIM, H. K., PARK, H. M., KANG, H. S., KIM, J. S., KIM, U. H. & HAN, M. K. 2012. NAADP mediates insulin-stimulated glucose uptake and insulin sensitization by PPARgamma in adipocytes. *Cell Rep,* 2**,** 1607-19.

SPURR, A. R. 1969. A low-viscosity epoxy resin embedding medium for electron microscopy. *J Ultrastruct Res,* 26**,** 31-43.

STAMMERS, A. N., SUSSER, S. E., HAMM, N. C., HLYNSKY, M. W., KIMBER, D. E., KEHLER, D. S. & DUHAMEL, T. A. 2015. The regulation of sarco(endo)plasmic reticulum calcium-ATPases (SERCA). *Can J Physiol Pharmacol,* 93**,** 843-54.

STRAND, A. H., GUDMUNDSDOTTIR, H., OS, I., SMITH, G., WESTHEIM, A. S., BJORNERHEIM, R. & KJELDSEN, S. E. 2006. Arterial plasma noradrenaline predicts left ventricular mass independently of blood pressure and body build in men who develop hypertension over 20 years. *J Hypertens,* 24**,** 905-13.

SUGDEN, P. H. & CLERK, A. 2005. Endothelin signalling in the cardiac myocyte and its pathophysiological relevance. *Curr Vasc Pharmacol,* 3**,** 343-51.

TANG, W. X., CHEN, Y. F., ZOU, A. P., CAMPBELL, W. B. & LI, P. L. 2002. Role of FKBP12.6 in cADPR-induced activation of reconstituted ryanodine receptors from arterial smooth muscle. *Am J Physiol Heart Circ Physiol,* 282**,** H1304-10.

TAPPER, H. & SUNDLER, R. 1990. Role of lysosomal and cytosolic pH in the regulation of macrophage lysosomal enzyme secretion. *Biochem J,* 272**,** 407-14.

TERENTYEV, D., VIATCHENKO-KARPINSKI, S., GYORKE, I., TERENTYEVA, R. & GYORKE, S. 2003. Protein phosphatases decrease sarcoplasmic reticulum calcium content by stimulating calcium release in cardiac myocytes. *J Physiol,* 552**,** 109-18.

TERENTYEV, D., VIATCHENKO-KARPINSKI, S., GYORKE, I., VOLPE, P., WILLIAMS, S. C. & GYORKE, S. 2003. Calsequestrin determines the functional size and stability of cardiac intracellular calcium stores: Mechanism for hereditary arrhythmia. *Proc Natl Acad Sci U S A,* 100**,** 11759-64.

TERMAN, A. & BRUNK, U. T. 1998. Lipofuscin: mechanisms of formation and increase with age. *APMIS,* 106**,** 265-76.

TERMAN, A. & BRUNK, U. T. 2005. The aging myocardium: roles of mitochondrial damage and lysosomal degradation. *Heart Lung Circ,* 14**,** 107-14.

TERMAN, A., DALEN, H., EATON, J. W., NEUZIL, J. & BRUNK, U. T. 2004. Aging of cardiac myocytes in culture: oxidative stress, lipofuscin accumulation, and mitochondrial turnover. *Ann N Y Acad Sci,* 1019**,** 70-7.

TIDBALL, J. G., CEDERDAHL, J. E. & BERS, D. M. 1991. Quantitative analysis of regional variability in the distribution of transverse tubules in rabbit myocardium. *Cell Tissue Res,* 264**,** 293-8.

TIMERMAN, A. P., ONOUE, H., XIN, H. B., BARG, S., COPELLO, J., WIEDERRECHT, G. & FLEISCHER, S. 1996. Selective binding of FKBP12.6 by the cardiac ryanodine receptor. *J Biol Chem,* 271**,** 20385-91.

TOMISAWA, M. 1969. Atrial specific granules in various mammals. *Arch Histol Jpn,* 30**,** 449-65.

TOPPING, T. M. & TRAVIS, D. F. 1974. An electron cytochemical study of mechanisms of lysosomal activity in the rat left ventricular mural myocardium. *J Ultrastruct Res,* 46**,** 1-22.

TOUCHBERRY, C. D., BALES, I. K., STONE, J. K., ROHRBERG, T. J., PARELKAR, N. K., NGUYEN, T., FUENTES, O., LIU, X., QU, C. K., ANDRESEN, J. J., VALDIVIA, H. H., BROTTO, M. & WACKER, M. J. 2010. Phosphatidylinositol 3,5-bisphosphate (PI(3,5)P2) potentiates cardiac contractility via activation of the ryanodine receptor. *J Biol Chem,* 285**,** 40312-21.

TRAFFORD, A. W., CLARKE, J. D., RICHARDS, M. A., EISNER, D. A. & DIBB, K. M. 2013. Calcium signalling microdomains and the t-tubular system in atrial mycoytes: potential roles in cardiac disease and arrhythmias. *Cardiovasc Res,* 98**,** 192-203.

TUGBA DURLU-KANDILCI, N., RUAS, M., CHUANG, K. T., BRADING, A., PARRINGTON, J. & GALIONE, A. 2010. TPC2 proteins mediate nicotinic acid adenine dinucleotide phosphate (NAADP)- and agonist-evoked contractions of smooth muscle. *J Biol Chem,* 285**,** 24925-32.

VALDIVIA, H. H., FARRELL, E. F., ANTARAMIAN, A., BENKUSKY, N., ZHU, X., RUEDA, A. & GOMEZ, A. M. 2004. Sorcin and ryanodine receptors in heart failure. *J Muscle Res Cell Motil,* 25**,** 605-7.

VALDIVIA, H. H., KAPLAN, J. H., ELLIS-DAVIES, G. C. & LEDERER, W. J. 1995. Rapid adaptation of cardiac ryanodine receptors: modulation by Mg2+ and phosphorylation. *Science,* 267**,** 1997-2000.

VAN OORT, R. J., MCCAULEY, M. D., DIXIT, S. S., PEREIRA, L., YANG, Y., RESPRESS, J. L., WANG, Q., DE ALMEIDA, A. C., SKAPURA, D. G., ANDERSON, M. E., BERS, D. M. & WEHRENS, X. H. 2010. Ryanodine receptor phosphorylation by calcium/calmodulin-dependent protein kinase II promotes life-threatening ventricular arrhythmias in mice with heart failure. *Circulation,* 122**,** 2669-79.

VAQUERO, M., CALVO, D. & JALIFE, J. 2008. Cardiac fibrillation: from ion channels to rotors in the human heart. *Heart Rhythm,* 5**,** 872-9.

VASUDEVAN, S. R., LEWIS, A. M., CHAN, J. W., MACHIN, C. L., SINHA, D., GALIONE, A. & CHURCHILL, G. C. 2010. The calcium-mobilizing messenger nicotinic acid adenine dinucleotide phosphate participates in sperm activation by mediating the acrosome reaction. *J Biol Chem,* 285**,** 18262-9.

WAGNER, L. E., 2ND, GROOM, L. A., DIRKSEN, R. T. & YULE, D. I. 2014. Characterization of ryanodine receptor type 1 single channel activity using "on-nucleus" patch clamp. *Cell Calcium,* 56**,** 96-107.

WAGNER, S., MAIER, L. S. & BERS, D. M. 2015. Role of sodium and calcium dysregulation in tachyarrhythmias in sudden cardiac death. *Circ Res,* 116**,** 1956-70.

WANG, X., ZHANG, X., DONG, X. P., SAMIE, M., LI, X., CHENG, X., GOSCHKA, A., SHEN, D., ZHOU, Y., HARLOW, J., ZHU, M. X., CLAPHAM, D. E., REN, D. & XU, H. 2012. TPC proteins are phosphoinositide- activated sodium-selective ion channels in endosomes and lysosomes. *Cell,* 151**,** 372-83.

WARSZTA, D., NEBEL, M., FLIEGERT, R. & GUSE, A. H. 2014. NAD derived second messengers: Role in spontaneous diastolic Ca(2+) transients in murine cardiac myocytes. *DNA Repair (Amst),* 23**,** 69-78.

WEHRENS, X. H., LEHNART, S. E., REIKEN, S., VEST, J. A., WRONSKA, A. & MARKS, A. R. 2006. Ryanodine receptor/calcium release channel PKA phosphorylation: a critical mediator of heart failure progression. *Proc Natl Acad Sci U S A,* 103**,** 511-8.

WEHRENS, X. H., LEHNART, S. E., REIKEN, S. R. & MARKS, A. R. 2004. Ca2+/calmodulin-dependent protein kinase II phosphorylation regulates the cardiac ryanodine receptor. *Circ Res,* 94**,** e61-70.

WEIDMANN, S. 1955. Effects of calcium ions and local anesthetics on electrical properties of Purkinje fibres. *J Physiol,* 129**,** 568-82.

WHALLEY, D. W., WENDT, D. J. & GRANT, A. O. 1995. Basic concepts in cellular cardiac electrophysiology: Part I: Ion channels, membrane currents, and the action potential. *Pacing Clin Electrophysiol,* 18**,** 1556-74.

WILKINS, B. J., DAI, Y. S., BUENO, O. F., PARSONS, S. A., XU, J., PLANK, D. M., JONES, F., KIMBALL, T. R. & MOLKENTIN, J. D. 2004. Calcineurin/NFAT coupling participates in pathological, but not physiological, cardiac hypertrophy. *Circ Res,* 94**,** 110-8.

WILSON, H. L. & GALIONE, A. 1998. Differential regulation of nicotinic acid-adenine dinucleotide phosphate and cADP-ribose production by cAMP and cGMP. *Biochem J,* 331 (Pt 3)**,** 837-43.

WINCHESTER, B. G. 2001. Lysosomal membrane proteins. *Eur J Paediatr Neurol,* 5 Suppl A**,** 11-9.

WOJCIKIEWICZ, R. J. 1995. Type I, II, and III inositol 1,4,5-trisphosphate receptors are unequally susceptible to down-regulation and are expressed in markedly different proportions in different cell types. *J Biol Chem,* 270**,** 11678-83.

WOLF, I. M., DIERCKS, B. P., GATTKOWSKI, E., CZARNIAK, F., KEMPSKI, J., WERNER, R., SCHETELIG, D., MITTRUCKER, H. W., SCHUMACHER, V., VON OSTEN, M., LODYGIN, D., FLUGEL, A., FLIEGERT, R. & GUSE, A. H. 2015. Frontrunners of T cell activation: Initial, localized Ca2+ signals mediated by NAADP and the type 1 ryanodine receptor. *Sci Signal,* 8**,** ra102.

WOODCOCK, E. A., ARTHUR, J. F. & MATKOVICH, S. J. 2000. Inositol 1,4,5-trisphosphate and reperfusion arrhythmias. *Clin Exp Pharmacol Physiol,* 27**,** 734-7.

WU, X., ZHANG, T., BOSSUYT, J., LI, X., MCKINSEY, T. A., DEDMAN, J. R., OLSON, E. N., CHEN, J., BROWN, J. H. & BERS, D. M. 2006. Local InsP3-dependent perinuclear Ca2+ signaling in cardiac myocyte excitation-transcription coupling. *J Clin Invest,* 116**,** 675-82.

XIAO, B., TIAN, X., XIE, W., JONES, P. P., CAI, S., WANG, X., JIANG, D., KONG, H., ZHANG, L., CHEN, K., WALSH, M. P., CHENG, H. & CHEN, S. R. 2007. Functional consequence of protein kinase A-dependent phosphorylation of the cardiac ryanodine receptor: sensitization of store overload-induced Ca2+ release. *J Biol Chem,* 282**,** 30256-64.

XIAO, B., ZHONG, G., OBAYASHI, M., YANG, D., CHEN, K., WALSH, M. P., SHIMONI, Y., CHENG, H., TER KEURS, H. & CHEN, S. R. 2006. Ser-2030, but not Ser-2808, is the major phosphorylation site in cardiac ryanodine receptors responding to protein kinase A activation upon beta-adrenergic stimulation in normal and failing hearts. *Biochem J,* 396**,** 7-16.

XIAO, R. P., VALDIVIA, H. H., BOGDANOV, K., VALDIVIA, C., LAKATTA, E. G. & CHENG, H. 1997. The immunophilin FK506-binding protein modulates Ca2+ release channel closure in rat heart. *J Physiol,* 500 (Pt 2)**,** 343-54.

XIE, G. H., RAH, S. Y., KIM, S. J., NAM, T. S., HA, K. C., CHAE, S. W., IM, M. J. & KIM, U. H. 2005. ADP-ribosyl cyclase couples to cyclic AMP signaling in the cardiomyocytes. *Biochem Biophys Res Commun,* 330**,** 1290-8.

YAMAGUCHI, S., JHA, A., LI, Q., SOYOMBO, A. A., DICKINSON, G. D., CHURAMANI, D., BRAILOIU, E., PATEL, S. & MUALLEM, S. 2011. Transient receptor potential mucolipin 1

(TRPML1) and two-pore channels are functionally independent organellar ion channels. *J Biol Chem,* 286**,** 22934-42.

YUE, D. T., HERZIG, S. & MARBAN, E. 1990. Beta-adrenergic stimulation of calcium channels occurs by potentiation of high-activity gating modes. *Proc Natl Acad Sci U S A,* 87**,** 753-7.

ZAGLIA, T., MILAN, G., RUHS, A., FRANZOSO, M., BERTAGGIA, E., PIANCA, N., CARPI, A., CARULLO, P., PESCE, P., SACERDOTI, D., SARAIS, C., CATALUCCI, D., KRUGER, M., MONGILLO, M. & SANDRI, M. 2014. Atrogin-1 deficiency promotes cardiomyopathy and premature death via impaired autophagy. *J Clin Invest,* 124**,** 2410-24.

ZHANG, F. & LI, P. L. 2007. Reconstitution and characterization of a nicotinic acid adenine dinucleotide phosphate (NAADP)-sensitive Ca2+ release channel from liver lysosomes of rats. *J Biol Chem,* 282**,** 25259-69.

ZHANG, F., XU, M., HAN, W. Q. & LI, P. L. 2011. Reconstitution of lysosomal NAADP-TRP-ML1 signaling pathway and its function in TRP-ML1(-/-) cells. *Am J Physiol Cell Physiol,* 301**,** C421-30.

ZHANG, F., ZHANG, G., ZHANG, A. Y., KOEBERL, M. J., WALLANDER, E. & LI, P. L. 2006. Production of NAADP and its role in Ca2+ mobilization associated with lysosomes in coronary arterial myocytes. *Am J Physiol Heart Circ Physiol,* 291**,** H274-82.

ZHANG, J., CHEN, B., ZHONG, X., MI, T., GUO, A., ZHOU, Q., TAN, Z., WU, G., CHEN, A. W., FILL, M., SONG, L. S. & CHEN, S. R. 2014. The cardiac ryanodine receptor luminal Ca2+ sensor governs Ca2+ waves, ventricular tachyarrhythmias and cardiac hypertrophy in calsequestrin-null mice. *Biochem J,* 461**,** 99-106.

ZHANG, L., KELLEY, J., SCHMEISSER, G., KOBAYASHI, Y. M. & JONES, L. R. 1997. Complex formation between junctin, triadin, calsequestrin, and the ryanodine receptor. Proteins of the cardiac junctional sarcoplasmic reticulum membrane. *J Biol Chem,* 272**,** 23389-97.
ZHAO, Y., GRAEFF, R. & LEE, H. C. 2012. Roles of cADPR and NAADP in pancreatic cells. *Acta Biochim Biophys Sin (Shanghai),* 44**,** 719-29.

ZHOU, J., TAN, S. H., NICOLAS, V., BAUVY, C., YANG, N. D., ZHANG, J., XUE, Y., CODOGNO, P. & SHEN, H. M. 2013. Activation of lysosomal function in the course of autophagy via mTORC1 suppression and autophagosome-lysosome fusion. *Cell Res,* 23**,** 508-23.

ZHU, H., TANNOUS, P., JOHNSTONE, J. L., KONG, Y., SHELTON, J. M., RICHARDSON, J. A., LE, V., LEVINE, B., ROTHERMEL, B. A. & HILL, J. A. 2007. Cardiac autophagy is a maladaptive response to hemodynamic stress. *J Clin Invest,* 117**,** 1782-93.

ZHU, M. X., MA, J., PARRINGTON, J., CALCRAFT, P. J., GALIONE, A. & EVANS, A. M. 2010. Calcium signaling via two-pore channels: local or global, that is the question. *Am J Physiol Cell Physiol,* 298**,** C430-41.

ZIMA, A. V., BARE, D. J., MIGNERY, G. A. & BLATTER, L. A. 2007. IP3-dependent nuclear Ca2+ signalling in the mammalian heart. *J Physiol,* 584**,** 601-11.

ZONG, X., SCHIEDER, M., CUNY, H., FENSKE, S., GRUNER, C., ROTZER, K., GRIESBECK, O., HARZ, H., BIEL, M. & WAHL-SCHOTT, C. 2009. The two-pore channel TPCN2 mediates NAADP-dependent Ca(2+)-release from lysosomal stores. *Pflugers Arch,* 458**,** 891-9.